AWARD NUMBER: W81XWH-18-1-0547

TITLE: Brigatinib and Its Combination with INK-128 as a Novel Treatment for NF2-Deficient Meningiomas

PRINCIPAL INVESTIGATOR: Long-Sheng Chang, Ph.D.

CONTRACTING ORGANIZATION: The Research Institute at Nationwide Children's Hospital, Columbus, OH

REPORT DATE: January 2023

TYPE OF REPORT: Final

PREPARED FOR: U.S. Army Medical Research and Development Command
Fort Detrick, Maryland 21702-5012

DISTRIBUTION STATEMENT: Approved for Public Release;
Distribution Unlimited

The views, opinions and/or findings contained in this report are those of the author(s) and should not be construed as an official Department of the Army position, policy or decision unless so designated by other documentation.

REPORT DOCUMENTATION PAGE

Form Approved
OMB No. 0704-0188

Public reporting burden for this collection of information is estimated to average 1 hour per response, including the time for reviewing instructions, searching existing data sources, gathering and maintaining the data needed, and completing and reviewing this collection of information. Send comments regarding this burden estimate or any other aspect of this collection of information, including suggestions for reducing this burden to Department of Defense, Washington Headquarters Services, Directorate for Information Operations and Reports (0704-0188), 1215 Jefferson Davis Highway, Suite 1204, Arlington, VA 22202-4302. Respondents should be aware that notwithstanding any other provision of law, no person shall be subject to any penalty for failing to comply with a collection of information if it does not display a currently valid OMB control number. **PLEASE DO NOT RETURN YOUR FORM TO THE ABOVE ADDRESS.**

1. REPORT DATE	2. REPORT TYPE	3. DATES COVERED
January 2023	Final	15Sep2018 – 14Sep2022

4. TITLE AND SUBTITLE

Brigatinib and Its Combination with INK-128 as a Novel Treatment for NF2-Deficient Meningiomas

5a. CONTRACT NUMBER
W81XWH-18-1-0547

5b. GRANT NUMBER
0011191673

5c. PROGRAM ELEMENT NUMBER

6. AUTHOR(S)

Long-Sheng Chang, Ph.D.

E-Mail: Long-Sheng.Chang@nationwidechildrens.org

5d. PROJECT NUMBER

5e. TASK NUMBER

5f. WORK UNIT NUMBER

7. PERFORMING ORGANIZATION NAME(S) AND ADDRESS(ES)

Research Institute at Nationwide Children's Hospital
700 Children's Drive
Columbus, OH 43205-2696

8. PERFORMING ORGANIZATION REPORT NUMBER

9. SPONSORING / MONITORING AGENCY NAME(S) AND ADDRESS(ES)

U.S. Army Medical Research and Development Command
Fort Detrick, Maryland 21702-5012

10. SPONSOR/MONITOR'S ACRONYM(S)

11. SPONSOR/MONITOR'S REPORT NUMBER(S)

12. DISTRIBUTION / AVAILABILITY STATEMENT

Approved for Public Release, Distribution Unlimited

13. SUPPLEMENTARY NOTES

14. ABSTRACT

Presently, an FDA-approved medical therapy for *NF2*-deficient meningiomas is not available. To identify a novel therapy for these tumors, we, as members of the Synodos for NF2 Consortium, in collaboration with the National Center for Advancing Translational Sciences (NCATS), identified brigatinib, a potent anaplastic lymphoma kinase (ALK) inhibitor, to be effective as a single agent in inhibiting proliferation of *NF2*-deficient meningioma cells and suppressing tumor growth in an orthotopic *NF2*-deficient meningioma mouse model. Additionally, INK128, a dual mTORC1/2 inhibitor, synergized with brigatinib to suppress meningioma cell proliferation *in vitro*. Based on these data, we have proposed to evaluate the brigatinib/INK128 combination as an effective treatment for *NF2*-deficient meningiomas and investigate their mechanisms of action. We have found that *NF2*-deficient meningiomas did not express ALK. Brigatinib suppressed the growth of *NF2*-deficient tumors via inhibition of multiple receptor tyrosine kinases (RTKs) and non-RTKs, such as focal adhesion kinase (FAK). These findings have led to a phase II clinical trial to evaluate brigatinib in patients with NF2. Also, we have generated a quantifiable, orthotopic, NF2-associated meningioma model using a luciferase-expressing, telomerase-immortalized meningioma cell line AG-NF2-Men-Luc2 derived from a grade-I tumor from an NF2 patient. Using this model and the *NF2*-deficient sporadic meningioma model that we established previously, we showed that combining the dual mTORC1/2 inhibitor INK128 with brigatinib enhanced the anti-tumor effects by eliciting major changes in the expression of genes including the upstream regulators of several signaling networks such as the AKT pathway that are important for meningioma growth. These results suggest that a clinical trial to evaluate the combination of brigatinib with an mTOR inhibitor in NF2 patients with progressive meningiomas is warranted.

15. SUBJECT TERMS

Neurofibromatosis type 2 (NF2), *NF2* gene, *NF2*-deficient, NF2-associated, meningioma, brigatinib, anaplastic lymphoma kinase (ALK), inhibitor, receptor tyrosine kinase (RTK), INK128, mTORC1/2, orthotopic, bioluminescence imaging (BLI)

16. SECURITY CLASSIFICATION OF:			17. LIMITATION OF ABSTRACT	18. NUMBER OF PAGES	19a. NAME OF RESPONSIBLE PERSON
a. REPORT	b. ABSTRACT	c. THIS PAGE			USAMRDC
Unclassified	Unclassified	Unclassified	Unclassified	177	19b. TELEPHONE NUMBER *(include area code)*

TABLE OF CONTENTS

Page

1. Introduction 4
2. Keywords 4
3. Overall Project Summary 4-5
4. Key Research Accomplishments 5-21
5. Impact 21-22
6. Changes/Problems 22
7. Publications, Abstracts, and Presentations 22-26
8. Participants & Other Collaborating Organizations 26
9. Reportable Outcomes 26
10. Other Achievements 26
11. References 27-28
12. Appendices 29-

1. INTRODUCTION

Meningiomas are the most common brain tumors, which originate from the meningothelial cells of the arachnoid layer lining the brain (Ostrom et al., 2018). The majority (~80%) of meningiomas are benign (WHO grade I), whereas the remaining are atypical (grade II) and anaplastic (grade III). Meningiomas can occur spontaneously in the general population or frequently found in patients with neurofibromatosis type 2 (NF2), an autosomal-dominant genetic disorder caused by mutations in the *NF2* tumor suppressor gene (Rouleau et al., 1993; Trofatter et al., 1993). Interestingly, about 50-60% of sporadic meningiomas also harbor *NF2* mutations, suggesting a critical role of *NF2* in tumor development. Surgery and radiation are the current treatment options for meningiomas; however, these treatments could cause severe complications, including seizure, intracranial bleeding, and stroke (Suppiah et al., 2019). As patients with NF2 often develop multiple meningiomas, surgery may not be possible due to too many tumors or the locations that are difficult to operate, such as in the skull base. Incomplete tumor resection is not uncommon and is a main cause of tumor recurrence. In addition, radiation therapy may induce malignant transformation of benign tumors and increase risk for secondary malignancies. Together, these factors underscore the importance of developing effective medical therapies that stop tumor growth or completely eradicate meningiomas. To accelerate drug development for NF2-associated tumors, the Children's Tumor Foundation previously sponsored the establishment of the multi-institutional Synodos for NF2 Consortium aiming to apply system biology to create tools and treatment paradigms for NF2-associated meningiomas and schwannomas (Synodos for NF2 Consortium, 2018). The Synodos for NF2 team, in which we are a member, collaborated with the NIH National Center for Advancing Translational Sciences (NCATS) to conduct high-throughput drug screening of isogenic pairs of *NF2*-deficient and *NF2*-expressing disease-relevant cells to identify actionable drug targets for the treatment of NF2-related tumors. From this screening, several targeted drugs and drug combinations with potent growth-inhibitory activities in NF2 cell panels were identified. Using a noninvasive, quantifiable, orthotopic *NF2*-deficient meningioma animal model, we showed that the FDA-approved, multi-receptor tyrosine kinase (RTK) inhibitor, brigatinib (ALUNBRIG®), caused tumor regression. Together with Dr. Vijaya Ramesh, also a member of the Synodos for NF2 Consortium at Massachusetts General Hospital (MGH), we found that INK128 (TAK228, Sapanisertib, MLN0128), an inhibitor of mTORC1 and mTORC2 which are aberrantly activated in *NF2*-deficient meningiomas, exhibited antitumor effects in the *NF2*-deficient meningioma mouse model (Angus et al., 2018) and synergized with brigatinib to suppress the growth of *NF2*-deficient meningioma cells *in vitro*. Based on these findings, we have proposed to evaluate brigatinib and INK128 as a novel drug combination to treat *NF2*-deficient meningiomas and to investigate its molecular mechanism of action. It is hoped that the results obtained from this study will potentially lead to an effective combination treatment approach for NF2.

2. KEYWORDS

Neurofibromatosis type 2 (NF2), *NF2* gene, *NF2*-deficient, NF2-associated, meningioma, brigatinib, anaplastic lymphoma kinase (ALK), inhibitor, receptor tyrosine kinase (RTK), INK128, mTORC1/2, orthotopic, bioluminescence imaging (BLI)

3. OVERALL PROJECT SUMMARY

Presently, an FDA-approved medical therapy for the treatment of NF2-associated tumors, including meningiomas, is not available. To identify novel targeted therapies, either alone or in combination, for these tumors, we, as members of the Synodos for NF2 Consortium and in collaboration with Dr. Marc Ferrer of the NCATS, conducted high-throughput drug screening of isogenic pairs of *NF2*-deficient and *NF2*-expressing tumor cells and identified brigatinib, an inhibitor of anaplastic lymphoma kinase (ALK) and several other RTKs, to be effective as a single agent in suppressing the growth of *NF2*-deficient meningioma *in vitro* and *in vivo*. In addition, we found that INK128, a dual mTORC1/2 inhibitor, synergizes with brigatinib to inhibit proliferation of *NF2*-deficient meningioma cells *in vitro*. Based on these findings, we propose to further evaluate the brigatinib/INK128 combination as an effective treatment for *NF2*-deficient meningiomas. In addition, we investigate the mechanistic aspects of brigatinib, either alone or in combination with INK128, in *NF2*-null *in vitro* and *in vivo* meningioma models. To achieve this goal, the following two specific aims are proposed:

Aim 1. To evaluate the mechanism by which brigatinib inhibits proliferation of *NF2*-null meningioma

cells and to understand the synergy between brigatinib and INK128 in growth inhibition. Brigatinib was originally designed as a highly selective and potent inhibitor of ALK. It also has activity against ROS1 and other RTKs (Huang et al., 2016; Zhang et al., 2016). We hypothesize that mutation-independent activation of ALK/ROS1 is likely in *NF2*-null meningioma cells. To test this hypothesis, we plan to examine the expression and activation of ALK and ROS1 upon *NF2* loss and addressed whether brigatinib functions in an ALK/ROS1-dependent manner or as an inhibitor of other kinases. Further, we will investigate how brigatinib synergizes with INK128 in growth inhibition by examining the bypass signaling after single and combination treatment with these two drugs.

Aim 2. To determine the anti-tumor activity of the brigatinib and INK128 combination in orthotopic *NF2*-deficient meningioma models. We have found that as a single agent, INK128 also effectively suppresses intracranial Ben-Men-1 meningioma growth in mice (Angus et al., 2018). We hypothesize that combined brigatinib and INK128 treatment restrains activation of bypass signaling pathways, such as the AKT-mTOR pathway, resulting in efficient tumor inhibition. In addition, we plan to evaluate the antitumor effects of the brigatinib/INK128 combination in orthotopic meningioma xenograft mouse models using *NF2*-deficient meningioma cell lines established from sporadic and NF2-associated tumors.

Brigatinib is an FDA-approved drug, and a recent Phase I clinical study of INK128 has demonstrated tolerability and encouraging tumor responses (Ghobrial et al., 2016). Should the proposed brigatinib/INK128 combination demonstrate synergistic anti-tumor efficacy in *NF2*-deficient meningiomas, the results could be quickly translated to human evaluation. Identification of a targeted drug or drug combination that effectively eradicates NF2-related tumors would significantly advance our current approach to NF2 treatment and greatly improve the clinical care and long-term treatment outcomes for patients afflicted by NF2.

4. KEY RESEARCH ACCOMPLISHMENTS:

(i) What were the major goals of the project?

The major **goals** of this project are to evaluate brigatinib and INK128 as a novel drug combination to treat *NF2*-deficient meningiomas and to investigate its molecular mechanism of action, ultimately translating this therapy into the clinic for treating NF2-associated meningiomas.

(ii) What was accomplished under these goals?

Aim 1: To investigate how brigatinib suppressed the growth of *NF2*-deficient meningioma, we first profiled the expression of 28 phosphorylated or activated RTKs (p-RTKs) and 11 downstream signaling nodes in *NF2*-deficient Ben-Men-1 meningioma cells treated with one-IC_{50} dose (50% inhibitory concentration) of brigatinib or dimethyl sulfoxide (DMSO) as the vehicle control under active growth conditions in 10% fetal bovine serum (FBS)-containing medium or in growth-arrested cells stimulated with 20% FBS using the PathScan® RTK Signaling Antibody Array (Cell Signaling Technology). Surprisingly, while brigatinib has been described as a potent ALK inhibitor and is used clinically to treat ALK+ non-small cell lung carcinoma (Huang et al., 2016; Zhang et al., 2016), we did not detect any ALK signal in Ben-Men-1 cells with or without brigatinib treatment under both growth conditions (Figure 1; [Chang et al., 2021]). Western blot analysis confirmed that ALK protein expression was not detected in Ben-Men-1 cells with or without brigatinib treatment, as well as with or without stimulation with various growth factors (Figure 2A). Also, ALK protein was not found in normal meningeal cells, three *NF2*-deficient meningioma cell lines (KT21-MG1, AG-NF2-Men-1, and Ben-Men-1), and four primary meningioma cell cultures with or without *NF2* loss (Figure 3A). Similarly, we did not detect ALK expression in normal Schwann cells, the vestibular schwannoma cell line hVS-16H, primary vestibular schwannoma cell cultures hVS-16S, 12J and 12G (Figure 3B, upper panel), as well as nine schwannoma tumors (Figure 3B lower panel).

In contrast, we observed a broad range of kinases that were active in Ben-Men-1 cells, with similar patterns of activity between logarithmically growing cells and growth-arrested cells stimulated with 20% serum (Figures 1A and 1C). Notably, strong expression of phosphorylated epidermal growth factor receptor (EGFR)-family members, ErbB2 and ErbB3, insulin receptor (INSR), fibroblast growth factor

receptor 1 (FGFR1), tropomyosin receptor kinase A (TRKA), c-Kit, vascular endothelial growth factor receptor 2 (VEGFR2), and several ephrin receptors (EPHs) was observed. Importantly, brigatinib treatment reduced the levels of most, if not all, of these p-RTKs with the most significant reduction in EGFR, ErbB2, ErbB3, VEGFR2, and EPH receptors, particularly in cells treated for 2h. In addition, brigatinib treatment led to attenuation of the downstream signals from these RTKs, including p-AKT(S473 and T308) and p-ERK1/2. The phosphorylation of most of the brigatinib-inhibited RTKs showed some recovery to baseline levels after 24h, although some of their downstream signaling proteins, such as ERK1/2, AKT, and S6, remained markedly suppressed (compare Figures 1A and 1C with Figures 1B and 1D).

Figure. 1. Inhibition of multiple RTKs and non-RTKs in Brigatinib-treated Ben-Men-1 cells grown under various conditions. PathScan® RTK signaling antibody array analysis was conducted using cells grown in 10% FBS and treated with 1x IC50 of brigatinib for 2h (A) and 24 h (B) or in growth-arrested cells stimulated with 20% FBS in the presence of 1x IC50 of brigatinib for 2h (C) and 24 h (D). The numeric table below each pair of arrays displays the fold-change in fluorescence detected for each phospho-protein expressed in cells treated with brigatinib relative to DMSO control after subtraction of the fluorescence in the background control spots (indicated as "-"). Positive control spots are denoted as "+".

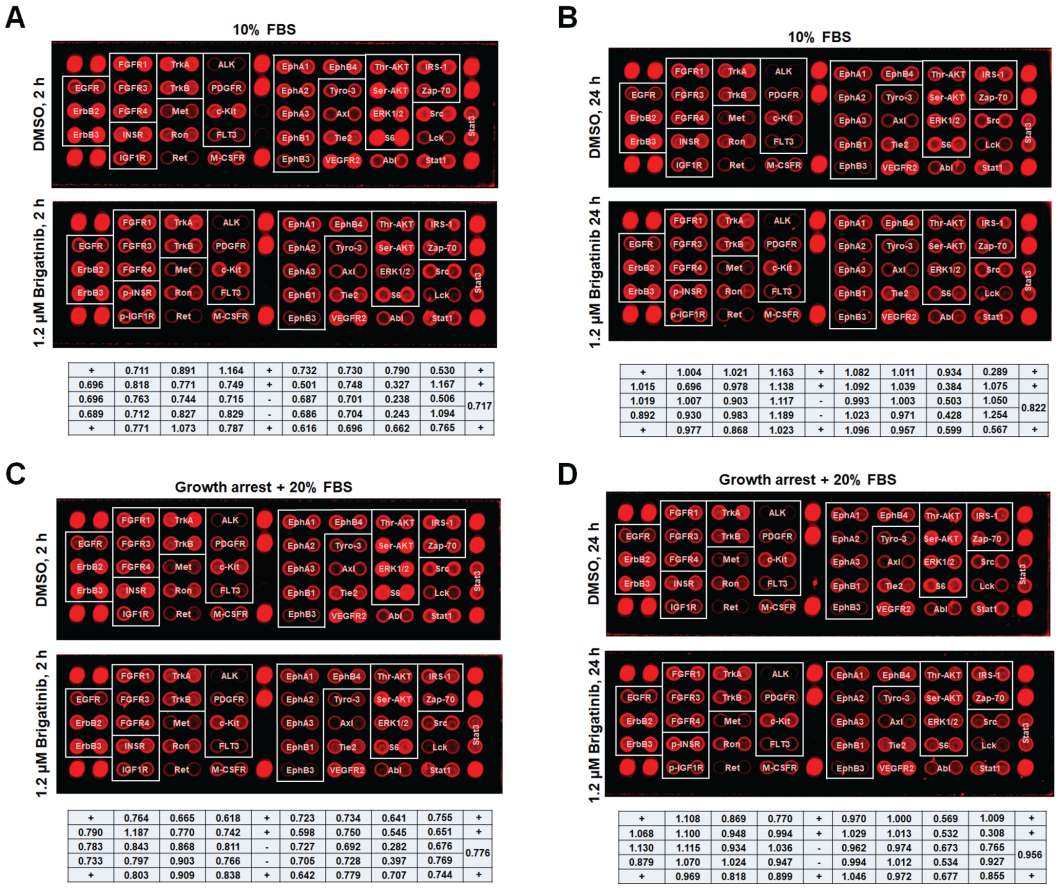

+	0.711	0.891	1.164	+	0.732	0.730	0.790	0.530	+
0.696	0.818	0.771	0.749	+	0.501	0.748	0.327	1.167	+
0.696	0.763	0.744	0.715	-	0.687	0.701	0.238	0.506	0.717
0.689	0.712	0.827	0.829	-	0.686	0.704	0.243	1.094	
+	0.771	1.073	0.787	+	0.616	0.696	0.662	0.765	+

+	1.004	1.021	1.163	+	1.082	1.011	0.934	0.289	+
1.015	0.696	0.978	1.138	+	1.092	1.039	0.384	1.075	+
1.019	1.007	0.903	1.117	-	0.993	1.003	0.503	1.050	0.822
0.892	0.930	0.983	1.189	-	1.023	0.971	0.428	1.254	
+	0.977	0.868	1.023	+	1.096	0.957	0.599	0.567	+

+	0.764	0.665	0.618	+	0.723	0.734	0.641	0.755	+
0.790	1.187	0.770	0.742	+	0.598	0.750	0.545	0.651	+
0.783	0.843	0.868	0.811	-	0.727	0.692	0.282	0.676	0.776
0.733	0.797	0.903	0.766	-	0.705	0.728	0.397	0.769	
+	0.803	0.909	0.838	+	0.642	0.779	0.707	0.744	+

+	1.108	0.869	0.770	+	0.970	1.000	0.569	1.009	+
1.068	1.100	0.948	0.994	+	1.029	1.013	0.532	0.308	+
1.130	1.115	0.934	1.036	-	0.962	0.974	0.673	0.765	0.956
0.879	1.070	1.024	0.947	-	0.994	1.012	0.534	0.927	
+	0.969	0.818	0.899	+	1.046	0.972	0.677	0.855	+

Western blot analysis corroborated that phosphorylation of the non-RTKs focal adhesion kinase (FAK)/PTK2 and Fps/Fes-related kinase (FER) were noticeably reduced in brigatinib-treated Ben-Men-1 cells under active growth conditions in 10% FBS or in growth-arrested cells stimulated with 20% serum (Figure 2B; [Chang et al., 2021]). Similar to p-RTK array analysis, we observed reduced phosphorylation of ErbB3 and EphA2 in brigatinib-treated cells. Also, the downstream signaling nodes of these RTKs, including ERK1/2, AKT, and S6, were all markedly decreased. However, under the same growth conditions, the basal levels of p-EGFR were minimally detectable and were lost following brigatinib treatment, particularly after 24h (Figure 4). Additionally, we did not detect p-IGF1R under these growth conditions (data not shown). Therefore, we investigated the effects of brigatinib in ligand-induced activation of insulin-like growth factor 1 receptor (IGF1R), EGFR, and ErbB3 in Ben-Men-1 cells. Upon each cognate ligand stimulation, p-EGFR, p-ErbB3, and p-IGF1R were readily detected in Ben-Men-1 cells, and brigatinib treatment abrogated their phosphorylation (Figure 2C).

Figure 2. Brigatinib inhibits multiple RTKs, non-RTKs, and their downstream signals. (A) Western blot analysis was conducted to detect ALK expression in Ben-Men-1 cells grown under various growth conditions and with or without brigatinib treatment. (B) Brigatinib treatment greatly reduced phosphorylation of non-RTKs FER and FAK, RTKs EPHA2 and ErbB3, and their downstream signaling molecules AKT, ERK1/2, and S6 in active growing Ben-Men-1 cells or growth-arrested cells stimulated with 20% serum. (C) Brigatinib blocked phosphorylation of EGFR, ErbB3, and IGF1R in growth-arrested Ben-Men-1 cells stimulated with each cognate ligand.

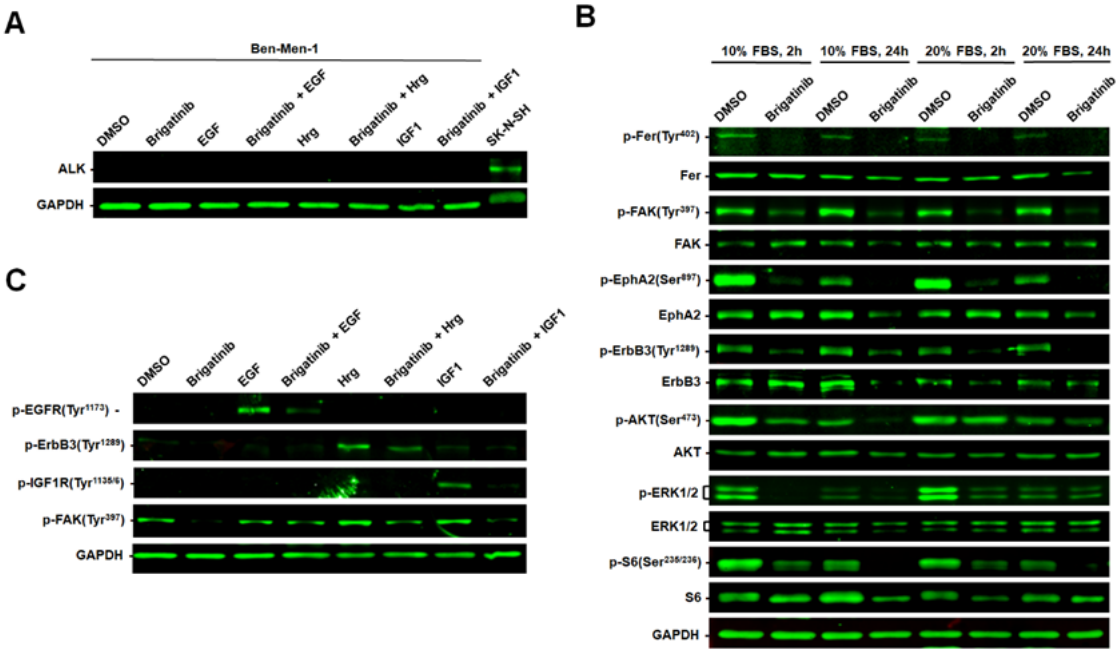

Figure 3. Meningioma and schwannoma cells do not express ALK. (A) ALK was not detected meningioma cells with or without *NF2* expression as well schwannoma cells and tumors. Equal amounts of protein lysates from three human meningioma cell lines (KT21-MG1-Luc, AG-NF2-Men, and Ben-Men-1), normal meningeal cells, and four primary meningioma cultures (hMen-10A, hMen-10B, hMen-12Ao, hMen-12B) were used in Western blot analysis to probe ALK and merlin expression. SK-N-SH neuroblastoma cells, which express ALK, were used as a positive control. (B) **ALK expression was not detected in Schwann and schwannoma cells.** Western blotting was performed to detect ALK expression in human Schwann cells, four primary vestibular schwannoma cultures (hVS-16H, hVS-16S, hVS-12J, hVS-12Ga), SK-N-SH neuroblastoma cells and nine vestibular schwannomas (VS). Tubulin or GAPDH was used as a loading control.

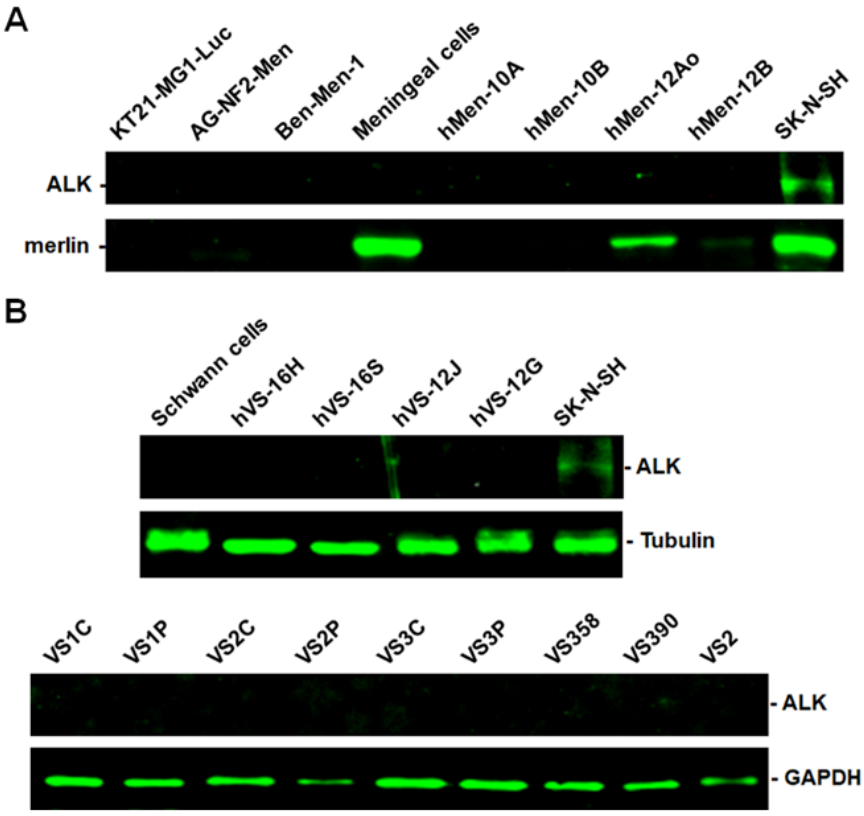

Figure 4. Ben-Men-1 cells expressed low levels of p-EGFR, which was abolished by brigatinib treatment. Western blot analysis revealed that while phosphorylated EGFR was robustly induced in EGF-stimulated Ben-Men-1 cells, only very low levels of p-EGFR were detected in actively-growing cells or growth-arrested cells stimulated with 20% serum for 24h. Brigatinib treatment diminished p-EGFR expression.

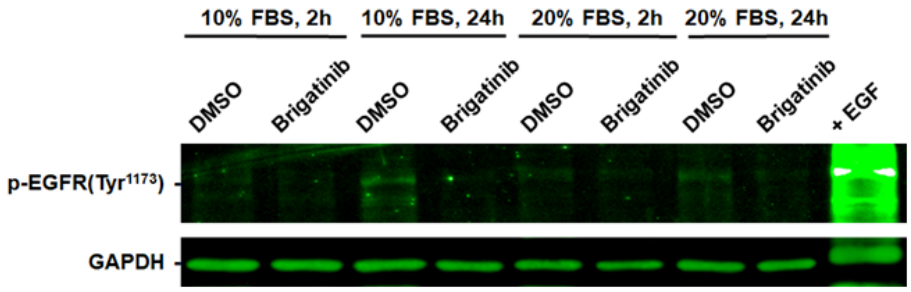

It should be mentioned that while brigatinib has been described as a potent ALK inhibitor, it also has multiple other kinase targets as well (Huang et al., 2016). Using multiplexed kinase inhibitor beads and mass spectrometry (MIB/MS), Dr. Gary Johnson's group at the University of North Carolina, together with other Synodos for NF2 members, conducted kinome profiling in isogenic NF2-related cell panels with or without brigatinib treatment. The MIBs are designed to bind kinases when they are in the "Asp-Phe-Gly (DFG)-in" (active) conformation. Kinases inhibited by brigatinib would not be bound by MIBs, while those bound are subsequently identified via MS (Duncan et al., 2012). Consistent with the RTK Signaling Antibody Array and Western blot studies that we conducted (Figures 1-4), the kinome analysis also did not detected any ALK or its related ROS1 in both merlin-expressing and merlin-null arachnoidal cells, as well as *NF2*-deficient Ben-Men-1 meningioma cells (Chang et al., 2021). Further, transcriptome analysis conducted by Dr. James Gusella and Dr. Vijaya Ramesh of Massachusetts General Hospital, also members of the Synodos for NF2 Consortium, confirmed the lack of expression of both *ALK* and *ROS1* in these cells. These results indicate that inhibition of meningioma cell proliferation by brigatinib is not ALK or ROS1-dependent. Therefore, we did not conduct the CRISPR experiment to knockout ALK or ROS1 as they do not express in meningioma cells. However, consistent with our PathScan® RTK Signaling Antibody Array and Western blot analyses (Figures 1, 2, and 4), the kinome profiling identifies the loss of MIB binding to several non-RTKs, including FER and PTK2/FAK, in brigatinib-treated cells (Chang et al., 2021). In addition, inhibition of EPHA2, which we previously showed increased expression and activation of this RTK in *NF2*-deficient cells (Angus et al., 2018), was detected in brigatinib-treated cells (Figure 2B; Chang et al., 2021). Collectively, these results suggest that the anti-tumor activity of brigatinib in *NF2*-deficient meningioma cells is mediated through blockade of multiple RTKs and non-RTKs, but not ALK or ROS1.

It should be mentioned that Wade Clapp of Indiana University, one of the leading members of the Synodos for NF2 Consortium, also demonstrated anti-tumor activity of brigatinib in a genetically engineered mouse model for NF2-associated schwannoma (Chang et al., 2021). Taken together, the results indicate that brigatinib possessed potent anti-tumor activity against both *NF2*-deficient meningioma and schwannoma via inhibition of multiple RTKs frequently activated in these tumors, but not ALK, as well as blockade of several non-RTKs, such as FAK, which has previously been recognized as an oncoprotein in NF2-related tumors (Ammoun and Hanemann, 2011; Blakeley and Plotkin, 2016). Based on these findings, the CTF, in collaboration with the brigatinib manufacturer Takeda Pharmaceutical Company, has launched a multi-site, phase II clinical trial to evaluate the efficacy of brigatinib in patients with NF2 with associated progressive tumors of vestibular schwannomas, non-vestibular schwannomas, meningiomas, and ependymomas (Innovative Trial for Understanding the Impact of Targeted Therapies in NF2 [INTUITT-NF2]; ClinicalTrials.gov Identifier: NCT04374305; Principal Investigator: Scott R Plotkin, MD, PhD, Massachusetts General Hospital).

Aim 2: To examine the growth inhibitory synergy of the brigatinib and INK128 combination, we collaborated with Vijaya Ramesh (Co-Investigator) and showed that brigatinib synergized with INK128 and another dual mTORC1/2 inhibitor, AZD2014, in inhibiting proliferation of *NF2*-deficient primary meningioma cells (Figures 5A and 5B). Interestingly, meningioma cells exhibited increased sensitivity to INK128 inhibition (>10-fold reduction in IC_{50}), compared to AZD2014, indicating that INK128 is more potent (Figure 5C). In addition, the growth-inhibitory synergy was detected in two primary *NF2*-null

meningioma cell cultures (Figure 6A) and the *NF2*-deficient Ben-Men-1 cell line (Figure 6B) treated with the brigatinib and INK128 combination, particularly at higher concentrations of brigatinib.

Figure 5. Combined treatment with Brigatinib and a dual mTORC1/2 inhibitor resulted in synergistic growth inhibition . Drug synergism experiments using the standard 6x6 dose matrix screen method were carried out for *NF2*-deficient primary meningioma cells treated with a combination of AZD2014 and Brigatinib (A) or INK128 and Brigatinib (B) for 72hr. Isobolograms were generated using Chalice Analyzer (Horizon CombinitoRx; http://chalice.horizondiscovery.com/analyzer-server/cwr/analyze.jsp) and show synergism, defined as combination index (CI) <1 (blue plot), compared to Loewe Additivity model (CI=1, red plot). (C) As a representative, single drug dose response curves generated reveal increased sensitivity of meningioma cells to INK128 (decreased IC_{50} dose) compared to AZD2014, defined by the shift of IC_{50} curve to the left (red arrow). The IC_{50} value for each drug is shown in the key.

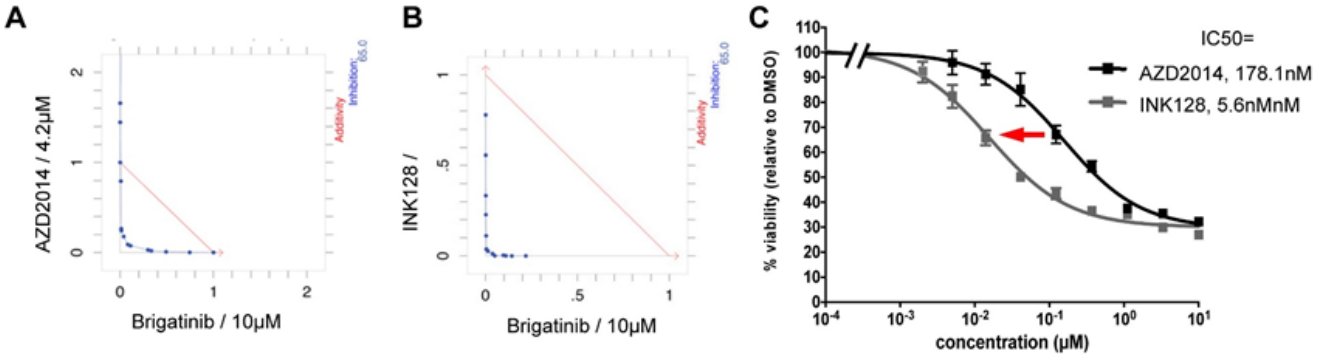

Figure 6. The Brigatinib and INK128 combination exhibits moderate synergy in growth inhibition of meningioma cells. (A) Two *NF2*-null primary meningioma cells were treated with 3-fold serial dilutions of each drug (0.002~10µM) or drug combination for 72 hrs. Cell viability was determined using CellTiterGlo (Promega). All assays were performed in triplicate and controls included wells incubated with vehicle (0.1% DMSO) or medium alone. The dose response curve for each drug was generated and plotted as % relative to DMSO-treated controls with the IC_{50} value shown in the key. Combination drug heatmaps were generated on a colorimetric scale using Combenefit software, which calculates the drug interaction effects (relative to DMSO controls). (B) *NF2*$^{-/-}$ Ben-Men-1 cells were treated with 2-fold serial dilutions of each drug (0.08~5µM) or drug combination for 72 hrs. Cell proliferation was assayed with resazurin (Sigma). The dose response curve for each drug and combination drug heatmaps were also generated using Combenefit software.

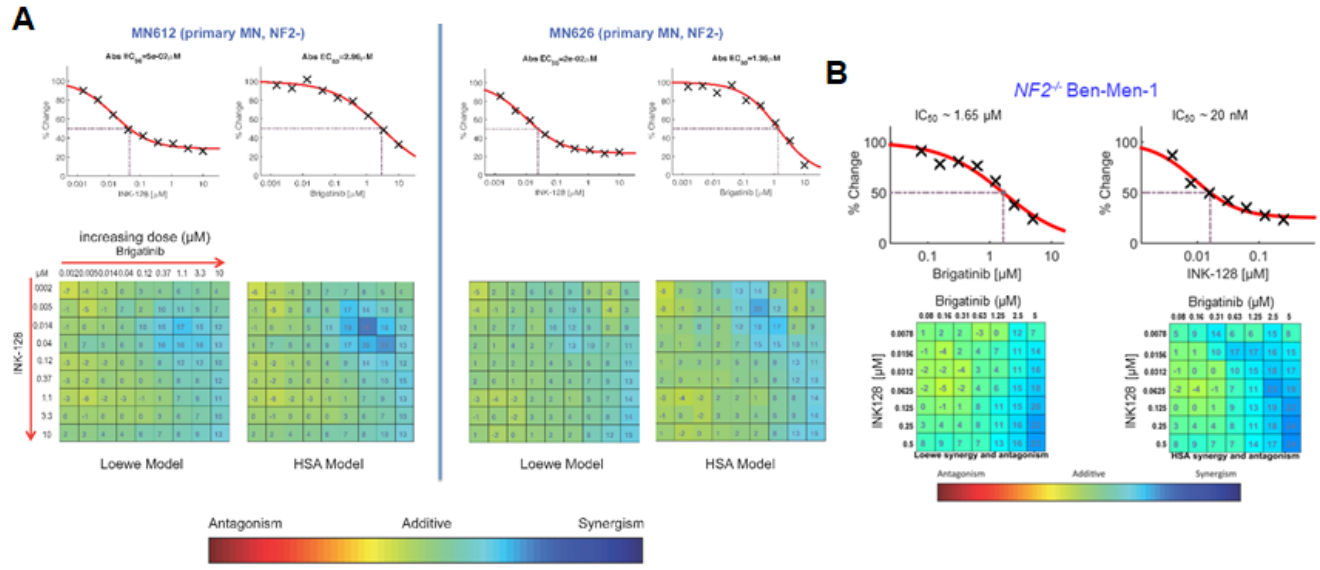

To determine the anti-tumor activity of the brigatinib and INK128 combination in orthotopic *NF2*-deficient meningioma models, we worked with the Human Research Protection Office (HRPO) of the US Army Medical Research and Materiel Command (USAMRMC) Office of Research Protections (OPR) and received approval for our Institutional Review Board (IRB)-approved Human Subjects protocol using established human cell lines. Also, we submitted ACURO Animal Use Appendix for Research Involving Animals to the Animal Care and Use Review Office (ACURO) and received

approval for our Institutional Animal Care and Use Committee (IACUC)-approved animal protocol. With these approvals, we first examined the anti-tumor effects of brigatinib, INK128, and their combination in the orthotopic *NF2*-deficient meningioma model. The maximal tolerable doses (MTDs) for brigatinib and INK128 were found to be 50 mg/kg/day of brigatinib (formulated in 90% polyethylene glycol and 10% 1-methyl-2-pyrrolidinone) and 0.75 mg/mg/kg/day of INK128 (dissolved in 5% 1-methyl-2-pyrrolidinone, 15% polyvinylpyrrolidone, and 80% water), either alone or in combination, in immunodeficient NSG (*NOD.Cg-Prkdc*^{scid} *Il2rg*^{tm1Wjl}*/SzJ*) mice. By stereotactically injecting luciferase-expressing Ben-Men-1-LucB meningioma cells into the skull base of NSG mice and monitoring tumor growth by bioluminescence imaging (BLI) (Burns et al., 2013), mice bearing established Ben-Men-1-LucB tumors, as defined by an increase in BL signal over at least two time points, were randomized into four treatment groups and treated with brigatinib, INK128, or their combination at the MTDs, or vehicle. BLI showed that vehicle-treated tumors grew steadily over time (Figure 7). Similar to our previous findings, brigatinib alone effectively blocked meningioma growth with slight tumor shrinkage over the 6-week treatment period. INK128 alone also blocked meningioma growth at the first two weeks, and treated tumors showed slight growth after four weeks. Nevertheless, treatment with INK128 for six weeks resulted in 85% reduction in tumor-emitted luminescence, compared to the vehicle control. Combined treatment with brigatinib and INK128 effectively shrank meningiomas over six weeks with a trend of more tumor shrinkage than brigatinib treatment alone, but not statistically significant.

Figure 7. Anti-tumor efficacy of Brigatinib and INK128, alone or in combination, in the *NF2*-deficient Ben-Men-1-LucB meningioma mouse model. Mice with established meningioma xenografts were treated with vehicle, Brigatinib, INK128, or Brigatinib+INK128 by oral gavage and tumor growth was monitored by BLI as previously described (Burns et al., 2013). The relative tumor-emitted BL signals were quantified and denoted as % of total flux after treatment relative to the total flux prior to treatment designated as one (100%). The data are shown as mean ± standard error.

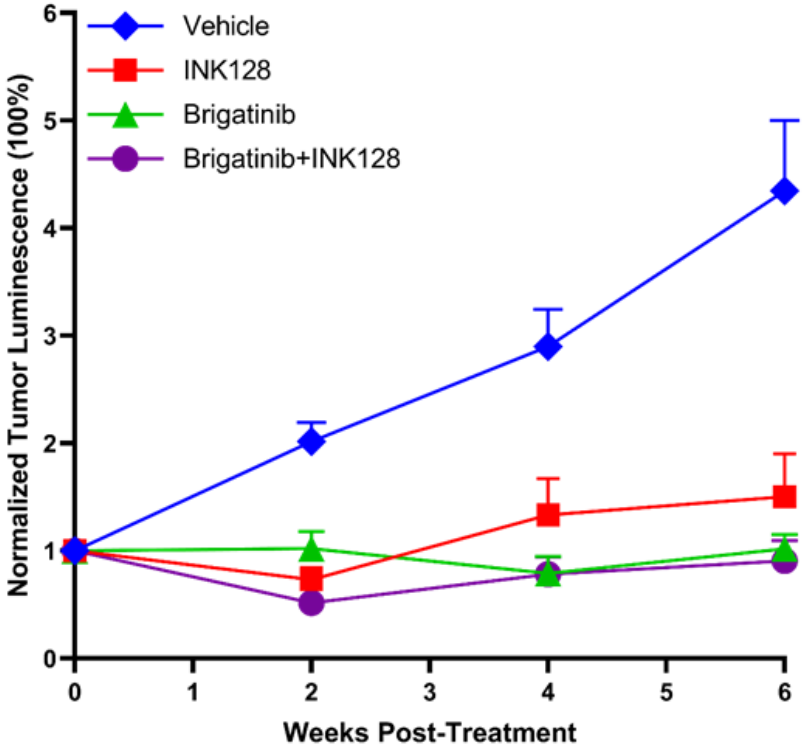

As brigatinib also decreased the growth of schwannoma-bearing dorsal root ganglion in *Postn-Cre*;*Nf2*$^{flox/flox}$ mice (Chang et al., 2021), we examined whether brigatinib alone and its combination with INK128 showed anti-tumor effects in malignant schwannomas, such as malignant peripheral nerve sheath tumors (MPNSTs). Brigatinib or INK128 alone had growth-inhibitory activity against MPNST cells, and combining brigatinib with INK128 further enhanced growth inhibition (Figure 8). Western blot analysis revealed that brigatinib, when combined with INK128, resulted in superior suppression of phosphorylated RTK p-IGF-1R, non-RTK p-FAK, and their downstream targets p-AKT, p-ERK1/2, and p-S6 in MPNST cells, compared with each individual drug (Figure 9).

Figure 8. The Brigatinib and INK128 combination exhibits enhanced growth inhibition in MPNST cells. *NF1*-deficient ST8814 (A) and *NF1*-expressing STS26T (B) cells were treated with 2-fold serial dilutions of each drug or drug combination for 72 hrs. Cell proliferation was assessed with resazurin assays. All assays were performed in triplicate and controls included wells incubated with vehicle (0.1% DMSO) or medium alone. The dose response curve for each drug was generated and plotted as % relative to DMSO-treated controls with the IC_{50} value shown in the key. Combination drug heatmaps were generated on a colorimetric scale using Combenefit software, which calculates the drug interaction effects (relative to DMSO controls),

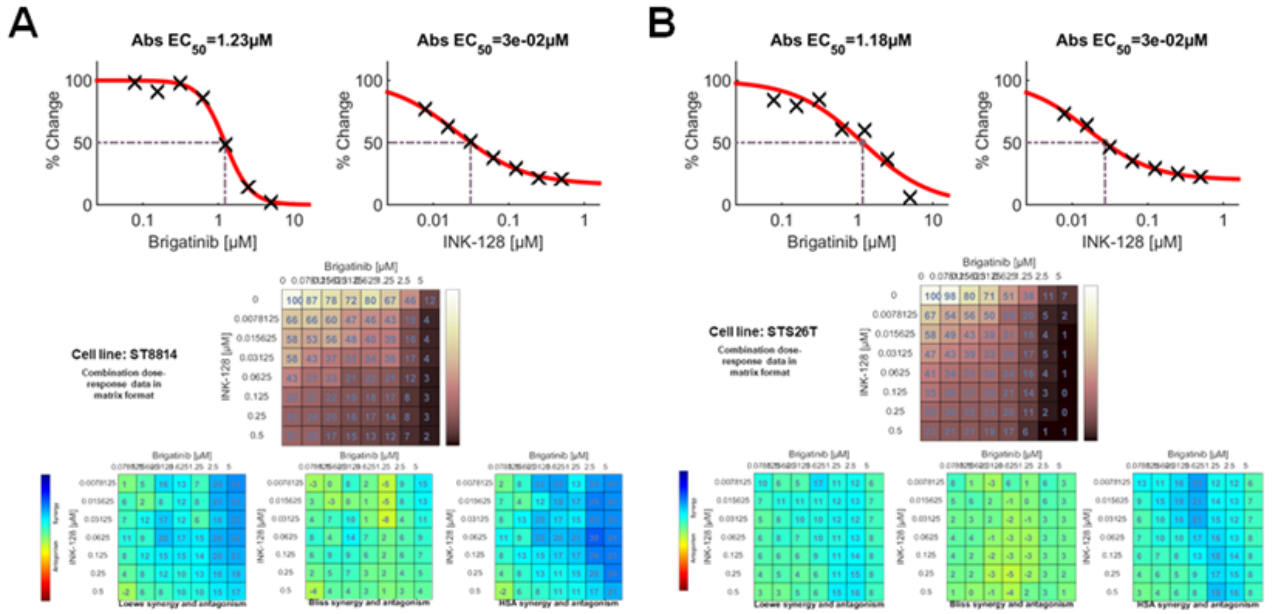

Figure 9. Combined Brigatinib and INK-128 treatment in MPNST cells resulted in superior suppression of RTKs, non-RTKs, and their downstream AKT and ERKs. (A) ST8814 cells were growth arrested over night and then stimulated with each indicated growth factor in the presence or absence or Brigatinib, INK128, or their combination, followed by Western blot analysis. The combined Brigatinib and INK128 treatment more effectively reduced phosphorylation of RTKs, such as IGF-1R, and their downstream signaling molecules AKT, ERK1/2, and S6 in growth factor-stimulated cells. (B) ST8814 cells were treated with vehicle (0.1% DMSO), Brigatinib, INK128, or Brigatinb+INK128 for various indicated times. Treated cells were lysed and equal amounts of protein lysates were Western blotted . The Brigatinib and INK128 combination greatly reduced phosphorylation of non-RTK FAK and their downstream signaling molecules AKT, ERK1/2, and S6 in actively growing ST8814 cells.

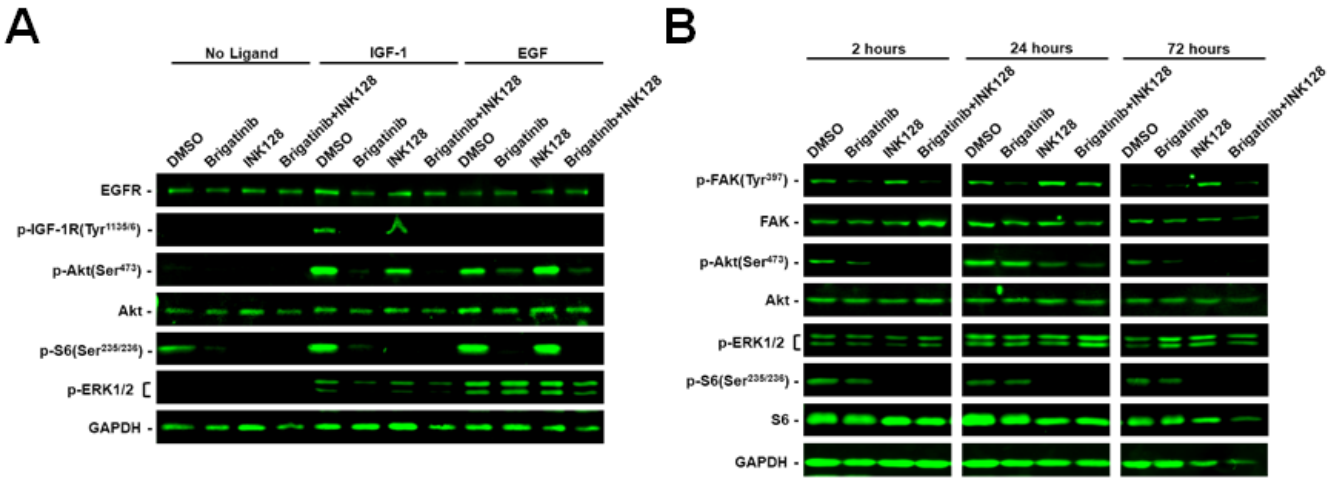

Next, we evaluated the *in vivo* efficacy of brigatinib, INK128, and their combination using a patient-derived xenograft (PDX) model of MPNST. Mice bearing growing MPNST PDXs were treated with brigatinib, INK128, or their combination at the MTDs, or vehicle, and tumor volumes were measured twice a week. As expected, vehicle-treated tumors grew ~13-fold larger in tumor volume after 28 days (Figure 10). Brigatinib alone suppressed the growth of MPNST PDXs by an average of 82% compared

with the vehicle control group over four weeks of treatment, while INK128 alone only modestly inhibited tumor growth by ~32%. Combined treatment with brigatinib and INK128 gave rise to a slightly stronger suppression of tumor growth (by ~86% over four weeks) than brigatinib alone.

Figure 10. Anti-tumor efficacy of Brigatinib and INK128, alone or in combination, in an MPNST PDX model. Mice with growing MPNST PDXs reaching ~100-200 mm^3 were treated with vehicle, Brigatinib, INK128, or Brigatinib+INK128 by oral gavage. Tumor diameters were measured twice weekly, and volumes calculated according to Chang et al. (2020). The normalized tumor volume, denoted as the ratio of the calculated tumor volume after treatment relative to the volume prior to treatment designated as one, was plotted as the mean tumor volume of the entire treatment group at each time point with standard error.

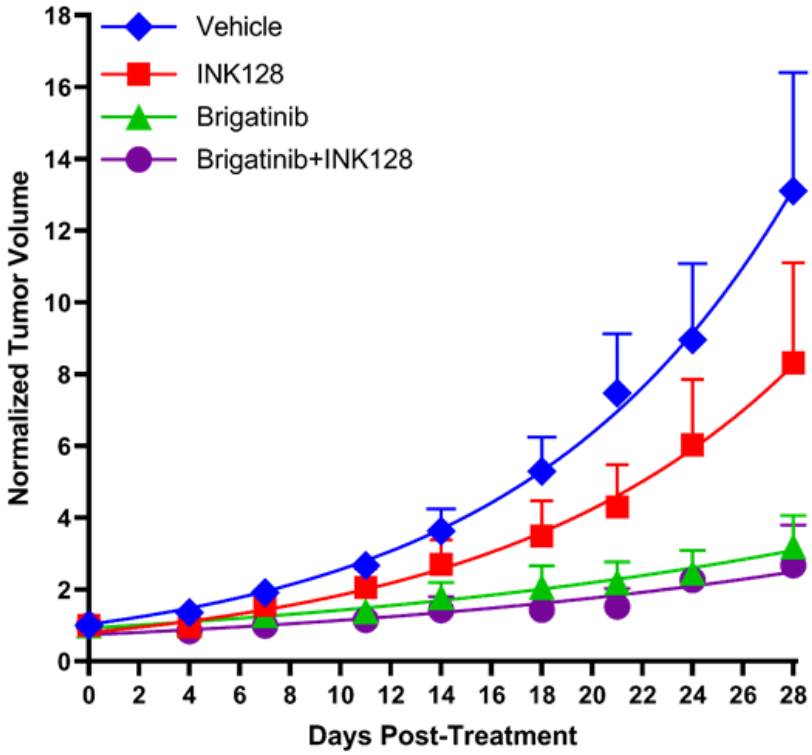

To compare the anti-tumor activity of brigatinib, INK128, and their combination in NF2-associated meningioma, we generated a meningioma cell line from a grade I tumor obtained from an NF2 patient by telomerase immortalization. This NF2-associated meningioma cell line, designated as AG-NF2-Men-1, retained many characteristics of the original tumor. Morphologically it looks fibroblastic (Figure 11A) and is slow growing in culture, relative to malignant cancer cell lines. AG-NF2-Men-1 cells expressed several meningioma markers, including desmoplakin and vimentin (Figures 11B and 11C), but not the *NF2*/merlin protein, indicating that they are *NF2*-null (Figure 11B). Like Ben-Men-1 cells, AG-NF2-Men-1 cells also expressed several RTKs, such as EGFR, ErbB3, and IGF-1R, and responded to their cognate ligands (Figure 12A). Interestingly, these *NF2*-deficient meningioma cells, including AG-NF2-Men-1, expressed EZH2, the catalytic subunit of the polycomb-repressive complex 2 (PRC2), at higher levels, compared to normal meningeal cells (Figure 12B). These results suggest possible changes in epigenetic regulation during meningioma tumorigenesis.

Figure 11. Generation of the telomerase-immortalized meningioma cell line AG-NF2-Men from a grade I tumor obtained from an NF2 patient. (A) The morphology of AG-NF2-Men cells in culture, exhibiting a spider web-like growth pattern. (B) Western blot analysis confirmed that like Ben-Men-1 meningioma cells, which was established from a sporadic grade I tumor (Püttmann et al., 2005), AG-NF2-Men cells did not express merlin, the NF2 gene product. In contrast, normal meningeal cells (MC) and HeLa cervical carcinoma cells readily express merlin. Also, the merlin protein was not detected in primary Men-10A meningioma cells prepared from a sporadic grade I meningioma. Desmoplakin, a component of desmosomes previously reported to be expressed in meningioma cells, was detected in AG-NF2-Men, Ben-Men-1, MC, and primary Men-10A cells. (C) Immunofluorescence staining confirmed that AG-NF2-Men cells also expressed vimentin, a marker commonly found in meningiomas.

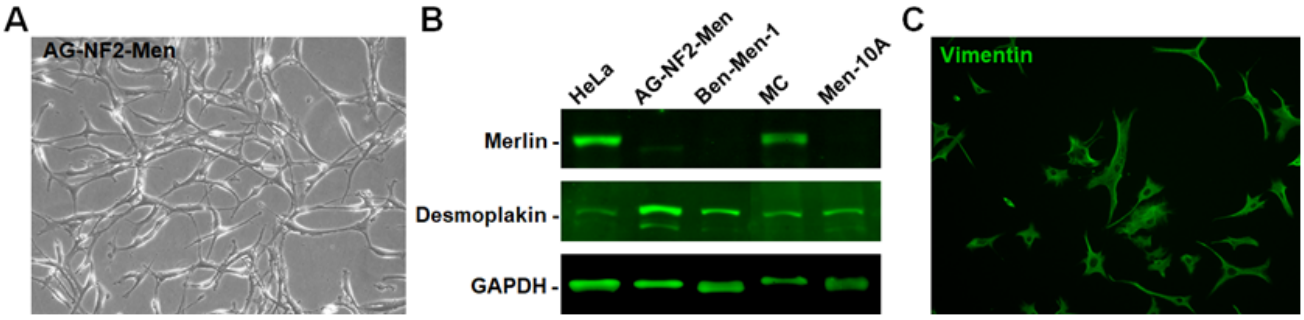

Figure 12. AG-NF2-Men-1 cells express several RTKs, such as EGFR, ErbB3, and IGF-1R, and EZH2, the catalytic subunit of the polycomb repressive complex 2 (PRC2), like Ben-Men-1 cells. (A) Western blot analysis confirmed that AG-NF2-Men-1, Ben-Men-1, and MEN-12Ao meningioma cells expressed the growth factor receptors EGFR, ErbB3, and IGF-1R and responded robustly to their cognate ligands. (B) These *NF2*-deficient meningioma cells also expressed higher levels of EZH2 than normal meningeal cells (MC).

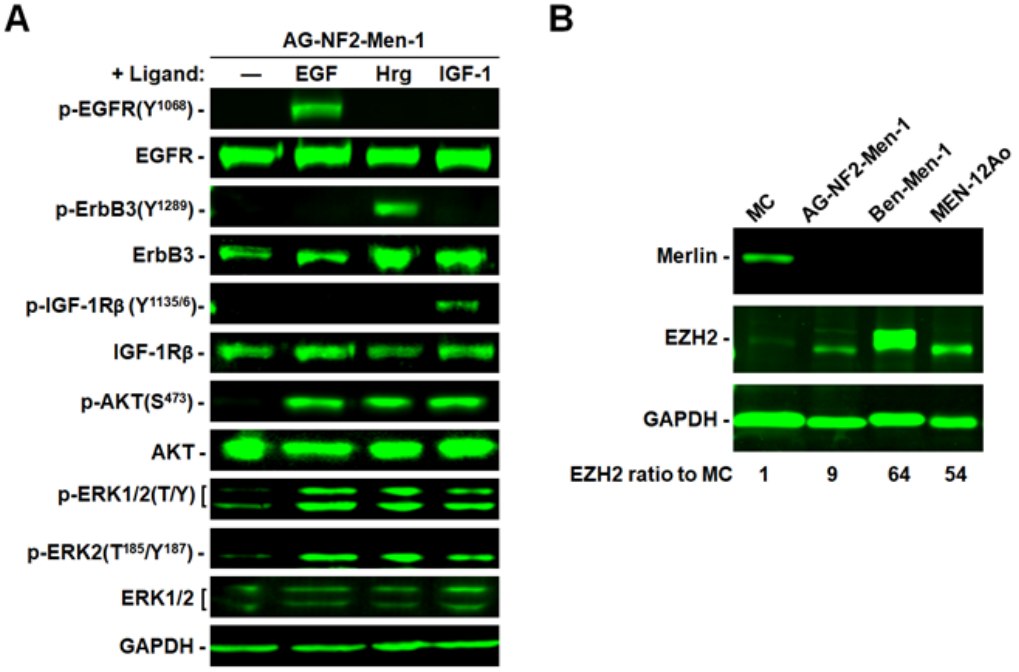

We next determined whether brigatinib and INK128 could elicit growth inhibition in AG-NF2-Men-1 cells. Similar to those detected in Ben-Men-1 cells (Figure 6), brigatinib and INK128 showed the IC_{50} concentrations of 1.1 μM and 20 nM, respectively, in AG-NF2-Men-1 cells (Figure 13A). Due to the slower growth rate of AG-NF2-Men-1 cells, the enhanced growth inhibitory activity of the brigatinib+INK128 combination was evaluated by counting treated AG-NF2-Men-1 cells over time to establish a growth curve. Using this method, we verified that brigatinib or INK128 alone reduced the growth rate of AG-NF2-Men-1 cells. Interestingly, the combined brigatinib+INK128 treatment further reduced the growth of AG-NF2-Men-1 cells with their proliferation almost completely abrogated (Figure 13B).

Figure 13. The brigatinib+INK128 combination treatment exhibited enhanced antiproliferative activity in AG-NF2-Men-1 cells. (A) Dose-response curves for AG-NF2-Men-1 cells treated for 3 days with serial drug dilutions established a mean IC_{50} of 1100 nM for brigatinib and 20 nM for INK128. (B) AG-NF2-Men-1 cells were treated for up to 14 days with DMSO vehicle or 1x IC_{50} doses of brigatinib or INK128 as single agents or in combination. Cells were harvested in technical duplicates and counted on a hemocytometer. Graphs depict means ± SEM for at least two independent experiments.

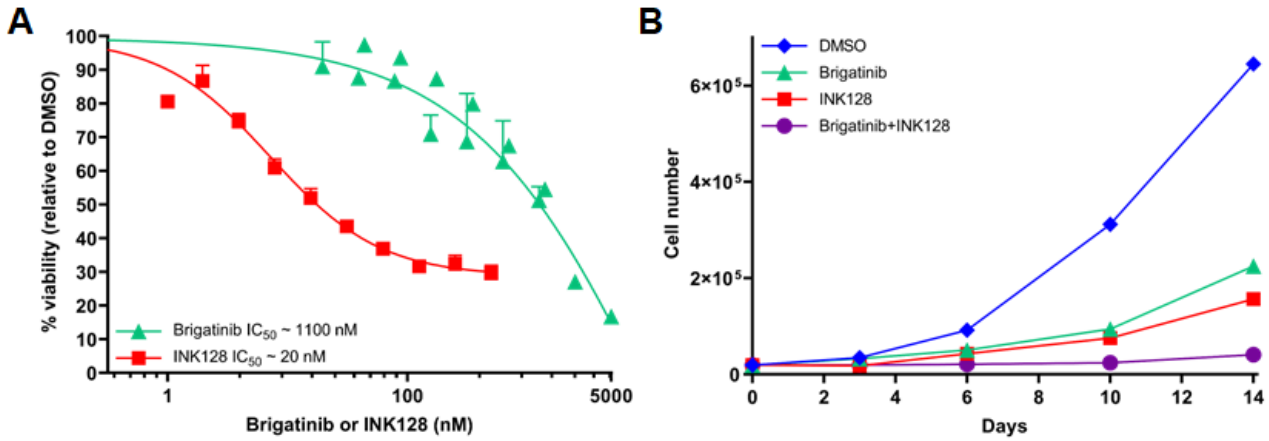

Western blot analysis showed that single-agent brigatinib decreased p-AKT on both S473 and T308 in AG-NF2-Men-1 cells (Figure 14). In contrast, 1-day of INK128 monotherapy reduced p-AKT only on S473, and this effect was transient as the p-AKT(S473) level almost returned to the control level by 3 days. Additionally, INK128 alone slightly increased p-AKT(T308) after 1 day of treatment, and the p-AKT(T308) level was greatly increased by 3 days, suggesting activation of feedback signaling and re-phosphorylation of AKT. Also, INK128 reduced p-4EBP1(S65), indicating that it enhances 4EBP1-mediated repression of protein translation. Importantly, the combined brigatinib+INK128 treatment not only decreased p-AKT(S473) more than either drug alone, but also completely prevented INK128-mediated re-phosphorylation of AKT on T308. While the combined brigatinib and INK128 treatment was as effective, if not more, at reducing p-4EBP1(S65) phosphorylation as INK128 alone, AG-NF2-Men-1 cells treated for 3 days with the brigatinib+INK128 combination had a greater proportion of 4EBP1 as faster-migrating, hypophosphorylated isoforms. Collectively, these results suggest that combining brigatinib with INK128 is more effective than INK128 at suppressing phosphorylation of 4EBP1 at multiple sites.

Figure 14. The brigatinib+INK128 combination elicits a superior and more durable suppression of the AKT pathway, compared to single drugs. AG-NF2-Men-1 cells were treated for 1 and 3 days with DMSO vehicle or 1x IC_{50} dose of brigatinib or INK128 as single agents or in combination. Treated cell lysates were subjected to Western blot analysis. While brigatinib alone decreased p-AKT on both S473 and T308, INK128 monotherapy only reduced p-AKT on S473 by one day, and the p-AKT(S473) level almost returned to the baseline after 3-day treatment. While INK128 alone also reduced the p-AKT(S473) level, it slightly increased p-AKT(T308) after 1 day of treatment. This p-AKT(T308) remained considerably elevated after treatment for 3 days, suggesting feedback reactivation. Importantly, the brigatinib+INK128 combination not only decreased p-AKT(S473) better than either drug alone, but also completely abolished this p-AKT(T308) reactivation.

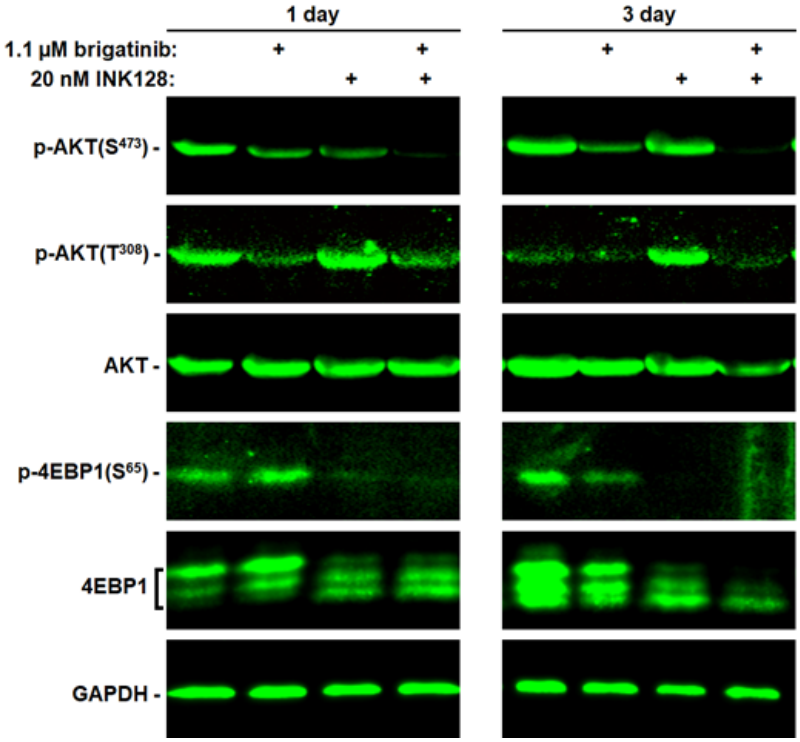

To further investigate the mechanism underlying the enhanced antiproliferative effects of the brigatinib+INK128 combination, we performed RNA sequencing and transcriptomic analyses on AG-NF-Men-1 cells treated for one day with 1x IC_{50} doses of brigatinib, INK128, or their combination. Differential gene analysis revealed that the single-agent treatments modestly affected gene expression patterns. However, the brigatinib+INK128 treatment resulted in an exceptionally large number of differentially expressed genes (DEG) (Figure 15). Among the top 50 protein-coding DEG, the brigatinib+INK128 treatment decreased transcripts encoding proteins important for DNA synthesis and cell cycle progression (e.g., *MCM10*, *CCNE2*, *CCND1*). Qiagen Ingenuity Pathway Analysis using the upstream regulator module revealed that 1-day of brigatinib or INK128 treatment was associated a trend toward inhibition of their target kinases (Table 1), although at this early timepoint, these effects did not reach full significance (absolute z-score ≥2). Critically, the combined brigatinib+INK128 treatment was associated with significant inhibition of multiple target upstream regulators, including growth factors/ligands (EGF, NRG1/Hrg), RTKs (EGFR, ErbB3), and downstream signaling pathways (mTOR, AKT, MEK1). Additionally, the combination treatment also inhibited upstream regulators involved with protein translation (eIF4E, eIF4G1), the Hippo pathway (YAP1, TAZ), and transcription (MYC). One of the upstream regulators predicted to be active is LATS1, a suppressor of the Hippo pathway. Additionally, FOXO3 and ATF4, transcription factors associated with apoptosis and cell stress responses, are predicted to be activated. Also scored as being activated were EIF2AK3 and EIF2AK4, proteins associated with the endoplasmic reticulum stress response and suppression of protein translation initiation. Intriguingly, our analysis also predicted activation of the SWI/SNF complex subunits ARID1A and SMARCA4 (BRG1). This chromatin remodeling complex is a well-known antagonist of PRC2, and we found that the z-scores for PRC2 subunits EZH2 and SUZ12 suggested a trend toward inhibition. These results suggest that the brigatinib+INK128 combination elicits major changes in the expression of genes including the upstream regulators of several signaling networks that are important for meningioma growth.

Figure 15. Differential gene analysis of treated AG-NF2-Men-1 cells reveals that the brigatinib+INK128 combination more significantly impacts gene expression than single-agent brigatinib or INK128. Volcano plots showing the $-\log_{10}$(P) versus the $\log_2$ fold-change of differentially expressed protein-coding genes in cells after one day of treatment with 1x-IC_{50} concentrations of brigatinib (left), INK128 (middle), and the brigatinib+INK128 combination (right). Colored dots represent transcripts with $\log_2$ fold-changes of -1 (blue, decreased) or +1 (red, increased). The top 50 most significantly affected transcripts are labelled. P-values are calculated from three technical replicates.

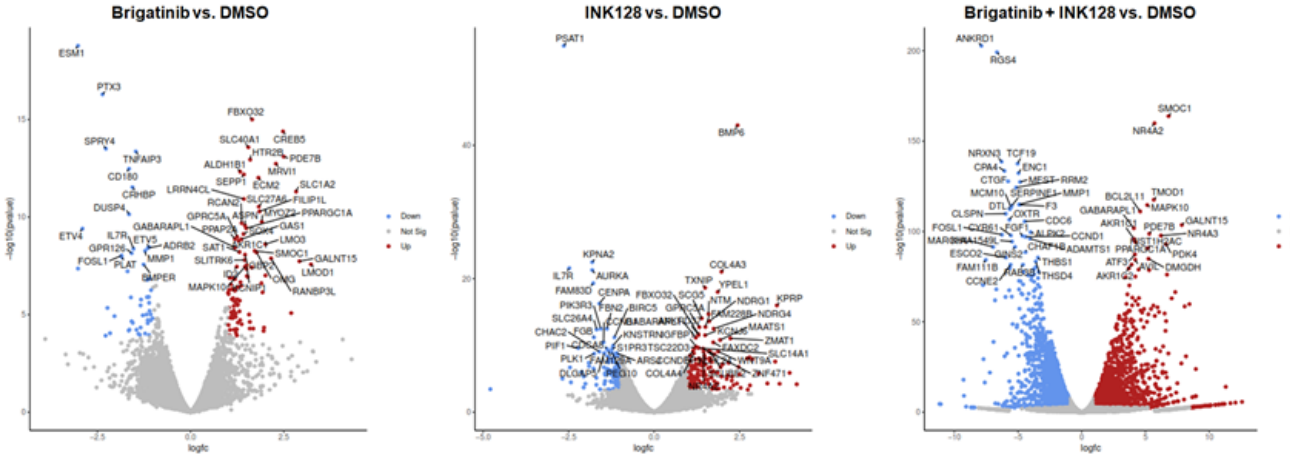

Table 1. Qiagen Ingenuity pathway analysis of upstream regulators affected by the brigatinib and INK128 combination treatment of AG-NF2-Men cells. The activation z-score is a statistical measure indicating the predicted activation state of the listed upstream regulator (negative = inhibited; positive = activated) with an absolute value of 2 being considered significant. Z-scores between 0 and 2 and 0 and -2 are considered to trend towards being activated or inhibited, respectively. Green shading indicates upstream regulators predicted to be activated and red shading for predicted inhibited upstream regulators. Dashes indicate that the drug treatment did not significantly affect the upstream regulators. The P-value of overlap is a statistical measure based on significant overlap between changes in dataset genes and known targets regulated by the listed upstream regulators.

Upstream regulator	Drug	Direction	Activation z-score	P-Value of overlap
Growth factor ligands				
Insulin/IGF family				
IGF1	Brigatinib+INK128	Trend down	-1.377	2.32E-17
IGF1	Brigatinib	Trend down	-0.259	3.60E-03
IGF1	INK128	Trend down	-0.886	2.44E-05
VEGF family				
VEGFA	Brigatinib+INK128	Inhibited	-3.002	2.62E-14
VEGFA	Brigatinib	Trend down	-1.238	4.41E-05
VEGFA	INK128	Trend up	0.736	5.97E-03
EGF family				
NRG1	Brigatinib+INK128	Inhibited	-4.595	1.42E-18
NRG1	Brigatinib	–	–	1.38E-04
NRG1	INK128	–	–	–
EGF	Brigatinib+INK128	Inhibited	-2.093	8.91E-20
EGF	Brigatinib	Trend down	-1.55	7.05E-08
EGF	INK128	Trend up	0.073	4.72E-03
Receptor tyrosine kinases				
Insulin/IGF family				
INSR	Brigatinib+INK128	Trend down	-1.304	4.20E-07
INSR	Brigatinib	–	–	–
INSR	INK128	Trend down	-1.067	1.21E-03
IGF1R	Brigatinib+INK128	Trend down	-0.671	3.97E-02
IGF1R	Brigatinib	–	–	–
IGF1R	INK128	–	–	–
EGFR family				
EGFR	Brigatinib+INK128	Inhibited	-3.689	4.18E-26
EGFR	Brigatinib	–	–	–
EGFR	INK128	–	–	–
ERBB2	Brigatinib+INK128	Inhibited	-5.347	1.14E-38
ERBB2	Brigatinib	–	–	–
ERBB2	INK128	Trend down	-1.614	1.17E-05
ERBB3	Brigatinib+INK128	Inhibited	-2.897	9.09E-13
ERBB3	Brigatinib	–	–	–
ERBB3	INK128	–	–	–
RAS/RAF/ERK signaling				
RAF1	Brigatinib+INK128	Inhibited	-3.183	2.67E-17
RAF1	Brigatinib	–	–	NS
RAF1	INK128	Trend up	1.732	3.07E-03
BRAF	Brigatinib+INK128	Inhibited	-2.535	2.92E-05
BRAF	Brigatinib	–	–	–
BRAF	INK128	–	–	–
DUSP4	Brigatinib+INK128	Activated	2	9.21E-02
DUSP4	Brigatinib	–	–	–
DUSP4	INK128	–	–	4.61E-03
MAP2K1 (MEK1)	Brigatinib+INK128	Inhibited	-2.794	3.88E-09
MAP2K1 (MEK1)	Brigatinib	Trend down	-1.58	0.00131
MAP2K1 (MEK1)	INK128	–	–	–
AKT/mTOR signaling				
PTEN	Brigatinib+INK128	Activated	3.285	1.56E-13
PTEN	Brigatinib	Trend up	1.134	4.09E-03
PTEN	INK128	Activated	2.252	1.12E-05
AKT1	Brigatinib+INK128	Trend down	-0.761	1.48E-11
AKT1	Brigatinib	Trend down	0.115	3.43E-05
AKT1	INK128	–	–	–
AKT2	Brigatinib+INK128	Trend down	-1.017	2.51E-02
AKT2	Brigatinib	–	–	–
AKT2	INK128	–	–	–
AKT3	Brigatinib+INK128	Trend up	0.57	3.92E-03
AKT3	Brigatinib	–	–	–
AKT3	INK128	–	–	–
MTOR	Brigatinib+INK128	Trend down	-1.216	2.30E-05
MTOR	Brigatinib	–	–	–
MTOR	INK128	Trend down	-1.231	3.74E-04
Translation				
EIF4E	Brigatinib+INK128	Inhibited	-3.314	3.97E-05
EIF4E	Brigatinib	–	–	–
EIF4E	INK128	–	–	–
EIF4G1	Brigatinib+INK128	Inhibited	-2.145	5.86E-05
EIF4G1	Brigatinib	–	–	–
EIF4G1	INK128	–	–	–
EIF4G2	Brigatinib+INK128	Trend down	-1.463	2.95E-03
EIF4G2	Brigatinib	–	–	–
EIF4G2	INK128	–	–	–
EIF2AK3	Brigatinib+INK128	Activated	2.178	3.24E-06
EIF2AK3	Brigatinib	–	–	–
EIF2AK3	INK128	–	–	–
EIF2AK4	Brigatinib+INK128	Activated	2.484	2.57E-03
EIF2AK4	Brigatinib	–	–	–
EIF2AK4	INK128	–	–	4.27E-03

Upstream regulator	Drug	Direction	Activation z-score	P-Value of overlap
Transcription factors				
MYC	Brigatinib+INK128	Inhibited	-6.819	1.26E-28
MYC	Brigatinib	Trend down	-0.925	7.63E-03
MYC	INK128	Inhibited	-2.672	8.03E-10
ATF4	Brigatinib+INK128	Activated	4.268	2.57E-08
ATF4	Brigatinib	–	–	–
ATF4	INK128	–	–	–
FOXO3	Brigatinib+INK128	Activated	3.83	2.10E-19
FOXO3	Brigatinib	–	–	–
FOXO3	INK128	Activated	2.594	7.35E-14
Hippo pathway				
LATS1	Brigatinib+INK128	Activated	2.345	3.32E-01
LATS1	Brigatinib	–	–	–
LATS1	INK128	–	–	–
LATS2	Brigatinib+INK128	Trend up	1.772	3.32E-02
LATS2	Brigatinib	–	–	–
LATS2	INK128	Trend up	0.254	1.91E-03
YAP1	Brigatinib+INK128	Inhibited	-4.304	6.67E-12
YAP1	Brigatinib	–	–	–
YAP1	INK128	Trend down	-1.158	3.57E-06
WWTR1 (TAZ)	Brigatinib+INK128	Inhibited	-2.649	5.60E-04
WWTR1 (TAZ)	Brigatinib	–	–	–
WWTR1 (TAZ)	INK128	–	–	–
Cell cycle				
AURKA	Brigatinib+INK128	Inhibited	-2.233	2.56E-01
AURKA	Brigatinib	–	–	–
AURKA	INK128	–	–	–
CCND1	Brigatinib+INK128	Inhibited	-3.551	6.83E-33
CCND1	Brigatinib	–	–	–
CCND1	INK128	Trend down	-1.342	8.25E-06
CCNE1	Brigatinib+INK128	Inhibited	-2.329	5.55E-07
CCNE1	Brigatinib	–	–	–
CCNE1	INK128	–	–	–
RB1	Brigatinib+INK128	Activated	2.445	6.00E-34
RB1	Brigatinib	Trend down	0.092	5.08E-05
RB1	INK128	Trend down	-0.103	5.37E-03
TP53	Brigatinib+INK128	Activated	4.026	6.58E-55
TP53	Brigatinib	Trend down	-0.011	6.94E-03
TP53	INK128	Activated	2.394	1.51E-07
CDKN1A	Brigatinib+INK128	Activated	4.799	1.20E-25
CDKN1A	Brigatinib	–	–	–
CDKN1A	INK128	Activated	2.102	1.68E-08
PRC2 complex				
EZH2	Brigatinib+INK128	Trend down	-1.663	5.91E-09
EZH2	Brigatinib	–	–	–
EZH2	INK128	Trend down	-1.568	4.31E-03
SUZ12	Brigatinib+INK128	Trend down	-1.134	1.32E-05
SUZ12	Brigatinib	–	–	–
SUZ12	INK128	–	–	–
EED	Brigatinib+INK128	Trend up	1	4.86E-02
EED	Brigatinib	–	–	–
EED	INK128	–	–	–
SWI/SNF complex				
SMARCA4 (BRG1)	Brigatinib+INK128	Activated	2.197	7.29E-14
SMARCA4 (BRG1)	Brigatinib	Trend down	-0.707	1.94E-05
SMARCA4 (BRG1)	INK128	Trend up	0.853	5.75E-03
ARID1A	Brigatinib+INK128	Activated	2.065	1.22E-05
ARID1A	Brigatinib	–	–	–
ARID1A	INK128	–	–	–
SMARCE1	Brigatinib+INK128	Trend up	0.478	1.13E-02
SMARCE1	Brigatinib	–	–	–
SMARCE1	INK128	–	–	–
BRD7	Brigatinib+INK128	Trend up	0.718	3.17E-04
BRD7	Brigatinib	–	–	–
BRD7	INK128	–	–	–
ACTL6A	Brigatinib+INK128	Inhibited	-2.714	5.41E-04
ACTL6A	Brigatinib	–	–	–
ACTL6A	INK128	–	–	1.96E-03
Chromatin readers				
BRD4	Brigatinib+INK128	Inhibited	-4.8	2.70E-15
BRD4	Brigatinib	–	–	8.41E-05
BRD4	INK128	Trend up	0.169	2.22E-05

To generate a quantifiable animal model for NF2-associated meningioma, we generated luciferase expressing AG-NF2-Men-Luc cells by transducing AG-NF2-Men-1 cells with the Lenti-CMV-Luc lentiviral vector carrying a luciferase-expressing cassette and a puromycin-resistant marker, similar to the Ben-Men-1-LucB cells that we established previously (Burns et al., 2013). Puromycin-resistant clones that express high levels of luciferase activity were isolated, and two such clones, designated AG-NF2-Men-Luc2 and AG-NF2-Men-LucG, were selected for generating animal models. First, we injected these luciferase-expressing cells subcutaneously in the back of NSG mice and monitored tumor growth by weekly BLI for 14 weeks. Intriguingly, these AG-NF2-Men-Luc cells did not grow when implanted at the subcutaneous location (Figure 16). Next, we stereotactically injected AG-NF2-Men-Luc2 and AG-NF2-Men-LucG cells into the skull base of NSG mice. BLI showed that in contrast to those inoculated subcutaneously, these orthotopically implanted xenografts readily grew over time with tumor-emitted luminescence increasing ~78-fold for AG-NF2-Men-Luc2 (Figure 17A) and ~20-fold for AG-NF2-Men-LucG over 12 weeks (Figure 17B). These results suggest that tumor microenvironment plays an important role in supporting the growth of NF2-associated meningiomas.

Figure 16. Luciferase-expressing AG-NF2-Men-Luc2 cells did not grow as subcutaneous xenografts in NSG mice. AG-NF2-Men-Luc2 cells (10^6 cells/mouse) were injected in the back of NSG mice. BLI was performed to monitor tumor growth (Burns et al., 2013). The tumor-emitted luminescence was captured every two weeks for 14 weeks and plotted for each mouse (A). The average relative luciferase unit (RLU) of tumor-emitted BL signal for the entire group (n=5) was calculated and denoted as % of total flux relative to that of the first scan at two weeks after AG-NF2-Men-Luc2 injection designated as one (100%). The data are shown as mean ± standard deviation (B).

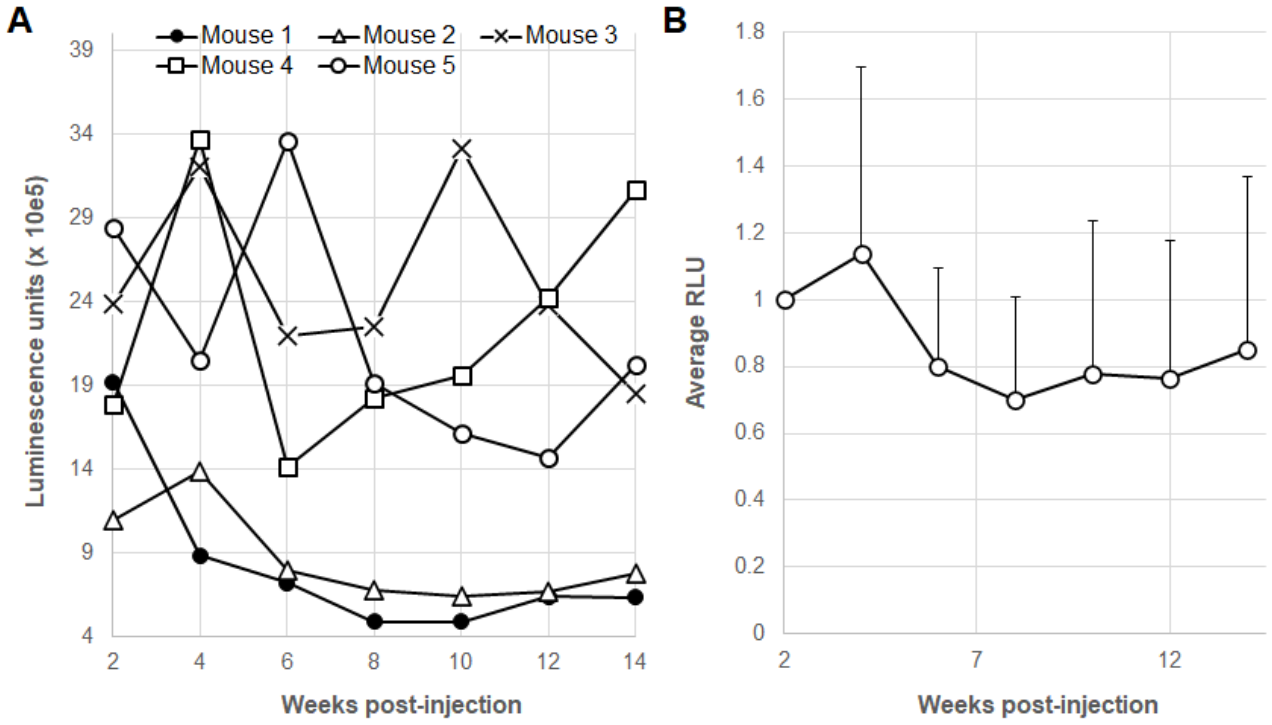

Figure 17. AG-NF2-Men-Luc cells readily grew as intracranial xenografts when implanted in the skull base of NSG mice. Luciferase-expressing AG-NF2-Men-Luc2 (A) and AG-NF2-Men-Luc2 (B) cells (10^6 cells/mouse) were stereotactically injected into the skull base of NSG mice (Burns et al., 2013). The tumor-emitted luminescence was captured by weekly BLI for 12 weeks. The mean relative luciferase unit (RLU) of tumor-emitted BL signal for the entire group was calculated and denoted as % of total flux relative to that of the first scan at one weeks after tumor cell injection designated as one (100%). The data are shown as mean ± standard deviation (B).

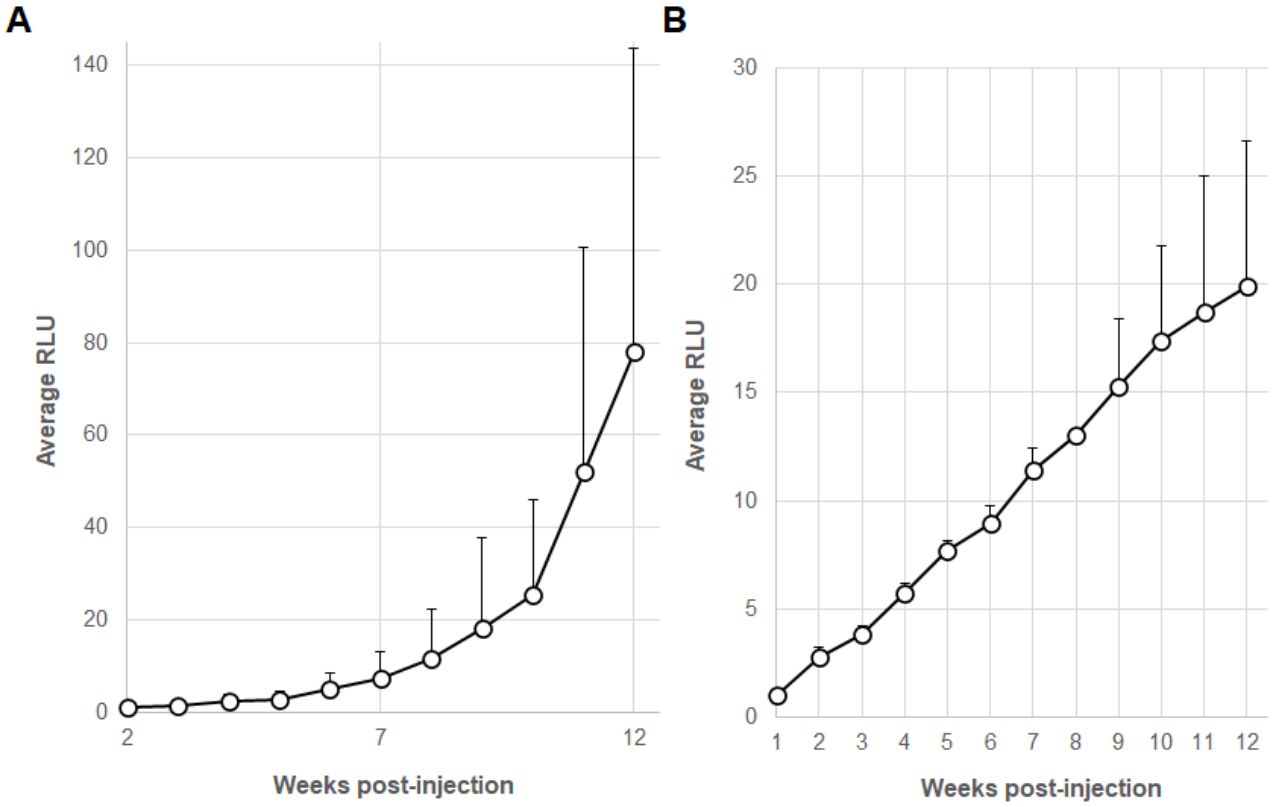

To examine the anti-tumor activities of brigatinib, INK128, and their combination, we generated and treated a cohort of NSG mice bearing intracranial AG-NF2-Men-Luc2 xenografts. As in the Ben-Men-1-LucB model, brigatinib alone effectively blocked AG-NF2-Men-Luc2 meningioma growth with some tumor shrinkage after six weeks of treatment (Figure 18A). INK128 alone also blocked meningioma growth with some tumor shrinkage particularly in the first two weeks. Combined treatment with brigatinib and INK128 further shrank meningiomas to smaller sizes to only ~18% (average) of the original tumors after six weeks. To assess potential tumor regrowth after cessation of treatment and the efficacy of re-treatment, we stopped treating two mice each in the groups that had been treated with INK128 or the brigatinib+INK128 combination for eight weeks and continued monitoring tumor growth by BLI for another six weeks. Upon cessation of treatment, both INK128- and brigatinib+INK128-treated tumors exhibited some regrowth; however, the brigatinib+INK128-treated tumors regrew at a much slower rate than those treated with INK128 alone. To examine the effects of re-treatment, we treated these mice for six more weeks. Curiously, tumor shrinkage was observed when the treatment was re-initiated (Figure 18B). In particular, the regrown tumors shrank substantially upon re-treatment with the brigatinib/INK128 combination, while the tumors re-treated with INK128 alone showed some transient tumor shrinkage only on the first week. Together, these results suggest that the brigatinib and INK128 combination can be repeatedly used to treat NF2-associated meningiomas.

Figure 18. The brigatinib and INK128 combination effectively shrank intracranial AG-NF2-Men-Luc2 meningioma xenografts. (A) Mice with established meningioma xenografts were treated with vehicle, brigatinib, INK128, or brigatinib+INK128 by oral gavage (n = 5/group) and tumor growth was monitored by BLI. The relative tumor-emitted BL signals were quantified and denoted as % of total flux after treatment relative to the total flux prior to treatment designated as one (100%). (B) To assess potential tumor regrowth, we stopped treating two mice each in the groups that had been treated with INK128 or the brigatinib+INK128 combination for 8 weeks and continued monitoring tumor growth by BLI for another 6 weeks. To examine the effects of re-treatment, we re-treated these mice and continued BLI monitoring for 6 more weeks. The data are shown as mean ± standard error.

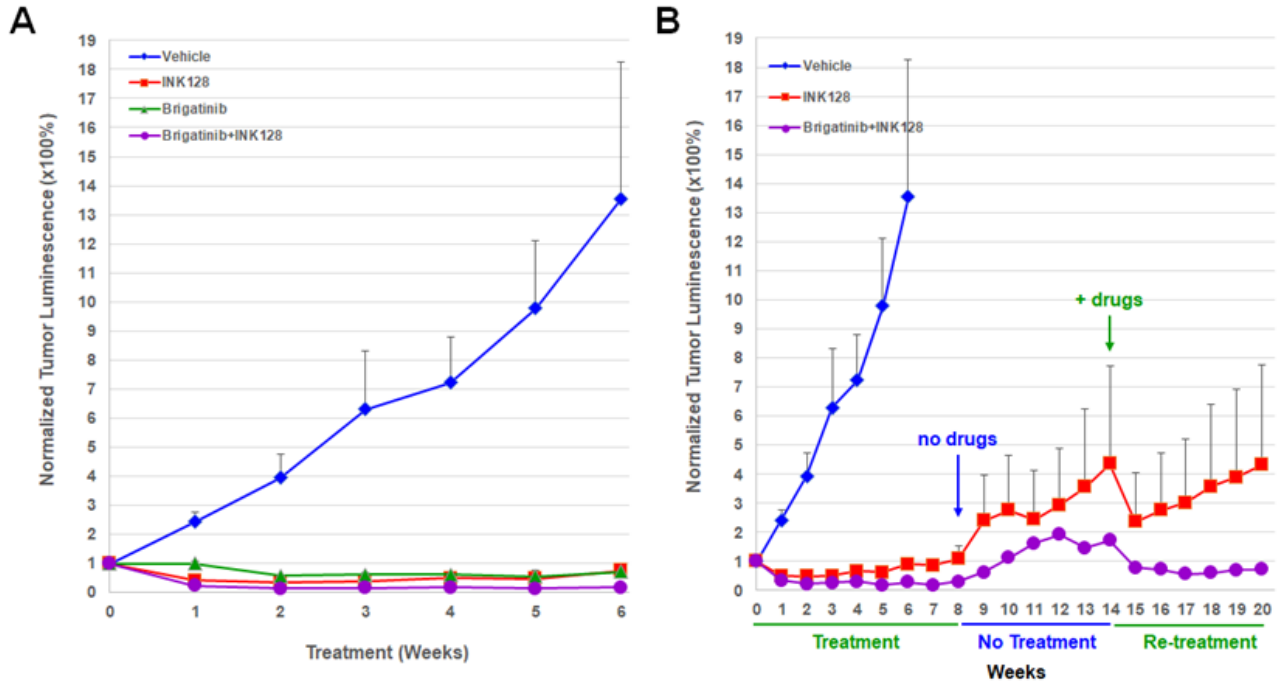

(iii) What opportunities for training and professional development has the project provided?

This project was not intended to provide training and professional development opportunities; therefore, we have "Nothing to Report."

(iv) How were the results disseminated to communities of interest?

Our data together with the results obtained by the Synodos for NF2 Consortium, in which I am a member, indicate that brigatinib possessed potent anti-tumor activity against *NF2*-deficient meningioma and schwannoma via inhibition of multiple RTKs, but not ALK, as well as blockade of several non-RTKs, such as FAK, which has previously been recognized as an oncoprotein in NF2-related tumors. All these findings have been combined into a publication (Chang et al., 2021). Also, we presented these findings at several national/international NF Conferences (see Appendix). Based on our and the Synodos for NF2 team findings, the CTF has collaborated with Takeda Pharmaceutical Company, the manufacturer of brigatinib, to conduct a multi-site, phase II clinical trial of brigatinib to treat NF2-associated progressive tumors of vestibular schwannomas, non-vestibular schwannomas, meningiomas, and ependymomas (Innovative Trial for Understanding the Impact of Targeted Therapies in NF2 [INTUITT-NF2]; ClinicalTrials.gov Identifier: NCT04374305; Principal Investigator: Scott R Plotkin, MD, PhD, Massachusetts General Hospital).

Previously, we generated an orthotopic, quantifiable, *NF2*-deficient meningioma model using luciferase-expressing Ben-Men-1-LucB cells, which were derived from a grade-I sporadic meningioma with NF2 loss (Burns et al., 2013). We have now established, for the first time, a grade-I meningioma cell line from an NF2 patient by telomerase immortalization. This NF2-associated meningioma cell line, designated AG-NF2-Men-1, does not express the *NF2*/merlin protein and retained many characteristics of the original tumor. By introducing a luciferase-expressing unit into AG-NF2-Men-1 cells and stereotactically injecting them into the skull base of NSG mice, we have established a quantifiable, intracranial model of NF2-associated meningioma. Intriguingly, AG-NF2-Men-Luc2 cells established

tumor xenografts only at the orthotopic location but did not grow when implanted subcutaneously, suggesting that tumor microenvironment plays an important role in supporting the growth of NF2-associated meningiomas. Using both the *NF2*-deficient sporadic Ben-Men-1 and the NF2-associated AG-NF2-Men-1 meningioma cell lines, we showed brigatinib, when combined with INK128, showed growth-inhibitory synergy. Mechanistically, the combined brigatinib+INK128 treatment not only decreased p-AKT(S473) more than either drug alone, but also completely prevented INK128-mediated re-phosphorylation of AKT on T308, as well as suppressing the downstream signaling of AKT. RNA sequencing analysis indicated that the brigatinib+INK128 combination elicited major changes in the expression of genes including the upstream regulators of several signaling networks that are important for meningioma growth. Further, combining INK128 with brigatinib enhanced anti-tumor effects in both the Ben-Men-1-LucB and AG-NF2-Men-Luc2 models. Also, the brigatinib and INK128 combination can be repeatedly used to treat NF2-associated meningiomas. All of these findings will be written into a manuscript for publication in the near future.

(v) What do you plan to do during the next reporting period to accomplish the goals?

This is the final report. We have completed all proposed experiments and are in the process of preparing a manuscript describing our new orthotopic NF2-associated meningioma AG-NF2-Men-Luc2 model and the anti-tumor effects of the brigatinib and INK128 combination.

5. IMPACT

(i) What was the impact on the development of the principal discipline(s) of the project?

Identification of a medical therapy that effectively eradicates NF2-related tumors would significantly advance our current approach to NF2 treatment and greatly improve the clinical care and long-term treatment outcomes for these patients. We have found that brigatinib caused tumor shrinkage in *NF2*-deficient meningiomas by inhibiting multiple RTKs, but not ALK, as well as blocking several non-RTKs, such as FAK. As brigatinib is an FDA-approved drug, a multi-center, phase II clinical trial (INTUITT-NF2) has been initiated to evaluate brigatinib in patients with NF2 with associated progressive tumors of vestibular schwannomas, non-vestibular schwannomas, meningiomas, and ependymomas (ClinicalTrials.gov Identifier: NCT04374305).

In addition, we have generated a quantifiable, orthotopic, NF2-associated meningioma model using a luciferase-expressing, telomerase-immortalized meningioma cell line AG-NF2-Men-Luc2 derived from a grade-I tumor from an NF2 patient. This NF2-associated meningioma model, together with the *NF2*-deficient sporadic meningioma Ben-Men-1-LucB model that we established previously, should enhance future therapeutic evaluation. Using both the AG-NF2-Men-Luc2 and Ben-Men-1-LucB models, we showed that brigatinib had anti-tumor activity in both *NF2*-deficient sporadic and NF2-associated meningiomas. Combining the dual mTORC1/2 inhibitor INK128 with brigatinib enhanced the anti-tumor effects. These results suggest that a clinical trial to evaluate the combination of brigatinib with an mTOR inhibitor in NF2 patients with progressive meningiomas is warranted.

(ii) What was the impact on other disciplines?

As we have found that brigatinib suppressed the growth of *NF2*-deficient sporadic and NF2-associated meningiomas via inhibition of multiple RTKs and non-RTKs, including FAK. Many of these kinases have also been found to be activated in many other human cancers, including malignant peripheral nerve sheath tumors (MPNSTs) which are frequently found in patients with NF1. Indeed, we showed that brigatinib also exhibited anti-tumor effects in MPNSTs. Combining INK128 with brigatinib gave rise to a slightly stronger tumor suppression of tumor growth than brigatinib alone, suggesting that brigatinib and its combination with an mTOR inhibitor should also be evaluated as potential treatments for MPNSTs.

(iii) What was the impact on technology transfer?

The AG-NF2-Men-Luc2 NF2-associated meningioma model, together with the Ben-Men-1-LucB *NF2*-deficient, sporadic meningioma model that we generated previously (Burns et al., 2013), will greatly enhance the translational research to identify additional targeted drugs/drug combinations to effectively treat NF2-associated meningiomas.

(iv) What was the impact on society beyond science and technology?

Identification of an effective medical therapy to treat NF2-associated tumors and other cancers would significantly advance our efforts to improve clinical care and long-term treatment outcomes for these patients.

6. CHANGES/PROBLEMS:

(i) Changes in approach and reasons for change

None

(ii) Actual or anticipated problems or delays and actions or plans to resolve them

None

(iii) Changes that had a significant impact on expenditures

None

(iv) Significant changes in use or care of human subjects

None

(v) Significant changes in use or care of vertebrate animals

None

(vi) Significant changes in use of biohazards and/or select agents

None

7. Publications, Abstracts, and Presentations

(1) Journal publications or manuscripts under review

The works described in the following six publications were supported, in part, by this grant.

(i) Fuse MA, Dinh CT, Vitte J, Kirkpatrick J, Mindos T, Plati SK, Young JI, Huang J, Carlstedt A, Franco MC, Brnjos K, Nagamoto J, Petrilli A, Copik AJ, Soulakova JN, Bracho O, Yan D, Mittal R, Shen R, Telischi FF, Morrison H, Giovannini M, Liu XZ, Chang LS, Fernandez-Valle C. Preclinical Assessment of MEK1/2 Inhibitors for Neurofibromatosis Type 2-Associated Schwannomas Reveals Differences in Efficacy and Drug Resistance Development. Neuro-Oncol. 2019;21:486-497. PMID: 30615146. https://pubmed.ncbi.nlm.nih.gov/30615146/

To identify an effective treatment for NF2-associated schwannomas, we collaborated with Dr. Cristina Fenandez-Valle at the University of Central Florida to investigate repurposing drugs targeting MEK1/2 kinases as merlin, the *NF2* gene product, has been shown to modulate activity of the Ras/Raf/MEK/ERK pathway. Among six MEK inhibitors examined, trametinib, PD0325901, and cobimetinib were most effective in reducing the viability of merlin-deficient mouse and human

Schwann cells. Also, the three inhibitors slowed the growth of schwannoma allografts. However, when we analyzed drug-treated tumors, we found decreased pERK1/2 levels only in the tumors treated with PD0325901 and cobimetinib, but not trametinib. Similarly, tumor burden and average tumor size were reduced in trametinib-treated NF2 transgenic mice, and we also did not find reduced pERK1/2 in treated mouse tumors. The results show that MEK inhibitors exhibited differences in anti-tumor efficacy resistance in schwannoma models with possible emergence of trametinib resistance.

(ii) Chang L-S, Oblinger JL, Burns SS, Huang J, Anderson LW, Hollingshead MG, Shen R, Pan L, Agarwal G, Ren Y, Roberts R, O'Keefe BR, Kinghorn AD, Collins JM. 2020. Targeting protein translation by rocaglamide and didesmethylrocaglamide to treat MPNST and other sarcomas. Mol Cancer Ther. 19:731-741. PMID: 31848295. https://pubmed.ncbi.nlm.nih.gov/31848295/

Previously we showed that malignant schwannomas, such as malignant peripheral nerve sheath tumors (MPNSTs) which are frequently found in patients with NF1, and benign schwannoma including those commonly seen in patients with NF2, often overexpress eIF4F components, and the eIF4A inhibitor silvestrol potently suppresses MPNST growth (Oblinger JL et al. Neuro-Oncol. 2016;18:1265-1277). However, silvestrol has suboptimal drug-like properties, including a bulky structure, poor oral bioavailability, sensitivity to MDR1 efflux, and pulmonary toxicity in dogs. We compared 10 silvestrol-related rocaglates lacking the dioxanyl ring and found that didesmethylrocaglamide (DDR) and rocaglamide (Roc) had growth-inhibitory activity comparable to silvestrol. Both DDR and Roc arrested MPNST cells at G_2/M, increased the sub-G_1 population, induced cleavage of caspases and poly(ADP-ribose) polymerase, and elevated the levels of the DNA-damage response marker γH2A.X, while decreasing the expression of AKT and ERK1/2, consistent with translation inhibition. Unlike silvestrol, DDR and Roc were not sensitive to MDR1 inhibition and pharmacokinetic analysis confirmed that Roc had 50% oral bioavailability. Importantly, Roc, when administered intraperitoneally or orally, showed potent anti-tumor effects in an orthotopic MPNST mouse model and did not induce pulmonary toxicity in dogs as found with silvestrol. Treated tumors displayed degenerative changes and had more cleaved caspase 3-positive cells, indicative of increased apoptosis. Furthermore, Roc effectively suppressed the growth of osteosarcoma, Ewing sarcoma, and rhabdomyosarcoma cells and patient-derived xenografts. Both Roc- and DDR-treated sarcoma cells showed decreased levels of multiple oncogenic kinases, including IGF-1R. The more favorable drug-like properties of DDR and Roc and the potent anti-tumor activity of Roc suggest that these rocaglamides could become viable treatments for MPNST and other sarcomas.

(iii) Chang LS, Oblinger JL, Smith AE, Ferrer M, Angus SP, Hawley E, Petrilli AM, Beauchamp RL, Riecken LB, Erdin S, Poi M, Huang J, Bessler WK, Zhang X, Guha R, Thomas C, Burns SS, Gilbert TSK, Jiang L, Li X, Lu Q, Yuan J, He Y, Dixon SAH, Masters A, Jones DR, Yates CW, Haggarty SJ, La Rosa S, Welling DB, Stemmer-Rachamimov AO, Plotkin SR, Gusella JF, Guinney J, Morrison H, Ramesh V, Fernandez-Valle C, Johnson GL, Blakeley JO, Clapp DW; Synodos for NF2 Consortium. Brigatinib causes tumor shrinkage in both *NF2*-deficient meningioma and schwannoma through inhibition of multiple tyrosine kinases but not ALK. PLoS One. 2021;16:e0252048. PMID: 34264955. https://pubmed.ncbi.nlm.nih.gov/34264955/

We, as members of the Synodos for NF2 Consortium in collaboration with the NIH-NCATS, conducted high-throughput drug screening of isogenic pairs of *NF2*-deficient and *NF2*-expressing disease-relevant cells and identified several actionable drug targets for the treatment of both NF2-related schwannomas and meningiomas. We also showed that brigatinib, which was originally developed for inhibition of ALK, potently suppressed the growth of *NF2*-deficient meningioma and schwannoma cells *in vitro* and established xenograft and spontaneous *NF2*-deficient meningiomas and schwannomas *in vivo*. With this support, we found that *NF2*-deficient meningioma and schwannoma cells do not express ALK or ROS1 and that brigatinib inhibited multiple RTKs and non-RTKs, such as focal adhesion kinase, but not ALK, in *NF2*-deficient tumor cells. These findings represent a major advance for the development of a treatment of NF2-related malignancies and demonstrate the power of a *de novo* unbiased approach to drug development.

(iv) Agarwal G, Chang L-S, Soejarto DD, Kinghorn AD. Update on Phytochemical and Biological Studies on Rocaglate Derivatives from *Aglaia* Species. Planta Med. 2021;87:937-948. PMID: 33784769 https://pubmed.ncbi.nlm.nih.gov/33784769/

Recent studies have shown that targeting translation initiation is a promising strategy for cancer treatment. In this review, we discussed the phytochemical and biological properties of rocaglates derived from tropical rainforest plants of Aglaia species. The varied biological properties of rocaglates, including rocaglamide (Roc), can be attributed to their unusual structures and their ability to act as inhibitors of the eukaryotic translation initiation factor 4A (eIF4A), affecting protein translation. Since the initial report of Roc as an antileukemic agent, the therapeutic potential of various rocaglates have been evaluated in a variety of tumor models including neurofibromatosis (NF)-associated tumors. From side-by-side comparison of ten rocaglates lacking the dioxanyl ring with silvestrol, Roc and didesmethylrocaglamide (DDR) were identified to exhibit potent growth-inhibitory activity comparable to silvestrol. Also, these rocaglamides show potent antitumor activities in NF-associated tumors and several other types of sarcoma. In addition, a synthetic derivative of rocaglamide named eFT-226 (Zotatifin) was reported to exhibit potent anti-tumor effects and has entered into a clinical trial to treat patients with advanced solid tumors. Collectively, these natural and synthetic rocaglamides have potential to become viable cancer treatments, including NF, in the future.

(v) Amaravathi A*, Oblinger JL*, Welling DB, Kinghorn AD, Chang L-S. Neurofibromatosis: Molecular Pathogenesis and Natural Compounds as Potential Treatments. Front Oncol. 2021;11:698192. PMID: 34604034 (*Co-first authors) https://pubmed.ncbi.nlm.nih.gov/34604034/

In this paper, we reviewed the neurofibromatosis tumor suppressor syndromes, including NF1, NF2, and schwannomatosis, which are characterized by multiple nervous system tumors, particularly Schwann cell neoplasms. NF-related tumors are mainly treated by surgery and often refractory to conventional chemotherapy. Recent advances in molecular genetics and genomics alongside the development of multiple animal models have provided a better understanding of NF tumor biology and facilitated target identification and therapeutic evaluation. Many targeted therapies have been evaluated in preclinical models and patients, including the MEK inhibitor selumetinib recently approved by the FDA for treating NF1-associated plexiform neurofibroma. Due to their anti-neoplastic, antioxidant, and anti-inflammatory properties, selected natural compounds could be useful as adjuvant therapy for patients with tumor predisposition syndromes as patients often take them as dietary supplements and for health enhancement purposes. Several natural compounds have been tested in NF models. Some have demonstrated potent anti-tumor effects and may become viable NF treatments in the future.

(vi) Welling DB*, Collier KA*, Burns SS*, Oblinger JL, Shu E, Miles-Markley B, Hofmeister CC, Makary MS, Slone HW, Blakeley JO, Mansouri SA, Neff BA, Jackler RK, Mortazavi A, Chang L-S. Early phase clinical studies of AR-42, a pan-histone deacetylase inhibitor, in patients with neurofibromatosis type 2-associated vestibular schwannomas and meningiomas. Submitted to Laryngoscope Investig Otolaryngol. 2021;6:1008-1019. PMID:34667843 (*Co-first authors) https://pubmed.ncbi.nlm.nih.gov/34667843/

This publication reported two pilot studies of AR-42, a pan-histone deacetylase, in human neurofibromatosis type 2 (NF2), vestibular schwannomas (VS), and meningiomas. The objectives are to evaluate the safety and intra-tumoral pharmacokinetics (PK) and pharmacodynamics (PD). The first study is a phase 1 clinical trial of AR-42 in solid tumors (ClinicalTrial.gov Identifier http://clinicaltrials.gov/show/NCT01129193). Five patients with NF2 and two with sporadic meningiomas were enrolled. It was found that AR-42 is safe. The six evaluable patients had 15 tumors (8 VS and 7 meningiomas). The analysis of tumor volumes in treated patients showed a mixed response, but most slowed growth. The second study is a phase 0 surgical study of AR-42 assessing intra-tumoral PK and PD in patients receiving oral AR-42 for three weeks pre-operatively (ClinicalTrial.gov Identifier http://clinicaltrials.gov/show/NCT02282917). We found that on a 40-mg regimen, drug concentrations in tumors and growth pathways were suppressed in most tumors, suggesting that this may be a well-tolerated and effective dose. A phase 2 study of AR-42 for NF2-associated tumors appears warranted. These two studies were supported by another DOD grant (W81XWH-14-1-0167; PI: D. Bradley Welling of MGH) and the current grant (which provided part of

personnel support and tumor specimens as untreated controls for the reported PK and PD analyses).

(2) Abstracts presented at national/international conferences

We presented a total of 16 abstracts with acknowledgement of this DOD award at the following national/international meetings.

(i) Chang L-S, SS Burns, JL Oblinger, M Ferrer, J Huang, M Poi, V Ramesh, On behalf of the Synodos for NF2 Consortium. 2018. Novel drug discovery for NF2-deficient meningiomas: Brigatinib causes tumor shrinkage in NF2-deficient meningiomas. The 2018 Joint Global NF Conference, Paris, France. (Platform presentation)

(ii) Chang L-S, JL Oblinger, SS Burns, J Huang, L Anderson, R Shen, L Pan, Y Ren, BR O'Keefe, AD Kinghorn, JM Collins. 2018. Identification of silvestrol-related rocaglates with better bioavailability and high potency against malignant peripheral nerve sheath tumors. The 2018 Joint Global NF Conference, Paris, France. (Poster presentation)

(iii) Fernandez-Valle C, M Fuse, C Dinh, J Vitte, J Kirkpatrick, T Mindos, S Campion, K Brnjos, MC Franco, J Huang, J Young, A Petrilli, D Yan, R Mittal, R Shen, F Telischi, L-S Chang, H Morrison, M Giovannini, X-Z Liu. 2018. Preclinical Assessment of MEK1/2 Inhibitors for Neurofibromatosis Type 2-Associated Schwannomas Reveals Differences in Efficacy and Drug Resistance Development. The 2018 Joint Global NF Conference, Paris, France. (Platform presentation)

(iv) Welling DB, SS Burns, JL Oblinger, B Miles-Markley, A Quinkert, J Blakeley, BA Neff, RK Jackler, L-S Chang. 2018. Phase 1 and Phase 0 studies of AR-42, a pan histone deacetylase inhibitor, in subjects with neurofibromatosis type 2 (NF2)-associated vestibular schwannomas and meningiomas. The 2018 Joint Global NF Conference, Paris, France. (Poster presentation)

(v) Beauchamp RL, S Erdin, SP Angus, TJ Stuhlmiller, JL Oblinger, JT Jordan, SJ Haggarty, SR Plotkin, L-S Chang, GL Johnson, JF Gusella, V Ramesh. 2018. High throughput kinome and transcriptome analyses reveal novel therapeutic targets in *NF2*-deficient meningioma. The 2018 Society for Neuro-Oncology Meeting, New Orleans, LA. (Poster presentation)

(vi) Oblinger J, L-S Chang. 2019. Brigatinib as a potential therapy for malignant peripheral nerve sheath tumors. The 2019 NF Conference, San Francisco, CA. (Poster presentation)

(vii) Chang L-S, JL Oblinger, SS Burns, J Huang, L Anderson, R Shen, L Pan, Y Ren, R Roberts, BR O'Keefe, AD Kinghorn, JM Collins. Targeting protein translation with rocaglamide and didesmethylrocaglamide to treat NF1 and NF2 tumors. The 2019 NF Conference, San Francisco, CA. (Platform presentation)

(viii) Chang L-S. 2019. Drug Discoveries from Synodos for NF2 and Identification of Natural Compounds to Treat NF1 and NF2 Tumors. NF Symposium and iNFo Fair 2019 - Annual NF Midwest Neurofibromatosis Family Symposium, Northern Illinois University, Hoffman Estates, IL. (Platform presentation)

(ix) Chang L-S. 2020. Targeting protein translation via eIF4A inhibition with didesmethylrocaglamide (DDR) and rocaglamide (Roc) to treat pediatric osteosarcoma. Keats Beating Cancer – Science Is the Cure Symposium, Orlando, FL. (Platform presentation)

(x) Chang L-S, JL Oblinger, G Agarwal, TA Wilson, R Roberts, J Fuchs, BR O'Keefe, AD Kinghorn, JM Collins. 2020. The eIF4A inhibitors didesmethylrocaglamide and rocaglamide as effective treatments for pediatric bone and soft-tissue sarcomas. AACR Annual Meeting 2020, San Diego, CA. (Poster presentation)

(xi) Chang L-S, Oblinger JL, Hawley E, Smith A, Ferrer M, Angus SP, Petrilli AM, Beauchamp R, Riecken LB, Erdin S, Poi M, Huang J, Bessler WK, Zhang X, Guha R, Thomas C, Burns SS, Jang L, Li X, Lu Q, Yuan J, He Y, Masters A, Jones DR, Yates CW, Haggarty SJ, La Rosa S, Welling DB, Stemmer-Rachamimov AO, Plotkin S, Gusella JF, Morrison H, Ramesh V, Fernandez-Valle C, Johnson GL, Blakeley J, Clapp DW, on behalf of the Synodos for NF2 Consortium. 2020. Novel drug discovery for NF2-deficient tumors: Brigatinib causes tumor shrinkage in NF2-deficient meningioma and schwannoma. Children's Tumor Foundation – NF2 Virtual Meeting 2020. (Invited oral presentation)

(xii) Chang L-S, Oblinger JL, Zhang X, Wu J, Fernandez-Valle C, Anderson LW, Ferrer M, Ratner N, Kinghorn AD, O'Keefe BR, Collins JM. 2021. Targeting Protein Translation in Combination with MEK Inhibition as an Effective Treatment for NF1, NF2, and Schwannomatosis-Related Tumors. The 2021 Virtual NF Conference. (Poster presentation)

(xiii) Chang L-S. 2021. eIF4A inhibitors in sarcoma. National Pediatric Cancer Foundation/Sunshine Project Summit. (Invited oral presentation)

(xiv) Chang L-S, Oblinger JL, Zhang X, Anksapuram H, Ferrer M, Roberts RD, Kinghorn AD. 2021. Targeting Inhibition of eIF4A and a High Throughput Screening to Identify Synergistic Drug Combinations to Treat Pediatric and Adult Sarcomas. 2021 CTOS 26th Annual Meeting Abstract Vancouver, Canada. (Poster presentation)

(xv) Chang L-S, Burns SS, Oblinger JL, Welling DB. 2022. Orthotopic Xenograft Models and Potential Treatments for *NF2*-Deficient Meningiomas. The 2022 NF Conference, Philadelphia, PA. (Oral presentation)

(xvi) Oblinger JL, Chang L-S. 2022. New patient-derived models of NF2-deficient vestibular schwannoma and meningioma to advance basic and preclinical investigations. The 2022 NF Conference, Philadelphia, PA (Poster presentation)

8. PARTICIPANTS & OTHER COLLABORATING ORGANIZATIONS

(i) What individuals who have worked on the project

The Research Institute at Nationwide Children's Hospital
Long-Sheng Chang, Ph.D., Professor, Principal Investigator
Janet Oblinger, Ph.D., Research Associate
Michael Hsu, M.S., Research Assistant
Massachusetts General Hospital
Vijaya Ramesh, Ph.D., Professor, Co-Investigator/Site Principal Investigator
Roberta Beauchamp, M.S., Research Associate

(ii) Has there been a change in the active other support of the PD/PI(s) or senior/key personnel since the last reporting period?

Nothing to report.

(iii) What other organizations were involved as partners

Massachusetts General Hospital - Vijaya Ramesh, Ph.D., Co-Investigator/Site Principal Investigator

9. Reportable Outcome

Six peer-reviewed publications and 16 abstracts presented at national/international conferences.

10. Other Achievements

Nothing to report.

11. References

Ammoun S, Hanemann CO. 2011. Emerging therapeutic targets in schwannomas and other merlin-deficient tumors. Nat Rev Neurol. 2011;7:392-399. https://www.ncbi.nlm.nih.gov/pubmed/21647202

Angus SP, Oblinger JL, Stuhlmiller TJ, DeSouza PA, Beauchamp RL, Witt L, Chen X, Jordan JT, Gilbert TSK, Stemmer-Rachamimov A, Gusella JF, Plotkin SR, Haggarty SJ, Chang LS, Johnson GL, Ramesh V; Children's Tumor Foundation Synodos for NF2 Consortium. EPH receptor signaling as a novel therapeutic target in NF2-deficient meningioma. Neuro Oncol. 2018;20:1185-1196. https://www.ncbi.nlm.nih.gov/pubmed/29982664

Blakeley JO, Plotkin SR. Therapeutic advances for the tumors associated with neurofibromatosis type 1, type 2, and schwannomatosis. Neuro Oncol. 2016;18:624-638. https://www.ncbi.nlm.nih.gov/pubmed/26851632

Burns SS, Akhmametyeva EM, Oblinger JL, Bush ML, Huang J, Senner V, Chen C-S, Jacob A, Welling DB, Chang L-S. 2013. AR-42, a Histone Deacetylase Inhibitor, Differentially Affects Cell-Cycle Progression of Meningeal and Meningioma Cells and Potently Inhibits NF2^{-} Meningioma Growth. Cancer Res. 73:792-804. http://www.ncbi.nlm.nih.gov/pubmed/23151902

Chang LS, Oblinger JL, Smith AE, Ferrer M, Angus SP, Hawley E, Petrilli AM, Beauchamp RL, Riecken LB, Erdin S, Poi M, Huang J, Bessler WK, Zhang X, Guha R, Thomas C, Burns SS, Gilbert TSK, Jiang L, Li X, Lu Q, Yuan J, He Y, Dixon SAH, Masters A, Jones DR, Yates CW, Haggarty SJ, La Rosa S, Welling DB, Stemmer-Rachamimov AO, Plotkin SR, Gusella JF, Guinney J, Morrison H, Ramesh V, Fernandez-Valle C, Johnson GL, Blakeley JO, Clapp DW; Synodos for NF2 Consortium. Brigatinib causes tumor shrinkage in both *NF2*-deficient meningioma and schwannoma through inhibition of multiple tyrosine kinases but not ALK. PLoS One. 2021;16:e0252048. PMID: 34264955. https://pubmed.ncbi.nlm.nih.gov/34264955/

Duncan JS, Whittle MC, Nakamura K, Abell AN, Midland AA, Zawistowski JS, Johnson NL, Granger DA, Jordan NV, Darr DB, Usary J, Kuan PF, Smalley DM, Major B, He X, Hoadley KA, Zhou B, Sharpless NE, Perou CM, Kim WY, Gomez SM, Chen X, Jin J, Frye SV, Earp HS, Graves LM, Johnson GL. 2012. Dynamic reprogramming of the kinome in response to targeted MEK inhibition in triple-negative breast cancer. Cell 149:307-321. PMID: 22500798. https://pubmed.ncbi.nlm.nih.gov/22500798/

Ghobrial IM, Siegel DS, Vij R, Berdeja JG, Richardson PG, Neuwirth R, Patel CG, Zohren F, Wolf JL. TAK-228 (formerly MLN0128), an investigational oral dual TORC1/2 inhibitor: A phase I dose escalation study in patients with relapsed or refractory multiple myeloma, non-Hodgkin lymphoma, or Waldenström's macroglobulinemia. Am J Hematol. 2016;91:400-405. https://www.ncbi.nlm.nih.gov/pubmed/26800393

Huang WS, Liu S, Zou D, Thomas M, Wang Y, Zhou T, Romero J, Kohlmann A, Li F, Qi J, Cai L, Dwight TA, Xu Y, Xu R, Dodd R, Toms A, Parillon L, Lu X, Anjum R, Zhang S, Wang F, Keats J, Wardwell SD, Ning Y, Xu Q, Moran Le, Mohemmad QK, Jang HG, Clackson T, Narasimhan NI, Rivera VM, Zhu X, Dalgarno D, Shakespeare WC. Discovery of brigatinib (ap26113), a phosphine oxide-containing, potent, orally active inhibitor of anaplastic lymphoma kinase. J Med Chem. 2016; 59:4948-4964. https://www.ncbi.nlm.nih.gov/pubmed/27144831

Ostrom Qt, Gittleman H, Truitt G, Boscia A, Kruchko C, Barnholtz-Sloan Js. CBTRUS statistical report: primary brain and other central nervous system tumors diagnosed in the united states in 2011-2015. Neuro Oncol. 2018;20(SUPPL_4):IV1-IV86. https://www.ncbi.nlm.nih.gov/pubmed/30445539

Püttmann S, Senner V, Braune S, Hillmann B, Exeler R, Rickert C, Paulus W. 2005. Establishment of a benign meningioma cell line by hTERT-mediated immortalization. Lab Invest. 85:1163-1171. http://www.ncbi.nlm.nih.gov/pubmed/15965488

Rouleau GA, Merel P, Lutchman M, Sanson M, Zucman J, Marineau C, Hoang-Xuan K, Demczuk S, Desmaze C, Plougastel B, et al. Alteration in a new gene encoding a putative membrane-organising protein causes neurofibromatosis type 2. Nature 1993;363:515-521. http://www.ncbi.nlm.nih.gov/pubmed/8379998

Suppiah S, Nassiri F, Bi WL, Dunn IF, Hanemann CO, Horbinski CM, Hashizume R, James CD, Mawrin C, Noushmehr H, Perry A, Sahm F, Sloan A, Von Deimling A, Wen PY, Aldape K, Zadeh G; International Consortium on Meningiomas. Molecular and translational advances in meningiomas. Neuro Oncol. 2019;21(Supplement_1):i4-i17. https://www.ncbi.nlm.nih.gov/pubmed/30649490

Synodos for NF2 Consortium, Allaway R, Angus SP, Beauchamp RL, Blakeley JO, Bott M, Burns SS, Carlstedt A, Chang LS, Chen X, Clapp DW, Desouza PA, Erdin S, Fernandez-Valle C, Guinney J, Gusella JF, Haggarty SJ, Johnson GL, La Rosa S, Morrison H, Petrilli AM, Plotkin SR, Pratap A, Ramesh V, Sciaky N, Stemmer-Rachamimov A, Stuhlmiller TJ, Talkowski ME, Welling DB, Yates CW, Zawistowski JS, Zhao WN. Traditional and systems biology based drug discovery for the rare tumor syndrome neurofibromatosis type 2. PLoS One. 2018;13:e0197350. https://www.ncbi.nlm.nih.gov/pubmed/29897904

Trofatter JA, MacCollin MM, Rutter JL, Murrell JR, Duyao MP, Parry DM, Eldridge R, Kley N, Menon AG, Pulaski K, Haase VH, Ambrose CM, Munroe D, Bove C, Haines JL, Martuza RL, MacDonald ME, Seizinger BR, Short MP, Buckler AJ, Gusella JF. A novel moesin-, ezxrin-, radixin-like gene is a candidate for the neurofibromatosis 2 tumor-suppressor. Cell 1993;72:791-800. http://www.ncbi.nlm.nih.gov/pubmed/8453669

Zhang S, Anjum R, Squillace R, Nadworny S, Zhou T, Keats J, Ning Y, Wardwell SD, Miller D, Song Y, Eichinger L, Moran L, Huang WS, Liu S, Zou D, Wang Y, Mohemmad Q, Jang HG, Ye E, Narasimhan N, Wang F, Miret J, Zhu X, Clackson T, Dalgarno D, Shakespeare WC, Rivera VM. The Potent ALK Inhibitor Brigatinib (AP26113) Overcomes Mechanisms of Resistance to First- and Second-Generation ALK Inhibitors in Preclinical Models. Clin Cancer Res. 2016;22:5527-5538. https://www.ncbi.nlm.nih.gov/pubmed/27780853

12. Appendices

The attachment includes six publications and 16 abstracts.

Neuro-Oncology
21(4), 486–497, 2019 | doi:10.1093/neuonc/noz002 | Advance Access date 6 January 2019

Preclinical assessment of MEK1/2 inhibitors for neurofibromatosis type 2–associated schwannomas reveals differences in efficacy and drug resistance development

Marisa A. Fuse, Christine T. Dinh, Jeremie Vitte, Joanna Kirkpatrick, Thomas Mindos, Stephani Klingeman Plati, Juan I. Young, Jie Huang, Annemarie Carlstedt, Maria Clara Franco, Konstantin Brnjos, Jackson Nagamoto, Alejandra M. Petrilli, Alicja J. Copik, Julia N. Soulakova, Olena Bracho, Denise Yan, Rahul Mittal, Rulong Shen, Fred F. Telischi, Helen Morrison, Marco Giovannini, Xue-Zhong Liu, Long-Sheng Chang, and Cristina Fernandez-Valle

Burnett School of Biomedical Sciences, College of Medicine, University of Central Florida (UCF), Orlando, Florida, USA (M.A.F., S.K.P., M.C.F., K.B., J.N., A.P., A.J.C., J.N.S., C.F-V.); Department of Otolaryngology, University of Miami Miller School of Medicine, Miami, Florida, USA (C.T.D., O.B., D.Y., R.M., F.F.T., X.Z-L.); Department of Head and Neck Surgery, David Geffen School of Medicine at UCLA and Jonsson Comprehensive Cancer Center, University of California at Los Angeles (UCLA), Los Angeles, California, USA (J.V., M.G.); Leibniz Institute on Aging, Fritz Lipmann Institute, Jena, Germany (J.K., T.M., A.C., H.M.); Department of Human Genetics, University of Miami Miller School of Medicine, Miami, Florida, USA (J.I.Y., X.-Z.L.); Center for Childhood Cancer and Blood Diseases, Nationwide Children's Hospital (J.H., L-S.C.) and Departments of Pediatrics (J.H., L.-S.C.) and Pathology, The Ohio State University (R.S.), Columbus, Ohio, USA

Corresponding Author: Cristina Fernandez-Valle, Ph.D., Burnett School of Biomedical Sciences, College of Medicine, University of Central Florida, 6900 Lake Nona Blvd, Orlando, FL 32827 (cfv@ucf.edu).

Abstract

Background. Neurofibromatosis type 2 (NF2) is a genetic tumor-predisposition disorder caused by *NF2*/merlin tumor suppressor gene inactivation. The hallmark of NF2 is formation of bilateral vestibular schwannomas (VS). Because merlin modulates activity of the Ras/Raf/mitogen-activated protein kinase kinase (MEK)/extracellular signal-regulated kinase (ERK) pathway, we investigated repurposing drugs targeting MEK1 and/or MEK2 as a treatment for NF2-associated schwannomas.

Methods. Mouse and human merlin-deficient Schwann cell lines (MD-MSC/HSC) were screened against 6 MEK1/2 inhibitors. Efficacious drugs were tested in orthotopic allograft and *NF2* transgenic mouse models. Pathway and proteome analyses were conducted. Drug efficacy was examined in primary human VS cells with *NF2* mutations and correlated with DNA methylation patterns.

Results. Trametinib, PD0325901, and cobimetinib were most effective in reducing MD-MSC/HSC viability. Each decreased phosphorylated pERK1/2 and cyclin D1, increased p27, and induced caspase-3 cleavage in MD-MSCs. Proteomic analysis confirmed cell cycle arrest and activation of pro-apoptotic pathways in trametinib-treated MD-MSCs. The 3 inhibitors slowed allograft growth; however, decreased pERK1/2, cyclin D1, and Ki-67 levels were observed only in PD0325901 and cobimetinib-treated grafts. Tumor burden and average tumor size were reduced in trametinib-treated *NF2* transgenic mice; however, tumors did not exhibit reduced pERK1/2 levels. Trametinib and PD0325901 modestly reduced viability of several primary human VS cell cultures with *NF2* mutations. DNA methylation analysis of PD0325901-resistant versus -susceptible VS identified genes that could contribute to drug resistance.

© The Author(s) 2019. Published by Oxford University Press on behalf of the Society for Neuro-Oncology. All rights reserved.
For permissions, please e-mail: journals.permissions@oup.com

Downloaded from https://academic.oup.com/neuro-oncology/article-abstract/21/4/486/5274482 by Medical Library 244 ED user on 10 August 2019

Conclusion. MEK inhibitors exhibited differences in antitumor efficacy resistance in schwannoma models with possible emergence of trametinib resistance. The results support further investigation of MEK inhibitors in combination with other targeted drugs for NF2 schwannomas.

Key Points

1. Cobimetinib and trametinib reduced NF2 schwannoma model cell proliferation in vitro and in vivo.
2. Biochemical/proteome analyses reveal cell cycle arrest and apoptosis of trametinib-treated cells.
3. Human vestibular schwannoma cell viability is modestly inhibited by PD0325901 and trametinib.

Importance of the Study

There are currently no FDA-approved drug therapies for the treatment of NF2-associated schwannomas. Clinical trials for selumetinib and cobimetinib are ongoing for assessment of efficacy for NF2-associated tumors and hearing loss; however, little preclinical data have been published. Here, we evaluated 6 MEK1/2 inhibitors for efficacy in mouse and human cell and animal models as well as patient-derived vestibular schwannoma cells with *NF2* mutations. We observed differences in efficacy among the inhibitors as well as the possibility of drug resistance development. Our work highlights the importance of comprehensive drug screening in multiple model systems and supports further investigation of MEK inhibitors alone and in combination with other targeted therapies.

Neurofibromatosis type 2 (NF2) is caused by mutations in the *NF2* gene encoding the merlin tumor suppressor.[1,2] NF2 patients classically present with bilateral vestibular schwannomas (VS) involving the cochleovestibular nerves important for hearing and balance, and can develop additional peripheral schwannomas, meningiomas, and ependymomas.[3] Management of NF2 requires a complex, multidisciplinary approach focused on balancing tumor control and nerve function preservation to improve quality of life and maximize survival.[4] Whereas microsurgical resection of tumors risks permanent nerve injury, radiation therapy increases the chance of malignant transformation of benign tumors and secondary malignancies.[5–10] Therefore, there is an ongoing search for effective drug therapies for NF2.

Schwann cells with loss of merlin tumor suppressor function have elevated levels of Ras/Raf/mitogen-activated protein kinase kinase (MEK)/extracellular signal-regulated kinase (ERK) signaling that promotes cell proliferation.[11–13] Sixteen small molecule MEK inhibitors have entered clinical trials for various cancers.[14] Among these MEK inhibitors, selumetinib (AZD6244) was recently granted Orphan Drug Designation by the FDA for treatment of inoperable plexiform neurofibromas in children with NF1.[15] Additionally, selumetinib reduced growth of an in vitro human schwannoma model.[16,17] This success has prompted additional trials of selumetinib for NF1 and NF2 (NCT numbers: 01089101, 01362803, 02839720, 03259633, 03095248).

Trametinib (Mekinist, GSK1120212, JTP-74057, GlaxoSmithKline) is an allosteric, second-generation, adenosine triphosphate non-competitive reversible MEK1/2 inhibitor that also blocks Raf-dependent phosphorylation of MEK Ser218.[14] Trametinib promotes cell cycle arrest and caspase cleavage in cultured colorectal cells, and demonstrates more potent antitumor activity than other second-generation MEK inhibitors, PD0325901 and selumetinib. It is FDA approved for metastatic melanoma and is in phase I clinical trial for NF1-associated plexiform neurofibromas (NCT02124772).[18]

PD0325901 (Pfizer) is also an allosteric MEK1/2 inhibitor and is a synthetic analog of the first-generation MEK1/2 inhibitor, CI-1040.[14,19] In an *Nf1* genetically engineered mouse model, PD0325901 prolonged survival of mice with malignant peripheral nerve sheath tumors and decreased neurofibroma size in over 80% of mice.[20] Tumor regrowth was observed when treatment was suspended.[21] A phase II open-label study is ongoing for PD0325901 in NF1 (NCT02096471).[14]

Cobimetinib (XL518, GDC-0973, Cotellic, Exelixis/Genentech) is derived from methanone and was FDA approved in 2015 for use in combination with vemurafenib, a BRAF inhibitor, for advanced melanoma with *BRAF* mutations.[22,23] Cobimetinib inhibited growth of tumors with *BRAF* and *KRAS* mutations in xenograft models.[24–26] Phase I studies of cobimetinib for solid tumors reported a manageable toxicity profile with signs of efficacy in tumors with $BRAF^{V600E}$ mutations.[27] Cobimetinib is in clinical trial for pediatric and young adult patients with rasopathies, including NF2 (NCT02639546), treated previously for solid tumors.

Here, we used mouse and human merlin-deficient Schwann cell lines (MD-MSC/HSC) and animal models to evaluate the growth-inhibitory and antitumor activities of a panel of MEK inhibitors. Also, we assessed their efficacy in primary human VS with NF2 mutations.

Downloaded from https://academic.oup.com/neuro-oncology/article-abstract/21/4/486/5274482 by Medical Library 244 ED user on 10 August 2019

Materials and Methods

Cell Culture

Wild-type (WT)-MSCs and MD-MSCs were generated and characterized in 2010.[28] MD-MSCs were transduced with lentiviral luciferase as previously reported.[29] MD-schwannoma (MD-SCN) cells were derived from paraspinal schwannomas of *Periostin-Cre*:*Nf2*$^{flox2/flox2}$ mice with *Nf2* inactivation (provided by Dr Wade Clapp, Indiana University). Human Schwann cells (HSCs) were purchased from ScienCell Research Laboratories (catalog #1700, lot #7228), and the generation of a merlin-deficient HSC (MD-HSC) line using lentiviral short hairpin (sh)RNA targeting *NF2* (Sigma Mission, SHCLNV-TRCN0000237845) was previously described.[30] Cells were tested monthly for *Mycoplasma* contamination (Lookout *Mycoplasma* PCR Detection Kit, Sigma).

Mouse Model Systems

NSG (*NOD.Cg-Prkdcscid Il2rgtmlWjl/SzJ*) mice were used at 6–10 weeks of age. *P0-SCH-Δ(39–121)-27* transgenic mice[31] in the BALB/c background were used as a genetically engineered mouse (GEM) model of NF2 schwannomas. Animal use was approved by the Institutional Animal Care and Usage Committees of UCF and UCLA, and the Animal Care and Use Review Office of the United States Army Medical Research and Materiel Command.

Human VS Samples

Through an institutional review board (IRB) approved protocol, the University of Miami Tissue Bank Core Facility (UM-TBCF) consented patients undergoing surgery for brain tumors to harvest samples for research purposes. De-identified fresh human VS were obtained from UM-TBCF through an IRB-exempt protocol. Primary VS cells were prepared and cultured as previously reported.[29,30]

Drug Formulations

MEK inhibitors were purchased from MedChemExpress. Drugs were prepared in dimethyl sulfoxide (DMSO) (stock 10 mM) and diluted to final concentrations in cell culture medium for in vitro work. For animal studies, drugs were solubilized in DMSO at 50–100 mg/mL and diluted in 0.1 M citrate buffer (pH 3) for oral dosing.

Cell Viability Assays

Cells were seeded in 384-well CellBind plates (Corning) at 2000–2500 cells/well in phenol red-free growth medium. WT-MSCs were seeded at 15 000 cells/well in 96-well plates coated with poly-L-lysine (200 μg/mL) and laminin (25 μg/mL). Attached cells were treated with drug or DMSO for 48 h (mouse) or 72 h (human); viability was measured with the CellTiter-Fluor Assay (Promega). Primary human VS cells were seeded (passage 1 or 2) in 96-well plates at 10 000 cells/well. After 24 hours, cells were treated with drug or DMSO for 72 h. Crystal violet assay was performed using a SpectraMax 190 microplate reader (Molecular Devices) to assess cell number, as previously described.[29,30]

Membrane Asymmetry Assay

MD-MSCs were grown at 200 000 cells/well in 12-well CellBind plates (Corning). When at ~80% confluency, cells were treated with drug for 18–24 h, then harvested with 0.05% trypsin and resuspended in Hanks Balanced Salt Solution. The Violet Ratiometric Membrane Asymmetry Assay (Invitrogen) was used to detect apoptosis per the manufacturer's instructions. Cell populations were measured by flow cytometry (Cytoflex, Beckman Coulter) and analyzed with CytExpert software (Beckman Coulter).

Mouse Studies

For pharmacokinetic analysis, at each timepoint 3 mice received drug (1 mg/kg trametinib, 1.5 mg/kg PD0325901, or 20 mg/kg cobimetinib); one mouse received vehicle alone (0.1 M citrate, pH 3, 2% DMSO). Mice were sacrificed after 0.5–32 h; blood and sciatic nerve samples were collected and analyzed by mass spectrometry at Sanford Burnham Prebys Medical Discovery Institute (Lake Nona, Florida).

The orthotopic allograft model using luciferase-expressing MD-MSCs was generated as previously described.[29] Upon confirmation of successful grafting, mice were randomized into treatment groups and received drug or vehicle at the above concentrations daily by oral gavage. Mice were imaged weekly for bioluminescence using the In Vivo Imaging System (IVIS, Caliper) or Bruker MI Imaging System. After 13–14 days of treatment, mice were sacrificed; grafts and contralateral sciatic nerves were removed, weighed, and photographed. Grafts were fixed overnight in 4% paraformaldehyde and stored in 30% sucrose (0.02% azide in phosphate buffered saline) at 4°C. List of antibodies used is provided in Supplementary Methods.

Four-week-old *P0-SCH-Δ(39–121)-27* transgenic mice[31] were treated daily with trametinib (1 mg/kg) or vehicle (0.1 M citrate buffer pH 3, 0.2% DMSO) by oral gavage for 8 weeks. Spinal nerve roots were histopathologically scored at the endpoint as previously described.[32] Following a blind procedure, measurements of tumors and nerve root areas were performed using Zeiss Axiovision software on hematoxylin and eosin stained parasagittal sections of cervical, thoracic, lumbar, and sacral spinal cord segments. The total area of nerve root analyzed was comparable between the trametinib and vehicle-treated groups ($P = 0.1541$).

Western Blotting

Western blots were performed as previously described.[29] Protein was extracted from human VS tumors using radioimmunoprecipitation buffer with protease and phosphatase inhibitors (ThermoFisher). Human VS blots were blocked in 3% bovine serum albumin and incubated

Downloaded from https://academic.oup.com/neuro-oncology/article-abstract/21/4/486/5274482 by Medical Library 244 ED user on 10 August 2019

overnight in primary antibody solution at 4°C, followed by incubation with Alexa Fluor 488 and 647 conjugated secondary antibodies (1:200; ThermoFisher) for 2 hours at room temperature and imaged using the ImageQuant LAS 4000 Imager (GE Healthcare).

NF2 Mutation Analysis

Total DNA was extracted from fresh tumor tissues using the QIAamp DNA Mini Kit (Qiagen) and purified using the QIAquick PCR Purification Kit (Qiagen). All VS were tested for mutations within the NF2 gene with multiplex ligation-dependent probe amplification using the Salsa MLPA NF2 Kit (MRC-Holland) per the manufacturer's instructions. Copy number alterations in all 17 exons of the NF2 gene (NM_000268.3) were analyzed with Coffalyser. Additional details are provided in the Supplementary Methods.

DNA Methylation Analysis

High-throughput DNA methylation analysis was performed for 7 human VS tumors using the Infinium MethylationEPIC Kit (Illumina) according to the manufacturer's instructions. Methylation patterns were compared between VS that had a statistically significant decrease in cell number following a 72 hour incubation with 3 μM PD0325901 and those with no response. Additional details are provided in Supplementary Methods.

Proteome

Protein from cell pellets of MD-MSCs treated with trametinib or vehicle was extracted, denatured and prepared for liquid chromatography–tandem mass spectrometry (LC-MS/MS) as described in the Supplementary Methods. MS/MS spectra were searched against the *Mus Musculus* Swiss-Prot entries of the Uniprot KB (database release 2016_01, 16755 entries) using the Andromeda search engine.[33] The specific search criteria and analytics used are provided in Supplementary Methods. Protein differential expression between the trametinib and vehicle control samples was evaluated using the Limma package.[34]

Statistics

Using GraphPad Prism 6, ANOVA with Bonferroni posttest, or Kruskal–Wallis test with Dunn's comparison was applied to all in vitro data. For in vivo allograft studies, we used SAS version 9.4 to test the overall differences in median tumor weight and median fold change in flux after 14 days treatment among the 4 cohorts (vehicle treatment served as the control). Nonparametric ANOVA with Bonferroni adjustments were used to adjust for small group sample sizes and non-normal distributions. The ANOVA for the median tumor weight and median fold change in flux indicated the overall significance differences. We tested 1-tailed hypothesis of improvements. For the *P0-SCH-Δ(39–121)-27* NF2 mouse model, 2-tailed unpaired Student's *t*-test was used to compare tumor burden and sizes in the trametinib- and vehicle-treated groups.

Results

We screened selumetinib, trametinib, PD0325901, MEK162, cobimetinib, and refametinib for effectiveness in reducing viability of 9 WT and MD-MSC/HSC lines after 48-hour (mouse) and 72-hour (human) treatments. Based upon 50% inhibitory concentration (IC_{50}) values, the inhibitors were overall more effective in MSCs compared with HSCs. Maximum loss of cell viability at 10 μM observed for all inhibitors tested was ~90–95% in MD-MSCs, compared with ~60% in MD-HSCs (Fig. 1A–B). The lowest inhibitor concentration tested produced a 20–40% reduction in MD-MSC viability. MEK inhibitors promoted a dose-dependent decrease in incorporation of 5-ethynyl-2'-deoxyuridine in both MD-MSC and MD-HSC (Supplementary Fig. 1). All 6 MEK inhibitors also exhibited less selectivity between WT- and MD-HSCs compared with MSC lines (2–5 fold compared with 6–15 fold; Fig. 1A–B and Supplementary Fig. 2).

Trametinib, PD0325901, and cobimetinib were further evaluated in vitro and in an allograft mouse model because each reduced viability of both MD-MSCs and MD-HSCs with submicromolar IC_{50} values and had some selectivity in HSCs. Each drug decreased phosphorylated pERK levels in MD-MSCs at 5 and 24 hours of treatment (Fig. 2A–B, Supplementary Fig. 3). Trametinib was the most potent, as pERK was not detected in the 0.001 μM sample. Among these 3 MEK1/2 inhibitors, cobimetinib was the least effective, based on sustained reduction of pERK levels over 24 hours. Higher cobimetinib concentrations (0.3–1 μM) were required to achieve an equivalent pERK reduction observed with 0.001 μM trametinib and PD0325901. As reported in other cell types, MEK inhibition is associated with a compensatory increase in pMEK levels (Fig. 2A–B, Supplementary Fig. 3).[35] In MD-MSCs, a more robust increase in pMEK levels was observed in cells treated with cobimetinib at 5 hours and PD0325901 at 24 hours. Because trametinib uniquely blocks Raf-dependent MEK phosphorylation,[14] the lowest increase in pMEK was observed in trametinib-treated cells. MD-HSCs also exhibited decreased pERK and increased pMEK following MEK inhibition, but at higher drug concentrations compared with MD-MSCs (Supplementary Fig. 4).

An examination of downstream MEK/ERK effectors in MD-MSCs treated with these inhibitors revealed decreased levels of cyclin D1, and increased $p27^{kip1}$ and cleaved caspase 3 levels (Fig. 2C–D). Membrane asymmetry assays confirmed an increase in apoptotic cell populations from ~2% in DMSO-treated to 20% and 45% in trametinib- and cobimetinib-treated MD-MSCs, respectively (Fig. 2E, Supplementary Fig. 4).

A proteomic analysis of trametinib-treated MD-MSCs was conducted to assess global changes in protein expression. The results were consistent with effective inhibition of MEK1/2 and downstream effectors and induction of apoptotic pathways. Trametinib-treated MD-MSCs had reduced expression of Ras/Raf/MEK/ERK pathway effectors including cyclin D1 and c-Myc and increased expression of pro-apoptotic proteins such as Bcl-2 interacting protein 3 like (BNIP3L) at 24 hours, compared with DMSO control (Fig. 3A). Ingenuity Pathway Analysis identified upstream regulators whose

Downloaded from https://academic.oup.com/neuro-oncology/article-abstract/21/4/486/5274482 by Medical Library 244 ED user on 10 August 2019

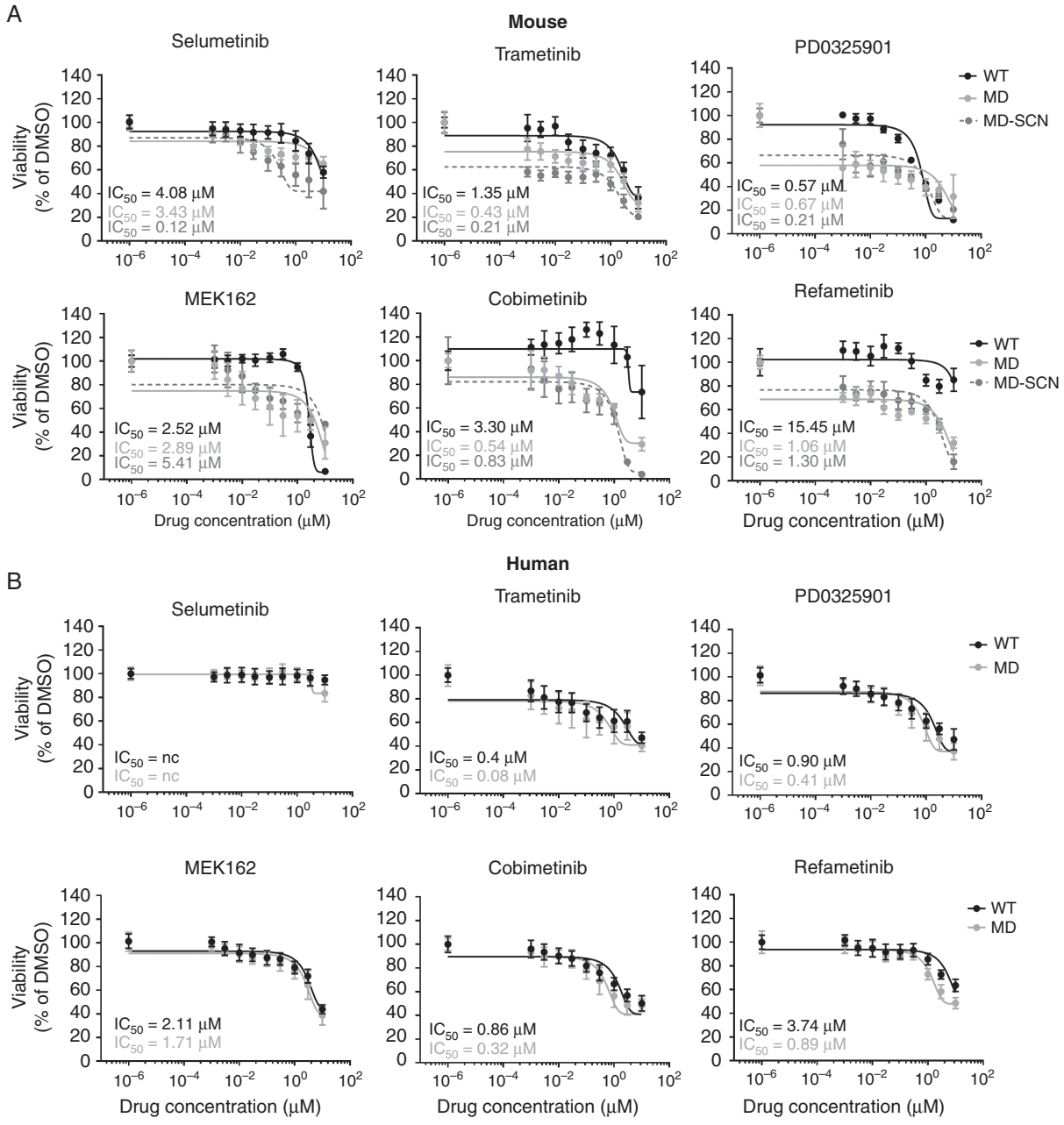

Fig. 1 MEK inhibitors reduce MD-MSC and MD-HSC viability. Screen of 6 MEK inhibitors against (A) mouse and (B) human WT and MD-SC lines treated for 48–72 h. Mean viability is plotted with IC_{50} values (n = 1–3 independent experiments; 8 replicates each).

modulation is consistent with the observed changes in protein levels. These included transforming growth factor beta (TGFβ), specificity protein 1, and p53 levels, whose levels were higher in trametinib-treated MD-MSCs compared with DMSO-treated controls (Fig. 3B–D).

To assess in vivo efficacy, we employed an orthotopic allograft model by grafting luciferase-expressing MD-MSCs into the sciatic nerves of NSG mice. Pharmacokinetic studies revealed that trametinib and cobimetinib had long $t_{1/2}$ values (~8 h and 4.8 h, respectively) and their nerve/plasma ratios increased with time (Fig. 4A). Upon confirmation of successful grafting (Supplementary Fig. 5), mice were gavaged daily for 14 days with trametinib (1 mg/ kg), PD0325901 (1.5 mg/ kg), or cobimetinib (20 mg/kg). All 3 MEK inhibitors significantly reduced the median tumor weight by 60–70% and the median fold change in flux from 0 to 14 days

Downloaded from https://academic.oup.com/neuro-oncology/article-abstract/21/4/486/5274482 by Medical Library 244 ED user on 10 August 2019

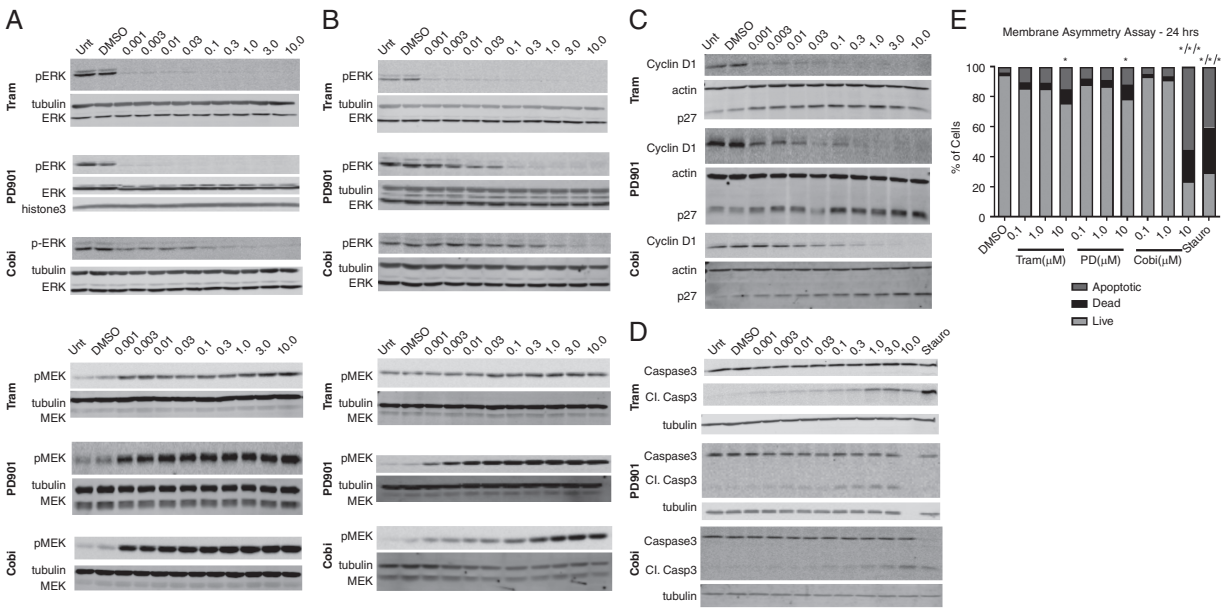

Fig. 2 MEK inhibitors promote G1 arrest and caspase-dependent apoptosis of MD-MSC in vitro. pERK1/2, pMEK1/2, cyclin D1, p27, and caspase-3 western blots of MD-MSC treated as indicated for (A) 5 h and (B-D) 24 h. All western blots are representative of 3–5 independent experiments. (E) Quantitation of membrane asymmetry assay of MD-MSC treated for 20 h with MEK inhibitors. Staurosporine (0.1 μM) served as a positive control for apoptosis ($n = 3$ independent experiments, 2-way ANOVA, $^*P < 0.05$).

by at least 80% compared with controls (Fig. 4B–D, Supplementary Fig. 6). Immunohistochemical analysis revealed that PD0325901 and cobimetinib were superior to trametinib in reducing pERK levels compared with the vehicle-treated group (Fig. 4E). Additionally, both inhibitors caused a more robust decrease in Ki-67 and cyclin D1 than trametinib, suggesting they were more potent inhibitors of graft growth in vivo. None of the inhibitors produced detectable caspase 3 cleavage nor did they affect vascularity as evidenced by CD31 staining (Fig. 4E).

Because trametinib is a well-tolerated FDA-approved drug and outperformed cobimetinib in cell assays, we assessed its efficacy in an 8-week study using the *P0-SCH-Δ(39–121)-27 NF2* schwannoma mouse model.[31,32] In this GEM model, trametinib efficacy was assessed by comparing the tumor burden, as defined by the percentage of tumor area versus total spinal nerve root area. Overall, trametinib promoted a 25% reduction in tumor burden ($P < 0.0001$) and a 37% decrease of average tumor size ($P = 0.0023$) (Fig. 5). Phosphorylated ERK immunohistochemistry of tumor samples revealed equivalent staining in trametinib- and vehicle-treated mice (data not shown), consistent with the allograft findings.

To examine the effect of MEK inhibition on human VS cells, primary cultures from 7 VS tumors were prepared and treated with PD0325901 or trametinib. All 7 VS tumors demonstrated ≥1 mutation in the *NF2* gene (Supplementary Table 1) and varying degrees of MEK1/2, pMEK, and pERK expression (Fig. 6A–B). Compared with DMSO-treated cells, trametinib (3 μM) moderately reduced cell viability of 2 of 7 VS, whereas PD0325901 (3 μM) reduced cell viability of 5 of the 7 VS tested (Fig. 6C–D). No significant correlations between viabilities and MEK1/2 and pMEK protein expression levels were identified, suggesting that drug response was independent of MEK expression.

To assess whether aberrant DNA methylation of the genome was associated with a lack of drug response, we compared methylation profiles of 2 VS with no response to PD0325901 tumors (VS27 and VS32) to the remaining 5 PD0325901-responsive tumors. In an unbiased evaluation, we identified 17 299 single cytosine-phosphate-guanine (CpG) sites with significantly different methylation levels ($P < 0.05$) between the drug responsive and nonresponsive VS. Among significant CpG sites, 4773 were hypermethylated (covering 3090 genes) and 12 526 were hypomethylated (covering 8051 genes) in the PD0325901-resistant compared with drug-sensitive VS. Supplementary Table 2 displays the top 20 hypermethylated and hypomethylated genes between the 2 groups. However, when false discovery rate (FDR) <0.05 was applied, *ELMOD1* (NM_001130037; Engulfment and cell motility domain 1) was the only gene that contained a CpG site (cg22355889) in the promoter region that was significantly hypermethylated in the PD0325901 nonresponsive VS.

Neighboring CpG sites often display closely related methylation patterns. To account for spatial correlations, we identified 34 differentially methylated regions (DMRs) with at least 5 consecutive

Downloaded from https://academic.oup.com/neuro-oncology/article-abstract/21/4/486/5274482 by Medical Library 244 ED user on 10 August 2019

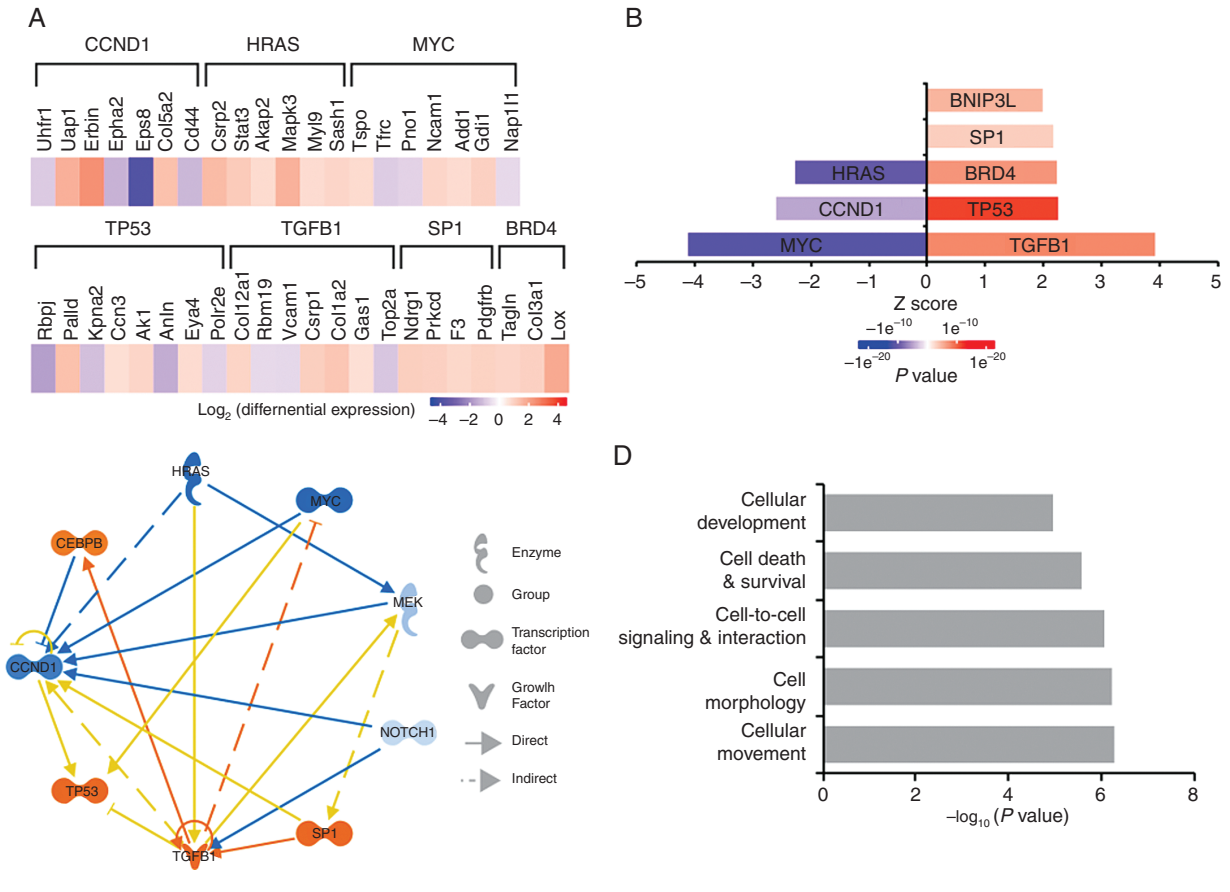

Fig. 3 Trametinib reduces signaling through Ras, Myc, and cyclin D1, and increases signaling through TP53 and TGFβ1. (A) Proteomic heat map showing differences in protein abundance in trametinib- versus DMSO-treated cells as determined by LC-MS/MS (blue: decreased expression, red: increased expression). (B) Predictions of upstream signaling pathways modulated by trametinib treatment. (C) Focus molecules and their connectivity based on Ingenuity Pathway Analysis of differentially expressed proteins in trametinib-treated versus DMSO-treated MD-MSC. (D) Differentially expressed proteins function in the indicated cellular processes ($n = 5$ replicate experiments).

hypermethylated or hypomethylated CpG loci in the PD0325901-nonresponsive compared with responsive VS (Supplementary Table 3). When examining individual DMRs, PD0325901 nonresponsive VS had DMRs in genes involved in non-MEK merlin signaling, including the *ATF6B* (activating transcription factor 6) and RXR (retinoid x receptor) genes associated with the phosphoinositide 3-kinase (PI3K/Akt) pathway and ATP6V1C1 (V-type proton ATPase subunit C1) of the mammalian target of rapamycin pathway. Gene ontology pathway analysis revealed no significant enrichment pathways for DMRs. However, when using a targeted approach assessing genes associated with merlin signaling, cancer, drug resistance, cell death, and survival, additional DMRs were identified. ARCHS4 pathway analysis revealed significant enrichment in epidermal growth factor receptor and tumor suppressor RPS6KA2 (ribosomal protein S6 kinase A2) human kinase pathways (http://amp.pharm.mssm.edu/Enrichr/. Accessed January 20, 2019).

Discussion

NF2 is a genetic disorder involving the development of multiple nervous system tumors that each impact neurological functions. Individuals affected by NF2 develop bilateral VS that cause severe hearing loss, disabling imbalance, and even life-threatening hydrocephalus from brainstem and cerebellar compression. Observation of tumor growth rate and hearing is standard as enthusiasm for microsurgical resection in NF2 is low due to consequential and irreversible limitations on nerve function and quality of life.[8] In the same respect, the long-term sequelae of utilizing radiotherapy is not so uncommon to disregard the risk of developing malignant transformation of benign tumors.[5–7,9,10] Off-label use of select FDA-approved chemotherapeutic agents for NF2 in clinical trials show moderate tumor control at best and hearing stabilization in only some NF2 patients.[36–41] However, even small effects

Downloaded from https://academic.oup.com/neuro-oncology/article-abstract/21/4/486/5274482 by Medical Library 244 ED user on 10 August 2019

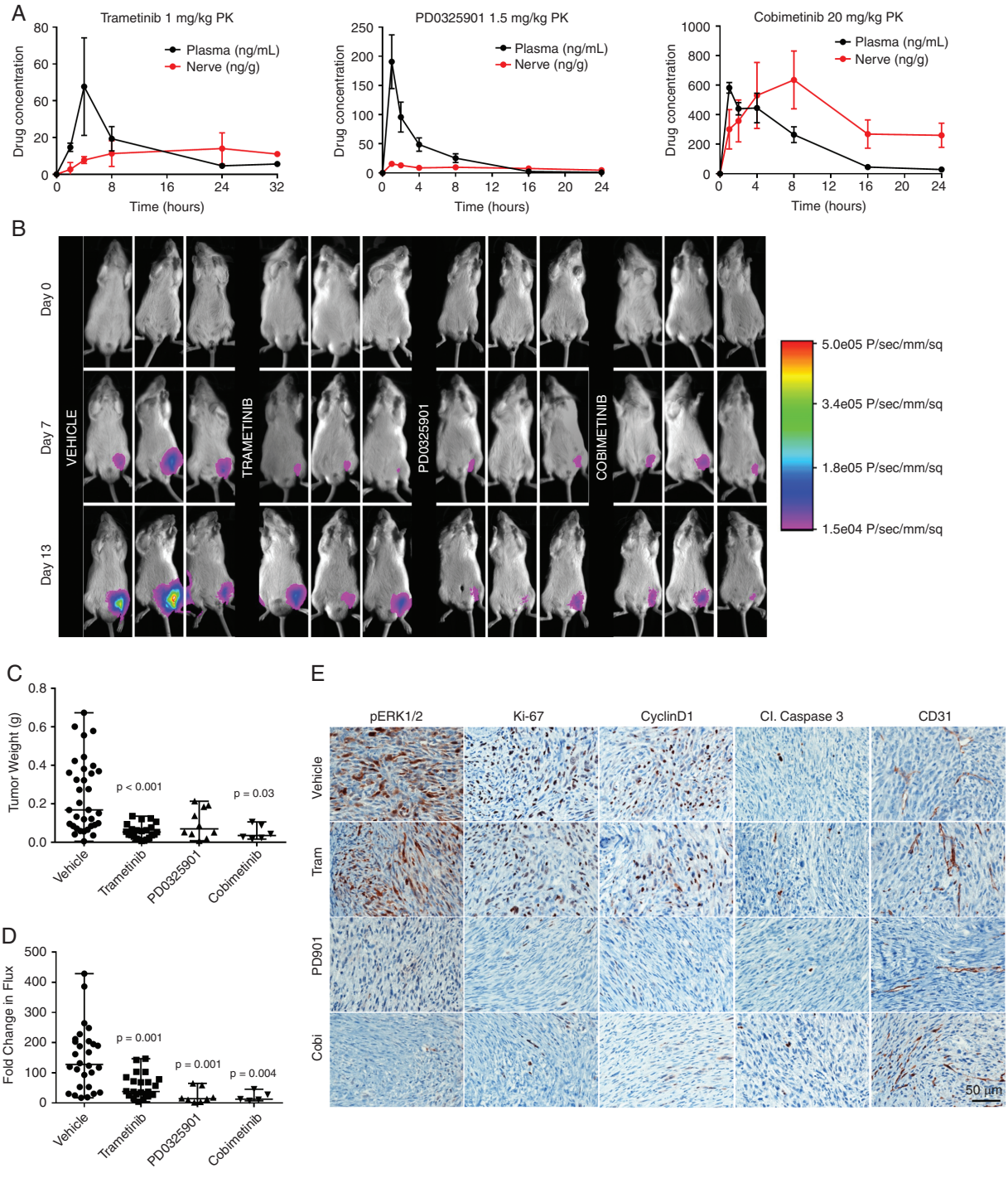

Fig. 4 MEK inhibitors slow MD-MSC growth in NSG mice. (A) Pharmacokinetic analysis for plasma and nerve following a single drug dose. (B) Representative bioluminescent (BL) images for indicated times. (C) Median tumor weights after 14 days of drug treatment compared with vehicle (n = 6–35 mice, nonparametric ANOVA). (D) BL signals were normalized to day 0 for each mouse and fold change in flux (photons/sec) after 14 days of treatment is shown (nonparametric ANOVA, median values shown). (E) Representative graft immunohistochemistry images for pERK1/2, Ki-67, cyclin D1, cleaved caspase 3, and CD31.

Downloaded from https://academic.oup.com/neuro-oncology/article-abstract/21/4/486/5274482 by Medical Library 244 ED user on 10 August 2019

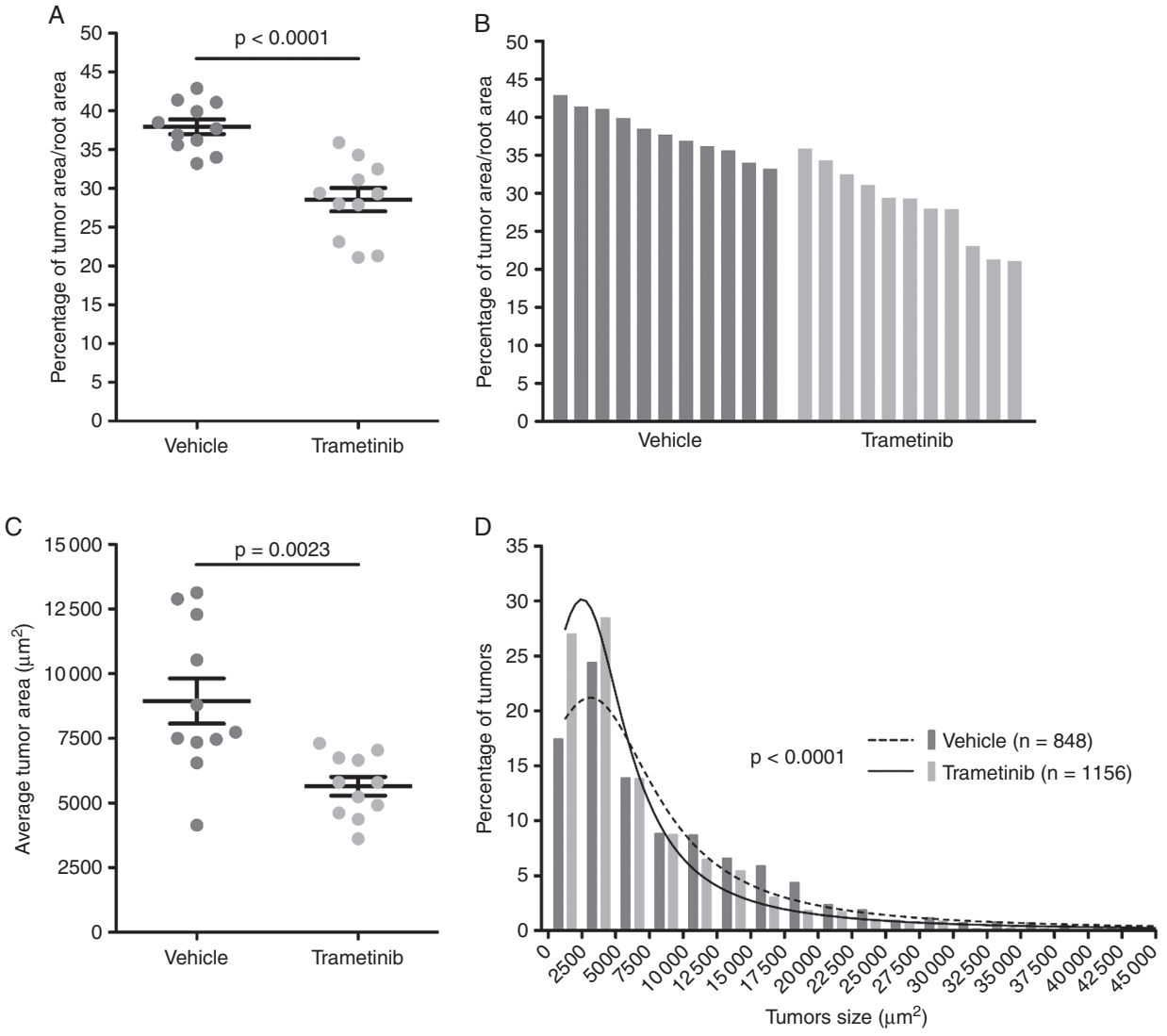

Fig. 5 Trametinib reduces schwannoma growth in the *P0-SCH-Δ(39–121)-27* NF2 mouse model. *P0-SCH-Δ(39–121)-27* mice were treated daily with trametinib (1 mg/kg, p.o., 7 d/wk) for 8 weeks starting at 4 weeks of age. (A) Reduction by 25% of the average tumor burden, calculated as percentage of tumor area versus total spinal nerve root area for trametinib-treated mice ($n = 11$) compared with vehicle-treated mice ($n = 11$). (B) Waterfall plot showing tumor burden for each vehicle- and trametinib-treated mouse. (C) Treatment with trametinib reduced average tumor size by 37% in trametinib-treated compared with vehicle-treated mice. (D) Histogram of tumor size distribution demonstrated a significantly higher percentage of smaller tumors in trametinib-treated ($n = 1156$ tumors) compared with vehicle-treated ($n = 848$ tumors) mice.

can impact survival and quality of life in individual NF2 patients. Therefore, the discovery of effective NF2 drug therapies is critical.

Currently, 2 clinical trials are enrolling pediatric NF2 patients to test effectiveness of selumetinib and cobimetinib in reducing tumor volume and preserving hearing (NCT03095248 and NCT02639546). However, the preclinical efficacies for selumetinib and cobimetinib have not been established. These trials are supported by knowledge that merlin loss is associated with increased mitogen-activated protein kinase signaling, and[42] success of selumetinib in shrinking plexiform neurofibromas in NF1 children.[15] Our study is the first to evaluate a panel of MEK inhibitors in mouse and human NF2 schwannoma models.

Of the 6 inhibitors screened against multiple mouse and human SC lines, trametinib, PD0325901, and cobimetinib reduced MD-SC viability at submicromolar IC_{50} values and were the most effective in non-immortalized human MD-SCs (Fig. 1A). Notably, selumetinib was the least effective in MD-HSCs and was not a top performer in MD-MSCs (based on maximum effect and IC_{50} values). In vitro, trametinib, PD0325901, and cobimetinib reduced pERK levels, modulated cyclin D1 and p27 levels in a manner consistent with a G_1/S cell cycle arrest, and induced caspase-dependent apoptosis in MD-MSCs. The proteomic study conducted in

Downloaded from https://academic.oup.com/neuro-oncology/article-abstract/21/4/486/5274482 by Medical Library 244 ED user on 10 August 2019

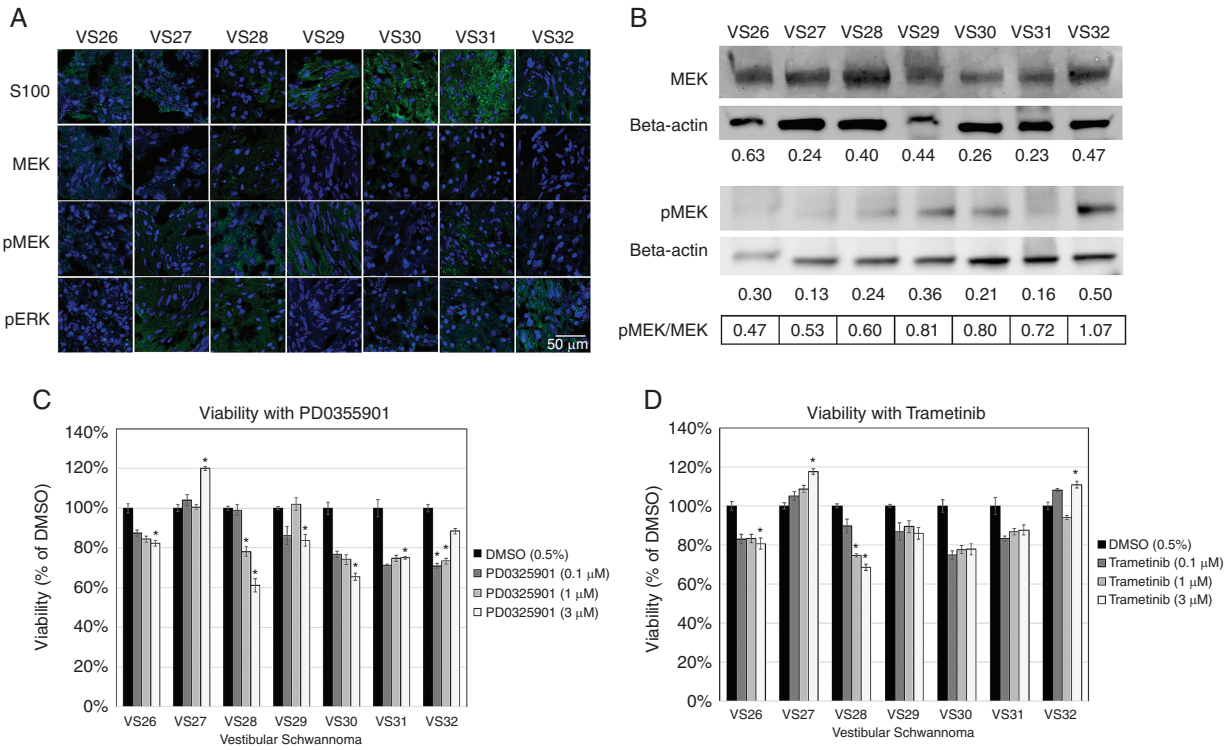

Fig. 6 MEK inhibitors reduce viability of a subset of primary human VS cells. (A) Immunohistochemistry shows S100 positivity and variable expression levels of MEK, pMEK, and pERK (green) in VS tumors (4′,6′-diamidino-2-phenylindole nuclear stain, blue). (B) Western blots demonstrate expression of MEK and pMEK for VS with beta-actin as the standard. Relative expression levels of MEK and pMEK were displayed and expressed as a ratio of pMEK/MEK. (C–D) Cell viability assays for PD0325901 and trametinib were performed and viability was normalized to 0.5% DMSO controls.

trametinib-treated MD-MSC further corroborated this conclusion by revealing decreased signaling in the Ras-ERK-cyclin D1 pathway and increased signaling from BNIP3L, a pro-apoptotic subfamily in the Bcl-2 family of proteins.

We used 2 in vivo models to evaluate drug efficacy: a 2-week treatment protocol aimed at slowing growth of established MD-MSCs nerve grafts in NSG mice, and an 8-week chemoprevention protocol aimed at preventing appearance of schwannomas in a GEM model. In the nerve grafts, PD0325901 and cobimetinib produced a stronger reduction in MD-MSC growth compared with trametinib, likely from persistent inhibition of pERK, cyclin D1, and Ki-67 levels.Trametinib did not significantly decrease pERK, cyclin D1 and Ki-67 levels in allografts at the study endpoint when compared with vehicle-treated controls, supporting the conclusion that cells in the allografts were developing resistance to trametinib. Similar responses to trametinib were obtained with the GEM model. Although the number and size of schwannomas were reduced in the GEM model following 8 weeks of trametinib treatment, immunohistochemically, pERK levels in trametinib-treated schwannomas were equivalent to controls. An adaptive response to trametinib has been reported in triple-negative breast cancer.[43] Trametinib treatment resulted in degradation of c-Myc and in assembly of bromodomain containing 4 (BRD4)-containing transcriptional enhancers on promoters of adaptive response genes, resulting in activation of compensatory pathways associated with drug resistance.[43] Our proteomic analysis similarly revealed decreased c-Myc levels and increased BRD4 levels in MD-MSCs treated with trametinib (Fig. 3). BRD4 in trametinib-induced adaptive response promoter complexes can be displaced by treatment with bromodomain and extraterminal domain family (BET) bromodomain inhibitors.[44] A study of BET bromodomain inhibitors in ovarian cancer revealed reduced activation of ERK, Akt, and Src kinase following treatment, suggesting that these pathways may be activated by bromodomain-containing transcriptional enhancers.[45] Additionally, BET family bromodomains were involved in reactivation of the Src/focal adhesion kinase pathway in breast cancer cells following inhibition of ErbB2 with lapatinib.[46] Collectively, these studies suggest that trametinib treatment may promote assembly of BRD-containing transcriptional enhancers that can activate compensatory proliferative pathways. Future studies examining the effects of bromodomain and Src inhibitors in combination with MEK inhibitors are warranted.

Of the 7 primary human VS cultures tested, only a subset responded to either PD0325901 or trametinib by reducing cell viability by 15–40% of controls. Although the trend of response to both drugs was similar within individual VS cultures, the differing response rate to the drugs was

Downloaded from https://academic.oup.com/neuro-oncology/article-abstract/21/4/486/5274482 by Medical Library 244 ED user on 10 August 2019

71% versus 29%, respectively, and did not correlate with baseline MEK or pMEK expression (Fig. 6A–D). The differing response rate can be attributed to the 10-fold higher potency of cobimetinib compared with PD0325901 (Fig. 6C–D).[18,19] VS cells also demonstrated a large variety of *NF2* mutations, which can have differential effects on merlin-dependent cell proliferation and survival pathways. Methylome exploration identified *ELMOD1* as the single gene with a hypermethylated promoter and an FDR <0.05 in nonresponsive VS compared with responsive VS. ELMOD1 is a GTPase activator for small GTPases in the ADP ribosylation factor (Arf) and Arf-like families (Arl2). In PD0325901 nonresponsive VS, a hypermethylated promoter in *ELMOD1* is expected to reduce ELMOD1 expression, increase Arl2 activity, and alter normal microtubule dynamics.[47] This may allow VS cells to circumvent traditional mechanisms of cell cycle arrest and cell death.[47] Further investigation into how tumor heterogeneity in NF2 contributes to drug resistance and disease progression is imperative for identifying treatment modalities to overcome resistance to MEK inhibition.

We present a comprehensive preclinical analysis of MEK inhibitors in mouse and human NF2 schwannoma models and primary human VS. Although differences in response were observed between drugs, species, and models, our cumulative results support MEK inhibitors for the treatment of a subset of NF2 schwannomas. We demonstrate that differences in treatment response to MEK inhibitors depends on genetic and epigenetic differences between tumors that can impact downstream merlin signaling, drug resistance mechanisms, and adaptive pathways to evade cell death or arrest. By understanding the mechanisms of drug response and resistance to MEK inhibitors in individual tumors, we can identify optimal combination therapies to maximize tumor control, determine important genetic and molecular biomarkers to predict patient outcomes, and develop precision medicine algorithms for NF2 treatment.

Supplementary Material

Supplementary data are available at *Neuro-Oncology* online.

Keywords

merlin tumor suppressor | methylome | NF2 transgenic mice | MEK inhibitors | patient-derived vestibular schwannomas

Funding

This work was supported by Department of Defense Congressionally Directed Medical Research Program (W81XWH-15-1-0446 to CFV and W81XWH-16-1-0104 to LSC), National Institutes of Health/National Institute on Deafness and Other Communication Disorders (R0-DC005575 and R01-DC012115 to XZL), and the Children's Tumor Foundation with contracts to CFV and MAF.

Acknowledgments

We thank Drs Jacques Morcos and Michael Ivan for their efforts harvesting human VS tumors and patients for donated tumor samples. We acknowledge Anthony Griswold, PhD, Division Head of the Center for Genetic Epidemiology and Statistical Genetics at the University of Miami Miller School of Medicine, for bioinformatics and statistical analysis of DNA methylation experiments.

Conflict of interest statement. CFV is a named inventor on unrelated patents. MG and JV receive research funding from Recursion Pharmaceuticals. Other authors report that no conflicts of interest exist.

Authorship statement. *Designed experiments*: CFV, MCF, MAF, JV, MG, JK and CTD. *Supervised work:* CFV, CTD, MG, HM, and LSC. *Cell and allograft studies*: MAF, SKP, JN, KB, AP, MCF. *Human VS work*: CTD, OB, RM, DY, XL, FT, JIY. *GEM model*: MG, JV. *Proteome analysis*: AC, JK, TM, HM. *Histology*: LSC, RS, JH. *Flow cytometry analysis*: AJC. *Statistical analysis*: JNS. CFV, MAF and LSC wrote the initial draft and all authors edited the manuscript.

Portions of Figs. 1, 3, and 5 were presented at the annual Neurofibromatosis Conference in Washington DC in June 2017.

References

1. Rouleau GA, Merel P, Lutchman M, et al. Alteration in a new gene encoding a putative membrane-organizing protein causes neuro-fibromatosis type 2. *Nature*. 1993;363(6429):515–521.
2. Trofatter JA, MacCollin MM, Rutter JL, et al. A novel moesin-, ezrin-, radixin-like gene is a candidate for the neurofibromatosis 2 tumor suppressor. *Cell*. 1993;72(5):791–800.
3. Evans DG. Neurofibromatosis type 2 (NF2): a clinical and molecular review. *Orphanet J Rare Dis*. 2009;4:16.
4. Blakeley JO, Evans DG, Adler J, et al. Consensus recommendations for current treatments and accelerating clinical trials for patients with neurofibromatosis type 2. *Am J Med Genet A*. 2012;158A(1):24–41.
5. Chung LK, Nguyen TP, Sheppard JP, et al. A systematic review of radiosurgery versus surgery for neurofibromatosis type 2 vestibular schwannomas. *World Neurosurg*. 2018;109:47–58.
6. Evans DG, Birch JM, Ramsden RT, Sharif S, Baser ME. Malignant transformation and new primary tumours after therapeutic radiation for benign disease: substantial risks in certain tumour prone syndromes. *J Med Genet*. 2006;43(4):289–294.
7. Kim BS, Seol HJ, Lee JI, et al. Clinical outcome of neurofibromatosis type 2-related vestibular schwannoma: treatment strategies and challenges. *Neurosurg Rev*. 2016;39(4):643–653.

Downloaded from https://academic.oup.com/neuro-oncology/article-abstract/21/4/486/5274482 by Medical Library 244 ED user on 10 August 2019

8. Nowak A, Dziedzic T, Czernicki T, et al. Strategy for the surgical treatment of vestibular schwannomas in patients with neurofibromatosis type 2. *Neurol Neurochir Pol*. 2015;49(5):295–301.
9. Seferis C, Torrens M, Paraskevopoulou C, Psichidis G. Malignant transformation in vestibular schwannoma: report of a single case, literature search, and debate. *J Neurosurg*. 2014;121(Suppl):160–166.
10. Sun S, Liu A. Long-term follow-up studies of Gamma Knife surgery for patients with neurofibromatosis type 2. *J Neurosurg*. 2014;121(Suppl):143–149.
11. Hilton DA, Ristic N, Hanemann CO. Activation of ERK, AKT and JNK signalling pathways in human schwannomas in situ. *Histopathology*. 2009;55(6):744–749.
12. Morrison H, Sperka T, Manent J, Giovannini M, Ponta H, Herrlich P. Merlin/neurofibromatosis type 2 suppresses growth by inhibiting the activation of Ras and Rac. *Cancer Res*. 2007;67(2):520–527.
13. Petrilli AM, Fernández-Valle C. Role of merlin/NF2 inactivation in tumor biology. *Oncogene*. 2016;35(5):537–548.
14. McDermott L, Qin C. Allosteric MEK1/2 inhibitors for the treatment of cancer: an overview. *J Drug Res Dev*. 2015;1:1–9. doi: 10.16966/jdrd.101.
15. Dombi E, Baldwin A, Marcus LJ, et al. Activity of selumetinib in neurofibromatosis type 1–related plexiform neurofibromas. *N Engl J Med*. 2016;375(26):2550–2560.
16. Ammoun S, Schmid MC, Ristic N, et al. The role of insulin-like growth factors signaling in merlin-deficient human schwannomas. *Glia*. 2012;60(11):1721–1733.
17. Ammoun S, Schmid MC, Triner J, Manley P, Hanemann CO. Nilotinib alone or in combination with selumetinib is a drug candidate for neurofibromatosis type 2. *Neuro Oncol*. 2011;13(7):759–766.
18. Yamaguchi T, Kakefuda R, Tajima N, Sowa Y, Sakai T. Antitumor activities of JTP-74057 (GSK1120212), a novel MEK1/2 inhibitor, on colorectal cancer cell lines in vitro and in vivo. *Int J Oncol*. 2011;39(1):23–31.
19. Barrett SD, Bridges AJ, Dudley DT, et al. The discovery of the benzhydroxamate MEK inhibitors CI-1040 and PD 0325901. *Bioorg Med Chem Lett*. 2008;18(24):6501–6504.
20. Jessen WJ, Miller SJ, Jousma E, et al. MEK inhibition exhibits efficacy in human and mouse neurofibromatosis tumors. *J Clin Invest*. 2013;123(1):340–347.
21. Jousma E, Rizvi TA, Wu J, et al. Preclinical assessments of the MEK inhibitor PD-0325901 in a mouse model of Neurofibromatosis type 1. *Pediatr Blood Cancer*. 2015;62(10):1709–1716.
22. Signorelli J, Shah Gandhi A. Cobimetinib. *Ann Pharmacother*. 2017;51(2):146–153.
23. Wong H, Vernillet L, Peterson A, et al. Bridging the gap between preclinical and clinical studies using pharmacokinetic-pharmacodynamic modeling: an analysis of GDC-0973, a MEK inhibitor. *Clin Cancer Res*. 2012;18(11):3090–3099.
24. Choo EF, Ng CM, Berry L, et al. PK-PD modeling of combination efficacy effect from administration of the MEK inhibitor GDC-0973 and PI3K inhibitor GDC-0941 in A2058 xenografts. *Cancer Chemother Pharmacol*. 2013;71(1):133–143.
25. Hoeflich KP, Merchant M, Orr C, et al. Intermittent administration of MEK inhibitor GDC-0973 plus PI3K inhibitor GDC-0941 triggers robust apoptosis and tumor growth inhibition. *Cancer Res*. 2012;72(1):210–219.
26. Rice KD, Aay N, Anand NK, et al. Novel carboxamide-based allosteric MEK inhibitors: discovery and optimization efforts toward XL518 (GDC-0973). *ACS Med Chem Lett*. 2012;3(5):416–421.
27. Rosen LS, LoRusso P, Ma WW, et al. A first-in-human phase I study to evaluate the MEK1/2 inhibitor, cobimetinib, administered daily in patients with advanced solid tumors. *Invest New Drugs*. 2016;34(5):604–613.
28. Petrilli AM, Fuse MA, Donnan MS, et al. A chemical biology approach identified PI3K as a potential therapeutic target for neurofibromatosis type 2. *Am J Transl Res*. 2014;6(5):471–493.
29. Fuse MA, Plati SK, Burns SS, et al. Combination therapy with c-Met and Src inhibitors induces caspase-dependent apoptosis of merlin-deficient schwann cells and suppresses growth of schwannoma cells. *Mol Cancer Ther*. 2017;16(11):2387–2398.
30. Petrilli AM, Garcia J, Bott M, et al. Ponatinib promotes a G1 cell-cycle arrest of merlin/NF2-deficient human schwann cells. *Oncotarget*. 2017;8(19):31666–31681.
31. Giovannini M, Robanus-Maandag E, Niwa-Kawakita M, et al. Schwann cell hyperplasia and tumors in transgenic mice expressing a naturally occurring mutant NF2 protein. *Genes Dev*. 1999;13(8):978–986.
32. Giovannini M, Bonne NX, Vitte J, et al. mTORC1 inhibition delays growth of neurofibromatosis type 2 schwannoma. *Neuro Oncol*. 2014;16(4):493–504.
33. Cox J, Neuhauser N, Michalski A, Scheltema RA, Olsen JV, Mann M. Andromeda: a peptide search engine integrated into the MaxQuant environment. *J Proteome Res*. 2011;10(4):1794–1805.
34. Smyth GK, Michaud J, Scott HS. Use of within-array replicate spots for assessing differential expression in microarray experiments. *Bioinformatics*. 2005;21(9):2067–2075.
35. Gilmartin AG, Bleam MR, Groy A, et al. GSK1120212 (JTP-74057) is an inhibitor of MEK activity and activation with favorable pharmacokinetic properties for sustained in vivo pathway inhibition. *Clin Cancer Res*. 2011;17(5):989–1000.
36. Blakeley JO, Plotkin SR. Therapeutic advances for the tumors associated with neurofibromatosis type 1, type 2, and schwannomatosis. *Neuro Oncol*. 2016;18(5):624–638.
37. Goutagny S, Raymond E, Esposito-Farese M, et al. Phase II study of mTORC1 inhibition by everolimus in neurofibromatosis type 2 patients with growing vestibular schwannomas. *J Neurooncol*. 2015;122(2):313–320.
38. Karajannis MA, Legault G, Hagiwara M, et al. Phase II trial of lapatinib in adult and pediatric patients with neurofibromatosis type 2 and progressive vestibular schwannomas. *Neuro Oncol*. 2012;14(9):1163–1170.
39. Karajannis MA, Legault G, Hagiwara M, et al. Phase II study of everolimus in children and adults with neurofibromatosis type 2 and progressive vestibular schwannomas. *Neuro Oncol*. 2014;16(2):292–297.
40. Plotkin SR, Halpin C, McKenna MJ, Loeffler JS, Batchelor TT, Barker FG 2nd. Erlotinib for progressive vestibular schwannoma in neurofibromatosis 2 patients. *Otol Neurotol*. 2010;31(7):1135–1143.
41. Plotkin SR, Merker VL, Halpin C, et al. Bevacizumab for progressive vestibular schwannoma in neurofibromatosis type 2: a retrospective review of 31 patients. *Otol Neurotol*. 2012;33(6):1046–1052.
42. Yi C, Troutman S, Fera D, et al. A tight junction-associated merlin-angiomotin complex mediates merlin's regulation of mitogenic signaling and tumor suppressive functions. *Cancer Cell*. 2011;19(4):527–540.
43. Bevill SM, Zawistowski JS, Johnson GL. Enhancer remodeling regulates epigenetic adaptation and resistance to MEK1/2 inhibition in triple-negative breast cancer. *Mol Cell Oncol*. 2017;4(6):e1300622.
44. Zawistowski JS, Bevill SM, Goulet DR, et al. Enhancer remodeling during adaptive bypass to MEK inhibition is attenuated by pharmacologic targeting of the P-TEFb complex. *Cancer Discov*. 2017;7(3):302–321.
45. Kurimchak AM, Shelton C, Duncan KE, et al. Resistance to BET bromodomain inhibitors is mediated by kinome reprogramming in ovarian cancer. *Cell Rep*. 2016;16(5):1273–1286.
46. Stuhlmiller TJ, Miller SM, Zawistowski JS, et al. Inhibition of lapatinib-induced kinome reprogramming in ERBB2-positive breast cancer by targeting BET family bromodomains. *Cell Rep*. 2015;11(3):390–404.
47. Zhou C, Cunningham L, Marcus AI, Li Y, Kahn RA. Arl2 and Arl3 regulate different microtubule-dependent processes. *Mol Biol Cell*. 2006;17(5):2476–2487.

Downloaded from https://academic.oup.com/neuro-oncology/article-abstract/21/4/486/5274482 by Medical Library 244 ED user on 10 August 2019

Published OnlineFirst December 17, 2019; DOI: 10.1158/1535-7163.MCT-19-0809

Targeting Protein Translation by Rocaglamide and Didesmethylrocaglamide to Treat MPNST and Other Sarcomas

Long-Sheng Chang[1,2,3,4], Janet L. Oblinger[1,2], Sarah S. Burns[1,2], Jie Huang[1,2], Larry W. Anderson[5], Melinda G. Hollingshead[5], Rulong Shen[4], Li Pan[6], Garima Agarwal[6], Yulin Ren[6], Ryan D. Roberts[1,2], Barry R. O'Keefe[5,7], A. Douglas Kinghorn[6], and Jerry M. Collins[5]

ABSTRACT

Malignant peripheral nerve sheath tumors (MPNST) frequently overexpress eukaryotic initiation factor 4F components, and the eIF4A inhibitor silvestrol potently suppresses MPNST growth. However, silvestrol has suboptimal drug-like properties, including a bulky structure, poor oral bioavailability (<2%), sensitivity to MDR1 efflux, and pulmonary toxicity in dogs. We compared ten silvestrol-related rocaglates lacking the dioxanyl ring and found that didesmethylrocaglamide (DDR) and rocaglamide (Roc) had growth-inhibitory activity comparable with silvestrol. Structure–activity relationship analysis revealed that the dioxanyl ring present in silvestrol was dispensable for, but may enhance, cytotoxicity. Both DDR and Roc arrested MPNST cells at G_2–M, increased the sub-G_1 population, induced cleavage of caspases and PARP, and elevated the levels of the DNA-damage response marker γH2A.X, while decreasing the expression of AKT and ERK1/2, consistent with translation inhibition. Unlike silvestrol, DDR and Roc were not sensitive to MDR1 inhibition. Pharmacokinetic analysis confirmed that Roc had 50% oral bioavailability. Importantly, Roc, when administered intraperitoneally or orally, showed potent antitumor effects in an orthotopic MPNST mouse model and did not induce pulmonary toxicity in dogs as found with silvestrol. Treated tumors displayed degenerative changes and had more cleaved caspase-3–positive cells, indicative of increased apoptosis. Furthermore, Roc effectively suppressed the growth of osteosarcoma, Ewing sarcoma, and rhabdomyosarcoma cells and patient-derived xenografts. Both Roc- and DDR-treated sarcoma cells showed decreased levels of multiple oncogenic kinases, including insulin-like growth factor-1 receptor. The more favorable drug-like properties of DDR and Roc and the potent antitumor activity of Roc suggest that these rocaglamides could become viable treatments for MPNST and other sarcomas.

Introduction

Malignant peripheral nerve sheath tumors (MPNST) are characterized as aggressive soft-tissue sarcomas with a high risk of recurrence and metastasis. Often refractory to current treatment, patients with these tumors have a poor 5-year survival rate of only about 20% to 50% (1). Therefore, development of a more effective medical therapy that eradicates MPNSTs is of significant clinical need. MPNSTs can occur sporadically or arise from preexisting plexiform neurofibromas in patients with neurofibromatosis type 1 (NF1), a tumor predisposition syndrome caused by mutations in the *NF1* gene which encodes the Ras-GTPase–activating protein neurofibromin. Importantly, even sporadic tumors frequently harbor mutations in the *NF1* gene or the Ras pathway. Consequently, both sporadic and NF1-associated MPNSTs exhibit upregulation of Ras downstream kinase signaling, including the PI3K–AKT–mTOR and Raf–MEK–ERK mitogen-activated protein kinases. MPNSTs also exhibit overexpression or aberrant activation of epidermal growth factor receptor (EGFR), platelet-derived growth factor receptor (PDGFR), and insulin-like growth factor-1 receptor (IGF-1R; refs. 2, 3). These reports suggest that these Ras downstream kinases and deregulated receptor tyrosine kinases (RTKs) may be therapeutic targets. In addition, recurrent mutations in the tumor-suppressor genes *CDKN2A* and *TP53* and the subunits of the chromatin-modifying polycomb repressor complex-2 (PRC2), *SUZ12* and *EED*, have been identified and are important for MPNST progression (4). Inactivation of *CDKN2A* and *TP53* disables the G_1–S checkpoint. The loss of PRC2 function can lead to enhanced Ras-driven gene transcription (5).

As MPNSTs often exhibit hyperactive Ras activity, statins and farnesyl transferase inhibitors, which prevent localization of Ras to the membrane and inhibit MPNST cell growth (6, 7), have been evaluated but do not improve survival in patients with advanced cancer (8–10). Drugs that target the deregulated RTKs and mitogenic kinases have also been investigated in patients with MPNSTs; however, the results have so far been disappointing. The EGFR inhibitor erlotinib elicited poor response rates in MPNSTs with only 1 of 20 patients exhibiting stable disease (11). The IGF-1R–blocking

[1]Center for Childhood Cancer and Blood Diseases, Abigail Wexner Research Institute, Nationwide Children's Hospital, Columbus, Ohio. [2]Department of Pediatrics, The Ohio State University College of Medicine, Columbus, Ohio. [3]Department of Otolaryngology-Head and Neck Surgery, The Ohio State University College of Medicine, Columbus, Ohio. [4]Department of Pathology, The Ohio State University College of Medicine, Columbus, Ohio. [5]Division of Cancer Treatment and Diagnosis, Center for Cancer Research, National Cancer Institute, NIH, Frederick, Maryland. [6]Division of Medicinal Chemistry and Pharmacognosy, The Ohio State University College of Pharmacy, Columbus, Ohio. [7]Molecular Targets Program, Center for Cancer Research, National Cancer Institute, NIH, Frederick, Maryland.

Note: Supplementary data for this article are available at Molecular Cancer Therapeutics Online (http://mct.aacrjournals.org/).

Corresponding Author: Long-Sheng Chang, Center for Childhood Cancer and Blood Diseases, Abigail Wexner Research Institute at Nationwide Children's Hospital and The Ohio State University College of Medicine, 700 Children's Drive, Columbus, OH 43205. Phone: 614-355-2658; Fax: 614-722-5895; E-mail: lchang@chi.osu.edu

Mol Cancer Ther 2020;19:731–41

doi: 10.1158/1535-7163.MCT-19-0809

©2019 American Association for Cancer Research.

Downloaded from mct.aacrjournals.org on May 28, 2020. © 2020 American Association for Cancer Research.

Published OnlineFirst December 17, 2019; DOI: 10.1158/1535-7163.MCT-19-0809

antibodies, such as ganitumab, show limited objective single-agent activity (12). Sorafenib, which inhibits Raf and several RTKs, has only minimal activity in patients with sarcomas (13). The mTOR inhibitor rapamycin and its derivatives, such as everolimus, cause cytostatic responses and are being evaluated in combination with other targeted drugs. However, a recent trial showed that combination of everolimus with bevacizumab, a monoclonal antibody that binds VEGF and prevents activation of the RTK VEGF receptor, was not effective in patients with refractory MPNSTs (14). A phase II study is ongoing to evaluate the dual mTOR complexes 1 and 2 inhibitor TAK-228 in soft-tissue sarcomas (https://clinicaltrials.gov Identifier: NCT02987959). Collectively, the modest and transient patient responses from the completed trials indicate that targeting more than one critical pathway is likely needed to achieve a cure.

To sustain uncontrolled growth, cancer cells commonly exhibit enhanced protein translation by upregulation of the translation machinery (15). The most highly regulated step in the protein biosynthetic pathway occurs during translation initiation, in which the eukaryotic initiation factor 4F (eIF4F) complex is recruited to the 5′ untranslated region (5′-UTR) of mRNA. This complex is composed of three subunits: eIF4G, a scaffolding protein; eIF4E, a cap-binding protein; and eIF4A, an RNA helicase which unwinds the secondary structure of the 5′-UTR. We have shown overexpression of the three eIF4F components in multiple types of human cancer, including MPNST (16, 17). Genetic inhibition of eIF4A and eIF4E using short-hairpin RNAs reduces MPNST cell proliferation. In addition, the prosurvival and progrowth activities of several signaling pathways, such as PI3K–AKT–mTOR and Raf–MEK–ERK frequently activated in human cancer, occur in part by facilitating eIF4F-mediated translation initiation. The mTOR kinase phosphorylates and inactivates the eIF4E-binding protein translational repressors (18). Both AKT and ERKs phosphorylate eIF4B, which then associates with and increases the helicase activity of eIF4A (19). Moreover, AKT, mTOR, and the downstream ERK1/2 kinase, p90 ribosomal S6 kinase, can phosphorylate and inactivate an endogenous repressor of eIF4A activity, the programmed cell death 4 protein. Further, the mRNAs that depend upon eIF4A for efficient translation usually contain long 5′-UTRs with guanine-rich sequences termed G-quadruplexes which can form four-stranded structures with G-tetrads stacked on one another (15). These eIF4A-dependent transcripts are often found in genes encoding oncoproteins, transcription factors associated with super enhancers, epigenetic regulators, and kinases (20). Interestingly, we found that the eIF4A inhibitor silvestrol suppresses MPNST cell growth at low nanomolar of IC_{50}, decreases the levels of multiple mitogenic kinases including AKT and ERKs, and profoundly impairs the growth of MPNST xenografts (16). These results suggest that direct targeting of the translation initiation components, particularly eIF4A, might be an effective treatment strategy for these tumors.

Silvestrol is part of a large family of compounds termed flavaglines or rocaglates, which share a cyclopenta[*b*]benzofuran structure (21, 22). It possesses potent antitumor activity in multiple other cancer models (23–25). However, silvestrol has some suboptimal drug-like properties. It is relatively large with a bulky dioxanyl ring, making the total synthesis of silvestrol laborious (26–28). It is a substrate for the multidrug resistance 1 (MDR1) transporter (29) and has very limited oral bioavailability of <2% (30).

To search for compounds with better drug-like properties, we analyzed ten rocaglates that lack the dioxanyl moiety and examined the structure–activity relationships for this compound class. We showed that two of these compounds, rocaglamide (Roc) and didesmethylrocaglamide (DDR), exhibited potent growth inhibitory activity with IC_{50} values comparable to silvestrol. Importantly, these rocaglamides were not sensitive to MDR1 inhibition, and Roc exhibited oral bioavailability and potent antitumor effects against multiple types of sarcomas.

Materials and Methods

Natural compounds

Ten silvestrol-related rocaglates, inclusive of (−)-didesmethylrocaglamide, were isolated from the tropical plant *Aglaia perviridis*, collected in Vietnam as part of a multi-institutional collaborative project on the discovery of new antineoplastic natural compounds. The full structures and absolute configurations of these rocaglates were determined (31). For *in vitro* studies, purified silvestrol and related rocaglates were dissolved as a 10 mmol/L stock in DMSO (Sigma-Aldrich). A 60-mg sample of (−)-rocaglamide (NSC326408) was prepared at the U.S. National Cancer Institute for *in vivo* studies.

Cell lines, cell proliferation assays, and flow cytometry

Various MPNST, Ewing sarcoma, osteosarcoma, rhabdomyosarcoma, schwannoma, meningioma, and leukemia cell lines used in this study are described in Supplementary Methods. All cell lines were authenticated by short tandem repeat genotyping and tested to be mycoplasma-free. Cell proliferation was assessed using resazurin assays, and cell-cycle analysis was performed as previously described (32).

Western blots

Subconfluent cells were treated with the indicated doses of Roc or DDR for 1 to 3 days and lysed. Equal amounts of protein lysates were analyzed by immunoblotting. Detailed procedures and the antibodies used are described in Supplementary Methods.

Pharmacokinetic analysis

Mice were administered with a 5 mg/kg dose of Roc by i.v. or i.p. injection or by oral gavage (p.o.). Blood samples were collected before and at multiple time-points after dosing ($n = 3$). Plasma concentrations of Roc were analyzed using a sensitive LC/MS-MS (Supplementary Methods).

Cell line–derived xenograft and patient-derived xenograft models and *in vivo* efficacy

All animal work was performed according to the protocols approved by the Institutional Animal Care and Use Committee at Nationwide Children's Hospital. For animal dosing, Roc was formulated in 30% hydroxypropyl-β-cyclodextrin (HPβCD). The quantifiable, orthotopic MPNST cell line–derived xenograft (CDX) model was generated as described previously (33). Mice bearing established ST8814-Luc tumors (16) were randomized into three groups ($n = 10$/group) and treated with the predetermined MTD of Roc at 4 mg/kg by i.p. or 1.2 mg/kg by oral gavage, or the vehicle HPβCD every other day. Tumor growth was measured weekly by bioluminescence imaging (BLI).

To generate patient-derived xenograft (PDX) models, the Nationwide Children's Hospital Institutional Review Board approved the Human Subjects Protocol. After obtaining informed written consents from the subjects, tumor specimens were used to establish PDX models. Mice with actively growing PDX tumors for a Ewing sarcoma (NCH-EWS-2), an osteosarcoma (NCH-OS-7), and an alveolar rhabdomyosarcoma (NCH-ARMS-2) reaching approximately 100 to 200 mm^3 were randomized into two treatment groups ($n = 10$/group) for each PDX model and treated with 3 mg/kg of Roc or HPβCD by i.p.

Downloaded from mct.aacrjournals.org on May 28, 2020. © 2020 American Association for Cancer Research.

Published OnlineFirst December 17, 2019; DOI: 10.1158/1535-7163.MCT-19-0809

every other day, followed by tumor measurement twice weekly (Supplementary Methods).

Immunohistochemistry

Sections from Roc or vehicle-treated MPNST tumors were prepared and stained with hematoxylin and eosin (H&E) or immunostained for p-histone H3(Ser^{10}) (pH3; ab32107, Abcam) or CC3 (#9664, Cell Signaling Technology) as previously described (32).

Results

DDR and Roc possess potent growth-inhibitory activity comparable with silvestrol

To search for compounds with better drug-like properties, we side-by-side compared ten rocaglates lacking the dioxanyl ring (31) with silvestrol for growth-inhibitory activity in a panel of MPNST, schwannoma, and meningioma cell lines, which we previously showed to be sensitive to the antiproliferative action of silvestrol (16, 17). We found that several of these rocaglates maintained potent growth inhibition comparable with silvestrol. In particular, the IC_{50} values of Roc were slightly higher than silvestrol, whereas DDR reliably demonstrated approximately 2-fold more potent than silvestrol in all cell lines tested (**Fig. 1**; **Table 1**; and Supplementary Fig. S1), indicating that the dioxanyl moiety is dispensable for cytotoxicity. Further structure–activity comparison discerned some positions on the cyclopenta[*b*]benzofuran scaffold that affected the antiproliferative activity of rocaglates. Similar to previous observations, the substitution of a methoxy group at position 8b, as in 8b-*O*-methylrocaglaol versus rocaglaol, abolished the activity (**Fig. 1**). This methoxy substitution at 8b could be partly mitigated by the addition of a methylenedioxy ring to phenyl ring B. In addition, the presence of amide or ester groups at position C-2 of the benzofuran scaffold appeared to enhance the activity, as compounds such as DDR, Roc, and methyl rocaglate were more potent than rocaglaol. Because the amide group at the C-2 position confers superior growth inhibition, we further evaluated DDR and Roc for their mechanisms of action.

Rocaglamides induce G_2–M arrest and cell death

Flow cytometry analysis revealed that human *NF1*-expressing STS26T and *NF1*-null ST8814 MPNST cells treated with one- or

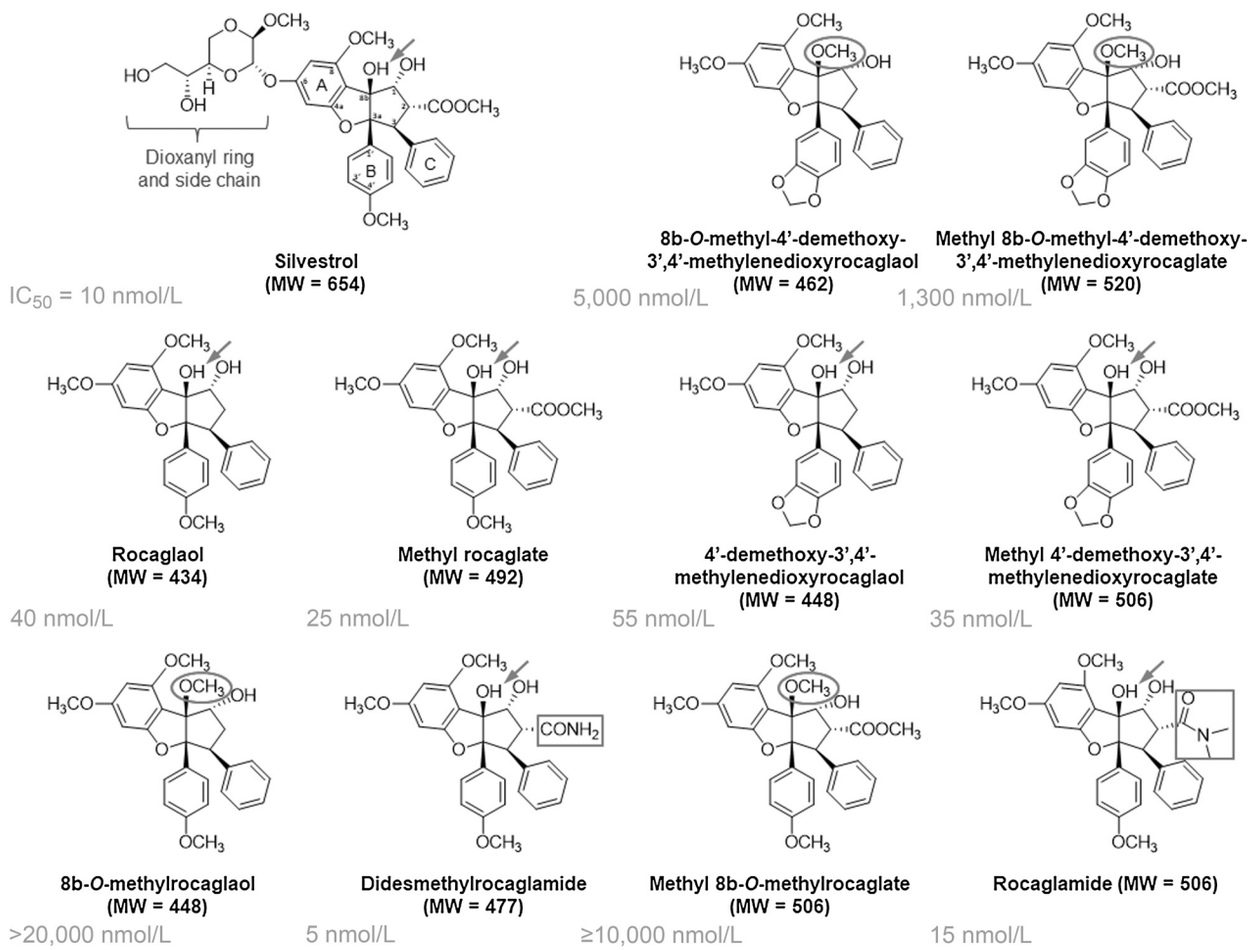

Figure 1.

Identification of DDR and Roc with potent growth-inhibitory activity comparable with silvestrol. The structure of each rocaglate is shown along with its IC_{50} value in STS26T MPNST cells as determined in **Table 1**. Structure–activity comparison revealed that the dioxanyl (dioxanyloxy) ring is dispensable but may enhance the cytotoxicity of rocaglates. An unmethylated C-8b hydroxyl group (arrow) and the amide functionality (rectangle) of DDR and Roc are important for optimum antiproliferative activity, whereas methylation of the C-8b hydroxyl group (oval) substantially impaired the activity.

Downloaded from mct.aacrjournals.org on May 28, 2020. © 2020 American Association for Cancer Research.

Published OnlineFirst December 17, 2019; DOI: 10.1158/1535-7163.MCT-19-0809

Table 1. The growth-inhibitory activity of silvestrol and 10 related rocaglates lacking the dioxanyl ring in *NF1*$^{+/+}$ STS26T and *NF1*$^{-/-}$ ST8814 MPNST, *Nf2*$^{-/-}$ schwannoma, and *NF2*$^{-/-}$ meningioma cells.

Compound	MW (Da)	IC_{50} (nmol/L) Sch10545 *Nf2*$^{-/-}$ schwannoma cells	Ben-Men-1 *NF2*$^{-/-}$ meningioma cells	STS26T *NF1*$^{+/+}$ MPNST cells	ST8814 *NF1*$^{-/-}$ MPNST cells
Silvestrol	654	70	10	10	40
8b-*O*-methyl-4′-demethoxy-3′,4′-methylenedioxyrocaglaol	462	>2,500	>2,500	5,000	10,000
Methyl 8b-*O*-methyl-4′-demethoxy-3′,4′-methylenedioxyrocaglate	520	1,900	3,800	1,300	2,000
Rocaglaol	434	60	100	40	90
Methyl rocaglate	492	50	55	25	35
4′-demethoxy-3′,4′-methylenedioxyrocaglaol	448	65	85	55	120
Methyl 4′-demethoxy-3′,4′-methylenedioxyrocaglate	506	60	80	35	70
8b-*O*-methylrocaglaol	448	>20,000	>20,000	>20,000	>20,000
Didesmethylrocaglamide	477	10	5	5	5
Methyl 8b-*O*-methylrocaglate	506	9,300	>10,000	>10,000	>20,000
Rocaglamide	506	ND	15	15	20

Note: The average IC_{50} value of each rocaglate was determined by 3-day resazurin proliferation assays as described in Materials and Methods. Didesmethylrocaglamide and rocaglamide were found to possess growth-inhibitory activity similar to or more potent than silvestrol.
Abbreviation: ND, not determined.

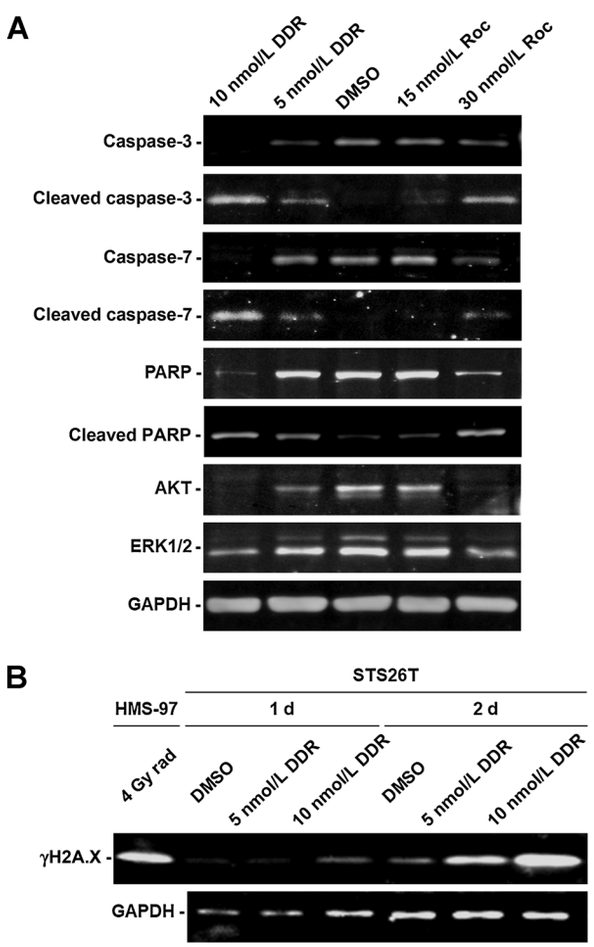

two-IC_{50} doses of DDR or Roc for 3 days exhibited a marked increase in the G_2–M fraction (Supplementary Fig. S2A and S2B). The sub-G_1 fraction, suggestive of apoptosis, was noticeably prominent in treated STS26T cells, especially at the two-IC_{50} dose (Supplementary Fig. S2A). Phase contrast micrographs taken of cells prior to cell-cycle analysis showed increased floating dead cells and debris in DDR- or Roc-treated dishes. Although ST8814 cells treated for 3 days did not show obvious signs of cell death (Supplementary Fig. S2B), a 6-day incubation resulted in increased numbers of floating dead cells with a commensurate expansion of the sub-G_1 fraction (Supplementary Fig. S2C). Collectively, these results indicate that, like silvestrol (16), DDR and Roc inhibit MPNST cell proliferation by inducing cell-cycle arrest at G_2–M and subsequently, cell death.

DDR and Roc increase caspase and PARP cleavage and activate the DNA damage response, while suppressing mitogenic signaling pathways

To confirm induction of apoptosis in Roc-treated MPNST cells, we analyzed protein expression of several markers important for this process. STS26T cells treated for 3 days with either DDR or Roc exhibited increased cleavage of the executioner caspases-3 and 7 and their downstream substrate PARP (**Fig. 2A**). A concomitant decrease in the amounts of intact

Figure 2.
DDR and Roc increase caspase and PARP cleavage and elevate the levels of γH2A.X while decreasing AKT and ERK expression in MPNST cells. **A,** Protein lysates prepared from STS26T cells treated for 3 days with 1- or 2-IC_{50} of DDR or Roc were analyzed by Western blots for full-length and cleaved caspase-3/7 and PARP, as well as AKT and ERK1/2. GAPDH served as a loading control. **B,** Protein lysates from STS26T cells treated for 1 and 2 days with 1- or 2-IC_{50} of DDR were probed for the expression of phosphorylated H2A.X (γH2A.X). As a positive control, lysates from HMS-97 human malignant schwannoma cells irradiated with 4 grays (Gy) of X-ray (rad) were used.

Downloaded from mct.aacrjournals.org on May 28, 2020. © 2020 American Association for Cancer Research.

Published OnlineFirst December 17, 2019; DOI: 10.1158/1535-7163.MCT-19-0809

caspases 3 and 7 and PARP was observed, consistent with the enhanced cleavage of these apoptotic markers and possibly due to direct effects of these rocaglamides on protein translation. Likewise, the levels of the prosurvival kinases AKT and ERK1/2 were diminished in Roc- and DDR-treated MPNST cells. Importantly, treatment with rocaglamides also resulted in higher levels of the DNA damage response marker γH2A.X. This increase occurred as early as one day after DDR treatment before the occurrence of cell death (**Fig. 2B**). Similarly, cleavage of caspase-3 and PARP and induction of γH2A.X were also detected in *NF1*-null ST8814 cells treated with DDR and Roc (Supplementary Fig. S3). These results demonstrate that DDR and Roc induce apoptosis in both *NF1*-expressing and *NF1*-deficient MPNST cells, possibly subsequent to the activation of the DNA damage response.

Rocaglamides are not sensitive to MDR1 inhibition, and Roc is orally bioavailable

The MDR1/P-glycoprotein (Pgp) encoded by the *ABCB1* (ATP-binding cassette subfamily B member 1) gene is implicated in limiting the bioavailability of several chemotherapeutics and confers drug resistance in tumors that overexpress this protein. Silvestrol is a substrate of MDR1/Pgp, which may be related to its poor oral bioavailability (29, 30). To determine whether there are any differences in the sensitivity to MDR1/Pgp between rocaglamides and silvestrol, we treated silvestrol-resistant 697-R leukemic cells, which overexpress MDR1/Pgp (Supplementary Fig. S4), and the parental silvestrol-sensitive 697 cells with various concentrations of each compound. Similar to previous findings (29), we found that 697-R cells were less sensitive to silvestrol inhibition than 697 cells (26 vs. 3.5 nmol/L of $IC_{50,}$ respectively; **Fig. 3A**). Surprisingly, DDR- and Roc-treated 697-R

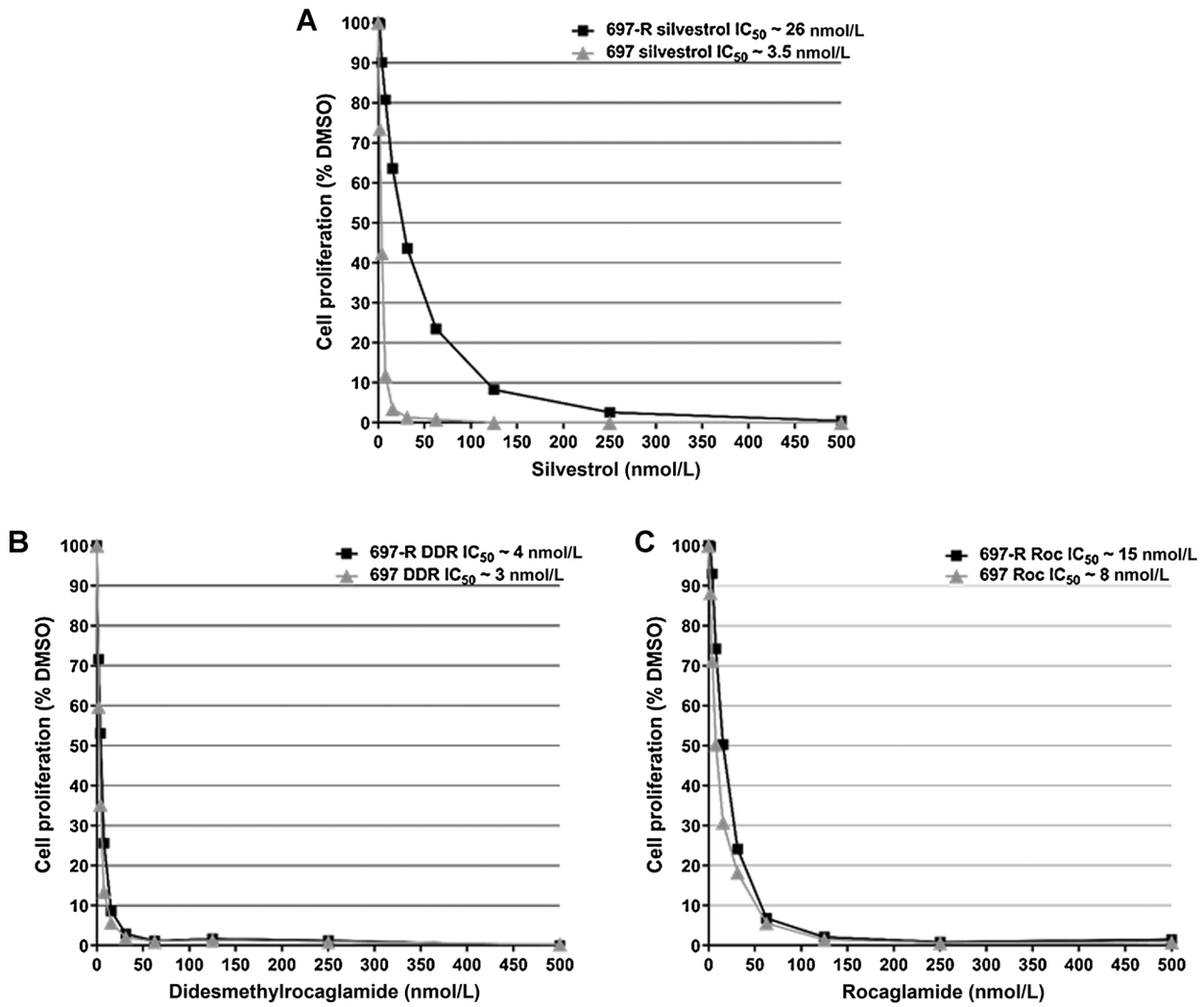

Figure 3.

Unlike silvestrol, DDR and Roc inhibit proliferation of MDR1-overexpressing 697-R leukemic cells at IC_{50} values similar to parental 697 cells. Cell proliferation was measured on 697-R and 697 cells treated for 3 days with various concentrations of silvestrol (**A**), DDR (**B**), and Roc (**C**). Each treatment was performed in six replicates, and each experiment was repeated twice. Shown are representative dose–response growth inhibition curves for all three drugs from experiments run in parallel. The insets show the IC_{50} values for each compound.

Downloaded from mct.aacrjournals.org on May 28, 2020. © 2020 American Association for Cancer Research.

Published OnlineFirst December 17, 2019; DOI: 10.1158/1535-7163.MCT-19-0809

cells exhibited IC_{50} values very similar to those of parental 697 cells (4 vs. 3 nmol/L of IC_{50}, respectively, for DDR and 15 vs. 8 nmol/L of IC_{50}, respectively, for Roc; **Fig. 3B** and **C**). Also, we observed that various MPNST cell lines expressed different levels of MDR1 protein (Supplementary Fig. S4). For example, ST8814 cells expressed a higher level of MDR1 than STS26T cells. Curiously, both cell lines showed similar sensitivity to growth inhibition by DDR and Roc (**Table 1**; Supplementary Fig. S1). Together, these results indicate that these rocaglamides are no longer sensitive to MDR1 inhibition.

To examine the oral bioavailability, we conducted pharmacokinetic (PK) studies to compare mice that had been dosed with Roc at 5 mg/kg via the i.v., i.p., or p.o. route, followed by measuring Roc concentrations in blood samples collected at various times post dosing. Two separate studies with 3 mice at each time point for each dosing route were conducted. The maximum mean observed concentration (C_{max}) reached approximately 11 μmol/L for the i.v. route, approximately 4 μmol/L for the i.p. route, and approximately 0.8 μmol/L for the p.o. route (**Fig. 4A**). Areas under the plasma concentration-time curves (AUC_{0-7h}) produced 245 μmol/L*min of exposure in the i.v. route and 142 μmol/L*min of exposure in the p.o. route. The concentrations of Roc appeared to decline more slowly in the plasma over 24 hours ($T_{½}$ = 2.4h) with the p.o. route compared with those dosed by the i.v. route ($T_{½}$ = 1.5h). Based on the estimation from AUC_{0-7h}, Roc exhibited approximately 50% oral bioavailability, confirming improved bioavailability of Roc over silvestrol.

Roc, when administered intraperitoneally or orally, exhibits potent antitumor effects in an orthotopic MPNST model

To evaluate the *in vivo* activity of Roc, we treated NSG mice bearing luciferase-expressing ST8814-Luc tumors implanted in the sciatic

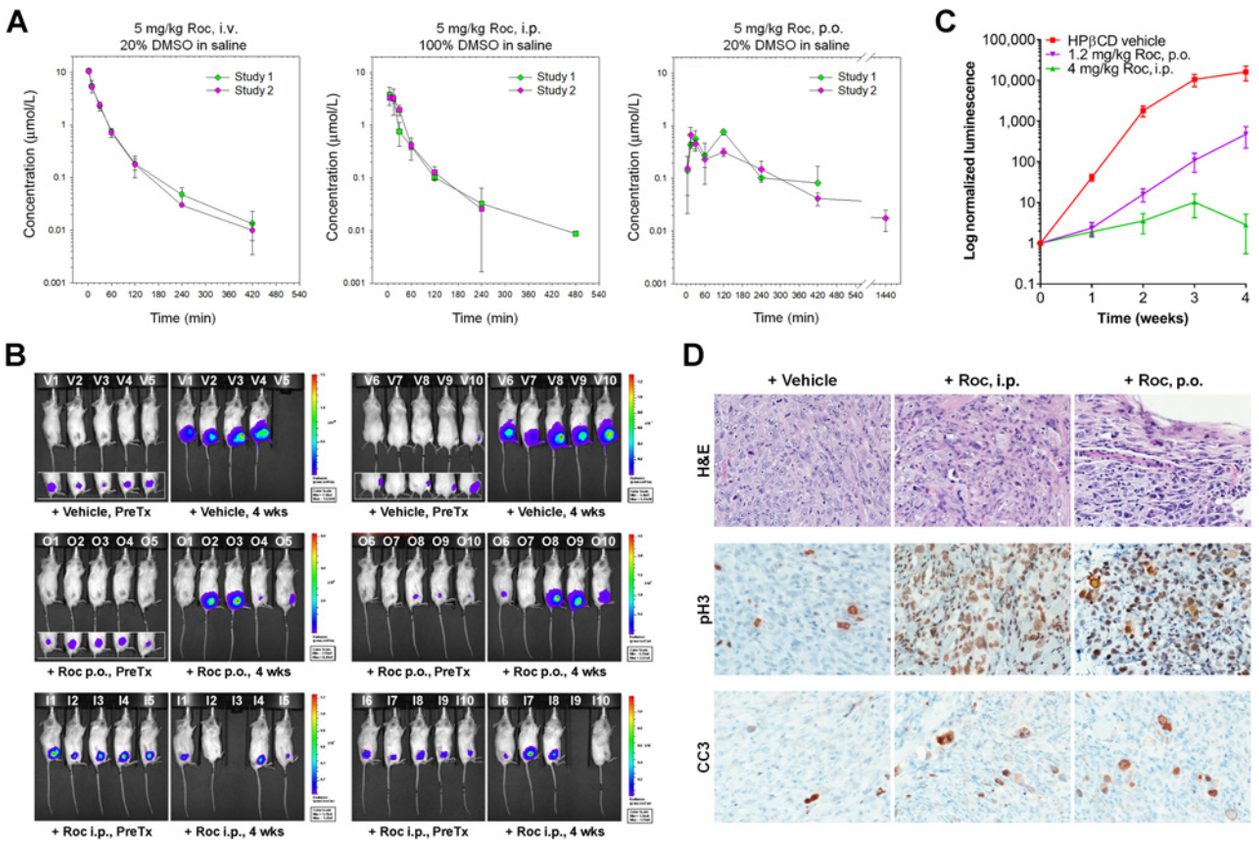

Figure 4.

Roc has 50% oral bioavailability and potently suppresses the growth of orthotopic MPNST xenografts. **A,** Plasma concentration-time profiles of Roc were obtained by PK analysis according to Materials and Methods. The mean concentration of Roc with SD in mouse plasma for each time point after i.v., i.p., and p.o. administration was plotted. For each dosing route, two independent studies were performed. **B,** Shown are representative BL images of ST8814-Luc MPNST-bearing mice prior to (PreTx) and 4 weeks (wks) after treatment with Roc at 4 mg/kg by i.p., 1.2 mg/kg by p.o., or HPβCD vehicle every other day. **C,** The relative tumor-emitted BL signals were denoted as percentage of total flux after treatment relative to the total flux prior to treatment designated as one (100%). The data are shown as mean ± SD. For each treatment group, at least 7 mice completed the full treatment schedule. Note that tumor bioluminescence from vehicle-treated mice rapidly increased by an average of approximately 17,000-fold over 4 weeks. However, tumor bioluminescence from the Roc i.p. group grew only by approximately 3-fold and from the Roc p.o. group increased approximately 470-fold on average. **D,** H&E staining shows that although vehicle-treated xenografts contained large vesicular nuclei with prominent nucleoli and mitotic activity, tumors treated with Roc by i.p. had pleomorphic nuclei, and many enlarged tumor cells had abundant foamy cytoplasm resembling histiocytoid degenerative changes along with scattered apoptosis (top panels). Degenerative tumor cells were also present in tumors treated with orally delivered Roc. Tumor necrosis with necrotic debris separating mostly degenerative tumor cells with viable vasculature was also observed. Immunostaining revealed abundant phospho-histone H3 (pH3)–labeled cells in Roc-treated tumors compared with vehicle-treated tumors (middle panels). Increased numbers of cleaved caspase-3 (CC3)–positive cells were detected in Roc-treated tumors (bottom panels).

Downloaded from mct.aacrjournals.org on May 28, 2020. © 2020 American Association for Cancer Research.

Published OnlineFirst December 17, 2019; DOI: 10.1158/1535-7163.MCT-19-0809

nerve with Roc at the predetermined MTD (4 mg/kg by i.p. or 1.2 mg/kg orally), or HPβCD vehicle every other day. As shown in **Fig. 4B** and **C**, tumor bioluminescence from vehicle-treated mice steadily and rapidly increased by >10,000-fold over 4-week treatment. In contrast, tumor bioluminescence from mice treated with Roc by i.p. only increased by an average of <10-fold, showing >99% reduction in tumor luminescence compared with controls. Similarly, Roc, when administered orally, also exhibited potent tumor inhibition with bioluminescence decreasing by >95%. In addition, we did not observe any significant changes in body weight of animals treated with the indicated doses of Roc, compared with vehicle-treated controls (Supplementary Fig. S5).

Histologic analysis revealed that although MPNSTs treated with HPβCD vehicle for 4 weeks had large nuclei with prominent nucleoli and displayed active mitotic figures (**Fig. 4D**, top left panel), tumors treated with Roc by i.p. had pleomorphic nuclei with abundant foamy cytoplasm resembling histiocytoid degenerative changes (top middle panel). A few enlarged tumor cells with multinucleated appearance and scattered apoptosis were present. Degenerative changes and cell death were also observed in tumors treated with orally delivered Roc (top right panel). Consistent with G_2–M arrest, tumor cells treated with i.p. or orally delivered Roc exhibited much higher prevalence of phospho-histone H3 labeling compared with vehicle-treated tumors (middle panel). In addition, Roc-treated tumors displayed increased numbers of cleaved caspase-3–positive cells which often coincided with those with multinucleated-like appearance (bottom panel). Taken together, these results indicate that Roc has oral bioavailability and possesses potent *in vivo* efficacy against MPNSTs.

Roc and DDR have broad antitumor activity against common types of pediatric sarcoma

Because MPNSTs comprise only approximately 2% of all sarcomas (34), we expanded our testing of Roc and DDR to three other types of sarcomas more prevalently seen in children and young adults: Ewing sarcoma, osteosarcoma, and rhabdomyosarcoma. Using a series of commonly used cell lines, including two Ewing sarcoma cell lines (A673 and TC32), four osteosarcoma cell lines (143B, MG-63, Saos2, and OS17), and one rhabdomyosarcoma cell line (RD), we showed that, as in MPNST cells, both rocaglamides were highly active against all of these sarcoma cell lines (Supplementary Fig. S6A–S6C). Also, we observed that DDR consistently exhibited lower IC_{50} values than Roc in every sarcoma cell line tested.

Subsequently, we evaluated the *in vivo* activity of Roc using PDX models for a Ewing sarcoma, an osteosarcoma, and an alveolar rhabdomyosarcoma. We discovered that Roc was highly potent in suppressing the growth of Ewing sarcoma PDXs and inhibited tumor growth by an average of approximately 90% over 4-week treatment (**Fig. 5A**). Similarly, the average size of Roc-treated osteosarcoma PDX tumors was reduced by approximately 80% compared with those of vehicle-treated tumors (**Fig. 5B**). Also, Roc inhibited the growth of rhabdomyosarcoma PDXs by approximately 70% (**Fig. 5C**). Notably, the volumes of tumors in individual Roc-treated mice showed very little overlap with those in

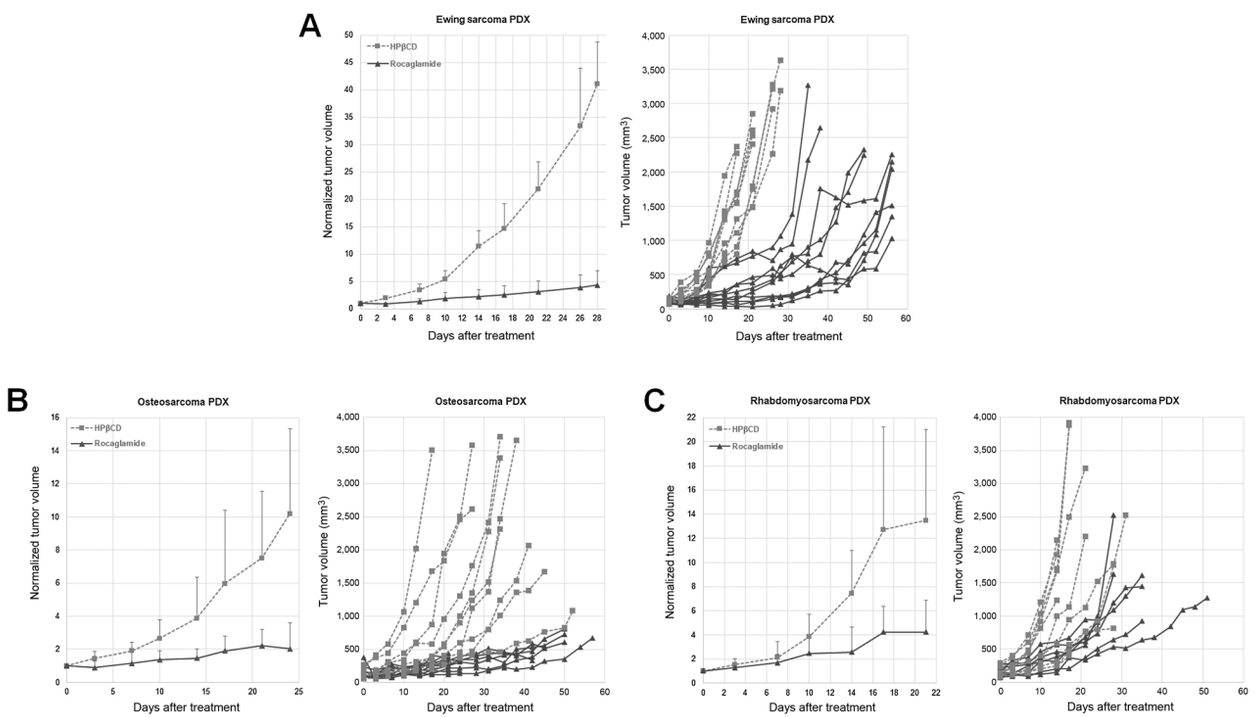

Figure 5.

Roc exhibits potent antitumor effects in multiple sarcoma PDX models. Mice with growing Ewing sarcoma (**A**), osteosarcoma (**B**), and rhabdomyosarcoma (**C**) PDXs were treated with 3 mg/kg of Roc or HPβCD vehicle by i.p. every other day. Tumor diameters were measured twice weekly, and volumes calculated according to Materials and Methods. The normalized tumor volume, denoted as the ratio of the calculated tumor volume after treatment relative to the volume prior to treatment designated as one, was plotted as the mean tumor volume of the entire treatment group at each time point with SD (left panels). The calculated tumor volume for each individual mouse over time was also plotted (right panels).

Downloaded from mct.aacrjournals.org on May 28, 2020. © 2020 American Association for Cancer Research.

Published OnlineFirst December 17, 2019; DOI: 10.1158/1535-7163.MCT-19-0809

vehicle-treated mice, particularly for the Ewing sarcoma and osteosarcoma PDX models (**Fig. 5**). Together with the findings from the MPNST model, these results demonstrate that Roc displays significant antitumor effects against multiple types of sarcoma.

Rocaglamides decrease multiple signaling kinases and transcription factors important for sarcoma cell growth

To further examine the molecular mechanisms underlying the antiproliferative effects of rocaglamides, we treated TC32 Ewing sarcoma, 143B osteosarcoma, and RD rhabdomyosarcoma cells with one- or two-IC_{50} dose of DDR or Roc for 1 to 2 days followed by Western blotting for several known drivers of cell survival and proliferation. Interestingly, we found that these rocaglamides reliably reduced the levels of the β subunit of IGF-1R, an upstream activator of PI3K–AKT signaling, in all three sarcoma cell lines (**Fig. 6A–C**). We also observed reduction of the IGF-1Rβ levels in Roc-treated MPNST cells (Supplementary Fig. S7). In addition, both rocaglamides decreased the levels of AKT, ERKs, cyclin D1 and survivin in treated TC32, 143B, and RD cells (**Fig. 6**). Intriguingly, the oncogenic fusion protein EWS-FLI1, which acts as an aberrant transcription factor in Ewing sarcoma (35), was not affected in Roc- and DDR-treated TC32 Ewing sarcoma cells (**Fig. 6A**). Consistent with this observation, these rocaglamides did not inhibit EWS expression in 143B osteosarcoma and RD rhabdomyosarcoma cells (**Fig. 6B** and **C**). However, the levels of lysine demethylase 1 (LSD1), which modulates EWS-FLI1 transcriptional activity (36), and NKX2.2, an EWS-FL11–regulated gene necessary for oncogenic transformation (37), were diminished by these rocaglamides in TC32 cells (**Fig. 6A**). Collectively, these results suggest that rocaglamides potently suppress sarcoma growth by decreasing multiple key signaling proteins important for tumor growth and survival.

Comparative toxicology studies in canines show that Roc does not induce pulmonary toxicity found with silvestrol

As the next part of the standard process for developing compounds as candidates for human evaluation, a toxicology study in dogs was conducted through a contractor of the NCI Experimental Therapeutics program. Unexpectedly, silvestrol was found to cause massive lung damage, whereas Roc did not produce adverse pulmonary findings when tested on the same protocol at the same lab. Further details are contained in the online summary reports for both silvestrol and Roc at https://dtp.cancer.gov/publications/silvestrol_rocaglamide_studies.pdf.

Discussion

For decades, treatments for MPNSTs and other sarcomas have remained largely unchanged with current standard of care combining surgical resection with intensive multiagent chemotherapy (1, 34, 38, 39). Radiation may be used depending upon the tumor type and clinical presentation. Although this multidisciplinary treatment strategy may help local control, it is not effective for metastatic and recurrent disease. Also, these multimodal regimens are associated with considerable acute and long-term toxicities that affect patients' quality of life. Despite recent advances in understanding tumor biology and targeted therapy development, an FDA-approved medical therapy for the treatment of these malignancies is still not available. We previously showed that eIF4A is a vulnerable point of disruption in MPNSTs and that the eIF4A inhibitor silvestrol potently suppresses MPNST growth (16). Regretfully, silvestrol exhibited an unexpected

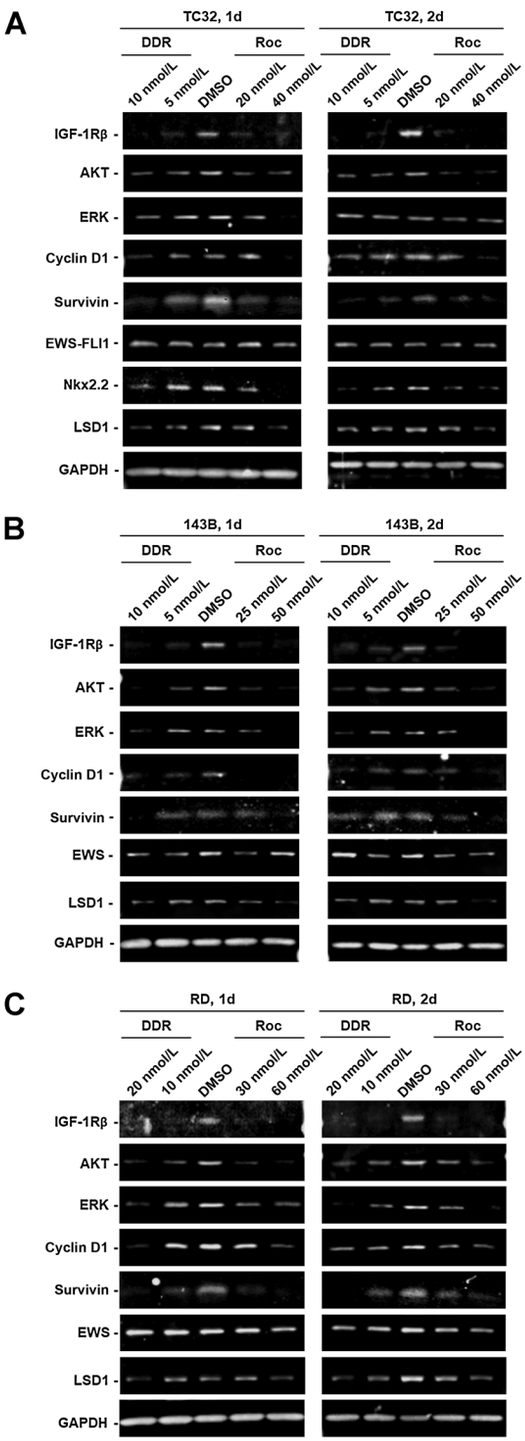

Figure 6.

DDR and Roc reduce multiple signaling proteins important for sarcoma cell growth and survival. Protein lysates from TC32 Ewing sarcoma (**A**), 143B osteosarcoma (**B**), and RD rhabdomyosarcoma (**C**) cells treated for 1 and 2 days with the indicated concentrations of DDR or Roc were analyzed by Western blotting for various oncogenic driver proteins. GAPDH was used as a loading control.

Downloaded from mct.aacrjournals.org on May 28, 2020. © 2020 American Association for Cancer Research.

Published OnlineFirst December 17, 2019; DOI: 10.1158/1535-7163.MCT-19-0809

pulmonary toxicity in dogs, and its further development as a cancer therapy was suspended (D.M. Lucas, M.A. Phelps, A.D. Kinghorn, M. Grever; in preparation). We have identified two rocaglates lacking the dioxanyl ring, Roc and DDR, with better drug-like properties than silvestrol and possessing antitumor efficacy in multiple sarcoma models, including MPNST. Most critically, Roc did not induce the toxicity found in dogs with silvestrol under the same conditions.

Our side-by-side comparison of ten rocaglates lacking the bulky dioxanyl ring present in silvestrol has allowed us to discern certain structure–activity relationships, particularly the C-8b, C-2, and C-6 positions along the cyclopenta[*b*]benzofuran core. Consistent with previous reports (22, 40), the hydroxy group at the C-8b position is essential for antiproliferative activity. This finding is consistent with the crystal structure of Roc complexed with eIF4A and polypurine RNA, which reveals hydrogen bonding between the 8b-OH of Roc and a guanine base in the RNA (41). Also, the phenyl rings A and B of Roc parallel stack with RNA bases, which may explain our finding that adding a methylenedioxy group to ring B modestly improved the growth-inhibitory activity of rocaglates with methylated 8b-OH (**Fig. 1**). It is possible that this methylenedioxy ring may enhance the affinity of the rocaglates to the eIF4A-RNA complex, partially compensating for the loss of 8b hydrogen bonding.

Among the rocaglates lacking the dioxanyl ring that we evaluated, DDR was the most potent, suggestive of the importance of having a simple primary amide group at the C-2 position. Although the presence of a dioxanyl ring instead of a methoxy group at the C-6 position enhances the potency of silvestrol compared with methyl rocaglate (22, 42), our data indicated that this ring is not required for cytotoxicity. However, it appears to play an important role in MDR1-induced resistance as Roc and DDR are no longer susceptible to this inhibitory effect. Consistent with this notion, we detected a higher level of MDR1 in ST8814 MPNST cells than that in STS26T cells (Supplementary Fig. S4), whereas the IC_{50} values of Roc and DDR in ST8814 cells were similar to those in STS26T cells (**Table 1**; Supplementary Fig. S1). The MDR1 transporter binds to silvestrol and is thought to limit its oral bioavailability (29). Our PK analysis demonstrating 50% oral bioavailability of Roc, a >25-fold improvement over silvestrol, confirms this prediction and strongly suggests a possible interaction of MDR1 with the dioxanyl moiety. The observed oral bioavailability of Roc allows a greater flexibility for dosing. More importantly, we found that Roc, when administered i.p. or p.o., showed potent antitumor effects in an orthotopic MPNST CDX mouse model and effectively suppressed the growth of PDX models for Ewing sarcoma, osteosarcoma, and rhabdomyosarcoma.

Like silvestrol, rocaglamides exert their potent growth-inhibitory and antitumor activities mainly through inhibition of eIF4A and protein translation (43, 44). Consistently, we observed that Roc and DDR decreased the levels of multiple signaling proteins important for tumor growth and survival, leading to G_2–M cell-cycle arrest and activation of executioner caspases. In addition to AKT and ERKs, rocaglamides reduced the levels of IGF-1R in all sarcoma cell lines tested. This decrease in IGF-1R expression, coupled with the simultaneous inhibition of AKT and ERKs, likely results in superior inhibition of IGF-1 signaling compared with the simple blockade at the receptor level. Our results further suggest that IGF-1R may serve as a biomarker for responsiveness to rocaglamides in sarcomas.

It should be noted that the effects of translation inhibition mediated by eIF4A are different from those by eIF4E, which can be activated by the AKT/mTOR pathway, a commonly deregulated event in sarcomas (18). The mTOR inhibitor, rapamycin and its analogs, and mTOR kinase inhibitors only cause cytostatic effects and tumor stabilization (45). Also, blocking mTOR signaling is associated with activation of bypass signaling pathways that can restore critical survival signals, enabling tumor regrowth. Inhibition of eIF4E tends to decrease translation of the mRNAs with 5′ terminal oligopyrimidine tracts, which encode ribosomal proteins, elongation factors, lysosomal-related and metabolic-related proteins. However, the eIF4A activity is more critical in unwinding the mRNAs with long 5′-UTRs that can form G-quadruplexes, such as *AKT* and *IGF-1R* (15, 20). In addition, some transcripts, e.g., *c-MYC*, are translated from internal ribosomal entry sites that do not require the cap binder eIF4E and are insensitive to eIF4E inhibition (46). Thus, blocking eIF4A may have a stronger effect on tumor growth and survival.

Ewing sarcoma is frequently driven by the chimeric fusion oncogene *EWS-FLI1* due to a chromosomal translocation that fuses an RNA-binding protein, EWSR1, with the FLI1 transcription factor (35). Surprisingly, we found that the levels of EWS-FLI1 remained unchanged in Roc-treated Ewing sarcoma cells (**Fig. 6A**). As a ubiquitously expressed protein, the EWSR1 levels were also not affected in other types of sarcoma cells treated with rocaglamides (**Fig. 6B** and **C**). In contrast, the levels of the epigenetic modulator LSD1, a protein needed for optimal activity of the EWS-FLI1 transcriptional complex (36), and a key EWS-FLI1 downstream target NKX2.2, a homeobox transcription factor implicated in development (37), were diminished by DDR and Roc treatment (**Fig. 6**). Upon inspection of these genes, we noted that the *EWSR1* transcript has a very short 5′-UTR, whereas the mRNAs for *NKX2.2* and *LSD1/KDM1A* contain longer G+C-rich 5′-UTRs. Therefore, we hypothesize that the *NKX2.2* and *LSD1/KDM1A* transcripts are eIF4A-dependent.

Intriguingly, prior to caspase activation, Roc-treated MPNST cells exhibited increased γH2A.X, suggesting that DNA damage may be a key underlying cause of the apoptosis seen at later time points. Rocaglamides may affect prohibitin-mediated ERK activation, cause the disruption of mitochondrial integrity, and/or promote the generation of reactive oxygen species (47, 48). Alternatively, they may affect translation of the proteins responsible for DNA replication and repair, resulting in stalled replication forks or inadequate repair of DNA damage. We are presently examining these possibilities.

Roc was the first member of the cyclopenta[*b*]benzofuran class identified as a novel antileukemic agent from *Aglaia elliptifolia* by King and colleagues (49). It is worth mentioning that the structures of Roc and DDR are simpler than silvestrol; therefore, they should be more amenable to chemical synthesis (50). As DDR exhibited higher *in vitro* potency against various types of sarcoma cells than Roc, we anticipate that DDR will have superior antitumor efficacy. Experiments are in progress to compare these rocaglamides in various sarcoma animal models.

In summary, we have demonstrated that Roc and DDR, as eIF4A inhibitors, simultaneously suppressed multiple growth-promoting signaling pathways and induced apoptosis in tumor cells. Roc was no longer sensitive to MDR1 inhibition. It was orally bioavailable and exhibited potent antitumor effects in multiple sarcoma models with no overt toxicity. These promising results indicate that these rocaglamides merit further investigation as treatments for patients with MPNSTs and other sarcomas.

Disclosure of Potential Conflicts of Interest

No potential conflicts of interest were disclosed.

Downloaded from mct.aacrjournals.org on May 28, 2020. © 2020 American Association for Cancer Research.

Published OnlineFirst December 17, 2019; DOI: 10.1158/1535-7163.MCT-19-0809

Authors' Contributions

Conception and design: L.-S. Chang, J.L. Oblinger, S.S. Burns, J.M. Collins
Development of methodology: L.-S. Chang, J.L. Oblinger, S.S. Burns, J. Huang, L.W. Anderson, R.D. Roberts
Acquisition of data (provided animals, acquired and managed patients, provided facilities, etc.): L.-S. Chang, J.L. Oblinger, S.S. Burns, J. Huang, L.W. Anderson, M.G. Hollingshead, R. Shen, G. Agarwal, R.D. Roberts
Analysis and interpretation of data (e.g., statistical analysis, biostatistics, computational analysis): L.-S. Chang, J.L. Oblinger, S.S. Burns, L.W. Anderson, M.G. Hollingshead, R. Shen, R.D. Roberts, J.M. Collins
Writing, review, and/or revision of the manuscript: L.-S. Chang, J.L. Oblinger, L.W. Anderson, M.G. Hollingshead, Y. Ren, R.D. Roberts, B.R. O'Keefe, A.D. Kinghorn
Administrative, technical, or material support (i.e., reporting or organizing data, constructing databases): L.-S. Chang, J.L. Oblinger, S.S. Burns, L. Pan, J.M. Collins
Study supervision: L.-S. Chang, B.R. O'Keefe, A.D. Kinghorn, J.M. Collins
Other (isolated and identified the test compounds, rocaglamide, and didesmethylrocaglamide): L. Pan

Acknowledgments

We thank Melissa Sammons of NCH Tumor Core for assistance with PDX models, Eva Majerova for technical help with plasma analysis, John Byrd for 697 and 697-R cells, Stephen Lessnick for Ewing sarcoma cells, and Ruoning Wang for rhabdomyosarcoma cells.

This study was supported by grants from CancerFree KIDS, Sunbeam Foundation, and Department of Defense (W81XWH-16-1-0104 and W81XWH-18-1-0547 to L.-S. Chang), National Cancer Institute (P01CA125066 to A.D. Kinghorn and P30CA16058 to The OSU Comprehensive Cancer Center), and NCI Experimental Therapeutics program (NCI Contract HHSN261200800001 to Leidos Biomedical Research).

The costs of publication of this article were defrayed in part by the payment of page charges. This article must therefore be hereby marked *advertisement* in accordance with 18 U.S.C. Section 1734 solely to indicate this fact.

Received August 19, 2019; revised December 2, 2019; accepted December 13, 2019; published first December 17, 2019.

References

1. Kim A, Stewart DR, Reilly KM, Viskochil D, Miettinen MM, Widemann BC. Malignant peripheral nerve sheath tumors state of the science: leveraging clinical and biological insights into effective therapies. Sarcoma 2017;2017:7429697.
2. Perrone F, Da Riva L, Orsenigo M, Losa M, Jocollè G, Millefanti C, et al. PDGFRA, PDGFRB, EGFR, and downstream signaling activation in malignant peripheral nerve sheath tumor. Neuro Oncol 2009;11:725–36.
3. Yang J, Ylipää A, Sun Y, Zheng H, Chen K, Nykter M, et al. Genomic and molecular characterization of malignant peripheral nerve sheath tumor identifies the IGF1R pathway as a primary target for treatment. Clin Cancer Res 2011;17:7563–73.
4. Kim A, Pratilas CA. The promise of signal transduction in genetically driven sarcomas of the nerve. Exp Neurol 2018;299(Pt B):317–25.
5. De Raedt T, Beert E, Pasmant E, Luscan A, Brems H, Ortonne N, et al. PRC2 loss amplifies Ras-driven transcription and confers sensitivity to BRD4-based therapies. Nature 2014;514:247–51.
6. Sebti SM, Tkalcevic GT, Jani JP. Lovastatin, a cholesterol biosynthesis inhibitor, inhibits the growth of human H-ras oncogene transformed cells in nude mice. Cancer Commun 1991;3:141–7.
7. Barkan B, Starinsky S, Friedman E, Stein R, Kloog Y. The Ras inhibitor farnesylthiosalicylic acid as a potential therapy for neurofibromatosis type 1. Clin Cancer Res 2006;12:5533–42.
8. Rao S, Cunningham D, de Gramont A, Scheithauer W, Smakal M, Humblet Y, et al. Phase III double-blind placebo-controlled study of farnesyl transferase inhibitor R115777 in patients with refractory advanced colorectal cancer. J Clin Oncol 2004;22:3950–7.
9. Cloughesy TF, Wen PY, Robins HI, Chang SM, Groves MD, Fink KL, et al. Phase II trial of tipifarnib in patients with recurrent malignant glioma either receiving or not receiving enzyme-inducing antiepileptic drugs: a North American Brain Tumor Consortium Study. J Clin Oncol 2006;24:3651–6.
10. Hanrahan EO, Kies MS, Glisson BS, Khuri FR, Feng L, Tran HT, et al. A phase II study of lonafarnib (SCH66336) in patients with chemorefractory, advanced squamous cell carcinoma of the head and neck. Am J Clin Oncol 2009;3:274–9.
11. Albritton KH, Rankin C, Coffin CM, Ratner N, Budd GT, Schuetze SM, et al. Phase II study of erlotinib in metastatic or unresectable malignant peripheral nerve sheath tumors (MPNST). J Clin Oncol 2006;24 Suppl 18:9518.
12. Tap WD, Demetri G, Barnette P, Desai J, Kavan P, Tozer R, et al. Phase II study of ganitumab, a fully human anti-type-1 insulin-like growth factor receptor antibody, in patients with metastatic Ewing family tumors or desmoplastic small round cell tumors. J Clin Oncol 2012;30:1849–56.
13. Maki RG, D'Adamo DR, Keohan ML, Saulle M, Schuetze SM, Undevia SD, et al. Phase II study of sorafenib in patients with metastatic or recurrent sarcomas. J Clin Oncol 2009;27:3133–40.
14. Widemann BC, Meyer CF, Cote GM, Chugh R, Milhem MM, Van Tine BA, et al. SARC016: phase II study of everolimus in combination with bevacizumab in sporadic and neurofibromatosis type 1 (NF1) related refractory malignant peripheral nerve sheath tumors (MPNST). J Clin Oncol 2016;34 Suppl 15:11053.
15. Malka-Mahieu H, Newman M, Désaubry L, Robert C, Vagner S. Molecular pathways: the eIF4F translation initiation complex-new opportunities for cancer treatment. Clin Cancer Res 2017;23:21–5.
16. Oblinger JL, Burns SS, Akhmametyeva EM, Huang J, Pan L, Ren Y, et al. Components of the eIF4F complex are potential therapeutic targets for malignant peripheral nerve sheath tumors and vestibular schwannomas. Neuro-Oncol 2016;18:1265–77.
17. Oblinger JL, Burns SS, Huang J, Pan L, Ren Y, Shen R, et al. Overexpression of eIF4F components in meningiomas and suppression of meningioma cell growth by inhibiting translation initiation. Exp Neurol 2018;299(Pt B):299–307.
18. Mamane Y, Petroulakis E, LeBacquer O, Sonenberg N. mTOR, translation initiation and cancer. Oncogene 2006;25:6416–22.
19. Chu J, Cargnello M, Topisirovic I, Pelletier J. Translation initiation factors: reprogramming protein synthesis in cancer. Trends Cell Biol 2016;26:918–33.
20. Wolfe AL, Singh K, Zhong Y, Drewe P, Rajasekhar VK, Sanghvi VR, et al. RNA G-quadruplexes cause eIF4A-dependent oncogene translation in cancer. Nature 2014;513:65–70.
21. Pan L, Woodard JL, Lucas DM, Fuchs JR, Kinghorn AD. Rocaglamide, silvestrol, and related bioactive compounds from Aglaia species. Nat Prod Rep 2014:31;924–31.
22. Kinghorn AD, DE Blanco EJ, Lucas DM, Rakotondraibe HL, Orjala J, Soejarto DD, et al. Discovery of anticancer agents of diverse natural origin. Anticancer Res 2016;36:5623–37.
23. Lucas DM, Edwards RB, Lozanski G, West DA, Shin JD, Vargo MA, et al. The novel plant-derived agent silvestrol has B-cell selective activity in chronic lymphocytic leukemia and acute lymphoblastic leukemia in vitro and in vivo. Blood 2009;113:4656–66.
24. Kogure T, Kinghorn AD, Yan I, Bolon B, Lucas DM, Grever MR, et al. Therapeutic potential of the translation inhibitor silvestrol in hepatocellular cancer. PLoS One 2013;8:e76136.
25. Boussemart L, Malka-Mahieu H, Girault I, Allard D, Hemmingsson O, Tomasic G, et al. eIF4F is a nexus of resistance to anti-BRAF and anti-MEK cancer therapies. Nature 2014;513:105–9.
26. El Sous M, Khoo ML, Holloway G, Owen D, Scammells PJ, Rizzacasa MA. Total synthesis of (−)-episilvestrol and (−)-silvestrol. Angew Chem Int Ed Engl 2007;46:7835–8.
27. Gerard B, Cencic R, Pelletier J, Porco JA Jr. Enantioselective synthesis of the complex rocaglate (-)-silvestrol. Angew Chem Int Ed Engl 2007;46:7831–4.
28. Adams TE, El Sous M, Hawkins BC, Hirner S, Holloway G, Khoo ML, et al. Total synthesis of the potent anticancer Aglaia metabolites (-)-silvestrol and (−)-episilvestrol and the active analogue (−)-4'-desmethoxyepisilvestrol. J Am Chem Soc 2009;131:1607–16.
29. Gupta SV, Sass EJ, Davis ME, Edwards RB, Lozanski G, Heerema NA, et al. Resistance to the translation initiation inhibitor silvestrol is mediated by ABCB1/P-glycoprotein overexpression in acute lymphoblastic leukemia cells. AAPS J 2011;13:357–64.
30. Saradhi UV, Gupta SV, Chiu M, Wang J, Ling Y, Liu Z, et al. Characterization of silvestrol pharmacokinetics in mice using liquid chromatography-tandem mass spectrometry. AAPS J 2011;13:347–56.

Downloaded from mct.aacrjournals.org on May 28, 2020. © 2020 American Association for Cancer Research.

Published OnlineFirst December 17, 2019; DOI: 10.1158/1535-7163.MCT-19-0809

31. Pan L, Acuña UM, Li J, Jena N, Ninh TN, Pannell CM, et al. Bioactive flavaglines and other constituents isolated from Aglaia perviridis. J Nat Prod 2013;76:394–404.
32. Burns SS, Akhmametyeva EM, Oblinger JL, Bush ML, Huang J, Senner V, et al. Histone deacetylase inhibitor AR-42 differentially affects cell-cycle transit in meningeal and meningioma cells, potently inhibiting NF2-deficient meningioma growth. Cancer Res 2013;73:792–803.
33. Burns SS, Chang LS. Generation of noninvasive, quantifiable, orthotopic animal models for NF2-associated schwannoma and meningioma. Methods Mol Biol 2016;1427:59–72.
34. Farid M, Demicco EG, Garcia R, Ahn L, Merola PR, Cioffi A, et al. Malignant peripheral nerve sheath tumors. Oncologist 2014;19:193–201.
35. Delattre O, Zucman J, Plougastel B, Desmaze C, Melot T, Peter M, et al. Gene fusion with an ETS DNA-binding domain caused by chromosome translocation in human tumours. Nature 1992;359:162–5.
36. Sankar S, Bell R, Stephens B, Zhuo R, Sharma S, Bearss DJ, et al. Mechanism and relevance of EWS/FLI-mediated transcriptional repression in Ewing sarcoma. Oncogene 2013;32:5089–100.
37. Smith R, Owen LA, Trem DJ, Wong JS, Whangbo JS, Golub TR, et al. Expression profiling of EWS/FLI identifies NKX2.2 as a critical target gene in Ewing's sarcoma. Cancer Cell 2006;9:405–16.
38. Brown HK, Schiavone K, Gouin F, Heymann MF, Heymann D. Biology of bone sarcomas and new therapeutic developments. Calcif Tissue Int 2018; 102:174–95.
39. Skapek SX, Ferrari A, Gupta AA, Lupo PJ, Butler E, Shipley J, et al. Rhabdomyosarcoma. Nat Rev Dis Primers 2019;5:1.
40. Ebada SS, Lajkiewicz N, Porco JA Jr, Li-Weber M, Proksch P. Chemistry and biology of rocaglamides (= flavaglines) and related derivatives from Aglaia species (Meliaceae). Prog Chem Org Nat Prod 2011;94:1–58.
41. Iwasaki S, Iwasaki W, Takahashi M, Sakamoto A, Watanabe C, Shichino Y, et al. The translation inhibitor rocaglamide targets a bimolecular cavity between eIF4A and polypurine RNA. Mol Cell 2019;73:738–48.
42. Kim S, Salim AA, Swanson SM, Kinghorn AD. Potential of cyclopenta[b]benzofurans from Aglaia species in cancer chemotherapy. Anticancer Agents Med Chem 2006;6:319–45.
43. Cencic R, Carrier M, Galicia-Vázquez G, Bordeleau ME, Sukarieh R, Bourdeau A, et al. Antitumor activity and mechanism of action of the cyclopenta[b]benzofuran, silvestrol. PLoS One 2009;4:e5223.
44. Sadlish H, Galicia-Vazquez G, Paris CG, Aust T, Bhullar B, Chang L, et al. Evidence for a functionally relevant rocaglamide binding site on the eIF4A-RNA complex. ACS Chem Biol 2013;8:1519–27.
45. D'Abronzo LS, Ghosh PM. eIF4E phosphorylation in prostate cancer. Neoplasia 2018;20:563–73.
46. Wiegering A, Uthe FW, Jamieson T, Ruoss Y, Hüttenrauch M, Küspert M, et al. Targeting translation initiation bypasses signaling crosstalk mechanisms that maintain high MYC levels in colorectal cancer. Cancer Discov 2015;5:768–81.
47. Polier G, Neumann J, Thuaud F, Ribeiro N, Gelhaus C, Schmidt H, et al. The natural anticancer compounds rocaglamides inhibit the Raf-MEK-ERK pathway by targeting prohibitin 1 and 2. Chem Biol 2012;19:1093–104.
48. Callahan KP, Minhajuddin M, Corbett C, Lagadinou ED, Rossi RM, Grose V, et al. Flavaglines target primitive leukemia cells and enhance anti-leukemia drug activity. Leukemia 2014;28:1960–8.
49. King ML, Chiang CC, Ling HC, Fujita E, Ochiai M, McPhail AT. X-ray crystal structure of rocaglamide, a novel antileukemic 1H-cyclopenta[b]benzofuran from Aglaia elliptifolia. J Chem Soc, Chem Commun 1982;20:1150–1.
50. Liu T, Nair SJ, Lescarbeau A, Belani J, Peluso S, Conley J, et al. Synthetic silvestrol analogues as potent and selective protein synthesis inhibitors. J Med Chem 2012; 55:8859–78.

Downloaded from mct.aacrjournals.org on May 28, 2020. © 2020 American Association for Cancer Research.

Published OnlineFirst December 17, 2019; DOI: 10.1158/1535-7163.MCT-19-0809

AACR American Association for Cancer Research

Molecular Cancer Therapeutics

Targeting Protein Translation by Rocaglamide and Didesmethylrocaglamide to Treat MPNST and Other Sarcomas

Long-Sheng Chang, Janet L. Oblinger, Sarah S. Burns, et al.

Mol Cancer Ther 2020;19:731-741. Published OnlineFirst December 17, 2019.

Updated version	Access the most recent version of this article at: doi:10.1158/1535-7163.MCT-19-0809
Supplementary Material	Access the most recent supplemental material at: http://mct.aacrjournals.org/content/suppl/2019/12/17/1535-7163.MCT-19-0809.DC1

Cited articles	This article cites 49 articles, 12 of which you can access for free at: http://mct.aacrjournals.org/content/19/3/731.full#ref-list-1

E-mail alerts	Sign up to receive free email-alerts related to this article or journal.
Reprints and Subscriptions	To order reprints of this article or to subscribe to the journal, contact the AACR Publications Department at pubs@aacr.org.
Permissions	To request permission to re-use all or part of this article, use this link http://mct.aacrjournals.org/content/19/3/731. Click on "Request Permissions" which will take you to the Copyright Clearance Center's (CCC) Rightslink site.

Downloaded from mct.aacrjournals.org on May 28, 2020. © 2020 American Association for Cancer Research.

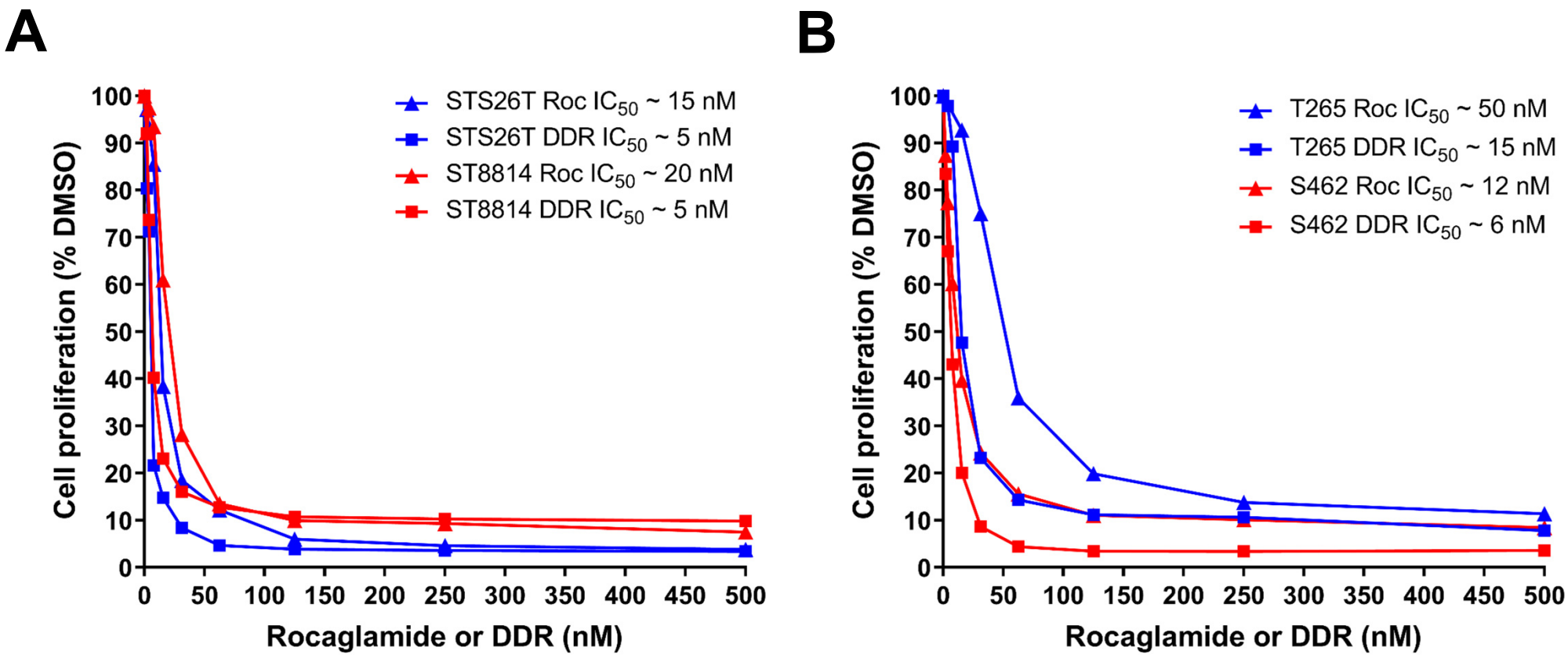

Supplementary Figure S1. Dose-response growth inhibition curves of DDR and Roc in MPNST cells. *NF1*-expressing STS26T (A) and T265 (B) (blue lines) and *NF1*-deficient ST8814 (A) and S462 (B) (red lines) MPNST cells were treated with various concentrations of DDR or Roc, followed by determination of cell proliferation as described in Methods. Experiments were performed in six replicates and were repeated three times. Data shown are the mean of replicates from one representative experiment for each cell line and compound. The graph inset shows the mean IC_{50} values derived from three independent experiments.

Supplementary Fig. S2A

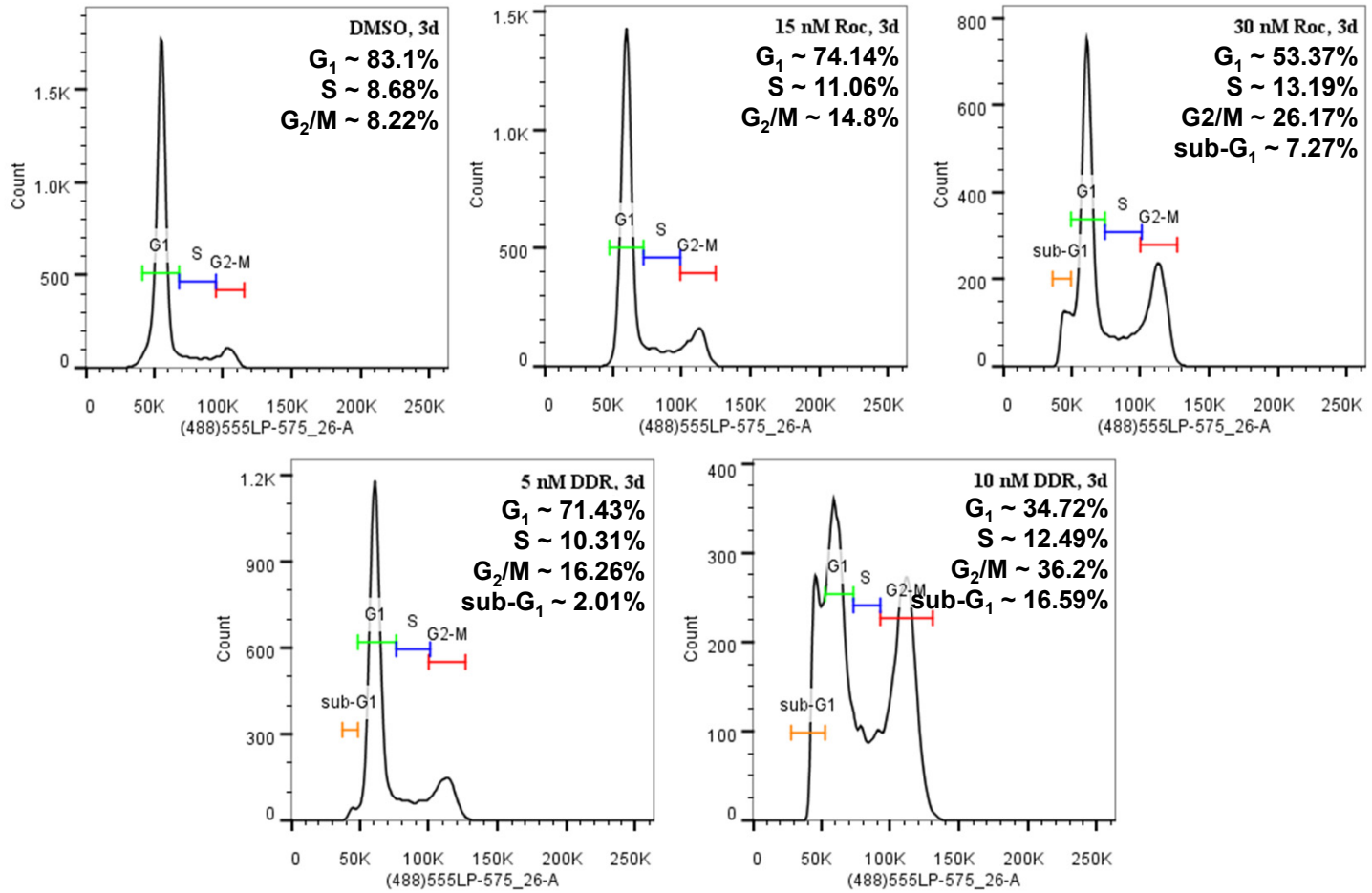

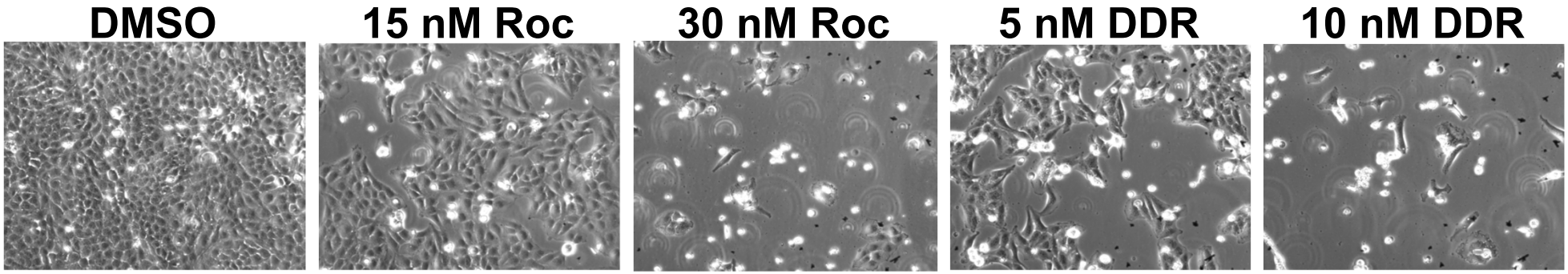

Supplementary Fig. S2B

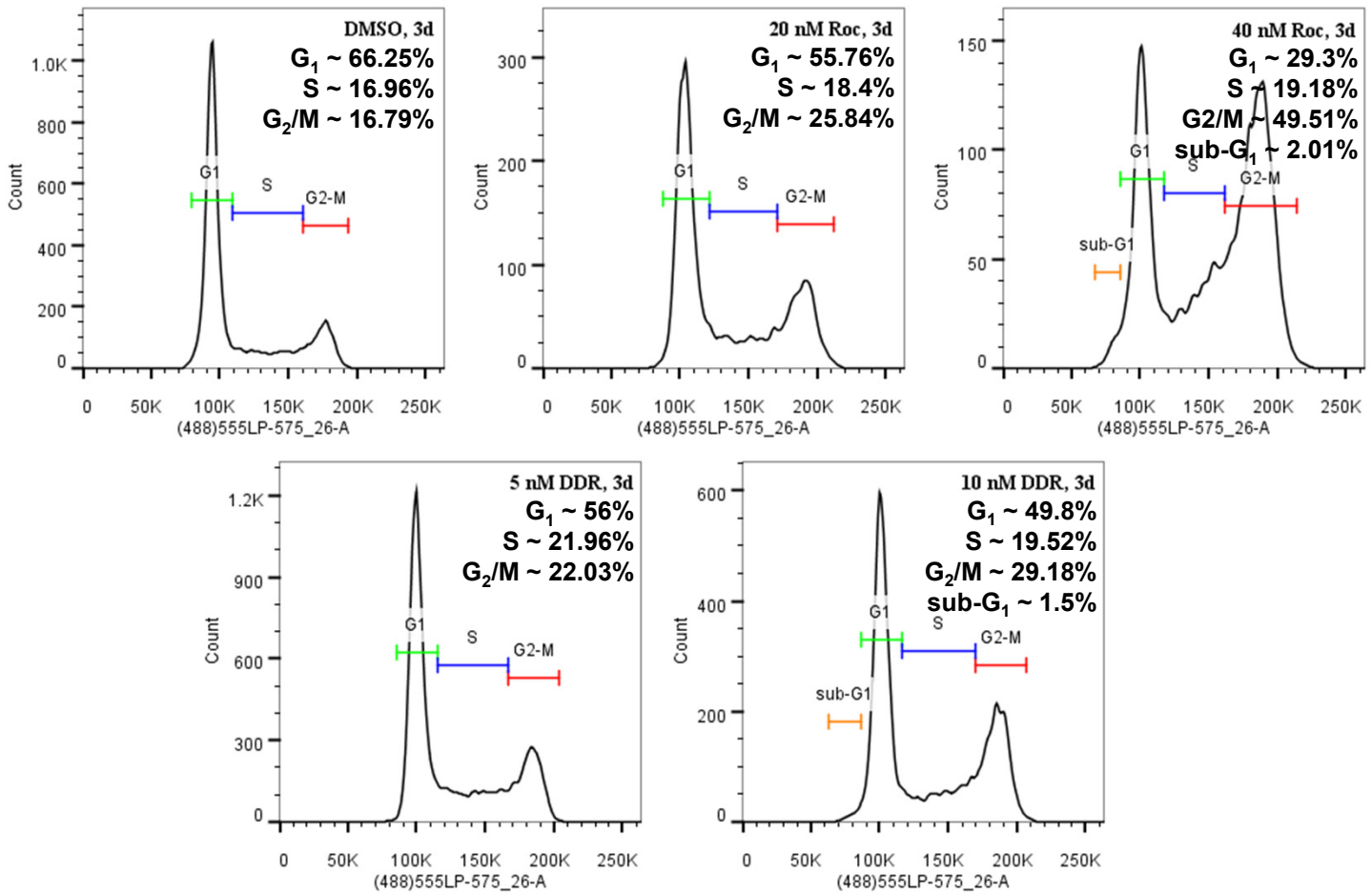

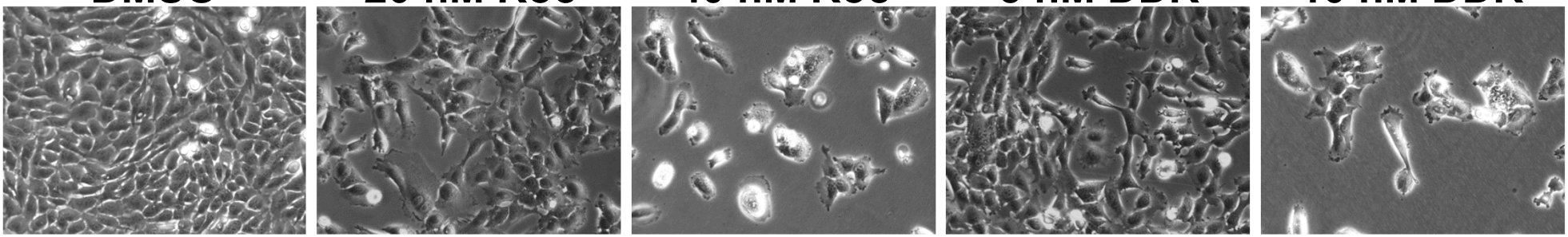

Supplementary Fig. S2C

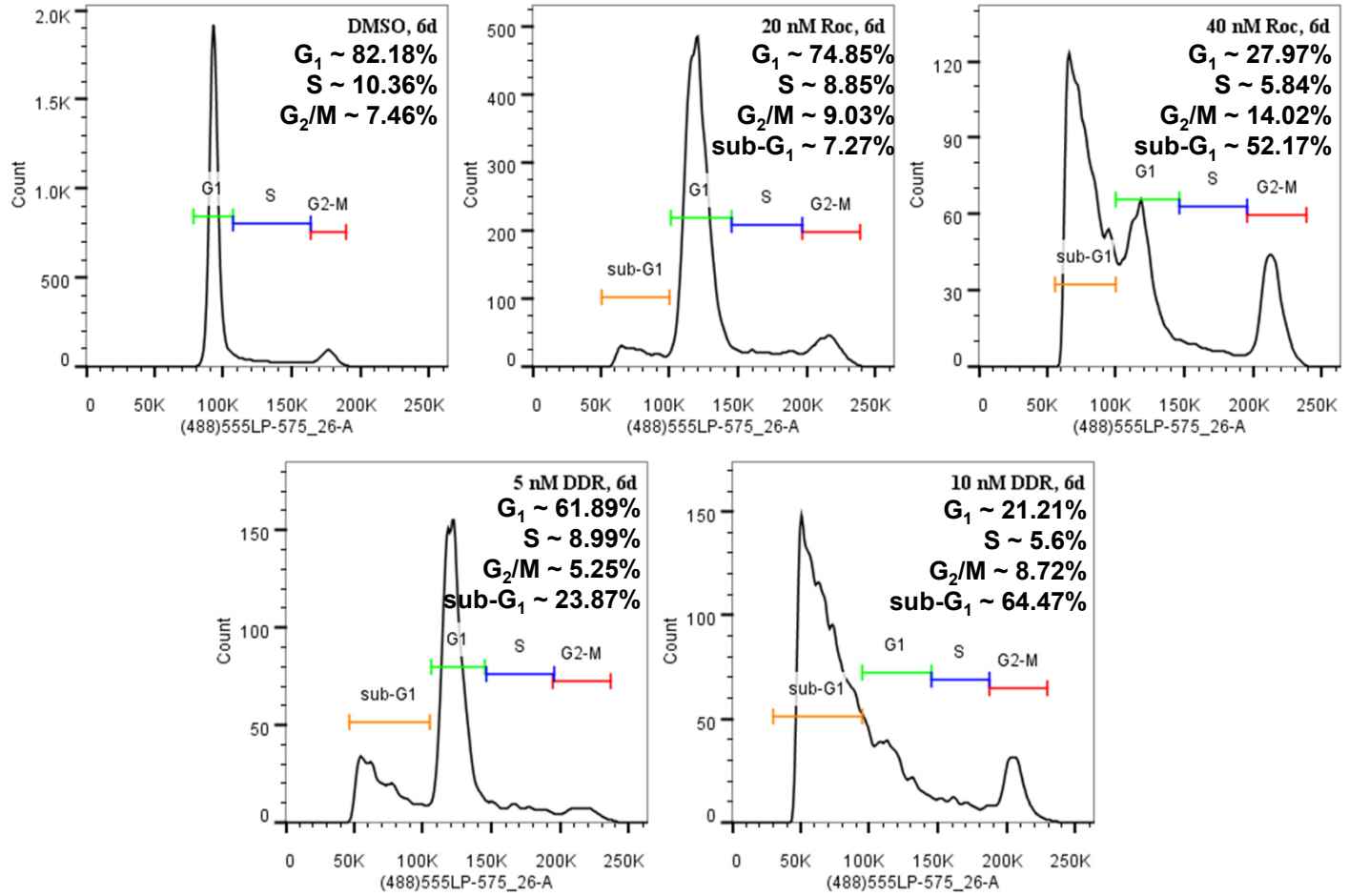

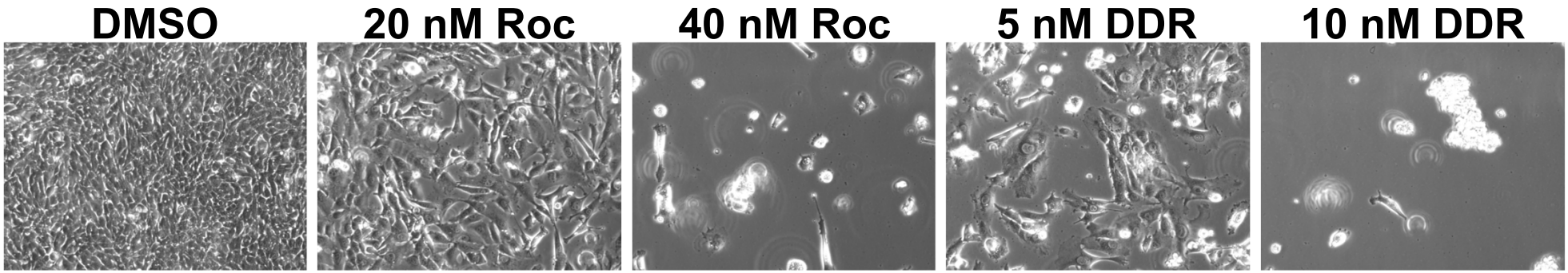

Supplementary Figure S2. DDR and Roc induce G_2/M arrest and increase sub-G_1 fraction in MPNST cells. (A) STS26T cells were treated with the indicated concentrations of DDR and Roc for three days, and phase-contrast images of treated cells were taken, followed by cell harvesting for flow cytometry analysis as described in Methods. Cell-cycle histograms of propidium iodide-labeled cells revealed a prominent increase in the G_2/M and sub-G_1 peaks after treatment. (B-C) Flow cytometry analysis and phase-contrast images of ST8814 cells treated with DDR or Roc for three (B) or six days (C) were conducted and showed an increased G_2/M fraction in treated cells. Also, a large increase in the sub-G_1 fraction was observed in cells treated for six days.

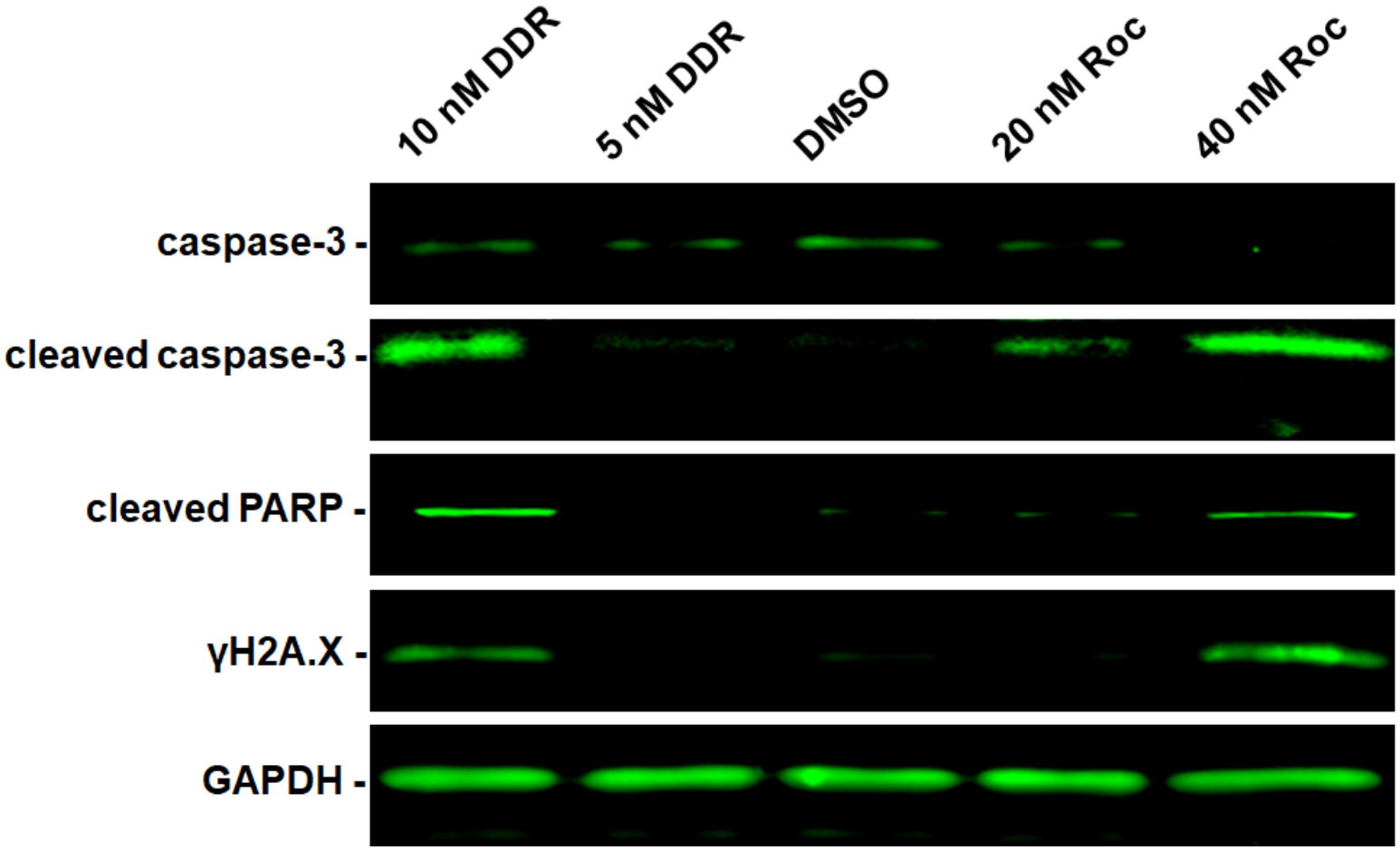

Supplementary Figure S3. DDR and Roc increase caspase-3 and PARP cleavage and elevate the levels of γH2A.X in *NF1*-deficient ST8814 cells. Protein lysates from ST8814 cells treated for 4 days with 1- or 2-IC_{50} of DDR or Roc were analyzed by Western blots for full-length and cleaved caspase-3, cleaved PARP, γH2A.X, and GAPDH as a loading control.

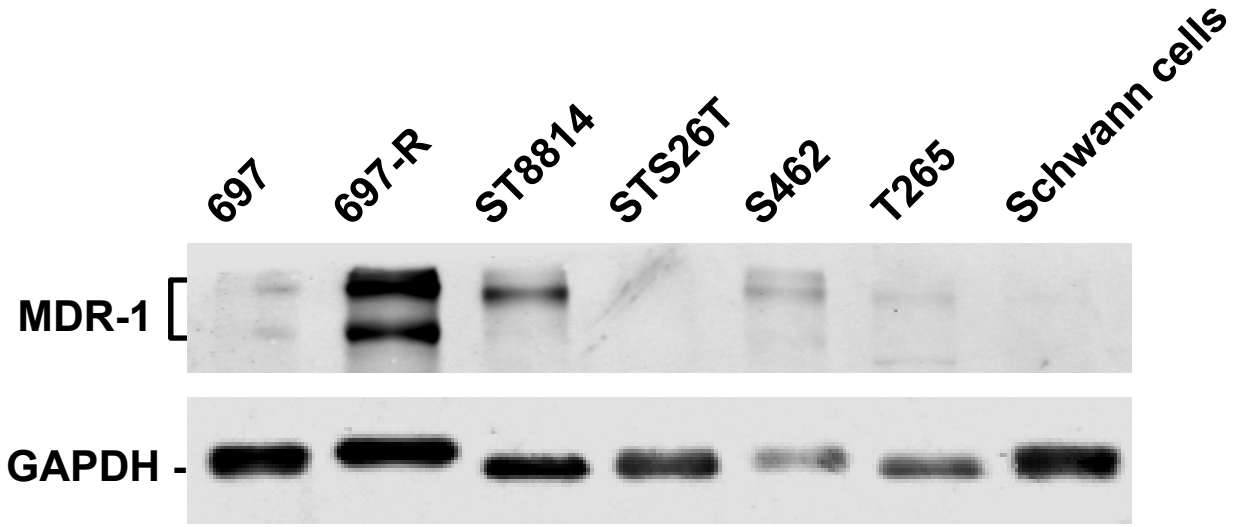

Supplementary Figure S4. Expression of the MDR1/Pgp protein in 697 and 697-R leukemic cells, various MPNST cell lines (ST8814, STS26T, S462, and T265), and primary human Schwann cells. Western blot analysis was conducted as described in Methods. GAPDH was used as a loading control.

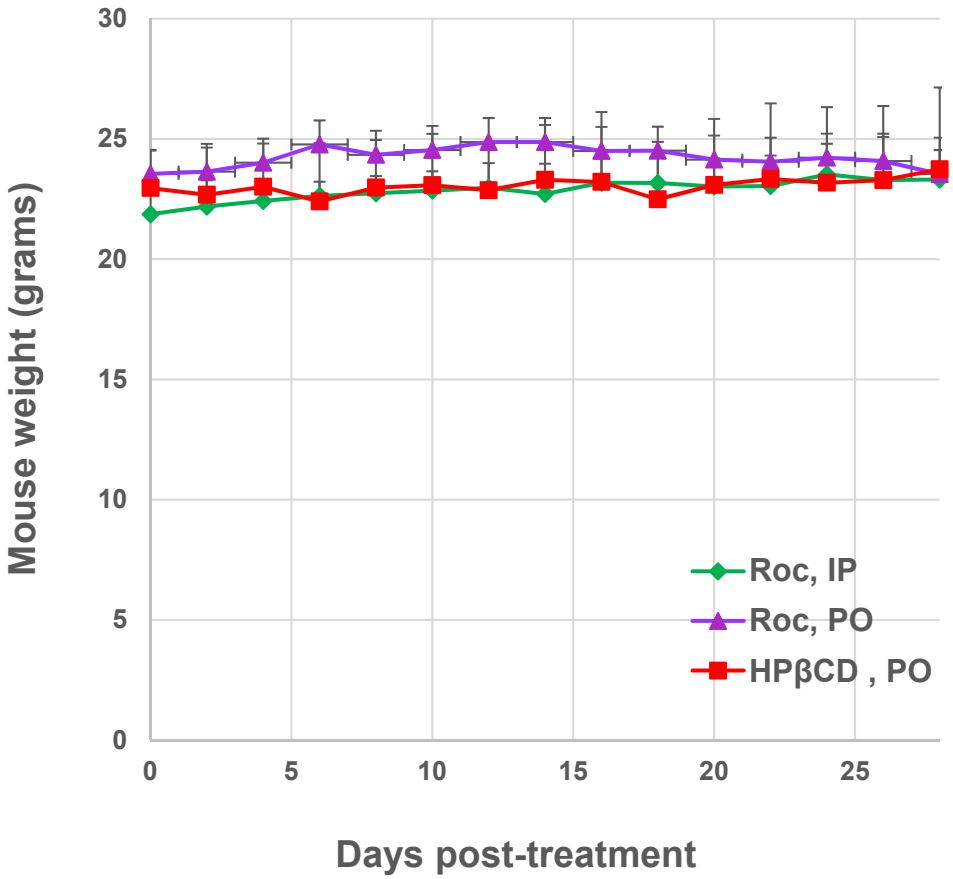

Supplementary Figure S5. Treatment with Roc did not significantly affect body weight, compared with vehicle-treated mice. ST8814-Luc MPNST-bearing NSG mice (n=10/group) were treated with Roc at 4mg/kg by IP, 1.2mg/kg by PO, or HPβCD vehicle every other day for four weeks. Mouse weights were measured every other day. Shown are the mean + standard deviation for each group of mice.

Supplementary Fig. S6A

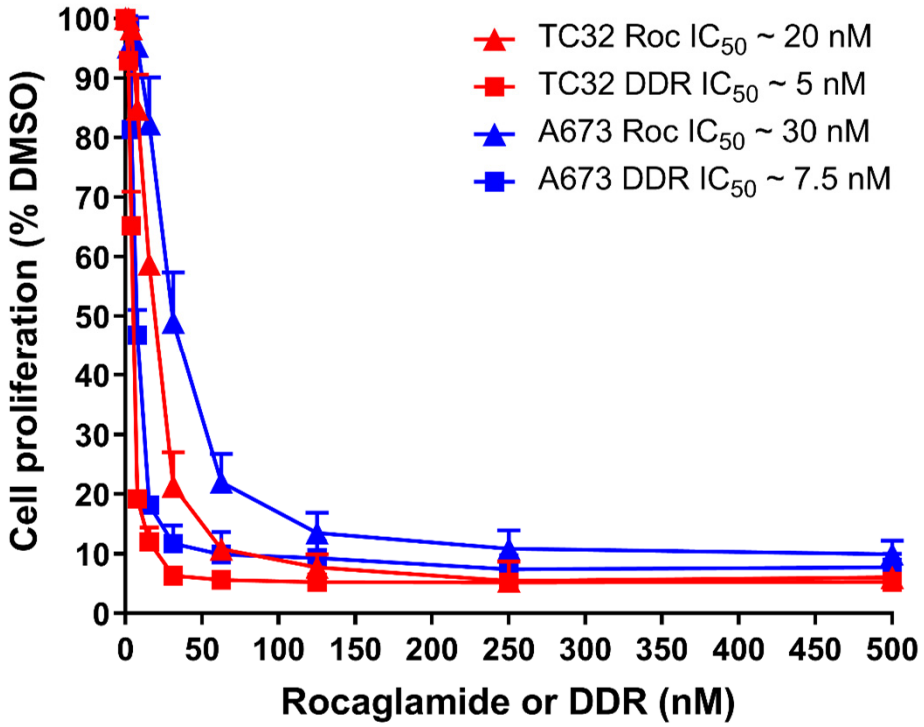

Supplementary Fig. S6B

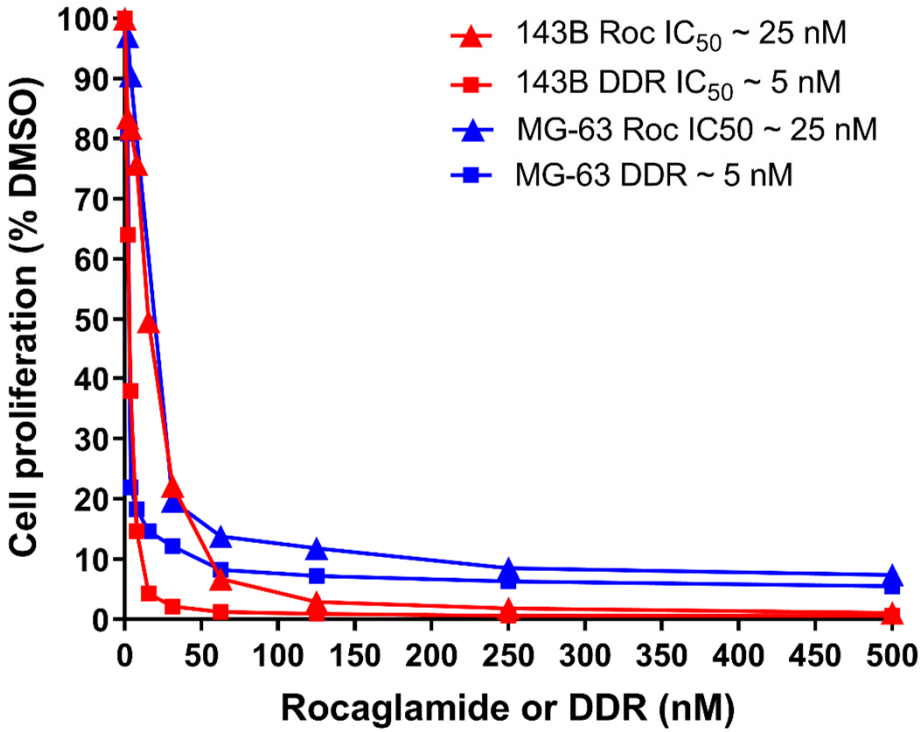

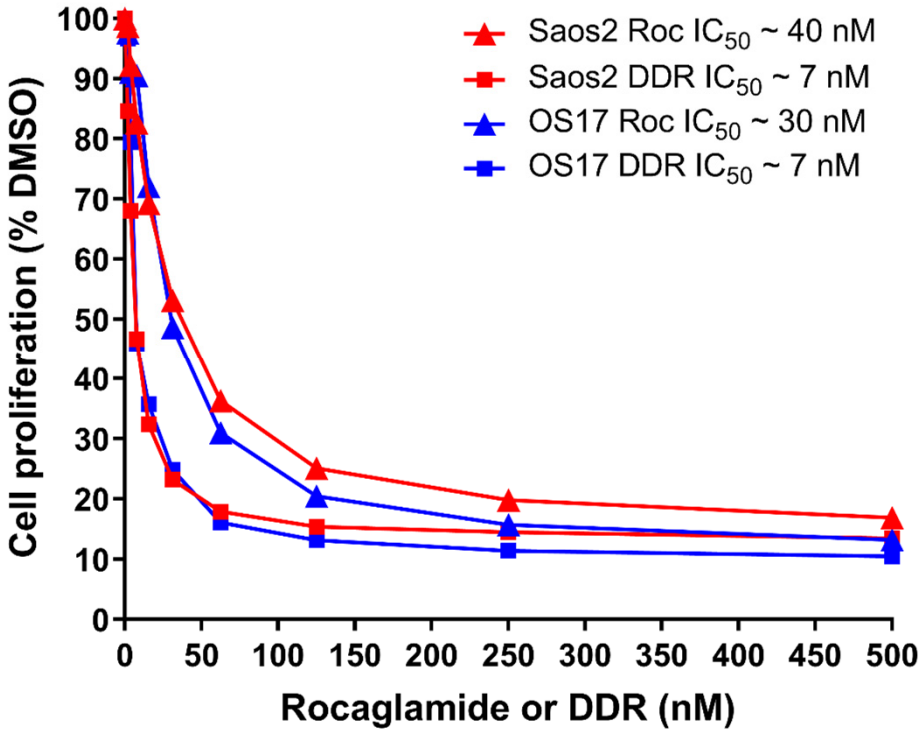

Supplementary Fig. S6C

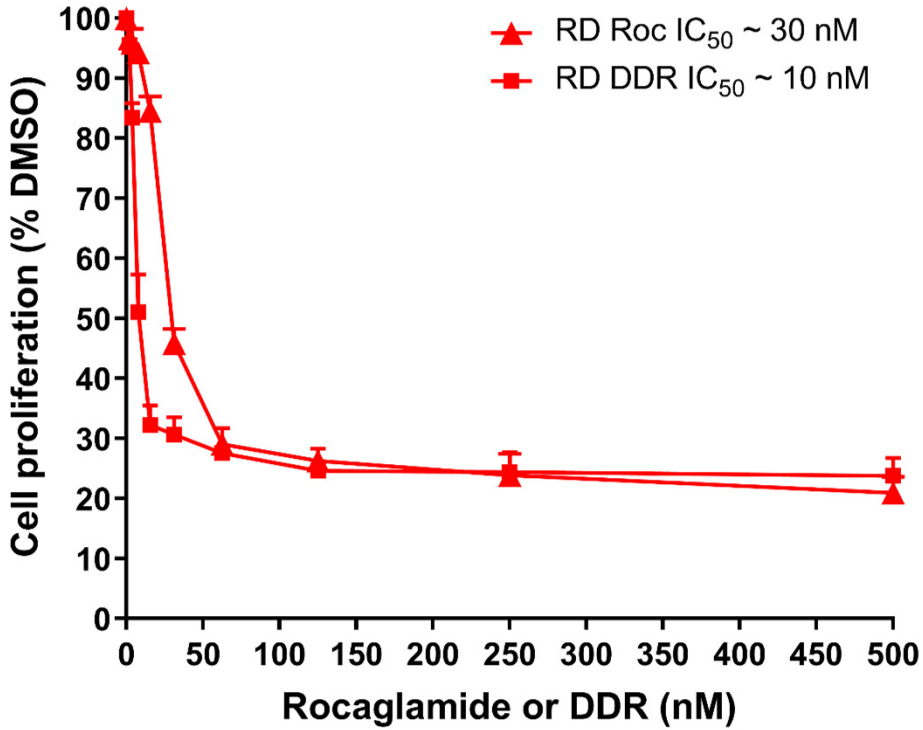

Supplementary Figure S6. DDR and Roc possess potent growth inhibitory activities against various Ewing sarcoma, osteosarcoma, and rhabdomyosarcoma cell lines. Cell proliferation assays were performed on the Ewing sarcoma cell lines A673 and TC32 (A), the osteosarcoma cell lines 143B, MG-63, Saos2, and OS17 (B), and the rhabdomyosarcoma cell line RD (C) treated with various concentrations of DDR (squares) or Roc (triangles) according to Methods. Each treatment was conducted in six replicates and the mean of replicates was calculated and used to generate the dose-response growth inhibition curve. Shown are representative curves for each cell line and treatment. The graph insets show the mean IC_{50} values derived from two independent experiments.

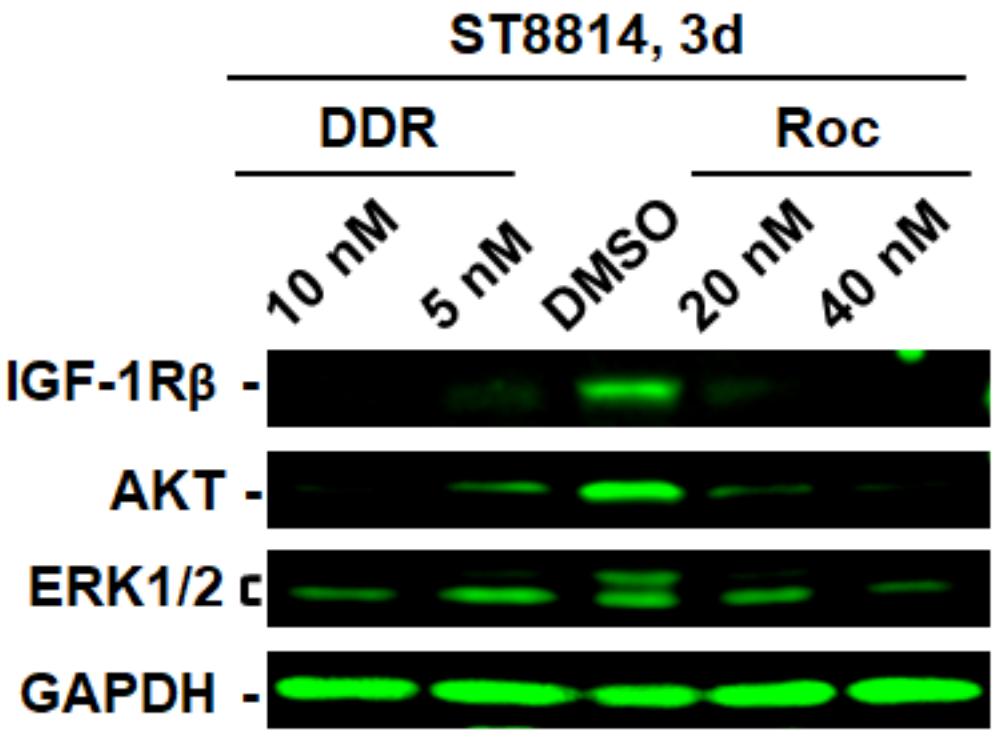

Supplementary Figure S7. DDR and Roc decrease the expression of IGF-1R, AKT and ERKs in MPNST cells. Protein lysates prepared from ST8814 cells treated for 3 days with 1- or 2-IC_{50} of DDR or Roc were analyzed by Western blots as described in Methods. GAPDH served as a loading control.

PLOS ONE

RESEARCH ARTICLE

Brigatinib causes tumor shrinkage in both NF2-deficient meningioma and schwannoma through inhibition of multiple tyrosine kinases but not ALK

Long-Sheng Chang[1¶]*, Janet L. Oblinger[1☯], Abbi E. Smith[2☯], Marc Ferrer[3], Steven P. Angus[2,4], Eric Hawley[2], Alejandra M. Petrilli[5], Roberta L. Beauchamp[6], Lars Björn Riecken[7], Serkan Erdin[6], Ming Poi[8], Jie Huang[1], Waylan K. Bessler[2], Xiaohu Zhang[3], Rajarshi Guha[3], Craig Thomas[3], Sarah S. Burns[1], Thomas S. K. Gilbert[4], Li Jiang[2], Xiaohong Li[2], Qingbo Lu[2], Jin Yuan[2], Yongzheng He[2], Shelley A. H. Dixon[2], Andrea Masters[2], David R. Jones[2], Charles W. Yates[9], Stephen J. Haggarty[6¶], Salvatore La Rosa[10¶], D. Bradley Welling[11¶], Anat O. Stemmer-Rachamimov[12¶], Scott R. Plotkin[6¶], James F. Gusella[13¶], Justin Guinney[14], Helen Morrison[7¶], Vijaya Ramesh[6¶], Cristina Fernandez-Valle[5¶], Gary L. Johnson[4¶], Jaishri O. Blakeley[15¶], D. Wade Clapp[2¶*], on behalf of the Synodos for NF2 Consortium

1 The Research Institute at Nationwide Children's Hospital and Department of Pediatrics, Center for Childhood Cancer and Blood Diseases, The Ohio State University College of Medicine, Columbus, Ohio, United States of America, **2** Department of Pediatrics, Indiana University, School of Medicine, Indianapolis, Indiana, United States of America, **3** Division of Preclinical Innovation, National Center for Advancing Translational Sciences, National Institutes of Health, Bethesda, Maryland, United States of America, **4** University of North Carolina School of Medicine, Chapel Hill, North Carolina, United States of America, **5** Burnett School of Biomedical Sciences, College of Medicine, University of Central Florida, Lake Nona-Orlando, Florida, United States of America, **6** Massachusetts General Hospital and Department of Neurology, Center for Genomic Medicine, Harvard Medical School, Boston, Massachusetts, United States of America, **7** Leibniz Institute on Aging–Fritz-Lipmann Institute (FLI), Jena, Germany, **8** Division of Pharmacy Practice and Science, The Ohio State University College of Pharmacy, Columbus, Ohio, United States of America, **9** Department of Otolaryngology and Head/Neck Surgery, Indiana University School of Medicine, Indianapolis, Indiana, United States of America, **10** Children's Tumor Foundation, New York, New York, United States of America, **11** Department of Otolaryngology, Massachusetts Eye and Ear Infirmary, Massachusetts General Hospital and Harvard University, Boston, Massachusetts, United States of America, **12** Department of Pathology, Massachusetts General Hospital and Harvard Medical School, Boston, Massachusetts, United States of America, **13** Center for Genomic Medicine, Massachusetts General Hospital and Department of Genetics, Blavatnik Institute, Harvard Medical School, Boston, Massachusetts, United States of America, **14** Sage Bionetworks, Seattle, Washington, United States of America, **15** Departments of Neurology, Neurosurgery and Oncology, Johns Hopkins University School of Medicine, Baltimore, Maryland, United States of America

☯ These authors contributed equally to this work.
¶ Members of the Synodos for NF2 Consortium. Please see the Acknowledgements for full member list.
* Long-Sheng.Chang@nationwidechildrens.org (L-SC); dclapp@iu.edu (DWC)

Check for updates

OPEN ACCESS

Citation: Chang L-S, Oblinger JL, Smith AE, Ferrer M, Angus SP, Hawley E, et al. (2021) Brigatinib causes tumor shrinkage in both NF2-deficient meningioma and schwannoma through inhibition of multiple tyrosine kinases but not ALK. PLoS ONE 16(7): e0252048. https://doi.org/10.1371/journal.pone.0252048

Editor: Piyali Dasgupta, Marshall University, Joan C. Edwards School of Medicine, UNITED STATES

Received: November 23, 2020

Accepted: May 7, 2021

Published: July 15, 2021

Copyright: This is an open access article, free of all copyright, and may be freely reproduced, distributed, transmitted, modified, built upon, or otherwise used by anyone for any lawful purpose. The work is made available under the Creative Commons CC0 public domain dedication.

Data Availability Statement: The data underlying the results presented in the study are available in the Supporting information Documents and in the NF Data Portal online: https://nf.synapse.org/ doi: 10.7303/syn2343195 The full, unedited blot images are included as a Supporting information PDF document titled "S1_Raw_Images".

Funding: The work in this manuscript was fully sponsored and managed by the Children's Tumor Foundation (www.ctf.org) through its Synodos for

Abstract

Neurofibromatosis Type 2 (NF2) is an autosomal dominant genetic syndrome caused by mutations in the *NF2* tumor suppressor gene resulting in multiple schwannomas and meningiomas. There are no FDA approved therapies for these tumors and their relentless progression results in high rates of morbidity and mortality. Through a combination of high throughput screens, preclinical *in vivo* modeling, and evaluation of the kinome *en masse*, we identified actionable drug targets and efficacious experimental therapeutics for the

NF2 Consortium program (CTF grants: 2014-18-001A to Gary L Johnson, 2014-18-001B to James F Gusella, 2014-18-001C to Jaishri O Blakeley, 2014-18-001D to D. Wade Clapp, 2014-18-001E to D Bradley Welling, 2014-18-001F to Cristina Fernandez-Valle, 2014-18-001G to Helen Morrison, 2014-18-001H to Long-Sheng Chang, 2014-04-008 to Justin Guinney). Salvatore La Rosa is the Chief Scientific Officer for CTF and was involved in the manuscript preparation.

Competing interests: No authors have competing interests.

treatment of NF2 related schwannomas and meningiomas. These efforts identified brigatinib (ALUNBRIG®), an FDA-approved inhibitor of multiple tyrosine kinases including ALK, to be a potent inhibitor of tumor growth in established *NF2* deficient xenograft meningiomas and a genetically engineered murine model of spontaneous NF2 schwannomas. Surprisingly, neither meningioma nor schwannoma cells express ALK. Instead, we demonstrate that brigatinib inhibited multiple tyrosine kinases, including EphA2, Fer and focal adhesion kinase 1 (FAK1). These data demonstrate the power of the *de novo* unbiased approach for drug discovery and represents a major step forward in the advancement of therapeutics for the treatment of NF2 related malignancies.

Introduction

Neurofibromatosis Type 2 (NF2) is a rare disease in which biallelic loss of the *NF2* gene leads to the development of tumors of neural crest derived origin [1–3]. *NF2* encodes the tumor suppressor Merlin, whose biochemical function is incompletely understood [4]. Bilateral vestibular schwannomas are pathognomonic for NF2 and the condition is also commonly associated with the development of multiple meningiomas. Further, approximately 90% of sporadic schwannomas and 60% of sporadic meningiomas, the most common intracranial tumor in humans, have inactivation of *NF2* [5,6]. There are no approved drug therapies for these common and relentlessly progressive tumors.

In this study, we applied a systems biology approach to: (1) utilize high throughput drug screens to identify FDA approved or late stage development compounds active against Merlin deficient schwannoma and meningioma cells, (2) integrate data from kinome profiling and transcriptome analysis to prioritize targets for future development and (3) utilize a genetically engineered mouse model and tumor xenograft model to establish preliminary preclinical efficacy data for a subset of compounds identified via the *in vitro* drug screening approaches with the goal of identifying at least one drug to move forward to a clinical trial. Using this approach, we have identified for the first time, single and combinatorial agents that positively impact the treatment of both schwannomas and meningiomas associated with *NF2*. Importantly, we established the FDA approved, multi-tyrosine kinase inhibitor (TKI), brigatinib, as a potent inhibitor of Merlin-deficient schwannoma and meningioma growth, both *in vitro* and in preclinical animal models. Interestingly, neither Merlin-deficient schwannoma nor meningioma cells express the primary published target of brigatinib, anaplastic lymphoma kinase (ALK). Rather, we demonstrate that mechanistically, this compound inhibits multiple kinases, including focal adhesion kinase (FAK) previously recognized as an oncoprotein in *NF2* related tumors [7–9]. These data demonstrate an effective systems biology approach for preclinical therapeutic discovery applicable to rare tumors and support the advancement of brigatinib, as a multi-TKI into clinical trials for the treatment of *NF2* associated meningiomas and schwannomas.

Results

Discovery of novel drug combinations for NF2-associated meningiomas and schwannomas

To identify novel chemotherapeutic agents for *NF2*-associated tumors, we screened the NCATS MIPE library 4.0 of 1,932 compounds in a high-throughput dose-response format

[9] using the isogenic pairs of *NF2*-expressing HS11 and *NF2*-deficient HS01 Schwann cells and *NF2*-expressing Syn1 and *NF2*-null Syn5 arachnoidal cells, as well as *Nf2*$^{-/-}$ mouse MS02 schwannoma cells and human Ben-Men-1 meningioma cells (Syn6). This panel of cell lines was used to assess selectivity of pharmacological responses based on *NF2* status and to distinguish the differences in compound responses between human and mouse *NF2*-related tumor cells to better predict the drug activity in animal models. The MIPE library was initially screened as single agents in dose-response mode, to determine the potency (IC_{50}), efficacy (maximum % inhibition), and area under the curve (AUC) for each compound in each cell line. Active compounds were selected using dose-response curve analysis algorithms, which assigns each tested compound a Curve Response Class (CRC) number [10]. This method classified primary hits into different categories according to their IC_{50}, magnitude of response, quality of curve fitting (r^2), and number of asymptotes. A CRC of -1.1 represents a compound with a complete curve and with high efficacy; a CRC of -1.2 represents a compound with a complete curve but with partial efficacy. Compounds with CRC 4 are inactive. Compounds with CRCs of -1.1, -1.2, and a maximum response of <30% cell viability were considered for further testing in a combination screen. The heat map of the maximal % activity using the hierarchical clustering function in Spotfire Tibco is shown in Fig 1A. The results of this single-agent screen demonstrated that the pharmacological responses clustered cells by tumor type (meningioma versus schwannoma) rather than *NF2*-expressing versus *NF2*-deficient cells. S1 Fig provides a view of the pharmacological responses according to different relevant targets, cellular pathways and mechanisms, based on the AUC parameters which include both potency and efficacy of the compounds. This high-level biological analysis of pharmacological responses confirms that all cell lines tested, independent of Merlin status or tumor type, behaved very similarly and that compounds targeting proteasome, chaperone, topoisomerase, RTK, serine-threonine kinase (STK), phosphatidylinositol 3-kinase (PI3K), and tubulin are the most active (S1 Fig). 62 and 82 compounds were active in all cells by a maximum response criteria of <30% cell viability and CRC of -1.1 and -1.2, respectively. Compounds with CRC -1.1 were hypothesized to be cytotoxic, while compounds that were -1.2 could either be cytostatic or induce senescence and slow cell growth. Targets that were enriched for these active compounds included inhibitors of histone deacetylase (HDAC), proteasome, Janus kinase 2 (JAK2), tubulin, mammalian target of rapamycin (mTOR), and cyclin-dependent kinase 1 (CDK1), PI3K, and topoisomerase (Figs 1B and S1).

We then selected 45 compounds to be tested in combination based on: (1) the potency and efficacy in each cell line, (2) the targets in key pathways regulated by Merlin, and (3) mechanisms of interest identified by genome and kinome analyses. These compounds were first tested using the CellTiterGlo assay at 72-h, in 6x6, all versus all dose-response matrices, for a total of 990-pairwise combinations (Fig 1C), with concentrations customized to include a range > 4-fold and < 4-fold the IC_{50}, to better determine possible synergies in both the meningioma (Syn1 vs Syn5) and the schwannoma cell (HSO1 vs HS11) models. Synergistic combinations were ranked based on the Delta Bliss Sum Negative (DBSumNeg) values [11] for each pairwise combination matrix. We detected 33 combinations that had a DBSumNeg value of <-2 in *Nf2*-deficient Syn5 cells, and 69 combinations, which had a DBSumNeg of <-2 in HS01 cells. A heat map of hierarchical clustering of DBSumNeg for each pairwise compound combination in each cell line showed that meningioma and schwannoma cells each clustered separately by DBSumNeg synergy scores, regardless of *NF2* status as seen in the single agent screen (Fig 1D).

Next we selected 176 pairwise compound combinations based on DBSumNeg values, synergy selectivity for *NF2*-deficient cells, mechanisms of interest, and clinical interest and

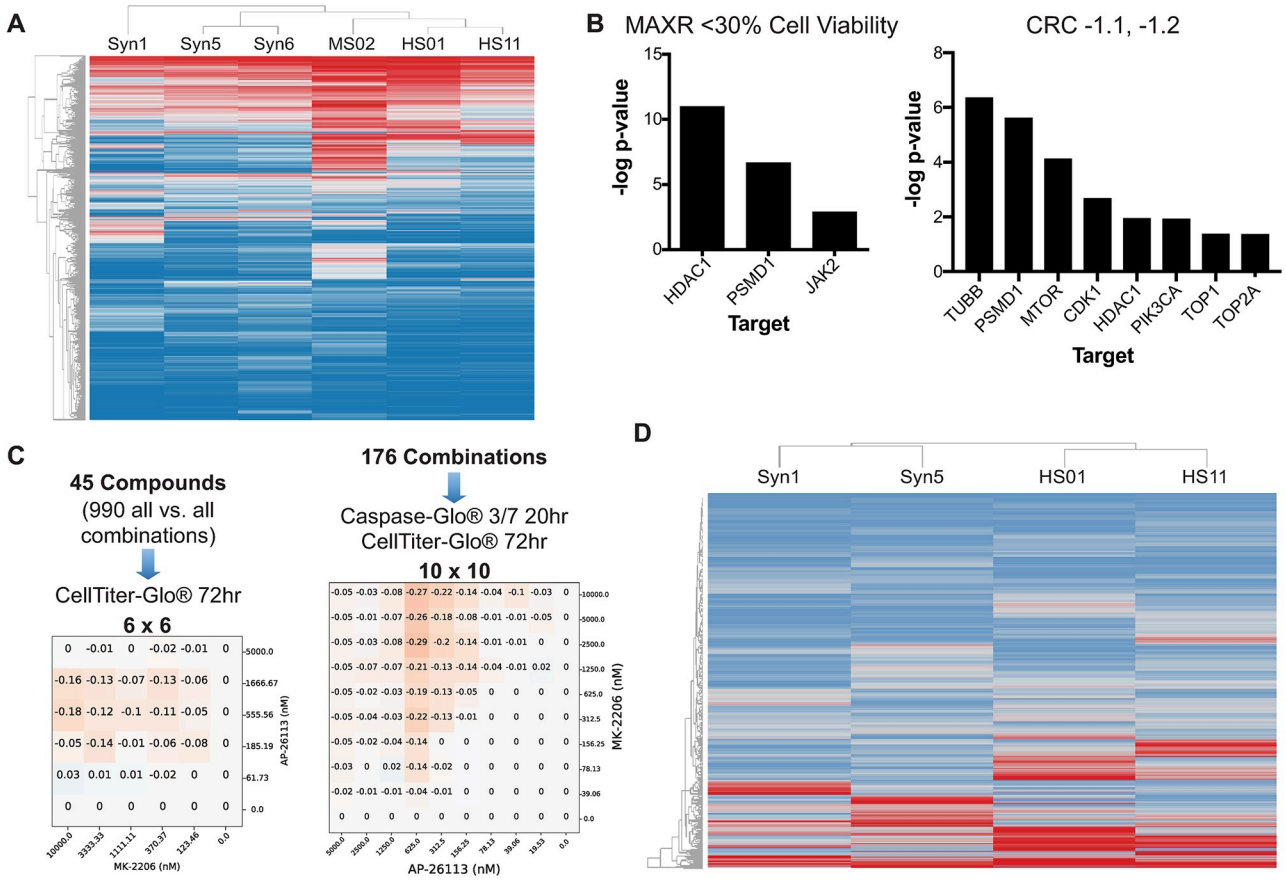

Fig 1. Single-agent and matrix HTS of the oncology MIPE 4.0 collection in meningioma and schwannoma cells. (A) Heat map of pharmacological responses (as % cell viability at the maximum dose tested, 46 μM, also called maximum response) of the MIPE 4.0 library in *NF2*-expressing Syn1 and *NF2*-null Syn5 human arachnoidal cells, *NF2*-deficient Ben-Men-1 (Syn6) meningioma cells, *NF2*-expressing HS11 and *NF2*-knockdown HS01 human Schwann cells, and *Nf2*$^{-/-}$ MS02 mouse schwannoma cells. Responses were clustered using a Hierarchical Clustering in Spotfire TIBCO. Red indicates low % cell viability and blue is high viability. (B) Target enrichment plots for pan active hits selected by % viability at the maximum concentration of compound tested (MAXR) <30% for both cell lines and all assay modes (top panel) and for pan active hits selected by CRCs -1.1 or -1.2 for both cell lines and all assay modes (bottom). The -log p-values were calculated as follows: Given a selection of compounds, the annotated targets for these compounds were identified and the enrichment for each target computed, compared to background, using the Fishers exact test. For this test, the background was defined as all the targets annotated in the MIPE collection. The p-value from the test was adjusted for multiple hypothesis testing using the Benjamini-Hochberg method. A -log p-value >1 was used as a cut-off to consider a target or processed being overrepresented. (C) Number of combinations tested and assays used for the 6x6 and 10x10 matrix combination HTS. Delta bliss 6x6 and 10x10 matrix plots for the combination of MK-2206 and ALK-IN-1 in Syn5 cells, using the CellTiterGlo viability assay. Darker color indicates higher DeltaBliss scores for synergy. (D) Heat map of DeltaBliss Sum Negative for the 990 6x6 all vs. all pairwise combinations of the 45 drugs selected from the single-agent testing. The IC_{50} and maximum % inhibition of each compound in each indicated cell line were calculated. Responses were clustered using a Hierarchical Clustering in Spotfire TIBCO. Red indicates low % cell viability and blue is high viability.

https://doi.org/10.1371/journal.pone.0252048.g001

tested them in 10x10 dose-response matrix format with the same set of meningioma and schwannoma cell models using both a cell viability readout (CellTiterGlo at 72h) and an apoptosis readout (CaspaseGlo, 20h). Based on differential drug synergy in *NF2*-deficient versus *NF2*-expressing cells, the stage of drug development, and compound performance in prior preclinical and clinical evaluations including pharmacology, response rate, toxicity, and availability, we selected and ranked the top three drug combinations for each *NF2* tumor type. These combinations in meningioma cells included: cabozantinib (an inhibitor of RTKs, including vascular endothelial growth factor receptor 2 [VEGFR2] and hepatocyte growth factor

A

Ranking	Drug Combination	Targets	DBSumNeg in Syn1 (*NF2+/+*) cells	DBSumNeg in Syn5 (*NF2-/-*) cells
1	Cabozantinib/Danusertib	VEGFR2/AURKa,b,c	-4.5557	-9.5633
2	Dasatinib/GSK2126458	BCR-ABL/PI3K	-0.3212	-4.9017
3	MK-2206/ALK-IN-1	AKT/ALK	-0.8899	-4.6811

E

Ranking	Drug Combination	Targets	DBSumNeg in HS11 (*NF2+/+*) cells	DBSumNeg in HS01 (*NF2-/-*) cells
1	ALK-IN-1/Dasatinib	ALK/BCR-ABL	-3.8977	-14.9019
2	TAE-226/Dasatinib	FAK/BCR-ABL	-3.1658	-8.9342
3	Simvastatin/Dasatinib	HMG CoA Reductase/BCR-ABL	-2.7972	-7.1197

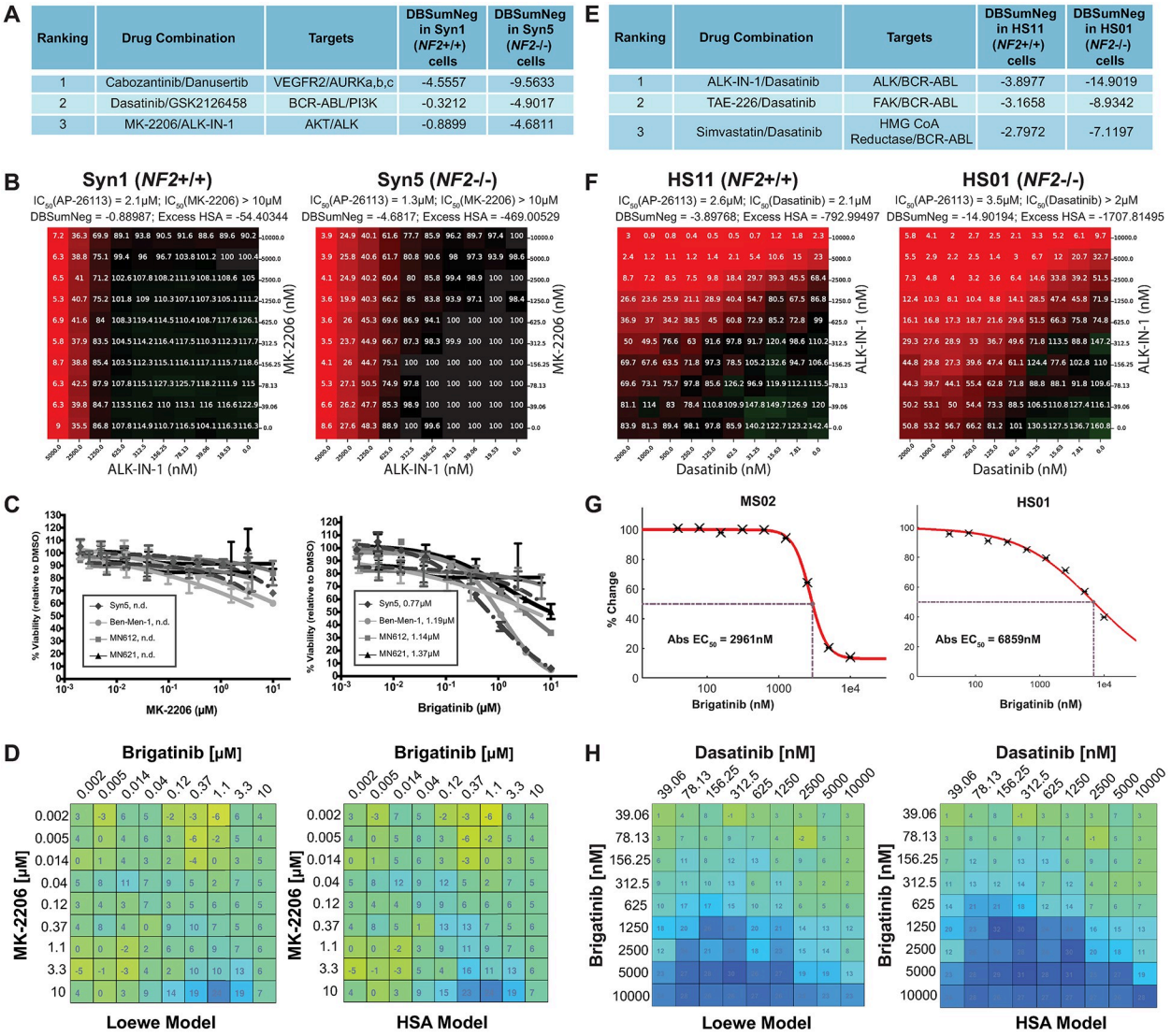

Fig 2. Like ALK-IN-1, brigatinib exhibited growth-inhibitory synergy with MK-2206 or dasatinib in meningioma and schwannoma cells. (A) The top synergistic drug combinations identified for *NF2*-deficient meningioma cells. (B) 10x10 dose-viability response matrix of ALK-IN-1 vs MK-2206 in Syn1 and Syn5 cells, assessed at 72h. (C) Single-drug dose-response curves (DRCs) for MK-2206 (left) or brigatinib (27) were generated for human *NF2*-null cell lines, including Syn5, Ben-Men-1, and two primary meningiomas (MN612, MN621). Drug concentrations are outlined under Supplementary Methods in S1 File. n.d., not determined. Data is expressed as +/- SEM. (D) Combination treatment of Ben-Men-1 cells was carried out in a 10x10 dose-matrix format using the same increasing concentration range of MK-2206 and brigatinib as with single DRCs. Heatmaps were generated on a colorimetric scale using Combenefit software, which calculates the drug interaction effects (relative to vehicle/DMSO control). (E) The top synergistic drug combinations identified for NF2-related schwannoma cells. (F) 10x10 dose-viability response matrix of ALK-IN-1 vs dasatinib in HS11 and HS01 cells, assessed at 72h. (G) Brigatinib dose-response in mouse MS02 and human HS01 cells at 60 and 72h, respectively. (H) Loewe and highest single agent (HSA) synergy matrix analysis of brigatinib vs. dasatinib in HS01 cells treated for 72h.

https://doi.org/10.1371/journal.pone.0252048.g002

receptor MET)/danusertib (an Aurora kinase inhibitor), dasatinib (an inhibitor of BCR-ABL and SRC-family TKs)/GSK2126458 (a dual PI3K/mTOR inhibitor), and MK-2206 (an AKT inhibitor)/ALK-IN-1 (an inhibitor of ALK and multiple other TKs) (Fig 2A). The most effective combinations in Schwann cells were slightly different and included: ALK-IN-1/dasatinib, TAE226 (a dual FAK/IGF-1R inhibitor)/dasatinib, and dasatinib/simvastatin (an HMG-CoA reductase inhibitor) for schwannoma (Figs 2E, S3 and S4).

ALK-IN-1 and its derivative brigatinib synergized with MK-2206 or dasatinib to inhibit *NF2*-deficient meningioma and schwannoma cell viability, respectively

ALK-IN-1 is a chemical analogue of the FDA-approved ALK inhibitor brigatinib (AP26113. ALUNBRIG®) [12]. As ALK-IN-1 is no longer in clinical development, we compared brigatinib with ALK-IN-1 for their ability to synergize with MK-2206 or dasatinib to inhibit viability of *NF2*-deficient cells. Similar to ALK-IN-1, brigatinib inhibited viability of *NF2*-deficient Syn5 arachnoidal and Ben-Men-1 meningioma cells and two independent primary meningioma cell lines with *NF2* loss (MN612 and MN621). MK-2206 alone showed little growth-inhibitory activity (Fig 2B and 2C), however, when combined with brigatinib, MK-2206 exhibited mild synergy in growth inhibition of Ben-Men-1 (Fig 2D) and Syn5, MN612, and MN621 cells (S2 Fig).

ALK-IN-1 and dasatinib combination treatment reduced cell viability in the human Schwann cell lines, and the *NF2*-deficient (HS01) cells were more sensitive to treatment (Fig 2F). As a single agent, brigatinib inhibited viability of mouse *Nf2*$^{-/-}$ schwannoma MS02 and human *NF2*-deficient HS01 Schwann cells (Fig 2G). Mouse MS02 cells appeared more sensitive to brigatinib inhibition than human HS01 cells. As with ALK-IN-1 in the broad screen (Fig 2F), brigatinib demonstrated significant synergy with dasatinib in reducing viability of both HS01 and MS02 cells (Figs 2H and S3). Based on these results, we further evaluated brigatinib monotherapy and in combination with either MK-2206 or dasatinib by transcriptome analysis of treated cells and for effects on tumor growth *in vivo*.

Transcriptome analysis of drug-treated *NF2*-expressing and *NF2*-deficient cells

Baseline transcriptome analysis revealed that ALK is not expressed in Syn1/Syn5 arachnoidal and HS01/HS11 Schwann cells, suggesting that brigatinib acts through another target. Consistent with its differential effect on their growth, brigatinib treatment, with (BTM) or without MK-2206 (BT), elicited an exaggerated transcriptomic response from Syn5 compared to Syn1 cells. MK-2206 treatment alone did not result in any DEGs. Most differentially expressed genes (DEGs) from treatment of Syn1 (560 BT and 830 BTM) were also DEGs in treated Syn5 (456 BT and 625 BTM), but the latter expressed far more DEGs overall (2605 BT and 2171 BTM of which 1658 DEGs were present and altered in the same direction by both treatments) (S5A Fig and S1 Table). DEGs shared by treated Syn5 and Syn1 were enriched in DNA replication and cell cycle pathways, but the more numerous Syn5-specific DEGs were enriched in pathways related to RNA (S2A Table). Interestingly, in untreated cells, *NF2* inactivation is associated with a similar level of dysregulation to that caused by drug treatment of Syn5 (2458 DEGs from untreated Syn5 vs untreated Syn1). A comparison of these 2458 DEGs caused by *NF2* inactivation with the DEGs elicited in Syn 5 by either brigatinib or brigatinib + MK-2206 revealed substantial overlap (988 and 832, respectively), with more than 99% of these shared DEGs being dysregulated in opposite directions by *NF2* inactivation and by drug treatment of the *NF2* deficient cells (S5B Fig and S1 Table).

Treatment of HS01 and HS11 cells with brigatinib did not significantly disrupt the transcriptome, while treatment with either dasatinib or simvastatin had modest effects (S1 Table, S5C Fig). The combination of brigatinib + dasatinib showed more robust effects, with DEGs in HS01 Schwann cells being enriched most significantly in cytoplasmic pathways, in contrast to the arachnoidal cells (S2B Table).

Kinome profiling in brigatinib- treated cells

Brigatinib is used clinically for the treatment of ALK-positive non small cell lung carcinoma, with reported IC50 of 0.6nM determined by in vitro kinase assay [13]. However, it has numerous kinase targets including FER, ROS1, FLT3, EGFR, FAK1 (PTK2), and KIT with IC50 values <250nM and additional kinases with IC50 ~500nM-1uM such as ABL, EPHA1, EPHA7, and EPHB1 [13,14]. As brigatinib administration at 90 mg or 180mg dosage has been shown to achieve Cmax of 552 (0.94 uM) or 1452 ng/ml (2.482 uM), respectively [15], we sought to determine the kinases affected using comparable or lower concentrations of brigatinib effective in schwannoma and meningioma cells. To address this question, we conducted multiplexed kinase inhibitor bead (MIB) kinome profiling experiments. MIBs are a mixture of Type I kinase inhibitors designed to bind kinases when they are in the "Asp-Phe-Gly (DFG)-in" (active) conformation [16,17]. A spectrum of MIBs capable of binding almost all expressed kinases is employed, and binding is influenced not only by kinase expression but kinase activity as well. Kinases bound to the MIBs are subsequently identified and quantified via mass spectrometry [17,18]. In *NF2*-expressing (Syn1) or *NF2*-deficient (Syn5) arachnoidal cells treated for 24 hours, brigatinib significantly reduced MIB binding of multiple tyrosine kinases including Aurora kinase A (AURKA), Cyclin G-associated kinase (GAK), Fps/Fes-related kinase (FER), Activated Cdc42-associated kinase (ACK1 or TNK2), and FAK1 (PTK2) (Fig 3A and 3B). Similar target effects were observed with the addition of MK-2206, an allosteric AKT inhibitor, to brigatinib though unique peptides were only detected for AKT3 and in insufficient samples to quantitate (Fig 3C and 3D).

By adding kinase inhibitors to lysate or briefly treating cells, the direct target spectrum can be more reliably assessed by kinome profiling. This overall approach has substantially informed our knowledge of polypharmacology for numerous inhibitors in clinical use [19]. As validation of the observed kinase targets in Syn1 and Syn5 cells, 2-hour incubation of 10 and 100nM brigatinib was performed prior to kinome profiling in an *NF2*-deficient meningioma cell line Ben-Men-1 (Fig 3E). Brigatinib reproducibly reduced MIB binding of FER, TNK2, and FAK1 (PTK2) at both 100 and 1000nM. In a compatible experiment using lysate prepared from schwannomas from a genetically engineered murine model (GEMM), $Nf2^{flox/flox}$;*Postn-Cre* mice, a MIB competition assay identified FAK1 (PTK2) and GAK as the primary targets of brigatinib (Fig 3F). Further, kinome profiling from dorsal root ganglia in $Nf2^{flox/flox}$;*Postn-Cre* mice treated for either 3 or 7 days with 50 mg/kg/qd brigatinib monotherapy demonstrated a significant reduction in activated FAK1 (PTK2) and GAK (Fig 3G). The target specificity of brigatinib in HS01 and HS11 cells was also analyzed by lysate treatment followed by kinome profiling and the kinases with the largest reduction in binding were FER, TNK2, FAK1 (PTK2) and FAK2 (PTK2B) (Fig 3H). In comparison, the kinase inhibition profile was distinct for dasatinib, which primarily inhibited Src family kinase and Ephrin receptors (S6B and S6C Fig). Consistent with the transcriptome analysis, ALK was not detected using MIB kinome profiling methodology in either schwannomas or meningiomas, suggesting that non-ALK targets of brigatinib were driving the phenotypic effects.

Many of the kinase targets identified by kinome profiling were published targets of brigatinib, including FAK1 (PTK2), FAK2 (PTK2B), FER, MARK3, MARK1, RPS6KAS3, AURKA, SIK2, JAK1, and STK22 [13]. However, several kinases were not previously published brigatinib targets, such as ACK1 (TNK2), GAK, NUAK2, AAK1, PLK4 and SIK1. Since GAK and ACK1 (TNK2) were strongly inhibited in our models, we performed NanoBRET™ TE (target engagement) intracellular kinase assays with brigatinib to determine the IC50 for (ACK1) TNK2 and GAK using FAK1 (PTK2) and FER as positive controls (NanoLuc fusions with ALK are not commercially available). As shown in S6D–S6G Fig, brigatinib potently impacted

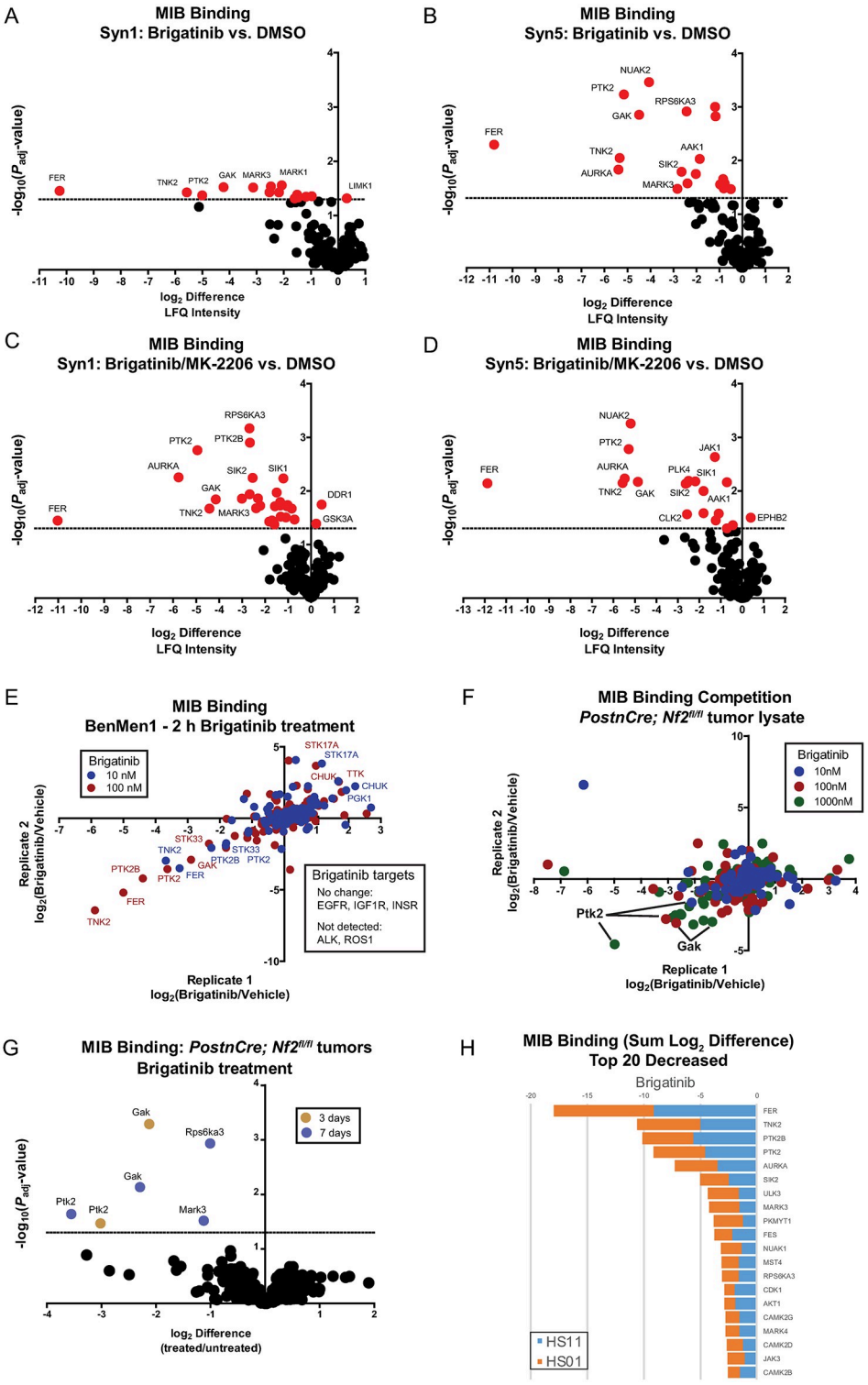

Fig 3. MIB/MS kinome profiling reveals brigatinib target specificity in multiple *NF2*-deficient cell models. (A-D) MIB/MS kinome profiling was performed following treatment of Syn1 and Syn5 cells with vehicle (DMSO), brigatinib (1μM) or the combination of MK-2206 (0.5μM) and brigatinib (1μM) for 24h in biological triplicate. MIB binding (log2LFQ intensities) were used for comparisons and the volcano plots indicate log2 difference and significance (5% FDR, indicated by dashed line). (E) MIB/MS kinome profiling was performed following treatment of Ben-Men-1 cells with vehicle (DMSO) or brigatinib (10nM, blue or 100nM, red) for 2h in biological duplicate. The log2 difference in

MIB binding (LFQ intensity) was calculated and plotted relative to vehicle for each replicate. (F) Tumor lysates from the *Postn-Cre;Nf2*$^{flox/flox}$ mouse model were prepared and equal amounts of total protein were incubated for 2h with vehicle (0.001% ethanol) or brigatinib (10nM, blue; 100nM, red; 1000nM, green) in biological duplicate prior to MIB/MS kinome profiling. The log2 difference in MIB binding (LFQ intensity) was calculated and plotted relative to vehicle for each replicate. (G) *Postn-Cre;Nf2*$^{flox/flox}$ mice were treated with vehicle or brigatinib for 3 or 7 days (gold and blue, respectively, for indicated kinases). Tumors were harvested and subjected to MIB/MS kinome profiling. MIB binding (log2LFQ intensities) was determined and used for comparisons of brigatinib to vehicle treatment. The volcano plot indicates log2 difference and significance (5% FDR, indicated by dashed line). (H) HS11 and HS01 cells were treated with vehicle (DMSO) or brigatinib (1μM) for 24h prior to MIB/MS kinome profiling. MIB binding (log2LFQ intensities) was determined and the top 20 kinases with decreased MIB binding compared to vehicle are shown as a stacked bar plot for the two cell lines.

https://doi.org/10.1371/journal.pone.0252048.g003

the BRET ratio for each of these kinases in HEK293T cells: FAK1 (PTK2), IC50 = 573.3nM; FER, IC50 = 303.6nM; GAK, IC50 = 154.6 nM; and TNK2, IC50 = 350.3 nM). Collectively, these data identify brigatinib as a direct and potent inhibitor of multiple kinases, including FAK1 (PTK2) and FAK2 (PTK2B), and novel targets, GAK and TNK2, in both arachnoid and schwannoma cells.

For validation of the targets identified in the kinome assay and to further probe known targets of brigatinib which were not altered in the kinome data set, a series of immunoblots were conducted on the Ben-Men-1 cell line. ALK expression was not observed in the Ben-Men-1 cells under any growth conditions (Figs 4A, S7 and S8). When EGF, HRG, or IGF-1 were added to the culture media to stimulate EGFR, ErbB3, and IGF-1R respectively, brigatinib potently inhibited the activation of these receptors (Fig 4B). Low levels of p-EGFR were detected in Ben-Men-1 cells whether actively growing, or growth-arrested and then stimulated with 20% serum. However, p-EGFR could be robustly stimulated with the addition of EGF to the media (S9 Fig). Therefore, it is possible that modulation of these known targets of brigatinib was not observed in the MIB experiments because appropriate stimulatory ligands were not present in those cell culture conditions. At 2 hours and 24 hours post stimulation with 10% or 20% FBS, treatment with brigatinib resulted in a significant reduction in FAK activation (Fig 4C). Treatment with brigatinib also reduced proliferative signaling as measured by p-ERK, p-AKT, p-S6 (Figs 4C and S8). Similarly, in Merlin-deficient (*NF2*-deficient) Schwann cells, ALK expression was not detected at baseline and treatment with brigatinib resulted in a reduction in FAK phosphorylation as well as reductions in p-ERK, p-AKT, and p-S6 (Figs 4D and S10). In human *NF2*-deficient Schwann cells, brigatinib treatment reduced phosphorylation of FAK, ERK, AKT, S6RP, GSK, p70S6K, and IGR at 2, 6 and 24 hours post-treatment with 2μM and 4μM brigatinib, while p-STAT3 and p-MEK were both reduced with 2μM but not 4μM brigatinib (Fig 4E). These data validate and recapitulate the mass spectrometry based findings that brigatinib is a potent inhibitor of FAK in both Merlin-deficient schwannoma and meningioma cell lines *in vitro*.

Brigatinib treatment of meningiomas and schwannomas in murine models of NF2

Patients with NF2 will often suffer from both meningiomas and schwannomas. Given the *in vitro* efficacy and the -omics supported mechanism of action in both tumor cell models, we chose to test brigatinib both alone and in combination with MK-2206 in a tumor xenograft model of meningioma. Mice were first injected with the human *NF2*-deficient Ben-Men-1 meningioma cells and then treated with either 120 mg/kg/qd MK-2206, 50 mg/kg/qd brigatinib, or the combination. Peak serum concentrations of brigatinib reached the 1.2μM concentration shown to be the IC50 of these cells *in vitro* with drug concentrations in the brain lagging by a little less than one order of magnitude (Figs 2C and 5A). Combination therapy

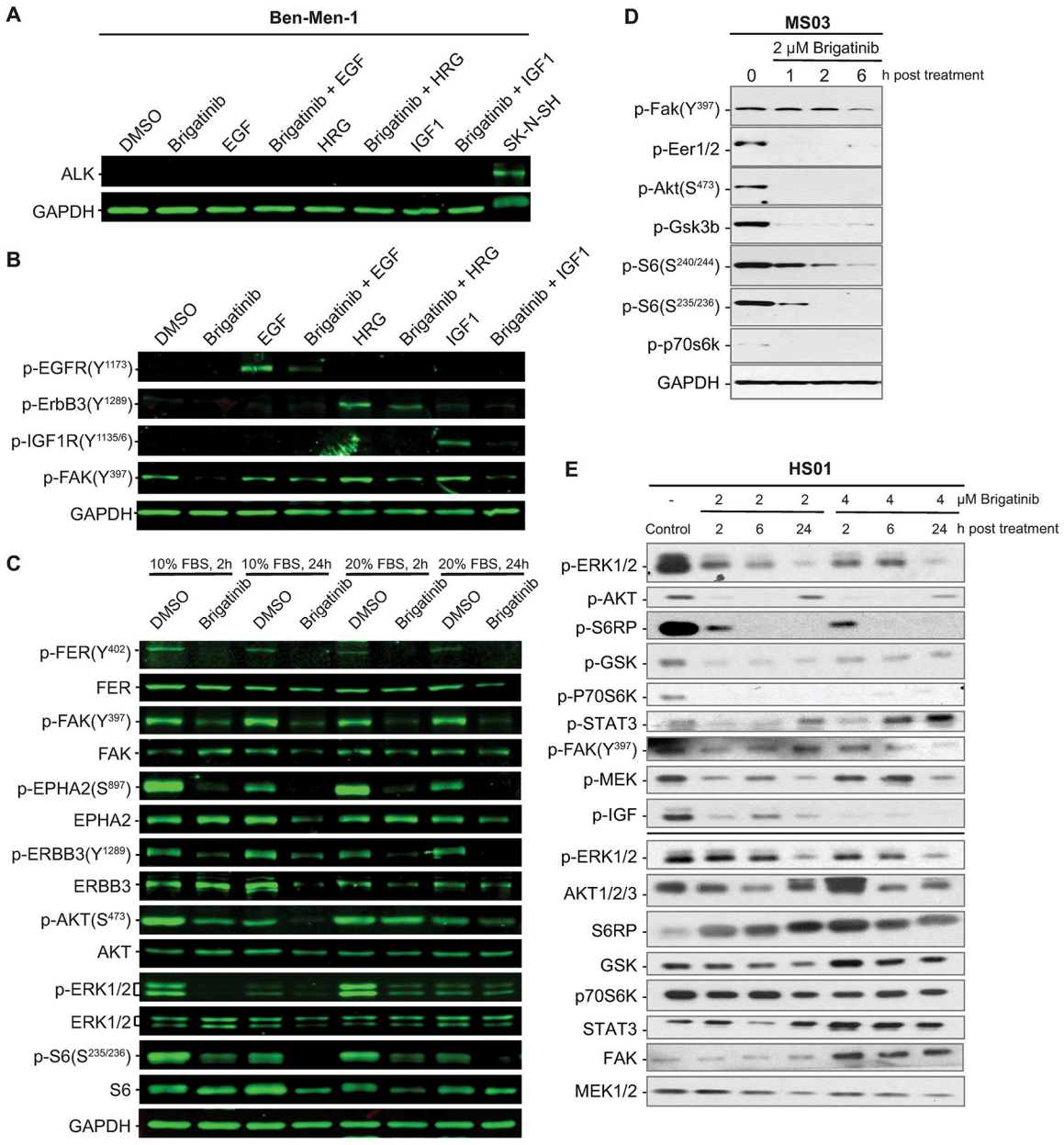

Fig 4. Brigatinib inhibits multiple RTKs, non-RTKs, and their downstream signals. (A) Western blot analysis was conducted to detect ALK expression in Ben-Men-1 cells grown under various growth conditions and with or without brigatinib treatment. (B) Brigatinib treatment greatly reduced phosphorylation of non-RTKs FER and FAK, RTKs EPHA2 and ErbB3, and their downstream signaling molecules AKT, ERK1/2, and S6 in active growing Ben-Men-1 cells or growth-arrested cells stimulated with 20% serum. (C) Brigatinib blocked phosphorylation of EGFR, ErbB3, and IGF1R in growth-arrested Ben-Men-1 cells stimulated with each cognate ligand. (D) Brigatinib reduced the levels of p-FAK, p-ERK1/2, p-AKT, p-S6, and p-Gsk in *Nf2* deficient murine Schwann Cells. (E) Brigatinib reduced phosphorylation of FAK, ERK1/2, MEK, AKT, S6RP, p70S6K, STAT3, and IGR in *NF2*-deficient HS01 human Schwann cells.

https://doi.org/10.1371/journal.pone.0252048.g004

increased concentrations of brigatinib in the serum but not in the CNS compared with treatment of brigatinib alone (Figs 5A and S11). As measured by luminescence engineered into the meningioma cells, brigatinib, both alone and in combination with MK-2206 blocked outgrowth of the xenograft (Figs 5B, 5C and S12).

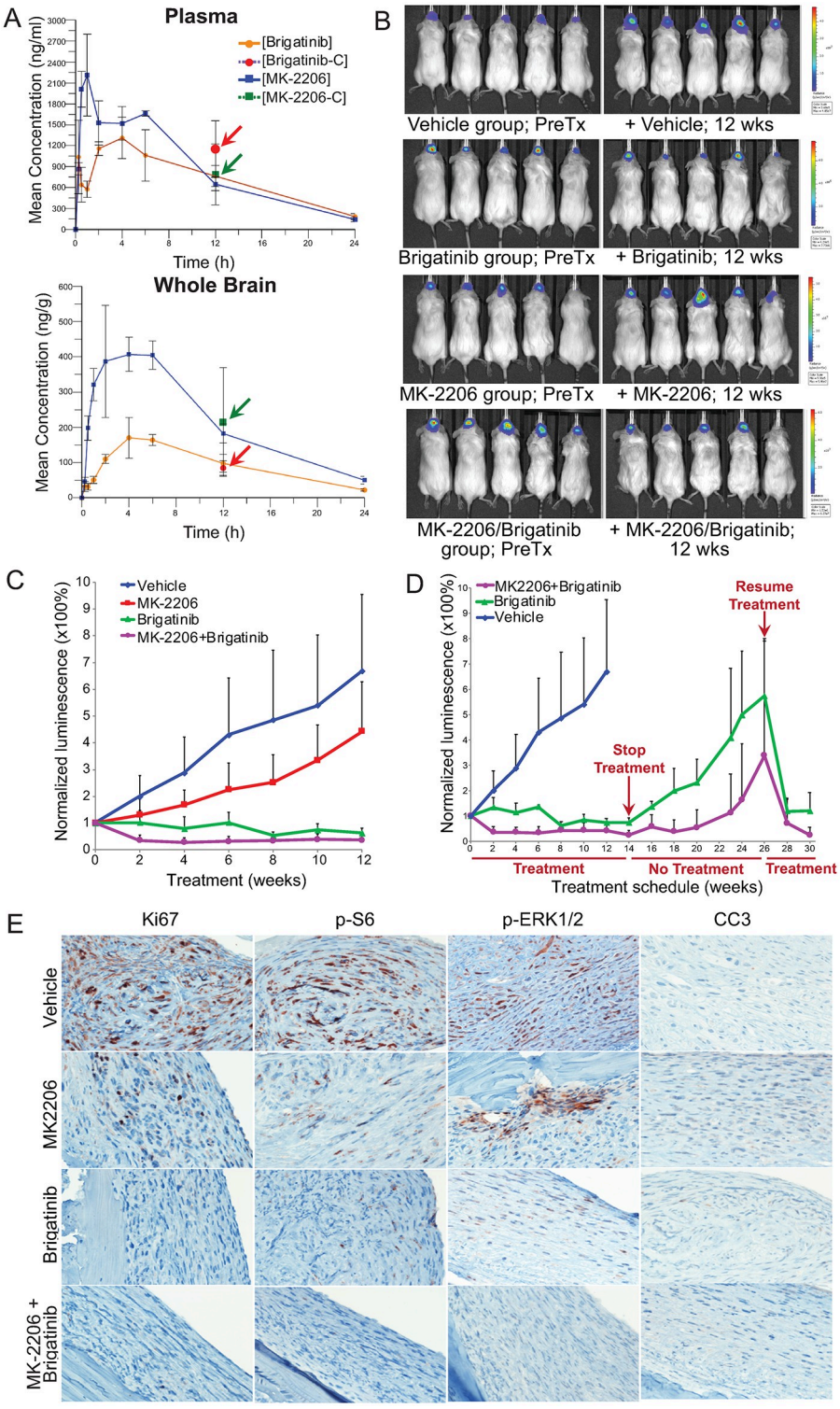

Fig 5. Brigatinib and its combination with MK-2206 effectively shrank intracranial meningioma xenografts. (A) Pharmacokinetic (PK) analysis was conducted to determine the concentrations of brigatinib and MK-2206 in mouse plasma and brain. Mice were treated with a single maximum tolerated dose (MTD) of brigatinib or MK-2206. Prior to and at various times after dosing (n = 3 per time point), blood and brain from each dosed mouse were collected for UHPLC-MS/MS. The mean concentration of each drug at each indicated time point with standard deviation was plotted. Also, mice were treated with a combined dose of brigatinib and MK-2206 at their MTD (n = 3), and the drug

concentration in the plasma and brain determined (indicated with arrows). (B-C) Mice with established meningioma xenografts were treated with vehicle, brigatinib, MK-2206, or brigatinib+MK-2206 by oral gavage (n = 10 each) and tumor growth was monitored by BLI. (B) Shown are representative BL images of tumor-bearing mice acquired prior to (PreTx) and 12 weeks (wks) after treatment. (C) The relative tumor-emitted BL signals were quantified and denoted as % of total flux after treatment relative to the total flux prior to treatment designated as one (100%). The data are shown as mean ± standard deviation. At least seven mice from each group completed the entire 12-week treatment. (D) Upon cessation of treatment, tumors in mice that had been treated with brigatinib or brigatinib+MK-2206 for 14 weeks (n = 4 each) regrew. However, tumor shrinkage was observed when the treatment was re-initiated. Data shown for mice treated with brigatinib or brigatinib+MK-2206 are only from the cage of mice that had undergone cessation of treatment and retreatment. (E) Representative images of immunostained sections of the heads of tumor-bearing mice after 12-week treatment with vehicle, MK-2206, brigatinib, or MK-2206+brigatinib for Ki67, p-S6, p-ERKs, and cleaved caspase 3 (CC3) expression.

https://doi.org/10.1371/journal.pone.0252048.g005

To assess whether brigatinib and/or MK-2206 were tumoristatic or tumoricidal, treatment was halted after 14 weeks of therapy. Cessation of treatment was associated with rapid xenograft expansion (Fig 5D). However, treatment re-initiation resulted in rapid loss of luminescence, indicating that the xenograft was still drug sensitive (Fig 5D). Immunohistochemistry showed a significant reduction in tumor cell proliferation consistent with luminescence signal and proliferative signaling in treated xenografts (Fig 5E).

In parallel *in vivo* studies in schwannomas, *Postn-Cre*;*Nf2*$^{flox/flox}$ mice were treated for 12 weeks with brigatinib and dasatinib, as single agents and in combination as well as dasatinib in combination with simvastatin, another FDA approved therapeutic which demonstrated synergy with dasatinib in the drug screens (S4 Fig). Mice treated with brigatinib alone received the maximum tolerated dose of 50 mg/kg/qd. Due to *in vivo* toxicity in the preclinical model, the dose of brigatinib in the brigatinib and dasatinib combination was reduced to 15 mg/kg/qd. The combination of the lower dosing and decreased half-life of brigatinib in the combination therapy group significantly reduced total drug exposure as measured by AUC (Fig 6A). While serum concentrations of brigatinib in the brigatinib alone treated mice came very close to the previously determined *in vitro* IC50 of MS02 cells, serum concentrations of brigatinib in the combination therapy group were much lower, in a range which we would predict to be less therapeutically efficacious given our *in vitro* data (Figs 2G and 6A). Brigatinib alone significantly reduced the volume of tumor-bearing dorsal root ganglion (DRG) tissue (Fig 6B). Finally, tissues from mice treated with brigatinib had some Schwann cell hypercellularity at the end of 12 weeks of treatment, but had far fewer areas of discrete schwannoma when compared to the other treatment conditions (Fig 6C). The brigatinib and dasatinib combination therapy also reduced the DRG volume, but by a smaller magnitude.

Discussion

In these studies, we undertook an unbiased, systems based approach to ultimately identify brigatinib as a novel monotherapy for the treatment of *NF2* related schwannomas and meningiomas. This work began with a series of cell based drug screens and utilized the ~2000 compounds contained in the MIPE 4.0 oncology collection. ALK-IN-1 was identified as a potent and selective inhibitor of *NF2*-deficient arachnoid and Schwann cell lines compared with otherwise isogenically matched *NF2/Nf2*-expressing cells. We chose not to pursue ALK-IN-1 directly as a therapeutic because ALK-IN-1 was originally generated as a part of a series of structural analogs which could inhibit ALK. Ultimately therapeutic development of that series of molecules favored a different analog, AP26113, now known as brigatinib. We confirmed that brigatinib had efficacy comparable to ALK-IN-1 in slowing the growth of schwannoma and meningioma cells lines and also exhibited modest *in vitro* synergy in growth inhibition of

A

Compound	Dosage (mg/kg)	C_{max} (ng/mL)	t_{max} (hours)	$AUC_{0-\infty}$ (ng*mL^{-1}*hr)	$t_{1/2}$ (hour)	Cl/F (L/hr)	VD_{SS}/F (L)
Brigatinib (alone)	50	2819	4	54907	8.8	0.019	0.26
Brigatinib (+ Dasatinib)	15	818	1	9529	6.3	0.034	0.32
Dasatinib (alone)	20	115	1	537	0.94	0.82	2.32
Dasatinib (+ Brigatinib)	20	507	1	2406	4.3	0.18	1.09

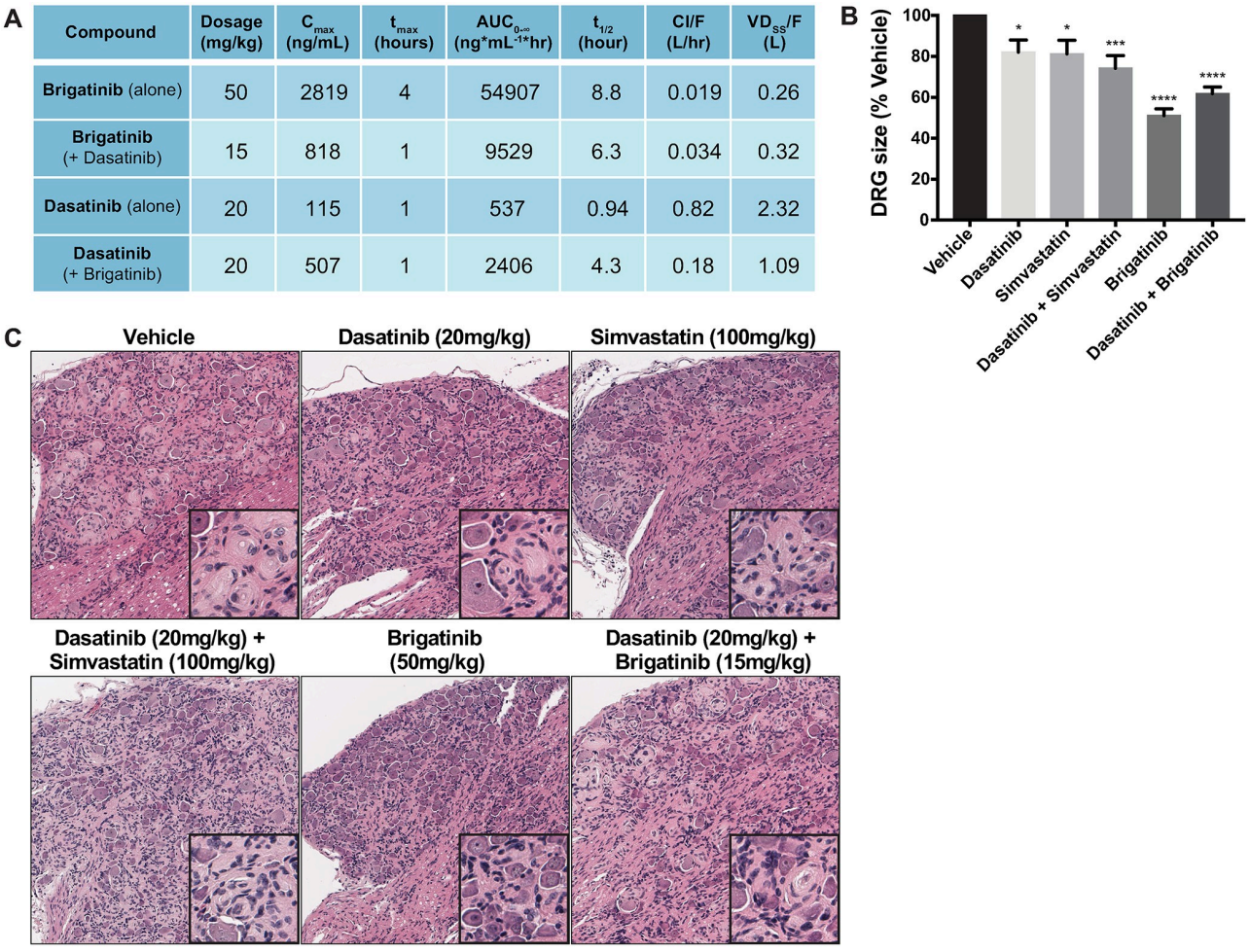

Fig 6. Brigatinib, dasatinib, simvastatin and combination treatments in the schwannoma mouse model. (A) Single-dose pharmacokinetics of compounds in *PostnCre; Nf2$^{flox/flox}$* mice. Plasma compound concentrations were measured at baseline, 1, 2, 4, 8 and 24 hours after administering a single oral dose to n = 3 *PostnCre; Nf2$^{flox/flox}$* mice. Parameters were calculated using a noncompartmental NCA-xls using PK add ins. (B) Volume of dorsal root ganglia (DRG) was measured post-mortem. All treatment groups had significantly smaller DRG volume when compared to vehicle, and brigatinib-treated DRGs showed the greatest reduction. One-Way ANOVA with Dunnett's multiple comparison's test; p = 0.0001(****), p = 0.0007 (***), p<0.05(*). (C) Representative hematoxylin and eosin stained DRGs following 12 weeks of continuous treatment with the indicated drugs.

https://doi.org/10.1371/journal.pone.0252048.g006

meningioma cells when combined with MK-2206 (Figs 2B–2D and S2). Hence, brigatinib replaced ALK-IN-1 for the *in vivo* studies.

The reasoning behind relying on an unbiased, systems based screen to identify novel therapeutics for NF2 was driven in part by our incomplete understanding of the biochemical functions of Merlin which has hampered prior efforts to advance therapeutics for this disease. Indeed, we would not have anticipated a drug known for its ability to inhibit ALK demonstrating preclinical efficacy in either *NF2* associated schwannoma or meningioma. Given this observation, we were surprised that ALK is not expressed in either tumorigenic cell type (Figs 4A, S7, S8 and S10). Following up on this unexpected finding, we demonstrated that in our particular cell culture conditions and in the primary tumors *in vivo*, the kinases most inhibited by brigatinib were non-RTKs (FER, PTK2B/FAK2, and PTK2/FAK) and serine/threonine kinases (TNK2, STK33, and GAK). Similarly, the non-RTK PTK2/FAK and the serine-threonine kinases GAK, RPS6KA3/RSK2, and MARK3 were also found to be greatly suppressed in

brigatinib-treated schwannoma cells (Fig 3). Our findings underscore the importance of kinome profiling in disease models of interest to identify potentially relevant but unanticipated drug targets [19].

From the New Drug Application [15] information of ALUNBRIG™ submitted to the FDA, we learned that while brigatinib has an IC_{50} of ~1 nM against ALK, it potently inhibits at relatively low IC_{50} values ($\leq$ 10 nM) other RTKs, like ROS1 and FLT3, several non-RTKs, including FER, FES/FPS, FAK/PTK2, and breast tumor kinase/protein tyrosine kinase 6 (BRK/PTK6), as well as the serine/threonine kinases STK22D and checkpoint kinase 2 (CHK2). Brigatinib is also active at IC50 $\leq$ 100 nM against several RTKs, including the various EGFR-family members, vascular endothelial growth factor receptor 3 (VEGFR3), RET, and IGF-1R, non-RTKs, such as YES and PTK2B/FAK2, and a number of serine/threonine kinases. In addition, brigatinib inhibits various fibroblast growth factor receptors (FGFRs), several EPH receptors, and non-RTKs at low micromolar concentrations that have been achieved clinically by many other RTK inhibitors. Using a proteome-wide drug screening approach, it was confirmed that brigatinib strongly interacts with ALK, PTK2/FAK1, and PTK2B/FAK2 and has a medium affinity to IGF-1R and EGFR [20]. These results suggest that the non-RTKs FAK/PTK2 and FER, which are strongly inhibited by brigatinib in *NF2*-deficient meningioma and schwannoma cells, are important for the growth and survival of these tumors. However, the multiple other targets of brigatinib in signaling pathways linked to Merlin may also impact the therapeutic efficacy of this drug.

It should be emphasized that even though we did not detect changes in the RTKs that are frequently activated in *NF2*-related tumors by MIB/MS, we were able to demonstrate suppression of phosphorylated EGFR, ErbB3, and IGF-1R in cells treated with 1x IC_{50} concentration of brigatinib under ligand-induced growth conditions (Fig 3B). At this brigatinib concentration, we also detected inhibition of EphA2, which we previously showed increased expression and activation of this RTK in *NF2*-deficient cells [21]. Consequently, activation of all these RTKs and non-RTKs leads to downstream activation of both PI3K-AKT and MEK-ERK signaling (Fig 3). Collectively, our results suggest that the anti-tumor activity of brigatinib in *NF2* associated schwannoma and meningioma is mediated through blockade of multiple RTKs and non-RTKs.

Consistent with previous reports [13,22], brigatinib and MK-2206 exhibited an overall favorable pharmacokinetic (PK) profiles. In the plasma, brigatinib reached a maximum of 2.2 μM when given orally (1,311 ng/ml of C_{max} in S11 Fig), which is above the IC_{50} in Ben-Men-1 cells. Our PK data also showed effective blood-brain penetration and further indicates no drug-drug interaction between brigatinib and MK-2206 (Fig 5A). These results should guide the dosing regimen for these drugs in a future clinical trial. Importantly, brigatinib monotherapy induced tumor regression in meningioma and its combination with MK-2206 resulted in further tumor shrinkage (Fig 5B and 5C). Although meningiomas regrew upon cessation of treatment, these tumors remained responsive to brigatinib, either alone or in combination with MK-2206 (Fig 5D). These results suggest that it is possible to have short breaks from treatment while maintaining therapeutic responses to retreatment, particularly after treatment with the brigatinib/MK-2206 combination.

Brigatinib as a single agent was well-tolerated and showed efficacy in the *NF2* GEMM animals. We observed a nearly 40% reduction in average DRG volume after 12 weeks of daily brigatinib treatment (Fig 6B) and reduced discrete schwannoma formation in the brigatinib-treated DRGs (Fig 6C). The two combinatorial therapeutics of brigatinib/dasatinib and dasatinib/simvastatin which were identified in the drug screen and tested *in vivo* were also efficacious in reducing schwannoma growth albeit to a lesser extent than what was observed with brigatinib alone at a higher concentration. Of note, significant toxicity was observed in the

brigatinib/dasatinib treatment group. Due to toxicity, the dose of brigatinib in the brigatinib/dasatinib combination had to be reduced from 50 mg/kg to 15 mg/kg. The lower dose of brigatinib in the combination therapy group significantly reduced total drug exposure as measured by AUC (Fig 6A). Therefore we believe the reduction in efficacy of the brigatinib/dasatinib combination therapy over the brigatinib single agent treatment may be a result of the greater than threefold reduction in brigatinib dosing given to the combination treated mice. The magnitude of the reduction in average DRG volume observed in the Brigatinib treated mice is the largest we have seen for any treatment in the *Postn-Cre*;*Nf2*$^{flox/flox}$ animals. DRG tissue harvested from mice at the end of the 12-week treatment period were evaluated by western blot and showed that brigatinib alone and brigatinib + dasatinib combination treatments resulted in greater inhibition of p-FAK, p-AKT and p-S6 pathways when compared to the other treatment groups (S13 Fig). Interestingly, dasatinib alone did not result in a significant inhibition of these kinases, also supporting the importance of brigatinib *in vivo* in the brigatinib + dasatinib combination group.

The studies executed here rely at least in part on xenograft and genetically engineered murine models. Consequently, we acknowledge that there could be important species-specific biological features of our studies compared to those in humans. However, in a closely related disease, Neurofibromatosis Type 1, we and others have found that genetically engineered murine models closely replicate the tumor pathogenesis and offer insights into a meaningful clinical signature in patients [23] for two distinctly different drugs [23–25]. Furthermore, the omics methodology utilized in one of these recent studies [25] was also key to identify specific activated kinases that may be important in tumor progression. The same methodologies were used in these studies. Finally, the kinases that were identified using MIB/MS were independently validated using other methodologies. Based on the data presented here, brigatinib possesses potent anti-tumor activity against *NF2*-deficient tumors via inhibition of multiple RTKs frequently activated in these tumors as well as blockade of several non-RTKs and serine-threonine kinases, but not ALK. Given the fact that brigatinib caused tumor shrinkage in both *NF2* associated schwannoma and meningioma, a clinical trial was initiated to assess the therapeutic effectiveness of brigatinib in NF2-associated tumors (ClinicalTrials.gov: NCT04374305).

Materials and methods

Compounds and library

The MIPE (Mechanism Interrogation Plates) oncology compound library 4.0 consisting of 745 FDA-approved drugs, 420 Phase I-III investigational agents, and 767 preclinical molecules was screened at the National Center for Advancing Translational Sciences (NCATS), National Institutes of Health. All compounds in the library have been annotated for their known nominal target, representing diverse and redundant mechanisms of action. Also, the library contains several compounds per target, allowing target-based enrichment analysis of responses; however, most compounds have polypharmacology. See Supplemental Methods in S1 File for additional details.

Cells and compound screening

A panel of NF2 tumor-relevant cells (Schwann cells for schwannoma and arachnoidal cells for meningioma with *NF2*-expressing or *NF2*-deficient) was previously assembled for systematic drug evaluation [1]. In this study, we used the isogenic pairs of *NF2*-expressing HS11 and *NF2*-deficient HS01 Schwann cells and *NF2*-expressing Syn1 and *NF2*-null Syn5 arachnoidal cells [26,27]. Also, human *NF2*-deficient meningioma Ben-Men-1, mouse *Postn-Cre*; *Nf2*$^{flox/flox}$ schwannoma MS02, and primary human meningioma and schwannoma cells were used

[28,29]. All cells were grown and tested for mycoplasma contamination as previously described [1].

For compound screening, actively-growing HS11 and HS01 Schwann cells and Syn1 and Syn5 arachnoidal cells as well as Ben-Men-1 cells were seeded in white 1536-well plates (Corning, NY) at a density of 750 cells/well using a Multidrop Combi Reagent dispenser with a small pin cassette (ThermoFisher, Fair Lawn, NJ). The next day, cells were treated for 72 hours with 11 two-fold serial dilutions of each compound in the MIPE 4.0 library. Cell viability was measured using CellTiter-Glo (Promega, Madison, WI). The potency (IC_{50}) and efficacy (maximum % inhibition) of each compound in each cell line were calculated as described [10].

HEK293T cells used for NanoBRET assays were cultured in Dulbecco's Modified Eagle Medium supplemented with 10% fetal bovine serum and penicillin-streptomycin. Cells were obtained from ATCC and routinely tested for mycoplasma contamination by DAPI staining.

In vitro confirmation of compound efficacy and synergism

Meningioma-relevant cells, including Syn1, Syn5, Ben-Men-1, and primary cultures of *NF2*-null meningioma cells, were seeded in 384-well plates and treated the next day with serial dilutions of brigatinib, MK-2206, or the combination of MK-2206 with brigatinib in a 10x10 matrix format. Cells were treated with 0.1% DMSO as the vehicle control. Cell viability was measured after 72 h of treatment using CellTiter-Glo. DRCs were generated using GraphPad Prism 7.0 (www.graphpad.com).

For the schwannoma-relevant cell panel, HS01, HS11, and MS02 cells were seeded in 384-well plates overnight and incubated with various dilutions of ALK-IN-1, brigatinib, dasatinib, or the combination of dasatinib with ALK-IN-1 or brigatinib in the 10x10 matrix format. Cell viability was measured after 60 or 72 h of treatment for mouse MS02 or human HS01 and HS11 cells, respectively, using CellTiter-Fluor (Promega). A similar study to validate the efficacy of dasatinib, simvastatin, and their combination was also conducted.

For both cell types, dose-response measurements were normalized to vehicle controls and dose-response curves were generated. Drug combination synergy was analyzed using the Loewe, Bliss, and HSA models as previously described using the Combenefit sotware [30].

RNA isolation and transcriptome analysis

RNA was isolated from all meningioma- and schwannoma-relevant cell lines treated in triplicate with single and combination drugs and used to prepare RNA libraries for RNAseq using Illumina HiSeq2000 and 2500 platforms [1]. Pairwise-compared, differentially-expressed genes were identified and gene ontology enrichment analysis for each comparison was conducted as described in Supplementary Methods in S1 File.

Kinome profiling

Multiplexed kinase inhibitor bead affinity chromatography and mass spectrometry (MIB/MS) was conducted to identify and quantitate the activity of the expressed kinome and their responses to drug treatment as previously described [1,17,31]. Lysates prepared from cells treated with the indicated concentrations of each drug or drug combination for various times or from tissues from animals treated with the indicated drugs were prepared and loaded onto the column containing multiple inhibitor-conjugated beads [31]. Kinase-bound inhibitor beads were stringently washed, followed by protein purification and trypsin digestion. Liquid chromatography, mass spectrometry, and analysis was essentially as previously described [31]. Peptide suspension was separated using an EASY nLC-1000 System with an Easy-Spray C-18 column (Thermo Fisher). Raw files were processed for label-free quantification using

MaxQuant LFQ and default parameters with the following modifications—razor plus unique peptides were used, matching between runs (3 min match time window), fixed modifications [cardbidomethy (C)] and dynamic modifications [phospho(STY)] [32]. Kinase LFQ intensities were used if two or more unique peptides were detected, and missing values were imputed in Perseus if observed in all replicates of another condition after log2 transformation for comparison. Data for each treated sample was plotted as a mean of fold change (log_2) relative to DMSO- or vehicle-treated control or untreated animals. When at least three replicates were available, unpaired Student's t-tests were performed in Perseus with Benjamini-Hochberg correction. FDR of 5% was used as a cut-off for significance.

NanoBRET™ TE intracellular kinase assays

NanoLuc fusion vectors were purchased from Promega Corporation (PTK2, NV1921; FER, NV1331; GAK, NV1421; and TNK2, NV4451). The Promega Kinase assay kit with K-10 tracer (N2641) was purchased and used for all kinase vectors. The optimized protocol from Promega was employed, with the following modifications. HEK293T cells were plated at a density of 20,000 cells per well in white 96-well plates in assay medium (Opti-MEM Reduced Serum Medium with no phenol red (Life technologies Cat.#11058–021) containing 1% fetal bovine serum). Four hours after plating, cells were transfected with 0.1 micrograms total DNA per well (9 parts carrier DNA: 1 part NanoLuc kinase fusion vestor) using jetPRIME transfection reagent (Polyplus) at a 2:1 ratio (microliters jetPRIME to micrograms DNA). Twenty hours later, the cells were treated with tracer according to protocol and serial dilutions of brigatinib or vehicle (ethanol) for 2 hours at 37 C, 5% CO_2. Substrate and inhibitor solutions were prepared according to protocol and incubated for 3–5 min before reading on a Synergy H4 (BioTek) plate reader using a 450/50 nm emission filter (BioTek Part no. 7082208) and a long-pass 610 nm filter (BioTek Part no. 7092209) with an integration time of 1 sec. BRET ratios were exported and multiplied by 1,000 to convert to NanoBRET ratios in milliBRET units (mBU), without background correction, according to Promega protocol. Values were plotted in GraphPad Prism 8 and the best-fit IC50 values were obtained by nonlinear regression fit using the log(inhibitor) vs. response–variable slope (four parameter) function in Prism. The experiments were performed at least twice, and representative data are shown.

Quantifiable orthotopic meningioma model

All animal studies conducted at Nationwide Children's Hospital were conducted in accordance with the Institutional Animal Care and Use Committee under the approved protocol number AR09-00054. Mice were housed in the barrier facility within the vivarium in our Abigail Wexner Research Institute with HEPA (high-efficient particulate air)-filtered room air, temperature control at 72˚F, and humidity set at 40–60%. Environmental parameters within each animal room were monitored electronically 24/7. The mouse rooms were equipped with micro-isolator caging on ventilated racks and class II biological safety cabinets. Each polycarbonate cage (30cm x 18cm x 15cm) housed a maximum of 5 mice and contained corn cob bedding and a polycarbonate hut or tube for hiding and climbing or a LifeSpan™ hanging devices for additional floor space above the cage bottom. Mice were fed non-fat rodent chow and filtered or sterile drinking water, and cages changed every week. All animals were euthanized by CO_2 asphyxiation, followed by cervical dislocation according to the approved IACUC protocol.

For animal dosing, MK-2206 was dissolved in 30% Captisol® and brigatinib was formulated in 90% polyethylene glycol 300 and 10% 1-methyl-2-pyrrolidinone. The MTD was determined as described (Plowman et al., 1999). Eight-to-12 week-old NSG (NOD-SCID gamma or

NOD.Cg-Prkdc^{scid} *Il2rg*^{tmlWjl}*/SzJ*) mice (The Jackson Laboratory) were treated with various doses of MK-2206 every other day or brigatinib every day by oral gavage for two weeks (n = 3 per dose). Treated mice were monitored daily for any signs of distress, such as significant weight loss (>20%), lethargy, and dehydration. Following MTD determination for each drug, a combination of MK-2206 and brigatinib at the MTD was also evaluated to ensure tolerability.

For PK analysis, NSG mice were fed a single oral dose of brigatinib, MK-2206, or their combination at the MTD. Prior to and at various times after dosing (n = 3 per time point), whole blood was collected from the facial vein into EDTA-containing Microtainer® (Becton Dickinson). Plasma samples were obtained by centrifugation. Immediately after blood sampling, mice were euthanized for brain harvesting. Both the plasma and brain samples were frozen at -80˚C until analysis of compound concentrations using ultra-high pressure liquid chromatography tandem-mass spectrometry (UHPLC-MS/MS). Plasma and brain samples were deproteinized and were analyzed in the presence of the brigatinib analogue ALK-IN-1 and dasatinib-d_8 as the internal standards for brigatinib and MK-2206, respectively.

To generate the orthotopic meningioma model, Ben-Men-1-LucB cells into the skull base of NSG mice as previously described [28]. Injected mice were monitored daily for any significant weight loss (>20%), lethargy, dehydration, and neurological problems. Mice with any of these abnormalities would have been euthanized, followed by a complete histopathological examination, however no mice met the criteria for early euthanasia in this study. In addition, we monitored tumor growth in mice by bioluminescence imaging (BLI) every two weeks using a Xenogen IVIS® Spectrum imaging system (Perkin Elmer). Mice with successful tumor engraftment were randomized into four groups (n = 10 each) and treated with MK-2206, brigatinib, MK-2206/brigatinib combination, or a mixture of the corresponding vehicles in which MK-2206 and brigatinib were formulated (1:1 ratio) by oral gavage. BLI was performed biweekly to assess the effects on tumor growth. The luminescence detected in each mouse was normalized to its pretreatment signal and expressed as the mean normalized luminescence ± standard deviation for each treatment group [28]. After 14 weeks of treatment, we stopped treating a cage of mice that had received brigatinib or the MK-2206/brigatinib combination and monitored possible tumor regrowth for 12 more weeks. Then, we retreated these mice to examine the effects of retreatment. All mice were humanely euthanized at the conclusion of the studies and tissues were collected for histopathological assessment.

Schwannoma model

All animal studies conducted at Indiana University were in accordance with the Institutional Animal Care and Use Committee under protocol number 11406. The methodologies of tumor assessment for the *PostnCre; Nf2*$^{flox/flox}$ mice were used as previously described [33]. Drugs were formulated as follows and administered by oral gavage: 50 mg/kg brigatinib dissolved in 90% PEG400 with 10% 1-metyl-2-pyrrolidinone; 20mg/kg dasatinib in pH3.0 citrate buffer; and 100 mg/kg simvastatin in 1% carboxymethylcellulosein water with 0.25% Tween80 and 0.05% antifoam 204 (Sigma). Cohorts of *Nf2*$^{f/f}$*; Postn-Cre+* mice were generated in-house, as previously described [33]. Animals were monitored daily for signs of distress such as hunched posture, labored breathing, scruffy coat, diarrhea, or lameness. All study mice began treatment at 4 months of age and were euthanized at the end of 12 weeks of treatment for histopathological assessment. Early endpoint criteria include: a palpable mass of more than of 1,000mm^3, greater than 20% reduction in body weight, any of the previously mentioned signs of distress that could not be remedied by the veterinary staff, or at the recommendation of the veterinarian. The total animals were enrolled in each treatment group are as follows: vehicle n = 17,

brigatinib n = 17, simvastatin n = 16, dasatinib n = 15, dasatinib and simvastatin n = 15 and dasatinib and brigatinib n = 16. The number of animals that met the criteria for euthanasia and were humanely euthanized according to the IACUC protocol or were found deceased prior to meeting criteria for euthanasia were as follows: vehicle, n = 1, brigatinib, n = 7, simvastatin n = 2, dasatinib n = 1, dasatinib and simvastatin n = 1, and dasatinib and brigatinib n = 4.

Tissue processing and DRG volume quantification methods were carried out as previously described [33]. Dissected nerve trees were pre-embedded in 2% agar, processed in a Leica tissue processor through graded alcohols, xylenes, and finally in molten paraffin. Five-micron thick sections were cut on a Leica rotary microtome and mounted on charged slides, then stained with hematoxylin and eosin. Images were acquired with an Aperio CS2 slide scanner (Leica).

HPLC/MS was performed by the IU Simon Cancer Center's Clinical Pharmacology Analytical Core. Six mice per drug dosage and three mice for vehicle only were used for pharmacokinetic experiments. Mice were given a single dose of drug and then blood was collected 1 and 4 hours later for one set of 3 mice and 2, 8, and 24 hours later for a second set of 3 mice. The blood was centrifuged at 4˚C, and then plasma was collected and stored at -80˚C. Samples were acidified and extracted in hexane:ethyl acetate (50:50, v/v). After solvent evaporation, mobile phase (acetonitrile:5mM ammonium acetate; 70:30, v/v) was mixed with residual sample and injected into an Agilent 1290 HPLC system with an Eskigent Autosampler. Mass spectrometry was performed using an ABSciex 5500 Q-TRAP.

Supporting information

S1 Fig. Cell survival responses to all MIPE 4.0 library agents (as judged by relative AUCs) binned per mechanistic classes with mechanistic superclasses listed in order from top to bottom: Transcriptional regulation, physiological homeostasis, other, metabolism, DNA repair, cell surface protein, cell signaling, cell growth, antimicrobial. Solid dots represent the median response for all the compounds, in each mechanistic class, and for each cell line.
(PDF)

S2 Fig. Single and combination drug treatment of meningioma-related cell lines. Drug treatment of the *NF2*-expressing Syn1(+) and *NF2*-null Syn5(-) cells (A), Ben-Men-1 cells (B), and two primary meningioma cultures MN612 and MN621 (C) was performed using the same drug doses as for Fig 2C and 2D. Single drug DRCs and combination drug heatmaps were generated using Combenefit software. Note that heatmap data for Ben-Men-1 (B) is the same as shown in Fig 2D.
(PDF)

S3 Fig. Brigatinib and dasatinib synergized to reduce *NF2*-deficient Schwann cell viability. (A) *Nf2*$^{-/-}$ mouse MS02 schwannoma and *NF2*-deficient human HS01 Schwann cells were plated and tested in dose-response 10x10 matrix format as described in Methods. Shown are single-agent dose response curves for ALK-IN-1 and brigatinib. (B) Brigatinib/dasatinib combination matrix analyses were conducted with HS01 cells. Shown are the brown-scale viability and synergy matrix plots with modeled surface synergy distributions in Loewe, Bliss, and HSA models. (C) Brigatinib/dasatinib combination matrix were analyzed with MS02 cells as described in S3B Fig.
(PDF)

S4 Fig. Dasatinib and simvastatin synergized to reduce the viability of Schwann and schwannoma cells. 10x10 matrix dose-response analysis was performed for *NF2*-deficient

HS01 (A) and *NF2*-expressing HS11 (B) human Schwann cells and *Nf2*$^{-/-}$ mouse schwannoma MS02 cells (C) treated with the brigatinib/simvastatin combination. Shown are the viability (brown scale) and synergy matrix (blue to red scale) plots with modeled surface synergy distributions in Loewe, Bliss, and HSA models.
(PDF)

S5 Fig. Gene expression changes caused by drug treatments. (A) Significant (Bonferroni-adjusted $p < 0.05$) changes in gene expression in Syn5 and Syn1 arachnoidal cells, which show extensive overlap with an overall greater response in the Syn5 merlin-null cells, are caused by brigatinib or brigatinib/MK-2206 treatment, but not by MK-2206 alone. (B) Genes whose expression is altered both by lack of merlin in Syn5 and by treatment of Syn5 with either brigatinib or brigatinib/MK-2206 treatment overwhelmingly show the expression change in opposite directions. (C) Significant changes in gene expression in HS01 and HS11 Schwann cells are limited in single drug treatments and most pronounced with the brigatinib/dasatinib combination. (D) The small number of genes differentially expressed in HS01 as a result of merlin expression do not overlap extensively with those altered in HS01 by the brigatinib/dasatinib treatment, and those overlaps that do occur are concordant in direction, contrasting with the arachnoidal cells.
(PDF)

S6 Fig. MIB/MS kinome profiling reveals dasatinib and brigatinib target specificity. (A) Control sciatic nerve tissues from *Postn-Cre; Nf2*$^{flox/flox}$ mice were used to prepare lysates. Equal amount of protein lysates (1mg) was incubated with vehicle (0.001% ethanol) or brigatinib (10nM, blue; 100nM, red; 1000nM, green) for 2h in biological duplicate. The log2 difference in MIB binding (LFQ intensity) was calculated and plotted relative to vehicle for each replicate. (B) HS11 and HS01 cells were treated with vehicle or brigatinib (1μM) for 24h prior to MIB/MS kinome profiling. MIB binding (log2LFQ intensities) was determined and PCA performed in Perseus. (C) HS11 and HS01 cells were treated with vehicle or dasatinib (0.6μM) for 24h prior to MIB/MS kinome profiling. MIB binding (log2LFQ intensities) was determined and the top 20 kinases with decreased MIB binding compared to vehicle are shown as a stacked bar plot for the two cell lines. (D-G). NanoBRET target engagement intracellular kinase assays were performed using the indicated kinases (PTK2/FAK1, FER, GAK, and TNK2) expressed as NanoLuc fusion constructs in HEK293T cells. Cells were treated with the indicated concentration of vehicle or brigatinib for 2 h prior to reading the plates. The 450/50 nm and long-pass 610 nm emission values were used to determine the NanoBRET™ ratios. Values were plotted in Prism and the best-fit IC50 values are indicated. Representative data is shown from experiments performed at least twice.
(PDF)

S7 Fig. ALK was not detected in normal meningeal and meningioma cells with or without *NF2* expression. Equal amounts of protein lysates from three human meningioma cell lines (KT21-MG1-Luc, NF2-Men-1, and Ben-Men-1), normal meningeal cells, and four primary meningioma cell cultures (hMen-10A, hMen-10B, hMen-12Ao, hMen-12B) were used in Western blot analysis to probe ALK and merlin expression. SK-N-SH neuroblastoma cells, which express ALK, were used as a positive control.
(PDF)

S8 Fig. Inhibition of multiple RTKs and non-RTKs in Ben-Men-1 cells treated with 1x IC_{50} of brigatinib under various growth conditions. PathScan® RTK signaling antibody array analysis was conducted according to Supplementary Methods in S1 File using cells grown in

10% FBS and treated with 1x IC_{50} of brigatinib for 2h (A) and 24 h (B) or in growth-arrested cells stimulated with 20% FBS in the presence of 1x IC_{50} of brigatinib for 2h (C) and 24 h (D). The numeric table below each pair of arrays displays the fold-change in fluorescence detected for each phospho-protein expressed in cells treated with brigatinib relative to DMSO control after subtraction of the fluorescence in the background control spots (indicated as "-"). Positive control spots are denoted as "+".
(PDF)

S9 Fig. Ben-Men-1 cells expressed low levels of p-EGFR, which was abolished by brigatinib treatment. Western blot analysis revealed that while phosphorylated EGFR was robustly induced in EGF-stimulated Ben-Men-1 cells, only very low levels of p-EGFR were detected in actively-growing cells or growth-arrested cells stimulated with 20% serum for 24h. Brigatinib treatment diminished p-EGFR expression.
(PDF)

S10 Fig. ALK expression was not detected in Schwann and schwannoma cells. (A) Western blotting was performed to detect ALK expression in human Schwann cells, four primary vestibular schwannoma cultures (hVS-16H, hVS-16S, hVS-12J, hVS-12Ga), and SK-N-SH neuroblastoma cells. Tubulin was used as a loading control. (B) Western blotting for ALK was also performed using extracts from nine vestibular schwannoma tumors. GAPDH was used as a loading control.
(PDF)

S11 Fig. Mouse PK parameters following a single oral dose of brigatinib or MK-2206 at the MTD. Mice were orally fed 50 mg/kg of brigatinib or 120 mg/kg of MK-2206. PK analysis was performed according to Supplementary Methods in S1 File.
(PDF)

S12 Fig. Relative tumor sizes in meningioma-bearing mice prior to or after treatment with MK-2206 and brigatinib, either alone or in combination, for 12 weeks. Detailed drug treatment and tumor measurement were as described in Fig 5B and 5C and Supplementary Methods in S1 File.
(PDF)

S13 Fig. Brigatinib inhibited p-FAK, p-AKT, and p-S6 target pathways in *Postn-Cre; Nf2$^{flox/flox}$* mice. DRGs from *Postn-Cre;Nf2$^{flox/flox}$* mice treated with the indicated drug or drug combination were used in Western blotting as described in Supplementary Methods in S1 File. Mice were treated for 12 weeks with the following drug dosages: 20mg/kg dasatinib, 50mg/kg brigatinib, 20mg/kg dasatinib + 15mg/kg brigatinib, 100mg/kg simvastatin, and 20mg/kg dasatinib + 100mg/kg simvastatin. DRG tissues were harvested 2 or 24 hours after the last dose of drug.
(PDF)

S1 Table. Fold-change and significance of differential expression in treated and untreated cells.
(XLSX)

S2 Table. Pathways enriched for differentially expressed genes.
(XLSX)

S3 Table. Kinome data plotted in Fig 3A–3D.
(XLSX)

S4 Table. Kinome data plotted in Fig 3E.
(XLSX)

S5 Table. Kinome data plotted in Figs 3F and S6A.
(XLSX)

S6 Table. Kinome data plotted in Fig 3G.
(XLSX)

S7 Table. Kinome data plotted in Figs 3H and S6B.
(XLSX)

S1 File. Supporting information methods.
(DOCX)

S1 Raw images.
(PDF)

Acknowledgments

We sincerely thank Tracy Galloway, mother of a person with NF2 and acting patient representative on the project, and the management team of the Children's Tumor Foundation for their contribution and support. We also wish to thank Children's Tumor Foundation President Dr. Annette Bakker. The Synodos for NF2 consortium members include Jaishri Blakely, D. Wade Clapp, Scott Plotkin, Long-Sheng Chang, Christina Fernandez-Valle, James Gusella, Stephen Haggarty, Gary Johnson, Helen Morrison, Vijaya Ramesh, Anat Stemmer-Rachamimov, and D. Bradley Welling (all contributing authors), along with the external advisors: Stephen Friend (President, Co-Founder and Director of Sage Bionetworks), Bruce Korf (Chair, Department of Genetics and Director, Heflin Center for Genomic Sciences at the University of Alabama at Birmingham), Gordon Mills (Chair of Gynecology and Chair of Systems Biology in the Division of Cancer Medicine, and co-head of the Kleberg Center for Molecular Markers at the University of Texas), Terry Van Dyke (Head of the Mouse Cancer Genetics Program at the National Cancer Institute), and Tracy Galloway (Synodos Founding Supporter, Children's Tumor Foundation Board Member, NF2 Patient Representative).

Author Contributions

Conceptualization: Long-Sheng Chang, Marc Ferrer, Steven P. Angus, David R. Jones, Charles W. Yates, D. Bradley Welling, Scott R. Plotkin, James F. Gusella, Helen Morrison, Vijaya Ramesh, Cristina Fernandez-Valle, Gary L. Johnson, Jaishri O. Blakeley, D. Wade Clapp.

Data curation: Long-Sheng Chang, Janet L. Oblinger, Abbi E. Smith, Marc Ferrer, Steven P. Angus, Eric Hawley, Waylan K. Bessler, Thomas S. K. Gilbert, Shelley A. H. Dixon, Andrea Masters, David R. Jones, D. Bradley Welling, James F. Gusella, Justin Guinney, Helen Morrison, Vijaya Ramesh, Cristina Fernandez-Valle, Gary L. Johnson, D. Wade Clapp.

Formal analysis: Long-Sheng Chang, Janet L. Oblinger, Abbi E. Smith, Marc Ferrer, Steven P. Angus, Waylan K. Bessler, Andrea Masters, David R. Jones, Anat O. Stemmer-Rachamimov, James F. Gusella, Helen Morrison, Vijaya Ramesh, Cristina Fernandez-Valle, Gary L. Johnson, D. Wade Clapp.

Funding acquisition: Long-Sheng Chang, Marc Ferrer, David R. Jones, Salvatore La Rosa, D. Bradley Welling, Anat O. Stemmer-Rachamimov, Scott R. Plotkin, James F. Gusella, Justin

Guinney, Helen Morrison, Vijaya Ramesh, Cristina Fernandez-Valle, Gary L. Johnson, Jaishri O. Blakeley, D. Wade Clapp.

Investigation: Long-Sheng Chang, Janet L. Oblinger, Abbi E. Smith, Marc Ferrer, Steven P. Angus, Eric Hawley, Alejandra M. Petrilli, Roberta L. Beauchamp, Lars Björn Riecken, Serkan Erdin, Ming Poi, Jie Huang, Waylan K. Bessler, Xiaohu Zhang, Rajarshi Guha, Craig Thomas, Sarah S. Burns, Thomas S. K. Gilbert, Li Jiang, Xiaohong Li, Qingbo Lu, Jin Yuan, Yongzheng He, Shelley A. H. Dixon, Andrea Masters, David R. Jones, Stephen J. Haggarty, D. Bradley Welling, Anat O. Stemmer-Rachamimov, James F. Gusella, Helen Morrison, Vijaya Ramesh, Cristina Fernandez-Valle, Gary L. Johnson, D. Wade Clapp.

Methodology: Long-Sheng Chang, Abbi E. Smith, Marc Ferrer, Steven P. Angus, Shelley A. H. Dixon, David R. Jones, Charles W. Yates, James F. Gusella, Helen Morrison, Vijaya Ramesh, Cristina Fernandez-Valle, Gary L. Johnson, D. Wade Clapp.

Project administration: Long-Sheng Chang, Marc Ferrer, Steven P. Angus, David R. Jones, Charles W. Yates, D. Bradley Welling, Anat O. Stemmer-Rachamimov, Scott R. Plotkin, James F. Gusella, Helen Morrison, Vijaya Ramesh, Cristina Fernandez-Valle, Gary L. Johnson, Jaishri O. Blakeley, D. Wade Clapp.

Resources: Long-Sheng Chang, David R. Jones, Anat O. Stemmer-Rachamimov, James F. Gusella, Helen Morrison, Vijaya Ramesh, Gary L. Johnson, D. Wade Clapp.

Supervision: Long-Sheng Chang, Marc Ferrer, Waylan K. Bessler, Charles W. Yates, D. Bradley Welling, Anat O. Stemmer-Rachamimov, D. Wade Clapp.

Writing – original draft: Long-Sheng Chang, Janet L. Oblinger, Abbi E. Smith, Marc Ferrer, Steven P. Angus, Eric Hawley, Andrea Masters, David R. Jones, Charles W. Yates, Salvatore La Rosa, D. Bradley Welling, Gary L. Johnson, Jaishri O. Blakeley, D. Wade Clapp.

Writing – review & editing: Long-Sheng Chang, Abbi E. Smith, Marc Ferrer, Steven P. Angus, Eric Hawley, David R. Jones, Charles W. Yates, Salvatore La Rosa, D. Bradley Welling, Anat O. Stemmer-Rachamimov, Scott R. Plotkin, James F. Gusella, Helen Morrison, Vijaya Ramesh, Cristina Fernandez-Valle, Gary L. Johnson, Jaishri O. Blakeley, D. Wade Clapp.

References

1. Synodos for NFC, Allaway R, Angus SP, Beauchamp RL, Blakeley JO, Bott M, et al. Traditional and systems biology based drug discovery for the rare tumor syndrome neurofibromatosis type 2. PLoS One. 2018; 13(6):e0197350. https://doi.org/10.1371/journal.pone.0197350 PMID: 29897904
2. Blakeley JO, Evans DG, Adler J, Brackmann D, Chen R, Ferner RE, et al. Consensus recommendations for current treatments and accelerating clinical trials for patients with neurofibromatosis type 2. Am J Med Genet A. 2012; 158A(1):24–41. https://doi.org/10.1002/ajmg.a.34359 PMID: 22140088
3. Evans DG, Kalamarides M, Hunter-Schaedle K, Blakeley J, Allen J, Babovic-Vuskanovic D, et al. Consensus recommendations to accelerate clinical trials for neurofibromatosis type 2. Clin Cancer Res. 2009; 15(16):5032–9. https://doi.org/10.1158/1078-0432.CCR-08-3011 PMID: 19671848
4. Cui Y, Groth S, Troutman S, Carlstedt A, Sperka T, Riecken LB, et al. The NF2 tumor suppressor merlin interacts with Ras and RasGAP, which may modulate Ras signaling. Oncogene. 2019; 38(36):6370–81. https://doi.org/10.1038/s41388-019-0883-6 PMID: 31312020
5. Hadfield KD, Smith MJ, Urquhart JE, Wallace AJ, Bowers NL, King AT, et al. Rates of loss of heterozygosity and mitotic recombination in NF2 schwannomas, sporadic vestibular schwannomas and schwannomatosis schwannomas. Oncogene. 2010; 29(47):6216–21. https://doi.org/10.1038/onc.2010.363 PMID: 20729918
6. Ruttledge MH, Sarrazin J, Rangaratnam S, Phelan CM, Twist E, Merel P, et al. Evidence for the complete inactivation of the NF2 gene in the majority of sporadic meningiomas. Nat Genet. 1994; 6(2):180–4. https://doi.org/10.1038/ng0294-180 PMID: 8162072

7. Ammoun S, Hanemann CO. Emerging therapeutic targets in schwannomas and other merlin-deficient tumors. Nat Rev Neurol. 2011; 7(7):392–9. https://doi.org/10.1038/nrneurol.2011.82 PMID: 21647202

8. Blakeley JO, Plotkin SR. Therapeutic advances for the tumors associated with neurofibromatosis type 1, type 2, and schwannomatosis. Neuro Oncol. 2016; 18(5):624–38. https://doi.org/10.1093/neuonc/nov200 PMID: 26851632

9. Troutman S, Moleirinho S, Kota S, Nettles K, Fallahi M, Johnson GL, et al. Crizotinib inhibits NF2-associated schwannoma through inhibition of focal adhesion kinase 1. Oncotarget. 2016; 7(34):54515–25. https://doi.org/10.18632/oncotarget.10248 PMID: 27363027

10. Ferrer M, Gosline SJC, Stathis M, Zhang X, Guo X, Guha R, et al. Pharmacological and genomic profiling of neurofibromatosis type 1 plexiform neurofibroma-derived schwann cells. Sci Data. 2018; 5:180106. https://doi.org/10.1038/sdata.2018.106 PMID: 29893754

11. Borisy AA, Elliott PJ, Hurst NW, Lee MS, Lehar J, Price ER, et al. Systematic discovery of multicomponent therapeutics. Proc Natl Acad Sci U S A. 2003; 100(13):7977–82. https://doi.org/10.1073/pnas.1337088100 PMID: 12799470

12. Markham A. Brigatinib: First Global Approval. Drugs. 2017; 77(10):1131–5. https://doi.org/10.1007/s40265-017-0776-3 PMID: 28597393

13. Zhang S, Anjum R, Squillace R, Nadworny S, Zhou T, Keats J, et al. The Potent ALK Inhibitor Brigatinib (AP26113) Overcomes Mechanisms of Resistance to First- and Second-Generation ALK Inhibitors in Preclinical Models. Clin Cancer Res. 2016; 22(22):5527–38. https://doi.org/10.1158/1078-0432.CCR-16-0569 PMID: 27780853

14. Huang WS, Liu S, Zou D, Thomas M, Wang Y, Zhou T, et al. Discovery of Brigatinib (AP26113), a Phosphine Oxide-Containing, Potent, Orally Active Inhibitor of Anaplastic Lymphoma Kinase. J Med Chem. 2016; 59(10):4948–64. https://doi.org/10.1021/acs.jmedchem.6b00306 PMID: 27144831

15. U.S. Food and Drug Administration, Center for Drug Evaluation and Research. Alunbrig (brigatinib). NDA 208772 Multidisciplinary Review and Evaluation. April 28, 2017. Retrieved April 15, 2021 from https://www.accessdata.fda.gov/drugsatfda_docs/nda/2017/208772Orig1s000MultidisciplineR.pdf.

16. Daub H, Olsen JV, Bairlein M, Gnad F, Oppermann FS, Korner R, et al. Kinase-selective enrichment enables quantitative phosphoproteomics of the kinome across the cell cycle. Mol Cell. 2008; 31(3):438–48. https://doi.org/10.1016/j.molcel.2008.07.007 PMID: 18691976

17. Duncan JS, Whittle MC, Nakamura K, Abell AN, Midland AA, Zawistowski JS, et al. Dynamic reprogramming of the kinome in response to targeted MEK inhibition in triple-negative breast cancer. Cell. 2012; 149(2):307–21. https://doi.org/10.1016/j.cell.2012.02.053 PMID: 22500798

18. Stuhlmiller TJ, Miller SM, Zawistowski JS, Nakamura K, Beltran AS, Duncan JS, et al. Inhibition of Lapatinib-Induced Kinome Reprogramming in ERBB2-Positive Breast Cancer by Targeting BET Family Bromodomains. Cell Rep. 2015; 11(3):390–404. https://doi.org/10.1016/j.celrep.2015.03.037 PMID: 25865888

19. Klaeger S, Heinzlmeir S, Wilhelm M, Polzer H, Vick B, Koenig PA, et al. The target landscape of clinical kinase drugs. Science. 2017; 358(6367). https://doi.org/10.1126/science.aan4368 PMID: 29191878

20. Zhou Y, Liu Z, Rothschild KJ, Lim MJ. Proteome-wide drug screening using mass spectrometric imaging of bead-arrays. Sci Rep. 2016; 6:26125. https://doi.org/10.1038/srep26125 PMID: 27194112

21. Angus SP, Oblinger JL, Stuhlmiller TJ, DeSouza PA, Beauchamp RL, Witt L, et al. EPH receptor signaling as a novel therapeutic target in NF2-deficient meningioma. Neuro Oncol. 2018; 20(9):1185–96. https://doi.org/10.1093/neuonc/noy046 PMID: 29982664

22. Yap TA, Yan L, Patnaik A, Fearen I, Olmos D, Papadopoulos K, et al. First-in-man clinical trial of the oral pan-AKT inhibitor MK-2206 in patients with advanced solid tumors. J Clin Oncol. 2011; 29(35):4688–95. https://doi.org/10.1200/JCO.2011.35.5263 PMID: 22025163

23. Beauchamp RL, James MF, DeSouza PA, Wagh V, Zhao WN, Jordan JT, et al. A high-throughput kinome screen reveals serum/glucocorticoid-regulated kinase 1 as a therapeutic target for NF2-deficient meningiomas. Oncotarget. 2015; 6(19):16981–97. https://doi.org/10.18632/oncotarget.4858 PMID: 26219339

24. Dombi E., Baldwin A., Marcus L. J., Fisher M. J., Weiss B., Kim A., et al. Activity of Selumetinib in Neurofibromatosis Type 1-Related Plexiform Neurofibromas. NEJMoa, 2016; 375(26):2550–2560. https://doi.org/10.1056/NEJMoa1605943 PMID: 28029918

25. Gross A. M., Wolters P. L., Dombi E., Baldwin A., Whitcomb P., Fisher M. J., et al. Selumetinib in Children with Inoperable Plexiform Neurofibromas. NEJMoa, 2020; 382(15):1430–1442. https://doi.org/10.1056/NEJMoa1912735 PMID: 32187457

26. Fisher M. J., Shih C. S., Rhodes S. D., Armstrong A. E., Wolters P. L., Dombi E., et al. Cabozantinib for neurofibromatosis type 1-related plexiform neurofibromas: a phase 2 trial. Nat Med., 2021; 27(1):165–173. https://doi.org/10.1038/s41591-020-01193-6 PMID: 33442015

27. Petrilli AM, Garcia J, Bott M, Klingeman Plati S, Dinh CT, Bracho OR, et al. Ponatinib promotes a G1 cell-cycle arrest of merlin/NF2-deficient human schwann cells. Oncotarget. 2017; 8(19):31666–81. https://doi.org/10.18632/oncotarget.15912 PMID: 28427224

28. Burns SS, Akhmametyeva EM, Oblinger JL, Bush ML, Huang J, Senner V, et al. Histone deacetylase inhibitor AR-42 differentially affects cell-cycle transit in meningeal and meningioma cells, potently inhibiting NF2-deficient meningioma growth. Cancer Res. 2013; 73(2):792–803. https://doi.org/10.1158/0008-5472.CAN-12-1888 PMID: 23151902

29. Puttmann S, Senner V, Braune S, Hillmann B, Exeler R, Rickert CH, et al. Establishment of a benign meningioma cell line by hTERT-mediated immortalization. Lab Invest. 2005; 85(9):1163–71. https://doi.org/10.1038/labinvest.3700307 PMID: 15965488

30. Di Veroli GY, Fornari C, Wang D, Mollard S, Bramhall JL, Richards FM, et al. Combenefit: an interactive platform for the analysis and visualization of drug combinations. Bioinformatics. 2016; 32(18):2866–8. https://doi.org/10.1093/bioinformatics/btw230 PMID: 27153664

31. Brighton HE, Angus SP, Bo T, Roques J, Tagliatela AC, Darr DB, et al. New Mechanisms of Resistance to MEK Inhibitors in Melanoma Revealed by Intravital Imaging. Cancer Res. 2018; 78(2):542–57. https://doi.org/10.1158/0008-5472.CAN-17-1653 PMID: 29180473

32. Cox J, Hein MY, Luber CA, Paron I, Nagaraj N, Mann M. Accurate proteome-wide label-free quantification by delayed normalization and maximal peptide ratio extraction, termed MaxLFQ. Mol Cell Proteomics. 2014; 13(9):2513–26. https://doi.org/10.1074/mcp.M113.031591 PMID: 24942700

33. Gehlhausen JR, Park SJ, Hickox AE, Shew M, Staser K, Rhodes SD, et al. A murine model of neurofibromatosis type 2 that accurately phenocopies human schwannoma formation. Hum Mol Genet. 2015; 24(1):1–8. https://doi.org/10.1093/hmg/ddu414 PMID: 25113746

Fig. S1

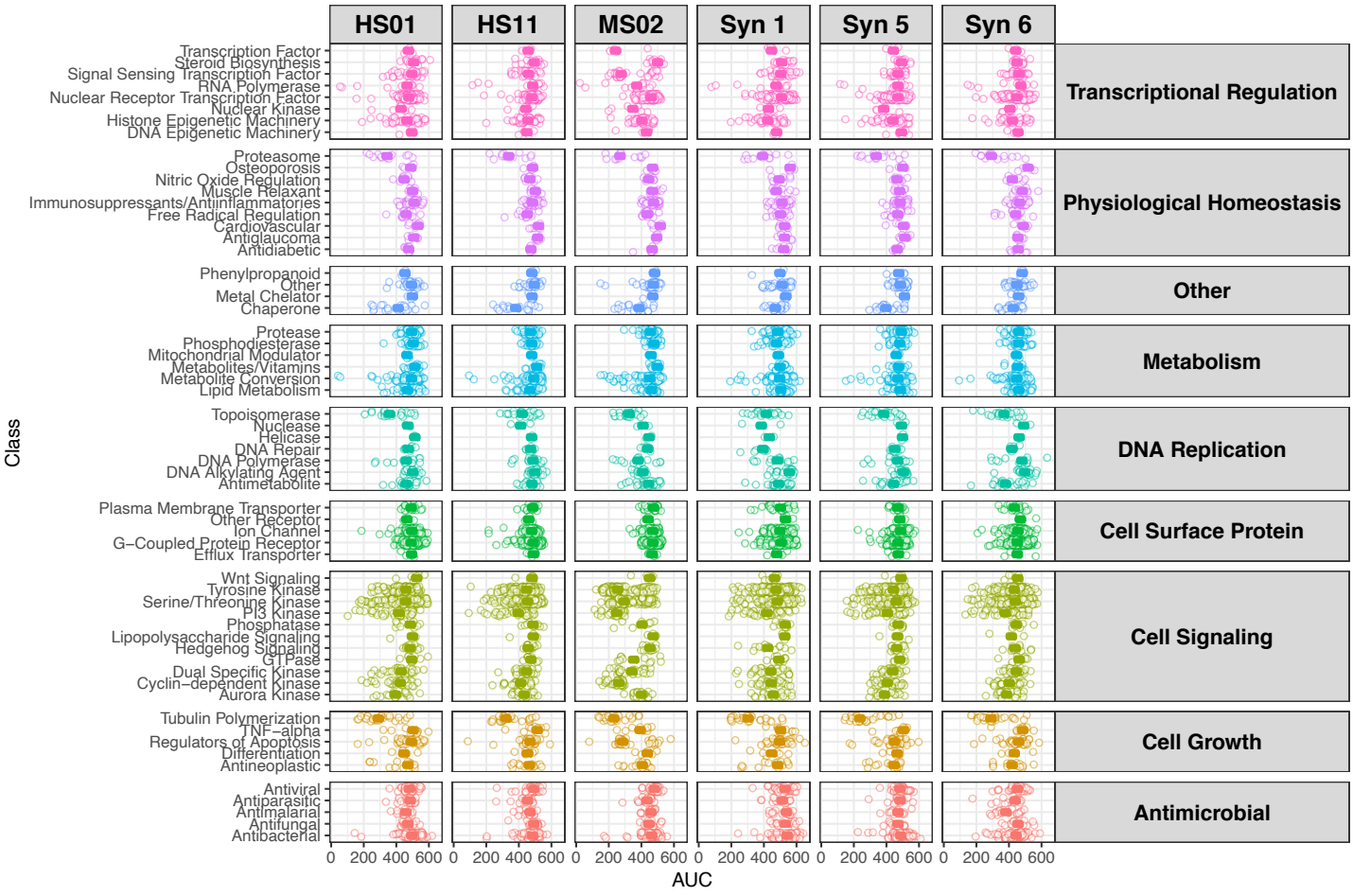
HS01
HS11
MS02
Syn 1
Syn 5
Syn 6
Transcription Factor
Steroid Biosynthesis
Signal Sensing Transcription Factor
RNA Polymerase
Nuclear Receptor Transcription Factor
Nuclear Kinase
Histone Epigenetic Machinery
DNA Epigenetic Machinery
Transcriptional Regulation
Proteasome
Osteoporosis
Nitric Oxide Regulation
Muscle Relaxant
Immunosuppressants/Antiinflammatories
Free Radical Regulation
Cardiovascular
Antiglaucoma
Antidiabetic
Physiological Homeostasis
Phenylpropanoid
Other
Metal Chelator
Chaperone
Other
Protease
Phosphodiesterase
Mitochondrial Modulator
Metabolites/Vitamins
Metabolite Conversion
Lipid Metabolism
Metabolism
Topoisomerase
Nuclease
Helicase
DNA Repair
DNA Polymerase
DNA Alkylating Agent
Antimetabolite
DNA Replication
Plasma Membrane Transporter
Other Receptor
Ion Channel
G−Coupled Protein Receptor
Efflux Transporter
Cell Surface Protein
Wnt Signaling
Tyrosine Kinase
Serine/Threonine Kinase
PI3 Kinase
Phosphatase
Lipopolysaccharide Signaling
Hedgehog Signaling
GTPase
Dual Specific Kinase
Cyclin−dependent Kinase
Aurora Kinase
Cell Signaling
Tubulin Polymerization
TNF−alpha
Regulators of Apoptosis
Differentiation
Antineoplastic
Cell Growth
Antiviral
Antiparasitic
Antimalarial
Antifungal
Antibacterial
Antimicrobial
Class
0 200 400 600
AUC

Fig. S2

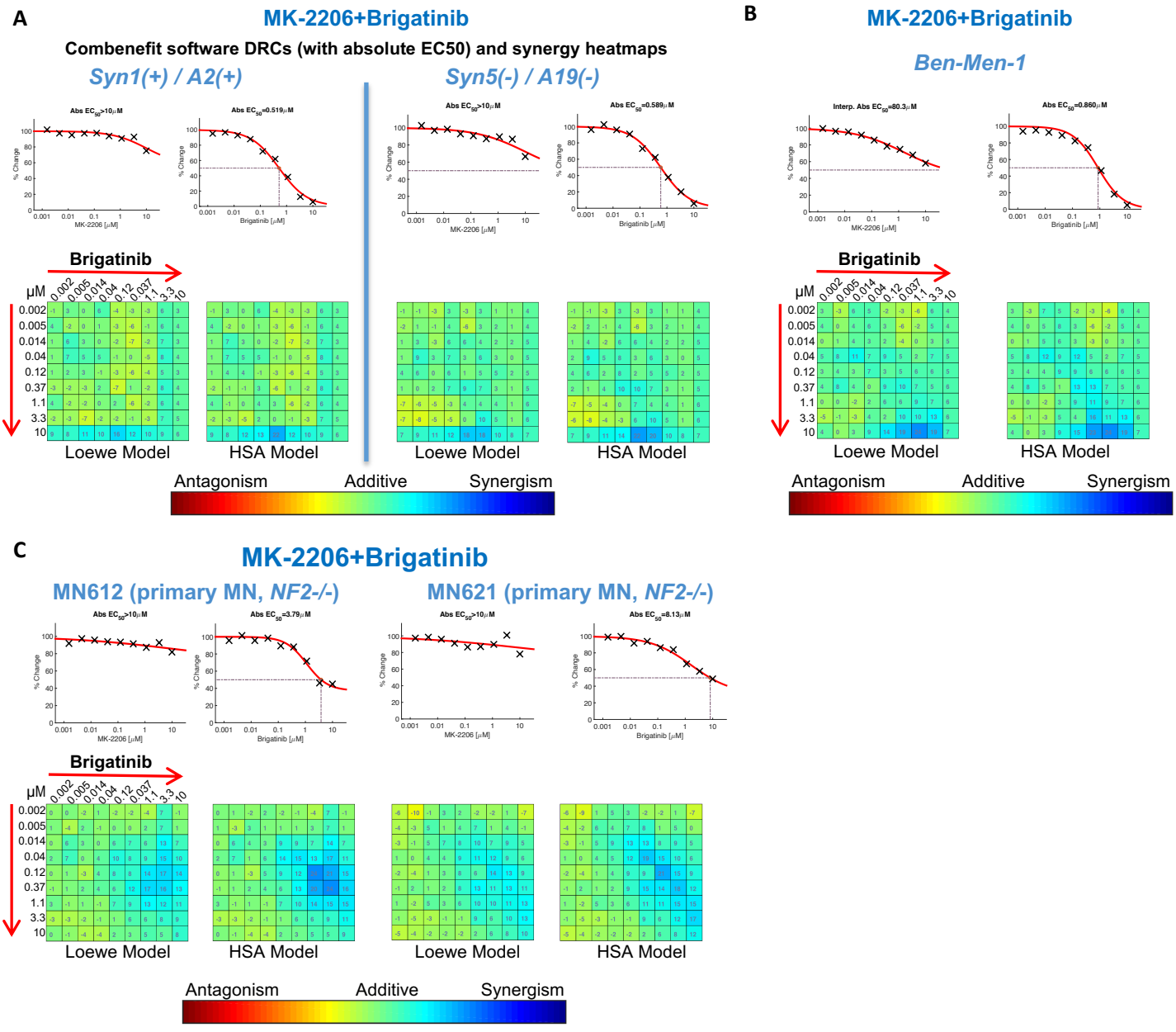
A
MK-2206+Brigatinib
Combenefit software DRCs (with absolute EC50) and synergy heatmaps
Syn1(+) / A2(+)
Syn5(-) / A19(-)
Brigatinib
μM
Loewe Model
HSA Model
Antagonism
Additive
Synergism
B
MK-2206+Brigatinib
Ben-Men-1
Brigatinib
Loewe Model
HSA Model
Antagonism
Additive
Synergism
C
MK-2206+Brigatinib
MN612 (primary MN, NF2-/-)
MN621 (primary MN, NF2-/-)
Brigatinib
Loewe Model
HSA Model
Loewe Model
HSA Model
Antagonism
Additive
Synergism

Fig. S3

A ALK inhibitors: Single Agent

Cell Line: HS01

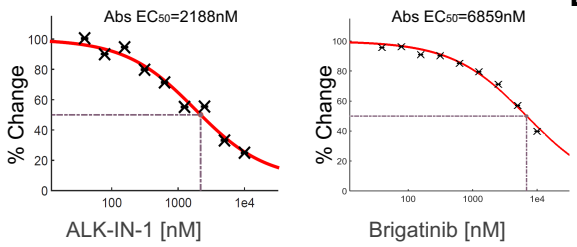

Cell Line: MS02

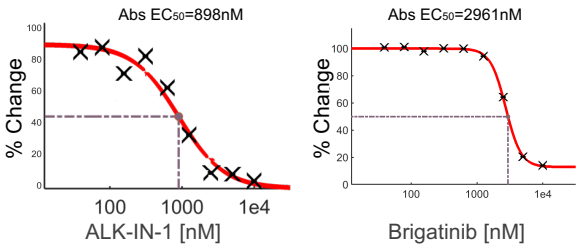

B

HS01
Brigatinib-Dasatinib
ALK-BCR/ABL

Combination dose-response data in matrix format

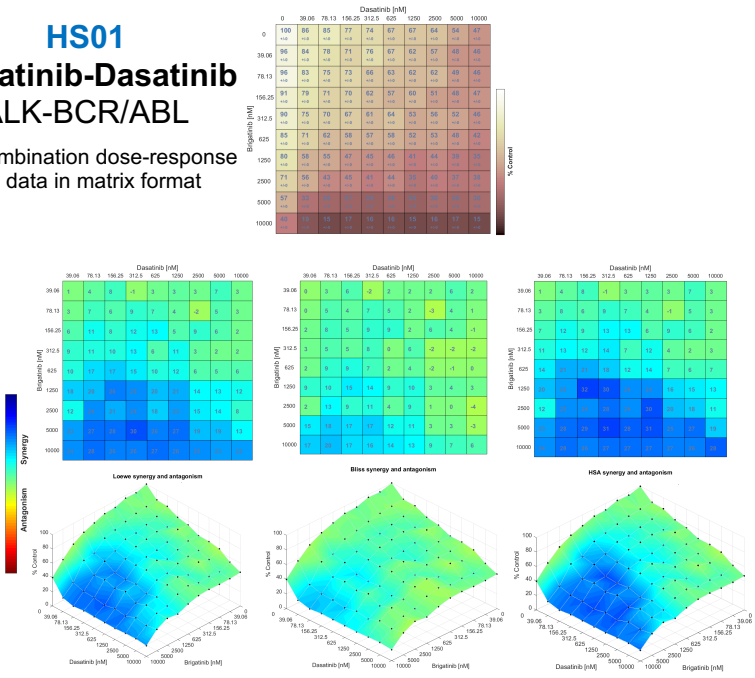

C

MS02
Brigatinib-Dasatinib
Alk-Bcr/Abl

Combination dose-response data in matrix format

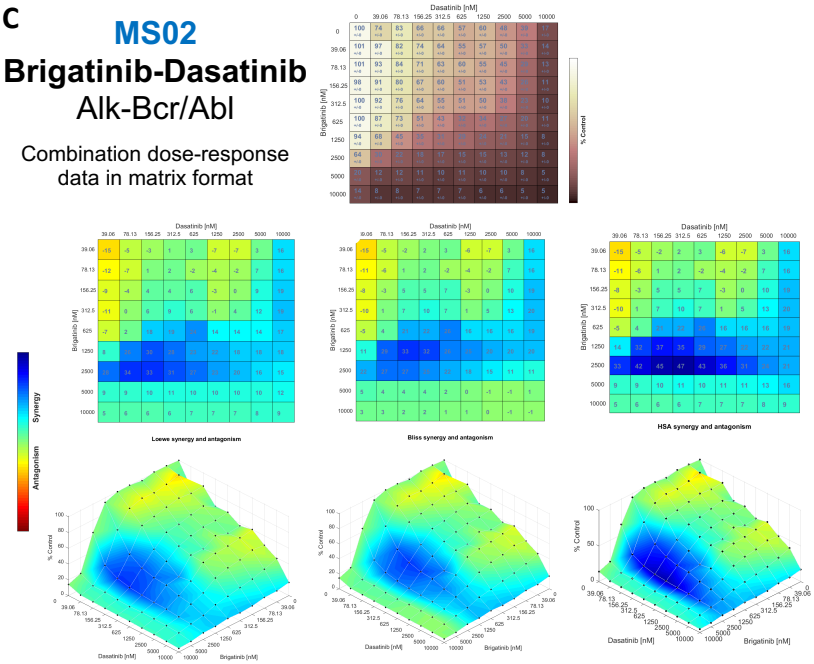

Fig. S4

A

HS01

Simvastatin-Dasatinib

HMG-CoA Reductase-BCR/ABL

Combination dose-response data in matrix format

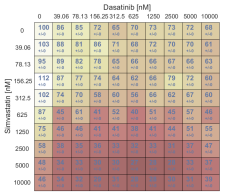

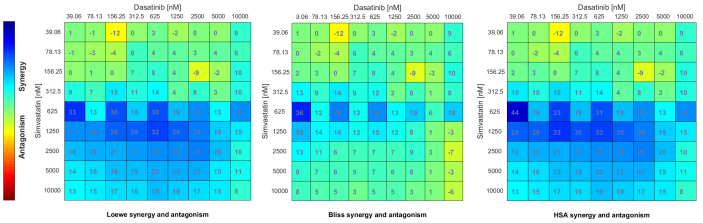

B

HS11

Simvastatin-Dasatinib

HMG-CoA Reductase-BCR/ABL

Combination dose-response data in matrix format

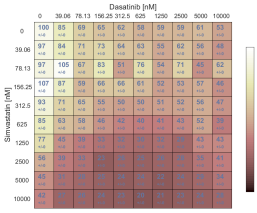

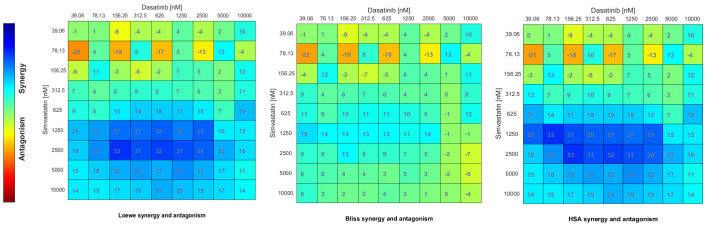

C

MS02

Simvastatin-Dasatinib

HMG-CoA Reductase-BCR/ABL

Combination dose-response data in matrix format

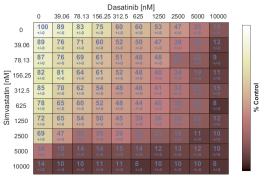

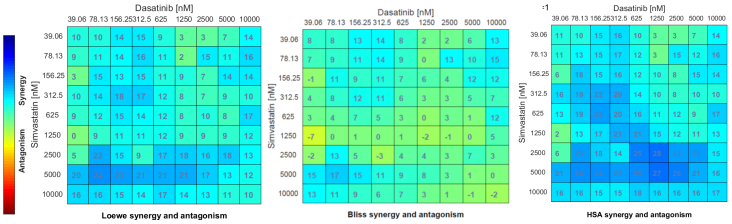

Fig. S5

A

		Syn5	Syn1	Shared	Discrepant
Brigatinib	Up	1281	242	180	0
	Down	1324	318	276	0
MK-2206	Up	0	0	0	0
	Down	0	0	0	0
Brigatinib + MK-2206	Up	1091	337	226	0
	Down	1080	493	399	0

B

		DEG in Syn5 + Brigatinib vs. Syn5 Untreated	
		Up (1281)	Down (1324)
DEG in Untreated Syn5 vs. Syn1	Up (1034)	5	327
	Down (1424)	653	3

		DEG in Syn5 + Brigatinib + MK-2206 vs. Syn5 Untreated	
		Up (1091)	Down (1080)
DEG in Untreated Syn5 vs. Syn1	Up (1034)	3	262
	Down (1424)	567	0

C

		HS01	HS11	Shared	Discrepant
Brigatinib	Up	0	0	0	0
	Down	0	1	0	0
Dasatinib	Up	18	19	8	0
	Down	7	21	2	0
Brigatinib + Dasatinib	Up	731	451	324	0
	Down	666	581	355	0
Simvastatin	Up	35	16	12	0
	Down	7	6	4	0
Dasatinib + Simvastatin	Up	171	102	72	0
	Down	174	283	108	0

D

		DEG in HS01 + Brigatinib + Dasatinib vs. HS01 Untreated	
		Up (731)	Down (666)
DEG in Untreated HS01 vs. HS11	Up (40)	11	0
	Down (15)	0	1

Fig. S6

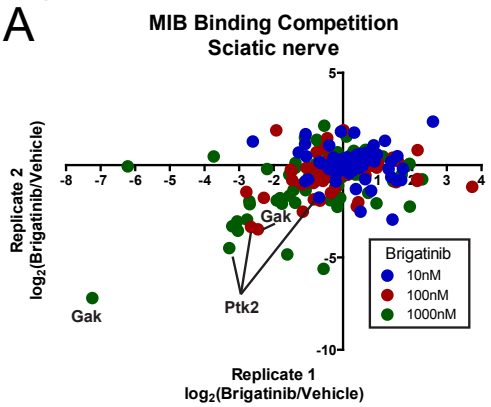
A
MIB Binding Competition
Sciatic nerve
Replicate 2
log2(Brigatinib/Vehicle)
Replicate 1
log2(Brigatinib/Vehicle)
Gak
Ptk2
Gak
Brigatinib
10nM
100nM
1000nM

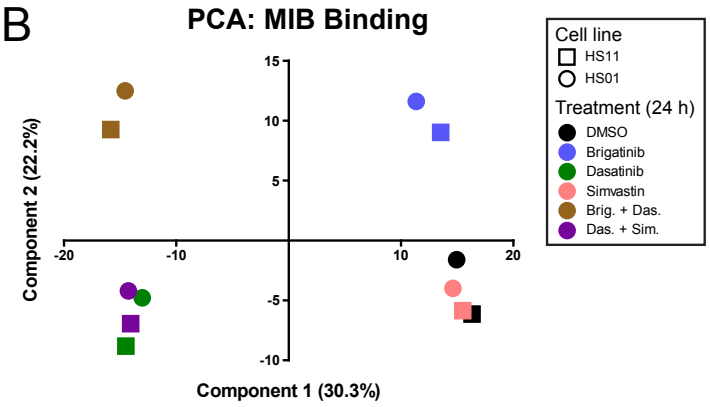
B
PCA: MIB Binding
Component 2 (22.2%)
Component 1 (30.3%)
Cell line
HS11
HS01
Treatment (24 h)
DMSO
Brigatinib
Dasatinib
Simvastin
Brig. + Das.
Das. + Sim.

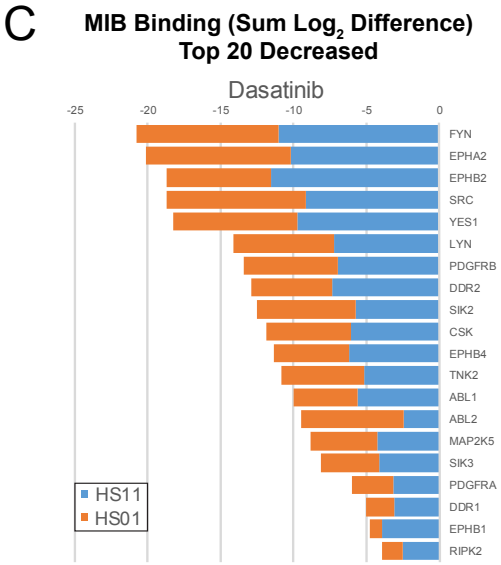
C
MIB Binding (Sum Log2 Difference)
Top 20 Decreased
Dasatinib
FYN
EPHA2
EPHB2
SRC
YES1
LYN
PDGFRB
DDR2
SIK2
CSK
EPHB4
TNK2
ABL1
ABL2
MAP2K5
SIK3
PDGFRA
DDR1
EPHB1
RIPK2
HS11
HS01

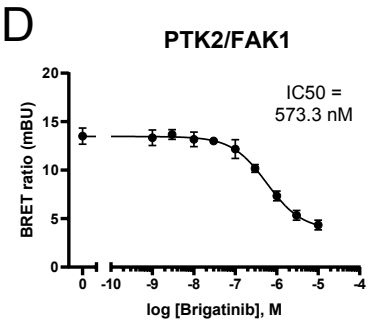
D
PTK2/FAK1
IC50 =
573.3 nM
BRET ratio (mBU)
log [Brigatinib], M

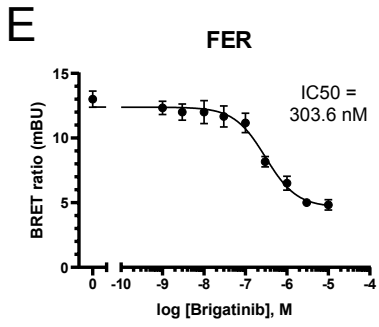
E
FER
IC50 =
303.6 nM
BRET ratio (mBU)
log [Brigatinib], M

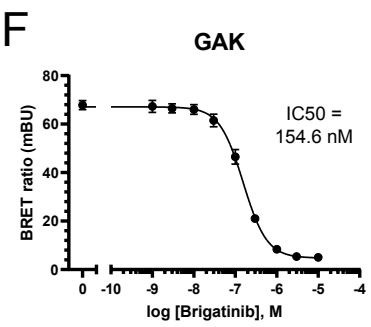
F
GAK
IC50 =
154.6 nM
BRET ratio (mBU)
log [Brigatinib], M

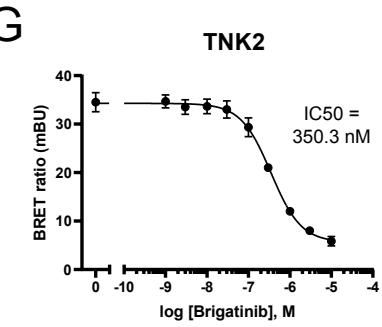
G
TNK2
IC50 =
350.3 nM
BRET ratio (mBU)
log [Brigatinib], M

Fig. S7

ALK was not detected in normal meningeal and *NF2*-deficient or expressing meningioma cells

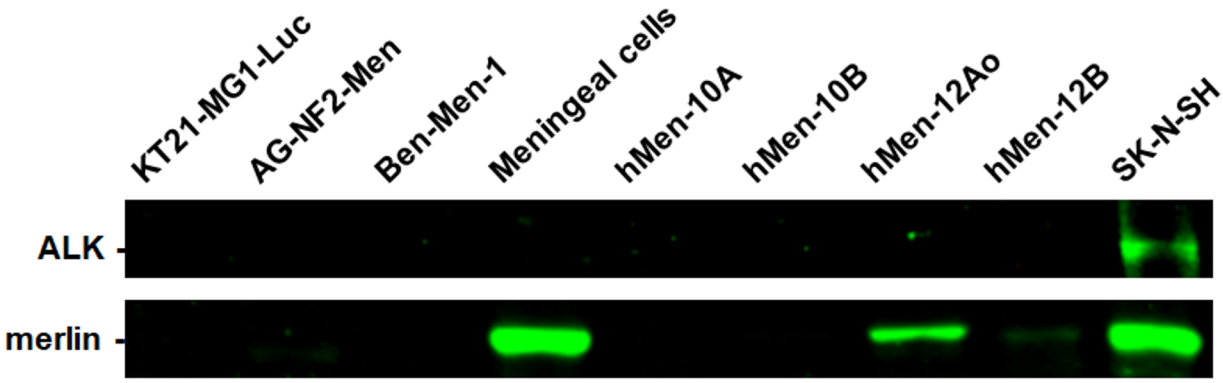

Fig. S8

A

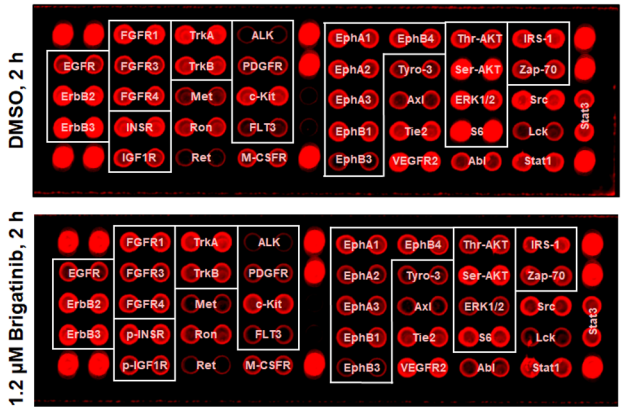

+	0.711	0.891	1.164	+	0.732	0.730	0.790	0.530	+
0.696	0.818	0.771	0.749	+	0.501	0.748	0.327	1.167	+
0.696	0.763	0.744	0.715	-	0.687	0.701	0.238	0.506	0.717
0.689	0.712	0.827	0.829	-	0.686	0.704	0.243	1.094	
+	0.771	1.073	0.787	+	0.616	0.696	0.662	0.765	+

B

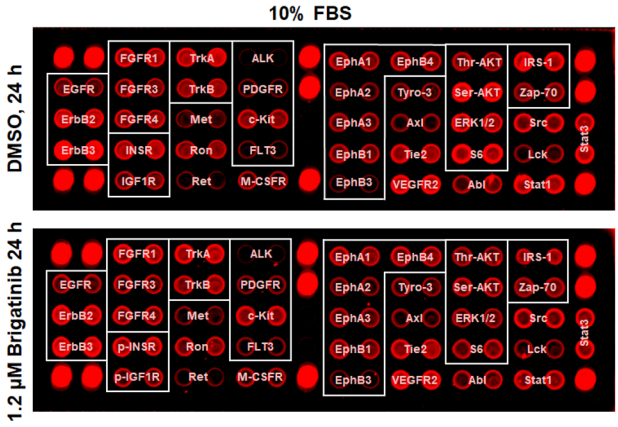

+	1.004	1.021	1.163	+	1.082	1.011	0.934	0.289	+
1.015	0.696	0.978	1.138	+	1.092	1.039	0.384	1.075	+
1.019	1.007	0.903	1.117	-	0.993	1.003	0.503	1.050	0.822
0.892	0.930	0.983	1.189	-	1.023	0.971	0.428	1.254	
+	0.977	0.868	1.023	+	1.096	0.957	0.599	0.567	+

C

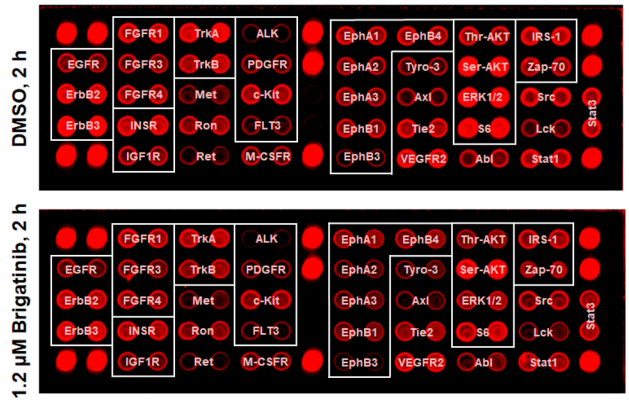

+	0.764	0.665	0.618	+	0.723	0.734	0.641	0.755	+
0.790	1.187	0.770	0.742	+	0.598	0.750	0.545	0.651	+
0.783	0.843	0.868	0.811	-	0.727	0.692	0.282	0.676	0.776
0.733	0.797	0.903	0.766	-	0.705	0.728	0.397	0.769	
+	0.803	0.909	0.838	+	0.642	0.779	0.707	0.744	+

D

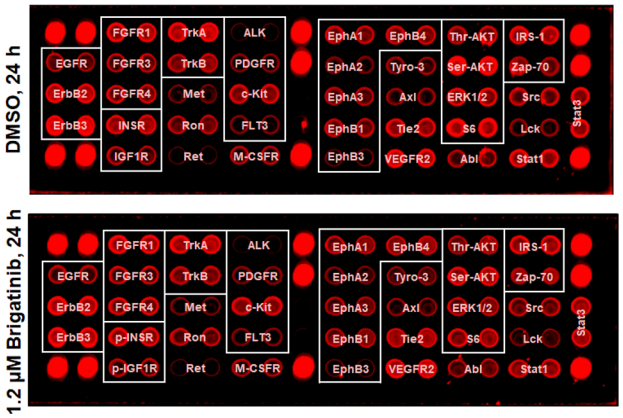

+	1.108	0.869	0.770	+	0.970	1.000	0.569	1.009	+
1.068	1.100	0.948	0.994	+	1.029	1.013	0.532	0.308	+
1.130	1.115	0.934	1.036	-	0.962	0.974	0.673	0.765	0.956
0.879	1.070	1.024	0.947	-	0.994	1.012	0.534	0.927	
+	0.969	0.818	0.899	+	1.046	0.972	0.677	0.855	+

Fig. S9

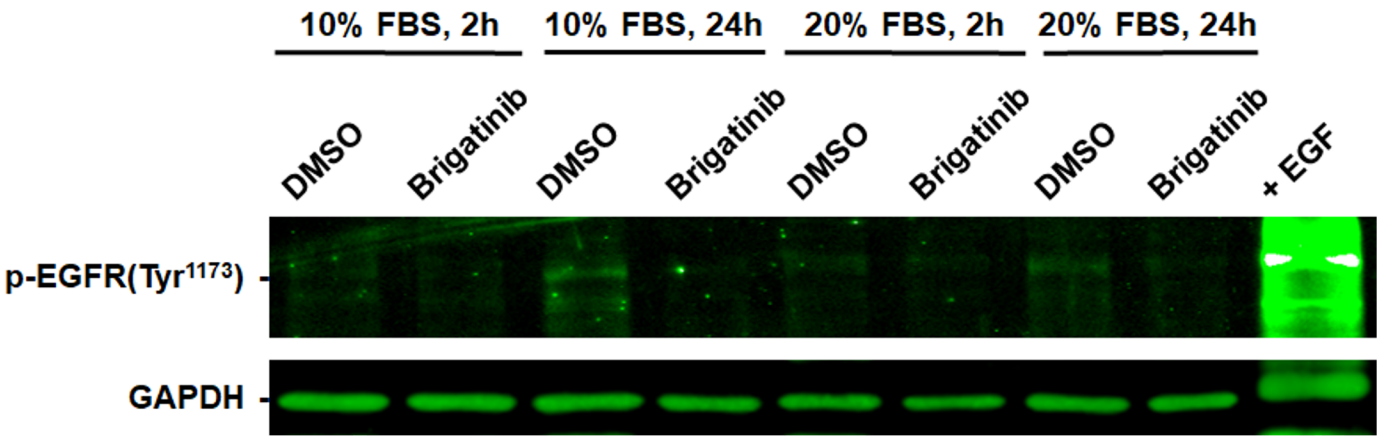
10% FBS, 2h
10% FBS, 24h
20% FBS, 2h
20% FBS, 24h
DMSO
Brigatinib
DMSO
Brigatinib
DMSO
Brigatinib
DMSO
Brigatinib
+ EGF
p-EGFR(Tyr1173)
GAPDH

Fig. S10

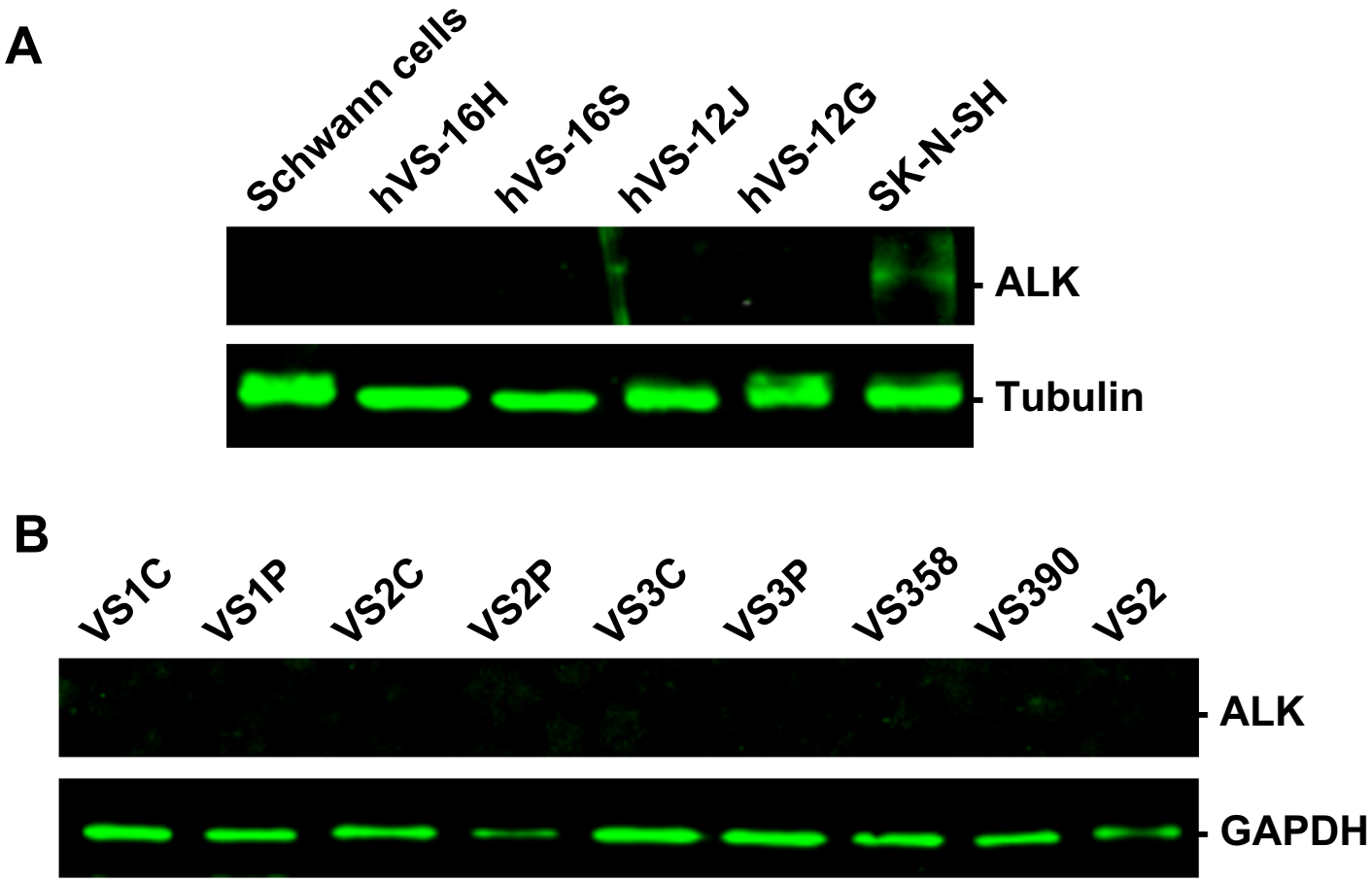
A
Schwann cells
hVS-16H
hVS-16S
hVS-12J
hVS-12G
SK-N-SH
ALK
Tubulin
B
VS1C
VS1P
VS2C
VS2P
VS3C
VS3P
VS358
VS390
VS2
ALK
GAPDH

Fig. S11

Mouse pharmacokinetic parameters following a single oral dose of brigatinib (50 mg/kg) or MK-2206 (120 mg/kg)

Drug	PK Parameters					
	$T_{1/2}$ (h)	T_{max} (h)	C_{max} (ng/mL)	$AUC_{0-\infty}$ (h*ng/mL)	V/F (L/kg)	CL/F (L/h/kg)
Plasma						
Brigatinib	7.2	4	1311	18662	27.8	2.7
MK2206	5.6	1	2208	21286	45.3	5.6
Brain (Gross)						
	$T_{1/2}$ (h)	T_{max} (h)	C_{max} (ng/g)	$AUC_{0-\infty}$ (h*ng/g)	V/F (kg/kg)	CL/F (kg/h/kg)
Brigatinib	6.2	4	170	2319	193.3	22.6
MK2206	6.0	4	406	5462	191.5	22.0

Fig. S12

Relative tumor sizes in meningioma-bearing mice prior to or after treatment with MK-2206 and brigatinib, either alone or in combination

Week	Vehicle control	SD	MK-2206	SD	Brigatinib	SD	MK-2206 + Brigatinib	SD
0	1	0	1	0	1	0	1	0
2	2.00	0.77	1.31	0.58	1.02	0.44	0.35	0.20
4	2.88	1.33	1.68	0.54	0.79	0.44	0.28	0.18
6	4.29	2.13	2.24	1.01	1.02	0.37	0.31	0.18
8	4.85	2.62	2.52	1.05	0.54	0.14	0.34	0.21
10	5.39	2.63	3.35	1.31	0.75	0.23	0.39	0.20
12	6.69	2.85	4.43	1.86	0.62	0.20	0.37	0.18

The relative tumor size shown following drug treatment was normalized to the tumor size prior to treatment (week 0), which is designated as 1 (100%).

Fig. S13

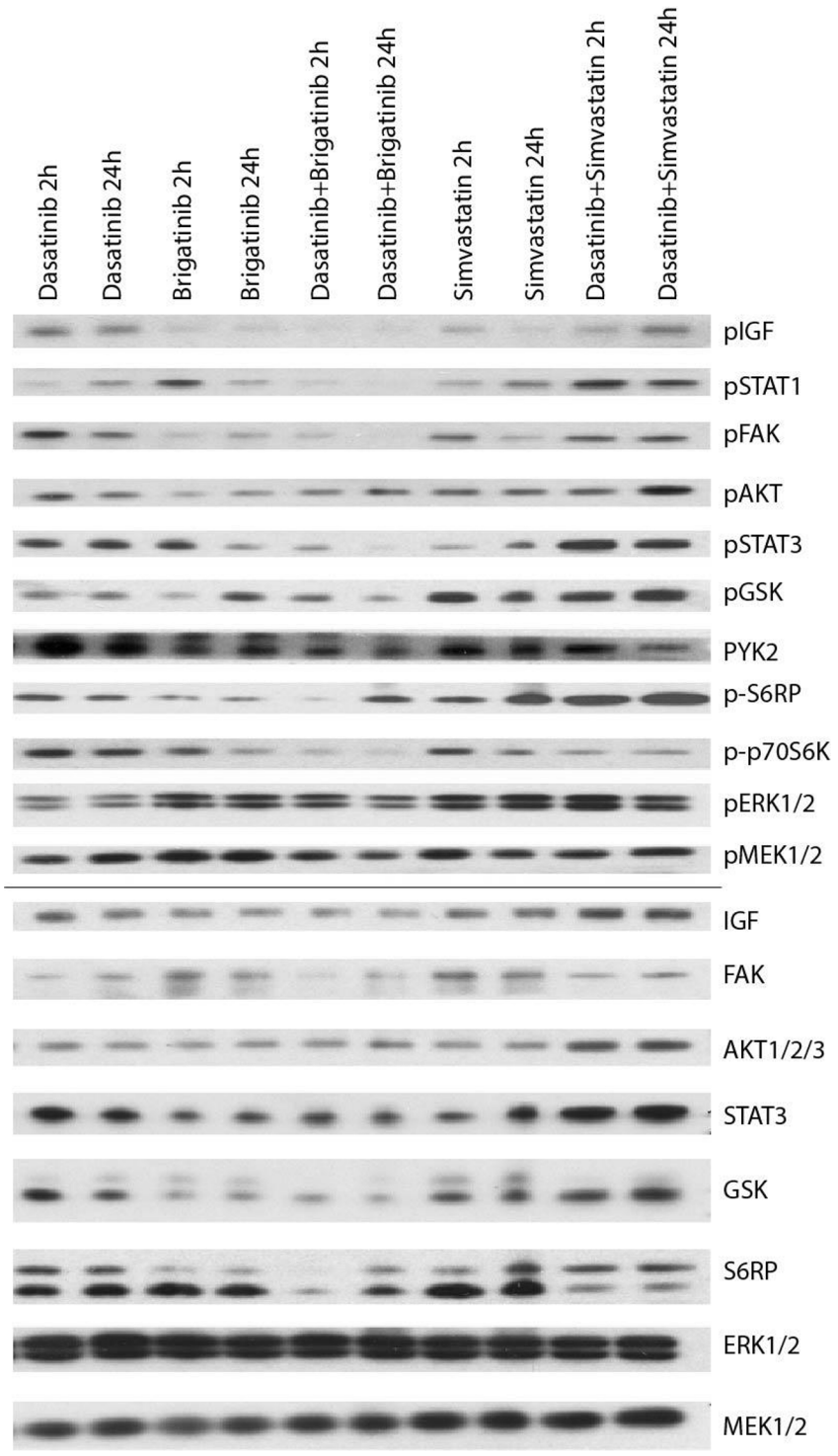
Dasatinib 2h
Dasatinib 24h
Brigatinib 2h
Brigatinib 24h
Dasatinib+Brigatinib 2h
Dasatinib+Brigatinib 24h
Simvastatin 2h
Simvastatin 24h
Dasatinib+Simvastatin 2h
Dasatinib+Simvastatin 24h
pIGF
pSTAT1
pFAK
pAKT
pSTAT3
pGSK
PYK2
p-S6RP
p-p70S6K
pERK1/2
pMEK1/2
IGF
FAK
AKT1/2/3
STAT3
GSK
S6RP
ERK1/2
MEK1/2

Supporing Information: Methods

Additional methods for MIPE screen

Brigatinib (ALUNBRIG®; CAS: 1197953-54-0), MK-2206 (CAS: 1032350-13-2), dasatinib (SPRYCEL®; CAS: 302962-49-8), and simvastatin (ZOCOR®; CAS: 79902-63-9) were synthesized by Proactive Molecular Research, Alachua, FL with purities of greater than 98-99% as determined by liquid chromatography-mass spectrometry (LC-MS) and nuclear magnetic resonance (NMR) spectroscopy. ALK-IN-1 (CAS: 1197958-12-5) was obtained from NCATS and Advanced ChemBlocks (Burlingame, CA) and dasatinib-d_8 (CAS: 1132093-70-9) was purchased from Cayman Chemical (Ann Arbor, MI). For *in vitro* study, all compounds were dissolved in DMSO as 10 mM stock solutions and diluted in medium prior to adding to cells with DMSO concentration kept constant at 0.1%.

Maximum tolerated dose (MTD) determination, and pharmacokinetic (PK) analysis in NSG mice

For animal dosing, MK-2206 was dissolved in 30% Captisol® and brigatinib was formulated in 90% polyethylene glycol 300 and 10% 1-methyl-2-pyrrolidinone. The MTD was determined as described (1). Eight-to-12 week-old NSG (NOD-SCID gamma or *NOD.Cg-Prkdc^{scid} Il2rg^{tm1Wjl}/SzJ*) mice (The Jackson Laboratory) were treated with various doses of MK-2206 every other day or brigatinib every day by oral gavage for two weeks (three mice per dose). The starting doses for MK-2206 and brigatinib were based on those used previously (2,3). Following MTD determination for each drug, a combination of MK-2206 and brigatinib at the MTD was also evaluated to ensure

tolerability.

For PK analysis, mice were fed a single oral dose of brigatinib, MK-2206, or their combination at the MTD. Prior to and at various times after dosing (n=3 per time point), whole blood was collected from the facial vein into EDTA-containing Microtainer® (Becton Dickinson). Plasma samples were obtained by centrifugation. Immediately after blood sampling, mice were euthanized for brain harvesting. Both the plasma and brain samples were frozen at -80 °C until analysis of compound concentrations using ultra-high pressure liquid chromatography tandem-mass spectrometry (UHPLC-MS/MS). Plasma and brain samples were deproteinized and were analyzed in the presence of the brigatinib analogue ALK-IN-1 and dasatinib-d_8 as the internal standards for brigatinib and MK-2206, respectively. Detailed UHPLC-MS/MS analysis is appended in Supplementary Methods.

Additional methods for Orthotopic Meningioma Model

The Institutional Animal Care and Use Committee at Nationwide Children's Hospital approved this animal study. The coordinates used were 1.5 mm anterior and 1.5 mm to the right of the bregma and 4.5 mm below the skull surface. The injected mice were monitored for tumor growth by bioluminescence imaging (BLI) every two weeks using a Xenogen IVIS® Spectrum imaging system (Perkin Elmer, Bradford, CT). Mice with successful tumor engraftment were randomized into four groups (n=10 each) and treated with MK-2206, brigatinib, MK-2206/brigatinib combination, or a mixture of the corresponding vehicles in which MK-2206 and brigatinib were formulated (1:1 ratio) by oral gavage. BLI was performed biweekly to assess the effects on tumor growth. Previously we showed that the BL signal detected in luciferase-expressing tumor

xenografts correlates with the tumor size (4). The luminescence detected in each mouse was normalized to its pretreatment signal and expressed as the mean normalized luminescence ± standard deviation for each treatment group. After 14 weeks of treatment, treatment was halted in a subset of mice in the brigatinib alone and MK-2206/brigatinib combination cohorts and monitored possible tumor regrowth for 12 more weeks. Then, treatment was reinitiated to determine tumor response.

Meningioma Model Immunohistochemistry

The heads of drug- or vehicle-treated mice bearing meningiomas were decalcified, followed by paraffin embedding as described previously (4). Serial 5-µm sections were cut and stained with hematoxylin and eosin to localize the tumor. Then, the sections containing tumors were processed for immunohistochemical staining using antibodies against Ki67 (RM-9106-S, Neomarkers), phospho-S6 (p-S6[$Ser^{235/236}$]; #4858, Cell Signaling), p-ERK1/2(Thr^{202}/Tyr^{204}) (#4370, Cell Signaling), and cleaved caspase 3 (CC3; #9664, Cell Signaling). Negative control slides were treated with the same procedures but without the primary antibody.

Additional methods for in vivo *Schwannoma Model*

Indiana University's Institutional Animal Care and Use Committee approved this study. *Postn-Cre; Nf2$^{flox/flox}$* mice were divided into treatment groups and administered drug by oral gavage. The number of animals used in analysis for each treatment group is as follows: Dasatinib (n=14), Simvastatin (n=15), Brigatinib (n=10), Dasatinib/Simvastatin (n=14), Dasatinib/Brigatinib (n=14), Vehicle Controls (n=37). Drugs were formulated as

follows and administered by oral gavage: 50 mg/kg brigatinib dissolved in 90% PEG400 with 10% 1-metyl-2-pyrrolidinone; 20mg/kg dasatinib in pH3.0 citrate buffer; and 100 mg/kg simvastatin in 1% carboxymethylcellulosein water with 0.25% Tween80 and 0.05% antifoam 204 (Sigma). Tissue processing and DRG volume quantification methods were carried out as previously described (29). Dissected nerve trees were pre-embedded in 2% agar, processed in a Leica tissue processor through graded alcohols, xylenes, and finally in molten paraffin. Five-micron thick sections were cut on a Leica rotary microtome and mounted on charged slides, then stained with hematoxylin and eosin. Images were acquired with an Aperio CS2 slide scanner (Leica).

PK analysis of brigatinib and dasatinib in plasma samples of PostnCre; Nf2$^{foxl/flox}$ mice

HPLC/MS was performed by the IU Simon Cancer Center's Clinical Pharmacology Analytical Core. Samples were acidified and extracted in hexane:ethyl acetate (50:50, v/v). After solvent evaporation, mobile phase (acetonitrile:5mM ammonium acetate; 70:30, v/v) was mixed with residual sample and injected into an Agilent 1290 HPLC system with an Eskigent Autosampler. Mass spectrometry was performed using an ABSciex 5500 Q-TRAP.

Phospho-receptor tyrosine kinase (RTK) array

Ben-Men-1 cells were plated in Dulbecco modified Eagle medium (DMEM) containing 10% fetal bovine serum (FBS). The following day, cells were growth-arrested in medium without serum for two days. Serum-starved cells were stimulated with 20% FBS-containing medium in the presence of 1x IC_{50} concentration of brigatinib or DMSO

vehicle. Also, cells grown in 10% FBS were treated with 1x IC_{50} concentration of brigatinib or DMSO in fresh 10% FBS-containing medium for 2 or 24 hours. Treated cells were lysed in 500 µL of 1x Cell Lysis buffer (#9803; Cell Signaling, Danvers, MA) with 1 mM freshly-added PMSF. Cell lysates were sonicated and their protein concentrations were assessed by microBCA assay (#23235; Thermo, Rockford, IL). 150 µg of total protein was added to each chamber of the PathScan RTK Antibody Array (#7949; Cell Signaling) according to the manufacturer's instructions. The fluorescent signal of the array was detected using an Odyssey CLx near-infrared scanner (LI-COR, Lincoln, NE), followed by quantitation using Image Studio software (LI-COR). Also, the remaining protein lysates from the above treated cells were analyzed by Western blotting to validate array findings.

Meningioma Cells Western blot analysis

Ben-Men-1 cells were growth-arrested in serum-free DMEM for two days and then pretreated for 2 hours with 1.5 µM of brigatinib or DMSO vehicle, followed by incubation for 10 minutes with 50 ng/mL each of the following ligands: epidermal growth factor (EGF) (#PHG0311; Thermo Fisher, Waltham, MA), heregulin (HRG) (#100-03; PeproTech, Rocky Hill, NJ), or insulin-like growth factor 1 (IGF1) (#1150-01; Gold Biotechnology, St. Louis, MO). Following ligand stimulation, cells were placed on ice, lysed in cold RIPA buffer containing protease/phosphatase inhibitor cocktail (#78440; Sigma-Aldrich, St. Louis, MO), and sonicated. Also, lysates were prepared from primary NF2-associated and sporadic meningioma, Ben-Men-1, normal human meningeal (ScienCell, Carlsbad, CA), and SK-N-SH neuroblastoma cells. Equal amounts of protein

lysates were used in Western blotting as previously described (4).

Drug concentrations used for Figure 2 (also used for Fig S2A-C).

For meningioma-related cells lines (Fig 2C), single drug dose response testing was carried out for MK-2206 or brigatinib at a concentration range of 0.0015 – 10 μM (3-fold dilutions seris, 9 dosage points) and DMSO (vehicle) control. For combination drug testing, cells were treated in a 10x10 dose matric format using same concentrations listed above.

Additional methods for RNAseq and transcriptome analysis

RNAseq reads were aligned to human reference genome Ensembl GRCh37 (v.75) using STAR (v. 2.5.2a) (5) with parameters '–outSAMunmapped Within –outFilterMultimapNmax 1 –outFilterMismatchNoverLmax 0.1 –alignIntronMin 21 –alignIntronMax 0 –alignEndsType Local –quantMode GeneCounts –twopassMode Basic'. In this step, STAR also generated gene level counts for all libraries. Quality checking of alignments was assessed by a custom script utilizing Picard Tools (http://broadinstitute.github.io/picard/), RNASeQC (6), RSeQC (7) and samTools (8). These analyses identified two samples, Syn1_1, and Syn1_11 (Brigatinib), as outlier samples as they failed to pass the following thresholds: exonic rate ≥ 0.8 and intergenic rate ≤ 0.1, and thus they were excluded from further analysis. Differentially expressed genes in pair-wise comparisons were identified by edgeR's quasi-likelihood F test (v. 3.18.1) (9), which was run at the R platform (v. 3.4) on genes with greater than 10 counts across replicates per condition in pair-wise comparisons. Gene ontology (GO) enrichment analysis for each comparison was performed on differentially expressed

genes at Bonferroni adjusted p values < 0.05, where all the analyzed genes in a given comparison were used as a background list, using DAVID (v. 6.8) (10). GO terms with Benjamini Hochberg adjusted p values < 0.05 were reported as significantly enriched for a given gene list.

Western blot of drug-treated DRG tumor samples from Postn-Cre;Nf2$^{flox/flox}$ mice

DRG tumor samples derived from mice shown in Figure 6 were collected at indicated time points after single dose oral gavage of indicated drugs. 9 DRGs for Dasatinib+Brigatinib treatment, 12 for all other conditions were collected in ice cold lysis buffer (1% IGEPAL; 0,1% DOC; 100 mM NaCl; 50 mM Tris pH 8.0) containing phosphatase and protease inhibitors (PhosSTOP, #04906837001 and cOmplete EDTA-free protease inhibitor cocktail, #4693132001, both from Roche). Lysis was performed in a Precellys 24 device (Bertin Technologies) at 2 x 5000 rpm for 30s with 5s break in-between. Cellular debris was removed twice by centrifugation at 12.000 rpm for 10 min and supernatant collected. Protein concentration was determined using a BCA protein assay kit (#23225; ThermorFisher). 10 µg each were separated by SDS-PAGE and transferred onto nitrocellulose membranes. Membranes were blocked in 5% milk/TBST and probed at 4°C overnight with the following primary antibodies in blocking buffer: p-AKT (Ser^{473}) (#4060), ERK1/2 (#9102), p-ERK1/2 (Thr^{202}/Tyr^{204}) (#4696), p-FAK (Tyr^{397}) (#8556), GSK (#9832), p-GSK (Ser^{9}) (#8213), IGF1R-beta (#9750), p-IGF1R-beta (Tyr^{1135}/Tyr^{1136}) (#3024), MEK1/2 (#8727), p-MEK1/2 (Ser^{217}/Ser^{221}), p-p70S6K (Thr^{389}) (#9234), S6RP (#2317), p-S6RP (Ser^{235}/Ser^{236}) (#4858), p-Stat1 (Tyr^{701}) (#7649), Stat3 (#9139), p-Stat3 (Tyr^{705}) (#9145) [all from Cell Signaling], Pyk2 (#ab32571; Abcam),

AKT1/2/3 (#sc-8312), FAK (#sc-271126) (both from Santa Cruz Biotechnology). Membranes were washed three times for 10 min each in TBST before probing with following secondary antibodies in blocking buffer for 1h at room temperature: Chemiluminescent signals were generated using ECL (#32106) or ECL+ (#32132) (both ThermoFisher) following manufacturer's instructions and detected on Super RX-N films (#4141019289; Fuji).

Supplemental Methods References

1. Plowman J CR, Alley M, Sausville E, Schepartz S. US-NCI testing procedures. Relevance of Tumor Models for Anticancer Drug Development: Karger; 1999. p 121-35.

2. Hirai H, Sootome H, Nakatsuru Y, Miyama K, Taguchi S, Tsujioka K*, et al.* MK-2206, an allosteric Akt inhibitor, enhances antitumor efficacy by standard chemotherapeutic agents or molecular targeted drugs i*n vitro* and *in vivo*. Mol Cancer Ther 2010;9:1956-67

3. Siaw JT, Wan H, Pfeifer K, Rivera VM, Guan J, Palmer RH*, et al.* Brigatinib, an anaplastic lymphoma kinase inhibitor, abrogates activity and growth in ALK-positive neuroblastoma cells, Drosophila and mice. Oncotarget 2016;7:29011-22

4. Burns SS, Akhmametyeva EM, Oblinger JL, Bush ML, Huang J, Senner V*, et al.* Histone deacetylase inhibitor AR-42 differentially affects cell-cycle transit in meningeal and meningioma cells, potently inhibiting NF2-deficient meningioma growth. Cancer Res; 2013; 73:792-803

5. Dobin, A., Davis, C.A., Schlesinger, F., Drenkow, J., Zaleski, C., Jha, S., Batut, P., Chaisson, M., and Gingeras, T.R. STAR: ultrafast universal RNA-seq aligner. Bioinformatics; 2013; 29, 15-21.

6. DeLuca, D.S., Levin, J.Z., Sivachenko, A., Fennell, T., Nazaire, M.D., Williams, C., Reich, M., Winckler, W., and Getz, G. RNA-SeQC: RNA-seq metrics for quality control and process optimization. Bioinformatics; 2012; 28, 1530-1532.

7. Li, H., Handsaker, B., Wysoker, A., Fennell, T., Ruan, J., Homer, N., Marth, G., Abecasis, G., Durbin, R., and Genome Project Data Processing, S. The Sequence Alignment/Map format and SAMtools. Bioinformatics; 2009; 25, 2078-2079.

8. Wang, L., Wang, S., and Li, W. RSeQC: quality control of RNA-seq experiments. Bioinformatics; 2012; 28, 2184-2185.

9. Robinson, M.D., McCarthy, D.J., and Smyth, G.K. edgeR: a Bioconductor package for differential expression analysis of digital gene expression data. Bioinformatics; 2010; 26, 139-140.

10. Huang da, W., Sherman, B.T., and Lempicki, R.A. Systematic and integrative analysis of large gene lists using DAVID bioinformatics resources. Nat Protoc; 2009; 4, 44-57.

Published online: 2021-03-30

Update on Phytochemical and Biological Studies on Rocaglate Derivatives from *Aglaia* Species#

Authors
Garima Agarwal[1], Long-Sheng Chang[2,3,4,5], Djaja Doel Soejarto[6,7], A. Douglas Kinghorn[1]

Affiliations
1 Division of Medicinal Chemistry and Pharmacognosy, College of Pharmacy, The Ohio State University, Columbus, Ohio, United States
2 Center for Childhood Cancer and Blood Diseases, Abigail Wexner Research Institute, Nationwide Children's Hospital, Columbus, Ohio, United States
3 Department of Pediatrics, The Ohio State University College of Medicine, Columbus, Ohio, United States
4 Department of Otolaryngology-Head and Neck Surgery, The Ohio State University College of Medicine, Columbus, Ohio, United States
5 Department of Pathology, The Ohio State University College of Medicine, Columbus, Ohio, United States
6 College of Pharmacy, University of Illinois at Chicago, Chicago, Illinois, United States
7 Science and Education, Field Museum, Chicago, Illinois, United States

Correspondence
Prof. A. Douglas Kinghorn
Division of Medicinal Chemistry and Pharmacognosy, College of Pharmacy, The Ohio State University
500 West 12th Avenue, Columbus, Ohio 43210, United States
Phone: + 1 614 247 8094, Fax: + 1 614 247 8642
kinghorn.4@osu.edu

Key words
Aglaia, Meliaceae, natural products, rocaglates, flavaglines, rocaglamide, silvestrol, biological effects, antineoplastic activity, antiviral activity, protein translation inhibition

received January 14, 2021
accepted after revision February 26, 2021
published online March 30, 2021

Bibliography
Planta Med 2021; 87: 937–948
DOI 10.1055/a-1401-9562
ISSN 0032-0943
© 2021. Thieme. All rights reserved.
Georg Thieme Verlag KG, Rüdigerstraße 14, 70469 Stuttgart, Germany

ABSTRACT

With about 120 species, *Aglaia* is one of the largest genera of the plant family Meliaceae (the mahogany plants). It is native to the tropical rainforests of the Indo-Australian region, ranging from India and Sri Lanka eastward to Polynesia and Micronesia. Various *Aglaia* species have been investigated since the 1960s for their phytochemical constituents and biological properties, with the cyclopenta[*b*]benzofurans (rocaglates or flavaglines) being of particular interest. Phytochemists, medicinal chemists, and biologists have conducted extensive research in establishing these secondary metabolites as potential lead compounds with antineoplastic and antiviral effects, among others. The varied biological properties of rocaglates can be attributed to their unusual structures and their ability to act as inhibitors of the eukaryotic translation initiation factor 4A (eIF4A), affecting protein translation. The present review provides an update on the recently reported phytochemical constituents of *Aglaia* species, focusing on rocaglate derivatives. Furthermore, laboratory work performed on investigating the biological activities of these chemical constituents is also covered.

Introduction

Since the first phytochemical report of the tetracyclic triterpene, aglaiol, from the leaves of the oriental plant *Aglaia odorata* in 1965 [1], many studies have appeared describing the chemical constituents of *Aglaia* species in terms of elucidating the structurally diverse natural products present. Examples of secondary metabolite compound classes isolated from *Aglaia* species include bisamides [2–4], flavonoids [2, 5], lignans [6], and triterpenoids, particularly of the baccharane, cycloartane, and dammarane types [7–9]. Also, more than 100 biogenetically related oxygen-containing heterocyclic secondary metabolites have been isolated to date. They are characteristic of many *Aglaia* species and are known col-

Dedicated to Professor Arnold Vlietinck to recognize his important contributions to natural product research on the occasion of his 80th birthday in 2021.

Downloaded by: Ohio State University. Copyrighted material.

ABBREVIATIONS

5′-UTRs	5′-untranslated regions
ADC	antibody-drug conjugate
BCSCs	breast cancer stem cells
CDX	cell line-derived xenograft
CPBF	cyclopenta[*b*]benzofuran ring system
DDR	didesmethylrocaglamide
DDX3	DEAD-box RNA helicase 3
EBOV	Ebola virus
eIF4A	eukaryotic initiation factor 4A
EV71	enterovirus 71
FLT3	FMS-like receptor tyrosine kinase 3
HCV	hepatitis C virus
HepG2	human hepatoblastoma cell line
HEV	hepatitis E virus
IRF1	interferon regulatory factor 1
MDR1	multidrug-resistance protein 1
MPNST	malignant peripheral nerve sheath tumor
NSCLC	non-small cell lung carcinoma
p53/Puma	p53 upregulated modulator of apoptosis
PC-3	prostate cancer cell line
PDA	pancreatic ductal adenocarcinoma
PDX	patient-derived xenograft
PHB1/2	prohibitins 1 and 2
PIM1	proto-oncogene serine/threonine-protein kinase
Raf-MEK-ERK	mitogen-activated protein kinases (MAPKs) involved in cell proliferation and survival

lectively as rocaglamide (**1**) derivatives. Such compounds have been divided into 3 sub-classes: (i) CPBFs ("flavaglines" or "rocaglates"); (ii) cyclopenta[b]benzopyrans ("thapsakins" or "aglain" derivatives), and (iii) benzo[*b*]oxepines ("thapoxepines" or "forbaglines"), which are thought to be formed by the cycloaddition of a cinnamic acid amide and a flavonoid unit [10, 11]. Of these 3 groups, rocaglates are the most potently bioactive and well-investigated chemical constituents of *Aglaia* species and thus the main focus of the present article.

(−)-Rocaglamide (**1**), a CPBF, was the first compound obtained in its class and was isolated in 1982 from the dried roots and stems of *Aglaia elliptifolia* as an *in vivo*-active antileukemic agent [12]. In subsequent years, more than 60 rocaglate derivatives have been isolated and structurally identified from several *Aglaia* species [13, 14]. With most substitutions occurring at the C-1 and C-2 positions of their phenyl rings (▶ **Fig. 1**), some examples of rocaglate derivatives are methyl rocaglate (**2**) [15, 16], DDR (**3**) [13, 15], rocaglaol (**4**) [17], aglaroxin C (**5**) [18], cyclorocaglamide (**6**) [19], and isothapsakon A (**7**) [20]. Another rocaglate derivative that has garnered much scientific attention is silvestrol (**8**), which was isolated and structurally characterized along with its 5‴-epimer, episilvestrol (**9**) [21]. These 2 rocaglate congeners were purified from the stem bark of *Aglaia foveolata* (originally misidentified taxonomically as *Aglaia silvestris*) collected in Indonesia and contain an unprecedented dioxanyl ring connected to the CPBF core at the C-6 position of the phenyl ring A (▶ **Fig. 1**). The presence of a dioxanyl ring was demonstrated to enhance the cytotoxic potency of rocaglates [2, 22, 23] and has led to extensive work on the synthesis and structure-activity requirement exploration of rocaglamide, silvestrol, and related analogs [22–28].

A pivotal paper exploring the cellular mechanism of activity of the rocaglates was published in 2008 [29], in which Pelletier and his associates reported silvestrol as an inhibitor of protein translation by modulating the activity of the eIF4A, an RNA helicase subunit of the eIF4F complex. This work has been complemented by further mechanistic reports from the same group [30, 31], with selected rocaglates also being documented to act at the cellular level to modulate the Raf-MEK-ERK pathway via targeting PHBs 1/2 [32], MAPK [33], and FLT3 and the microRNA-155 (*miR-155*) gene [34]. Such biological studies have laid the foundation for developing rocaglamide and silvestrol as potential drug leads against different disease states, including, in particular, cancer, and more recently, certain viruses.

This review describes the work on rocaglates from *Aglaia* species, primarily in terms of their phytochemical isolation, structural characterization, and biological activities, as reported from 2014 to 2020. It is intended as an update of the 2 previous review articles we wrote on this same topic in 2006 [22] and 2014 [23] and includes experimental contributions from the respective laboratories of the 3 current senior authors. Additionally, a summary is included of the collection of several *Aglaia* species from 3 Southeast Asian countries (Indonesia, Laos, and Vietnam) under various formal Memoranda of Agreement (MOA) with the University of Illinois at Chicago, as part of 2 multi-institutional collaborative research projects funded by the U. S. National Cancer Institute (NCI) [35–37]. To assist with the writing of this review, we searched the SciFinder literature database (Chemical Abstracts Service, Columbus, OH, USA) using keywords such as *Aglaia*, rocaglamide, and silvestrol and then categorized and refined for relevant publications and patents from 2014 onward.

Taxonomy and Collection

The genus *Aglaia* is a large group of plants, mostly comprised of trees, belonging to the family Meliaceae. These species have a natural distribution spanning the tropics from Sri Lanka and India, east to the Pacific through Burma, southern mainland China, Taiwan, Vietnam, Malaysia, Indonesia, the Philippines, New Guinea, Northern Australia, and the Western Pacific. In the volume "A Taxonomic Monograph of The Genus *Aglaia* Lour. (Meliaceae)", Dr. Caroline Pannell (University of Oxford, Oxford, U. K.), a leading taxonomic specialist of this genus, included 104 species belonging to *Aglaia* [38]. However, today, approximately 120 *Aglaia* species are recognized [39]. The largest concentration of this genus is found in Indonesia, followed by Malaysia, the Philippines, and the Indochina region (including Thailand and southern mainland China). In the taxonomic system, *Aglaia* belongs to the tribe Aglaieae within the subfamily Melioideae and is made up of 2 taxonomic sections, namely, the section *Aglaia* and the section *Amoora* [38]. In 2005, based on a phylogenetic study, Muellner and coworkers [40] recognized 3 taxonomic sections within the genus, viz., the

Downloaded by: Ohio State University. Copyrighted material.

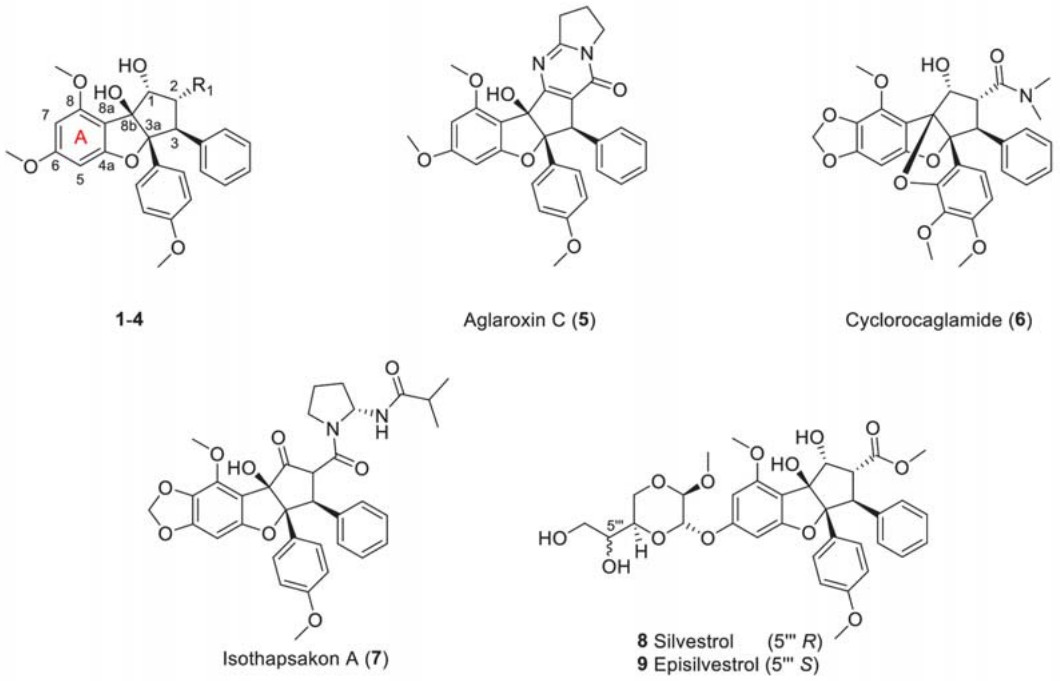

		R_1
1	Rocaglamide	$CONMe_2$
2	Methyl rocaglate	COOMe
3	Didesmethylrocaglamide (DDR)	$CONH_2$
4	Rocaglaol	H

▶ **Fig. 1** Examples of selected flavaglines (**1**–**9**) isolated from various *Aglaia* species.

sections *Amoora, Neoaglaia*, and *Aglaia*, which are defined morphologically primarily by their fruit characteristics and by the numbers of flower parts.

All *Aglaia* species are woody, ranging in size from a few meters high to large trees up to 40 m tall. The bark of these trees and their branches tend to exude a sticky white latex when incised. Most species have imparipinnate leaves, although these are occasionally simple or trifoliolate. Characteristically, branchlets and leaves are covered by an indumentum of peltate scales or stellate hairs, which may be used to identify specific species. The flowers of the genus members are small (1–10 mm long) and subglobose or ellipsoid and unisexual, typically set in a terminal and axillary paniculate inflorescence. In classifying the species, the staminal tube in the female flower provides the most taxonomic information. The fruits are either ellipsoid or pear-shaped, dehiscent or indehiscent, and covered by a stellate type of scales or hairs, with the pericarp thick and pliable. The outer layer of the seed coat (referred to as the aril) is usually fleshy [38].

Members of the genus *Aglaia* are found growing in both evergreen and monsoon primary and secondary forests, from sea level to an altitude of 1,500 m, or, rarely, higher, and occur mostly in evergreen forests and less commonly in monsoon forests. *Aglaia* species populations are normally scattered, not in a dense and dominant cluster, and many species have become rare due to forest clearance and may be threatened. Examples include *A. foveolata, A. spectabilis,* and *A. perviridis* [41]. Most species yield good hardwood timber used in construction for buildings, bridges, houses, and furniture. Several species have found traditional medicinal uses, especially the leaves, to treat bodily afflictions, such as wounds, fever, headache, asthma, and jaundice, and as a tonic, e.g., after childbirth [42, 43]. One species, *A. odorata*, often found in cultivation, has a history of wide use in traditional medicine to treat various diseases [44, 45].

During the time of operation of the 2 NCI-supported multi-institutional research projects [35–37], a total of 17 identified species of *Aglaia* were collected for investigation for potential anticancer activity (▶ **Table 1**). The greatest number of collections came from Indonesia (11 species), while a small number each came from Laos (3 species), Vietnam (2 species), and Thailand (one species). Voucher specimens of these collections are in deposit at the Herbarium of the Field Museum of Natural History, Chicago, IL, USA, and at herbarium institutions in the county where each collection was made.

Downloaded by: Ohio State University. Copyrighted material.

Phytochemical Reports of Rocaglate (Cyclopenta[*b*]benzofurans) Constituents of *Aglaia* Species (2014–2020)

In 2014, our group at The Ohio State University (OSU) published a comprehensive review focusing on rocaglamide (**1**), silvestrol (**8**), and their structurally related bioactive compounds [23], inclusive of isolation of several new rocaglates from 4 *Aglaia* species (*Aglaia cucullata, A. edulis, A. odorata*, and *A. perviridis*). Recent reports published mainly during the period 2014–2020 have described the isolation of new rocaglate derivatives from only a relatively few *Aglaia* spp., namely, *A. odorata, A. oligophylla, A. perviridis*, and *A. stellatopilosa*. Many of the research reports on the *Aglaia* CPBFs published over the last few years have focused on their syntheses, analog development, and biological activity evaluation, with the last-mentioned topic, in particular, to be covered in subsequent sections of this review.

In 2015, An et al. reported the structures of 8 new benzo[*b*]oxepine derivatives (aglaodoratins A–H) [46], and 8 new cyclopenta[*b*]benzopyrans, biosynthetic precursors to rocaglates (aglapervirisins B–J) [47], from the leaves of *A. odorata* and *A. perviridis*, respectively. Of these 16 secondary metabolites, aglaodoratins C (**10**), D (**11**), and E (**12**) (▶ **Fig. 2**) were observed to exhibit moderate cytotoxicity, with their IC_{50} values in the range from 0.097 to 6.25 µM, against 3 human cancer cell lines (HT-29 colon cancer, SMMC-7721 hepatocellular cancer, and MG-63 osteosarcoma). Additionally, aglaodoratin C (**10**) inhibited cellular proliferation by arresting cells at the G2/M cell-cycle phase and thereby inducing apoptosis in HepG2 liver cancer cells *in vitro* [46]. In contrast, aglapervirisins B–J were either only weakly active or noncytotoxic for a panel of 4 human cancer cell lines [47]. Interestingly, Kong and colleagues recently published a further phytochemical investigation on the leaves of *A. perviridis*, where they reported 4 new aglain glycosides (aglapervirisins J–M) with weak anti-inflammatory activity, as determined by an *in vitro* nitric oxide inhibition assay using the RAW264.7 mouse macrophage tumor cell line [48].

Two separate groups reported the similar compounds rocaglamide AY (**13**) [49] and aglaodoratin I (**14**) [46], isolated from the leaves of *A. oligophylla* and *A. odorata*, respectively. Both these rocaglates have an oxime group at the C-1 position, but aglaodoratin I (**14**) possesses a hydroxy group at the C-3′ position instead of a hydrogen atom, as seen in rocaglamide AY (**13**) (▶ **Fig. 2**). The limited quantity of **14** obtained prevented it from being evaluated for cytotoxicity [46]. Although no biological test results were reported for rocaglamide AY (**13**) either, it was mentioned that many rocaglamide congeners possess insecticidal properties against the agricultural insect pest, *Spodoptera littoralis* [49]. Another paper published in 1999 reported a similar compound **15**, also from the twigs and leaves of *A. odorata*, which exhibited moderate insecticidal activity (LC_{50} of 1.3 ppm) toward *S. littoralis* larvae [10]. Additionally, a rocaglaol derivative **16**, with a formamide group at the C-1 (*S*) position and a bromine at C-4′ instead of a methoxy group, was found to have cytotoxic activity ranging from 0.5–2.3 nM against an array of human cancer cell lines [50], suggesting an amide at C-1 may lead to a more potent cytotoxic effect when compared to rocaglate derivatives with a more typical hydroxy group found at this position.

▶ **Table 1** *Aglaia* species collected in Southeast Asia under 2 NCI-funded research projects.

Country	Species	Voucher specimen
Thailand	*Aglaia elliptica* Bl.	Nantasan s. n.
Laos	*Aglaia* cf. *macrocarpa* King	Soejarto et al. 15399
Laos	*Aglaia* cf. *oligophylla*	Soejarto et al. 15396
Laos	*Aglaia spectabilis* (Miq.) Jain & Bennet	Soejarto et al.15410
Vietnam	*Aglaia* cf. *aquatica* (Pierre) Harms	Soejarto et al. 15176
Vietnam	*Aglaia perviridis* Hiern	Soejarto et al. 14863
Indonesia	*Aglaia* cf. *argentea* Bl.	Riswan ML-039
Indonesia	*Aglaia edulis* (Roxb.) Wall.	Riswan SR-022
Indonesia	*Aglaia elliptica* Bl.	Riswan ML-033
Indonesia	*Aglaia foveolata* Pannell	Riswan KP-034
Indonesia	*Aglaia foveolata* Pannell	Riswan SR-IS02
Indonesia	*Aglaia foveolata* Pannell	Riswan SR-IS17
Indonesia	*Aglaia foveolata* Pannell	Riswan SR-IS18
Indonesia	*Aglaia foveolata* Pannell	Riswan SR-IS23
Indonesia	*Aglaia foveolata* Pannell	Riswan SR-IS24
Indonesia	*Aglaia foveolata* Pannell	Riswan SR-IS24
Indonesia	*Aglaia foveolata* Pannell	Riswan SR-IS25
Indonesia	*Aglaia foveolata* Pannell	Riswan SR-IS26
Indonesia	*Aglaia foveolata* Pannell	Riswan SR-IS26
Indonesia	*Aglaia foveolata* Pannell	Riswan SR-IS27
Indonesia	*Aglaia foveolata* Pannell	Riswan SR-IS28
Indonesia	*Aglaia foveolata* Pannell	Riswan Z-34
Indonesia	*Aglaia korthalsii* (Miq.) Pellegr.	Kardono SC87
Indonesia	*Aglaia leptantha* Miq.	Riswan SR-IS01
Indonesia	*Aglaia odorata* Lour.	Riswan A-12
Indonesia	*Aglaia odoratissima* Bl.	Riswan SR-072
Indonesia	*Aglaia rubiginosa* (Hiern) Pannell	Riswan Z-55
Indonesia	*Aglaia silvestris* Merr.	Riswan SR-J17
Indonesia	*Aglaia silvestris* Merr.	Riswan SR-068
Indonesia	*Aglaia silvestris* Merr.	Riswan SR-CJR068
Indonesia	*Aglaia teysmanniana* (Miq.) Miq.	Riswan SR-J20
Indonesia	*Aglaia tomentosa* Teijsm. & Binn.	Riswan B-037

In 2016, Othman and colleagues published the isolation of silvestrol (**8**) and its epimer 5‴-episilvestrol (**9**), in addition to several new 2,3-seco-dammarane triterpenoids, from the stems of *A. stellatopilosa*, collected in Sarawak, Malaysia [51]. Earlier, silvestrol (**8**) was reported in a patent application as an antineoplastic constituent of the Malaysian plant *Aglaia leptantha*, which was lat-

Downloaded by: Ohio State University. Copyrighted material.

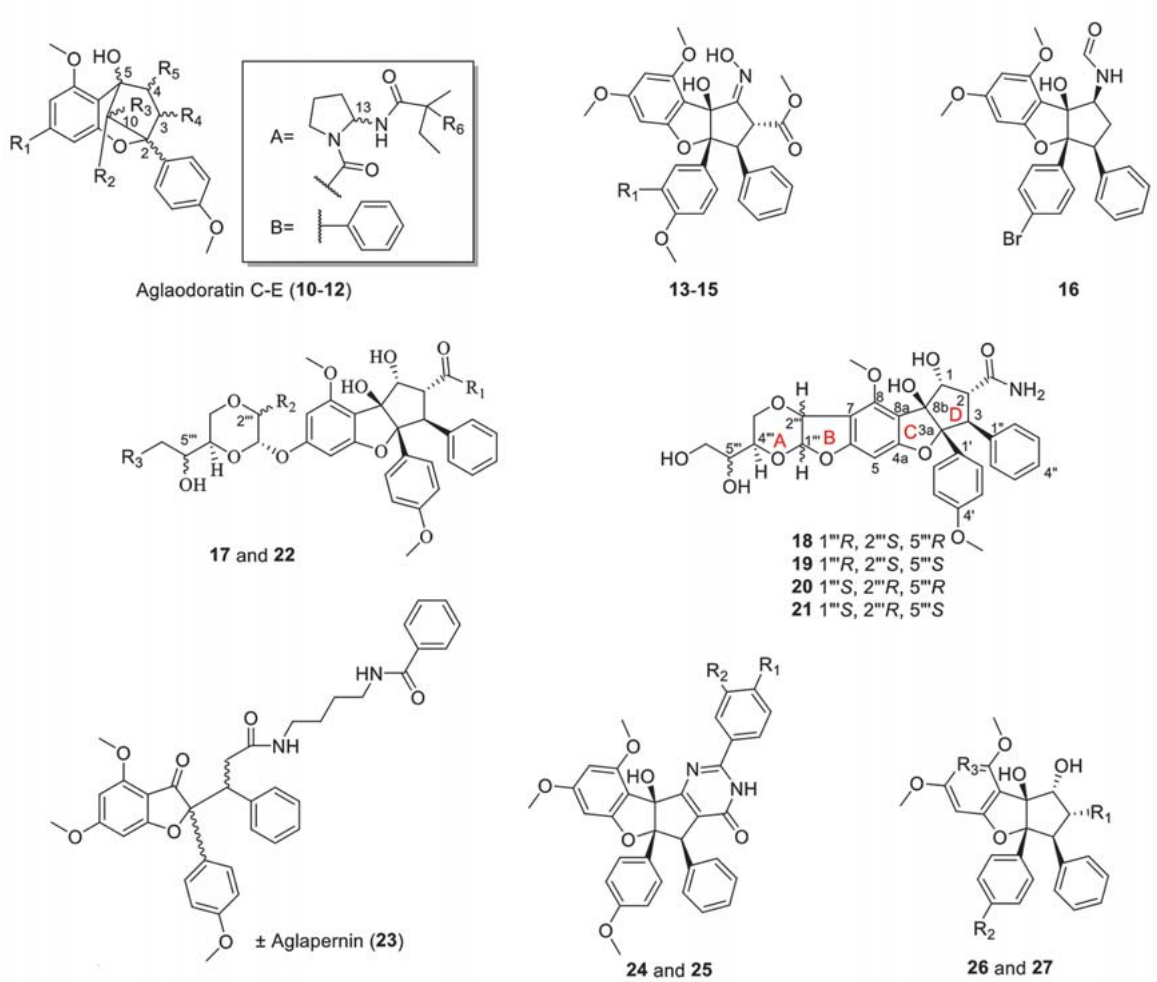

		R_1	R_2	R_3	R_4	R_5	R_6
10	Aglaodoratin C (2*S*, 3*R*, 4*S*, 5*S*, 13*R*)	OMe	$R_2 = R_3 = O$		unit B	unit A	OH
11	Aglaodoratin D (2*S*, 3*S*, 4*R*, 5*S*, 10*R*, 13*S*)	OH	H	OH	unit A	unit B	H
12	Aglaodoratin E (2*R*, 3*R*, 4*S*, 5*R*, 10*S*, 13*R*)	OMe	H	OH	unit A	unit B	OH
13	Rocaglamide AY	H	-	-	-	-	-
14	Aglaodoratin I	OH	-	-	-	-	-
15		OMe	-	-	-	-	-
17	Aglapervirisin A (5‴ *R*, 2‴ *S*)	OMe	OMe	Ac	-	-	-
22	2‴ (*R*/*S*) (5‴ *S*)	NH_2	OH	OH	-	-	-
24		Me	H	-	-	-	-
25		H	OMe	-	-	-	-
26	(–)-CR-31-B	CONHOMe	OMe	C	-	-	-
27	eFT-226	CH_2NMe_2	CN	N	-	-	-

▶ **Fig. 2** Structures of cytotoxic rocaglates isolated from various *Aglaia* species and several related synthetic congeners (**10**–**27**).

er re-identified as *A. stellatopilosa* [52]. However, the structures for the isolated compound described in this patent did not show full configurational details and did not distinguish between compounds **8** and **9**. Silvestrol (**8**) and episilvestrol (**9**) were also purified from the leaves of *A. perviridis* in 2016, collected in Yunnan Province of the People's Republic of China [47]. Moreover, our group confirmed the presence of compounds **8** and **9** in a root sample of *A. perviridis* collected in Vietnam [53]. Therefore, to date, cyclopenta[b]benzopyrans containing a dioxanyl ring as in silvestrol (**8**) have been found in only 3 of the approximately 120 *Aglaia* species (i.e., *A. foveolata*, *A. perviridis*, and *A. stellatopilosa*), making them rare constituents of this genus.

In addition to episilvestrol (5‴-episilvestrol) (**9**), a small number of additional structural modified variants of silvestrol (**8**) have

Downloaded by: Ohio State University. Copyrighted material.

been reported from *Aglaia* species. In 2010, as a result of a large-scale recollection of the stem bark of *A. foveolata* from Kalimantan, Indonesia, the compounds 2‴-episilvestrol and 2‴,5‴-diepisilvestrol were obtained as trace constituents, with both having reduced cytotoxic potencies when compared to silvestrol [8]. As a result of this work, which utilized specialized large-scale isolation facilities available at NCI, a sufficient amount of silvestrol (ca. 100 mg) was purified from the recollected plant material to conduct extensive biological testing at OSU and elsewhere [34, 54, 55]. An et al. in 2016 reported aglapervirisin A (**17**) as a new silvestrol analog with an acetate group at the C-6‴ position of the dioxanyl ring side chain (▶ **Fig. 2**) [47]. Cytotoxic profiling of aglapervirisin A (**17**) in 4 human cell lines (HT-29 colon cancer, HepG2 hepatocarcinoma, HL-60 leukemia, MCF-7 breast cancer) showed that it had comparable potencies to silvestrol (**8**) and episilvestrol (**9**), with IC_{50} values ranging from 8–14 nM. Further mechanistic evaluation of **17** against HepG2 cells uncovered the ability of this mono-acetylated molecule to lower the expression levels of tyrosine phosphatases, Cdc2, and Cdc25, thereby causing apoptosis by arresting cells at the G2/M phase [47].

In 2019, our group at OSU reported 5 new cyclopenta[*b*]benzofuran analogs (**18**–**22**) from the leaves of *A. perviridis* collected in the Nui Chua National Park in Vietnam [53]. Of these compounds, **18**–**21** were observed to have a fused dihydrofuran ring to both the dioxanyl and aryl rings of the rocaglate core (▶ **Fig. 2**) and an amide moiety at C-2. Compound **22**, elucidated as a 2‴-hydroxy derivative of episilvestrol (**9**) with an amide moiety at C-2, was isolated as an enantiomeric mixture (▶ **Fig. 2**). Of these isolates, only compound **22** exhibited low micromolar cytotoxic potency against the human colon (HT-29) and prostate cancer (PC-3) cell lines. However, this study provided some structure-cytotoxic activity information, in that a hydroxy group at C-2‴ and the rigidity in structure between the dioxanyl and CPBF core might be detrimental to the cytotoxic activity of these flavaglines [53].

In the most recent report on *A. perviridis* by Kong and colleagues [48], a novel rocaglate derivative was described, (±) aglapernin (**23**), which did not show cytotoxicity against cancer cell lines but exhibited weak antibacterial activity (125 µM) against *Porphyromonas gingivalis*.

Another recent development worthy of mention is the silvestrol-based antibody-drug conjugates (ADCs), developed in 2017 by Genentech, Inc. [56]. ADCs are target-specific prodrugs, with a warhead (the cytotoxic drug) connected to a specific antibody via a linker [57–59]. The warhead bioactive moiety of the ADC provides the biological activity to the macromolecule in antibody-targeted cells. The Genentech team synthesized various silvestrol-ADC analogs in their patent, incorporating a dioxanyl ring system with different antibodies. These ADCs were then evaluated both *in vitro* and *in vivo* in breast cancer cells and B-cell malignancies. Silvestrol-ADCs connected to cysteine-modified CD22 antibodies demonstrated promising results against a CD22-expressing xenograft mouse model [56].

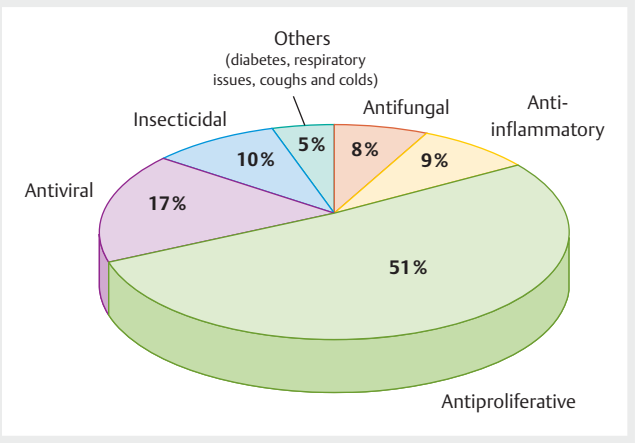

▶ **Fig. 3** Graphical representation of publications on *Aglaia* spp. and rocaglate derivatives, concerning different disease states, 2014–2020 (n = 77, primary research articles).

Therapeutic Potential of Rocaglates (Update 2014–2020)

Since the initial report of rocaglamide (**2**) from *A. elliptifolia* as an antileukemic agent in the early 1980s [12], the therapeutic potential of CPBFs has been evaluated and reported by several research groups. The diverse range of biological activities evaluated for these compounds has included antineoplastic, insecticidal, anti-inflammatory, neuroprotective, and, more recently, antiviral properties [2, 22, 23, 60]. ▶ **Fig. 3** gives a graphical representation of the published work on these compounds from 2014 to 2020. Continued modifications of the functional groups at specific positions have contributed to a better understanding of the structure-activity relationships of rocaglates as potential therapeutic agents. Substantial work has been conducted in establishing their biological targets, of which 2 have been explored to the greatest extent, namely, eIF4A [29, 30, 61] and PHB1/2 [32, 62, 63].

The initial studies exploiting the cellular mechanistic action of silvestrol (**8**) were published just a few years after its isolation, where it was observed to influence the interaction between eIF4A and RNA [29, 30]. This work was followed by demonstrating that synthesized biotinylated 5‴-episilvestrol selectively inhibits eIF4AI/II [26].

Over the last few years, several studies have been published from our collaborative work on the effects of various rocaglate derivatives against several neurofibromatosis-associated tumors and pediatric sarcomas, with the biological testing experimental work performed at the Nationwide Children's Hospital, Columbus, Ohio, USA. In an initial study using silvestrol (**8**), it was shown that the eIF4F components, including eIF4A, are potential therapeutic targets in MPNSTs and vestibular schwannomas [64]. Genetic depletion of eIF4A using short-hairpin RNAs and pharmacological inhibition using the natural eIF4A inhibitor silvestrol potently suppresses the growth of MPNSTs and schwannomas by decreasing the levels of multiple mitogenic signaling molecules, including AKT, ERKs, Aurora A, and cyclins, essential for tumor growth. The

Downloaded by: Ohio State University. Copyrighted material.

decrease of tumor growth was correlated with elevated phosphohistone H3 and with G2/M arrest and apoptosis observed in the tumor cells treated with silvestrol [64].

The inhibition of the overexpressed eIF4F components in meningiomas was also investigated using a panel of 23 natural products, inclusive of representatives of the cucurbitacin, diarylheptanoid, rocaglate, simaroubolide, stilbenoid, sesquiterpene lactone, and xanthone structural classes [65]. Of the compounds examined, silvestrol (**8**) and episilvestrol (**9**) were the 2 most growth-inhibitory compounds, with silvestrol being more potent (IC_{50} 10 nM) than episilvestrol (IC_{50} 32 nM) against *NF2*-deficient meningioma Ben-Men-1 cells. As in MPNSTs and schwannoma cells, silvestrol (**8**) treatment induced G_2/M arrest in the meningioma cells. These data suggested that inhibiting protein translation is a potential treatment approach for MPNSTs, schwannomas, and meningiomas, including those associated with neurofibromatosis [64, 65].

However, silvestrol (**8**) has suboptimal drug-like properties, including a bulky structure, poor oral bioavailability [66], and sensitivity to MDR1 efflux [67]. Moreover, a toxicity study in larger animals conducted by our colleagues and collaborators at OSU and the NCI Developmental Therapeutic Program (DTP) revealed toxic effects of silvestrol in dogs' lungs [68]. Consequently, further development of silvestrol as a cancer therapy was suspended. To search for compounds with better drug-like properties, alternative rocaglate congeners to silvestrol (**8**) were sought as potential growth inhibitors of MPNST, schwannoma, and meningioma cells [68]. Upon side-by-side comparison of 10 rocaglates lacking the dioxanyl ring with silvestrol (**8**), both rocaglamide (**1**) and DDR (**3**) were found to exhibit growth-inhibitory activity comparable to silvestrol (**8**). Like silvestrol, rocaglamide (**1**) and DDR (**3**) arrested tumor cells at G_2/M and induced apoptosis and a DNA-damage response while decreasing the expression of multiple mitogenic kinases, consistent with translation inhibition. In collaboration with colleagues at the NCI DTP, rocaglamide (**1**) was observed to be 50% orally bioavailable and did not show any discernible pulmonary toxicity in dogs. Also, both rocaglamide (**1**) and DDR (**3**) were not sensitive to MDR1 inhibition, possibly due to the lack of a dioxanyl ring. Most importantly, when administered either intraperitoneally or orally, rocaglamide (**1**, NSC326408) potently inhibited tumor growth in an orthotopic MPNST model. In addition, rocaglamide (**1**) exhibited broad antitumor activity in PDX models for a Ewing sarcoma, an osteosarcoma, and an alveolar rhabdomyosarcoma. In a comparative *in vitro* study of 11 rocaglate congeners, including rocaglamide (**1**), methyl rocaglate (**2**), DDR (**3**), rocaglaol (**4**), and silvestrol (**8**), DDR (**3**, IC_{50} between 5 and 15 nM) was found to be the most potent compound, when tested against a panel of MPNST, a schwannoma, and a meningioma cell lines [68]. (−)-DDR (**3**) was obtained earlier in our work as a trace constituent from the combined leaves, twigs, and fruits of *A. perviridis* when collected in Vietnam and differs from rocaglamide (**1**) in possessing an amide unit instead of a dimethylamide functionality at the C-2 position of the CPBF core (▶ **Fig. 1**) [13]. In a follow-up investigation, chemically synthesized DDR (**3**) was also found to effectively block tumor growth in CDX and PDX models of osteosarcoma [69]. It was suggested that both rocaglamide (**1**) and DDR (**3**) are worthy of further evaluation as potential treatments for pediatric bone and soft tissue sarcomas.

Additional studies have been performed on the cellular mechanism of action of rocaglate family members as eIF4A inhibitors. Chu and colleagues used CRISPR-Cas9 as a tool for drug-target validation *in vivo*. They validated the rocaglate-eIF4A relationship by introducing an eIF4A1 mutant allele (F163L) into cells and showed that eIF4A1(F163L) retains helicase activity but was unresponsive to rocaglates, such as silvestrol (**8**) [70]. Iwasaki et al. reported that rocaglamide (**1**) does not repress translation of specific messenger RNAs by reducing cellular eIF4A availability but rather by clamping eIF4A onto the polypurine sequences in an ATP-independent manner [71]. This same group later elucidated the crystal structure of a complex of human eIF4A-rocaglamide-polypurine RNA and showed rocaglamide to target a bimolecular cavity between eIF4A and polypurine RNA [72]. Recently, Sidraharan et al. treated breast cancer stem cells (BCSCs) with rocaglamide (**1**), determining eIF4A as a valid molecular target for both BCSCs and bulk tumor cells. They further suggested that eIF4A inhibitors may be combined synergistically with existing chemo-, radio- and/or immunotherapies [73].

Extensive follow-up work has been done more recently since the initial documentation of rocaglates and their inhibitory effect on PHB1/2 [32]. This includes not only the investigation of their antineoplastic activity but also their potential antiviral effects. Liu and colleagues evaluated rocaglamide (**1**) and aglaroxin C (**5**) in HCV-infected human hepatoma cells [63]. HCV, responsible for hepatitis C and liver cancer in humans, enters human hepatocyte cells utilizing different membrane proteins, particularly based on the interaction between its glycoprotein E2 and PHB1/2 [74]. Rocaglamide (**1**) inhibits HCV entry into human hepatoma cells by targeting PHB1/2, which in turn inhibits the CRaf/RAS pathway, an integral component in cell proliferation and signaling [75]. While synthesized aglaroxin C (**5**, ▶ **Fig. 1**) was found to exhibit a weak effect on HCV replication or entry into cells, several further analogs of **5** were shown to be more effective HCV entry inhibitors, including **24** and **25**, in which the C-aryl group of the pyramidinone is differentially substituted [76, 77]. These 2 compounds exhibited low cytotoxicity (EC_{50} = 0.5 µM), 3-fold greater in comparison to aglaroxin C (**5**), against human hepatoma Huh-7.5.1 cells infected with HCV and were suggested to inhibit viral entry rather than replication as their mechanism of action [76]. Another similar study with EV71, responsible for hand, foot, and mouth disease in humans, demonstrated dependence on PHB for cell entry, with rocaglamide (**1**) used to investigate EV71 translation and entry inhibition [78]. An *in vivo* study of EV71-infected mice showed that mice survived longer, with lower viral loads in the brain and spinal cord, on treatment with rocaglamide (**1**, 0.25 mg/kg), as compared to those treated with vehicle (0.25% DMSO in olive oil). These data were supported by an *in vitro* study of EV71-infected motor-neuron NSC-34 cells, where a dose-dependent reduction in viral load was observed in cells treated with rocaglamide (**1**, 10–100 nM) [78].

In 2017, silvestrol (**8**) was evaluated *in vitro* for its antiviral activity against the EBOV [79]. This study by Biedenkof et al. demonstrated the ability of silvestrol (**8**) to inhibit EBOV infection at a low noncytotoxic concentration (10 nM). Additionally, they demon-

Downloaded by: Ohio State University. Copyrighted material.

strated that reduction of EBOV propagation correlated with the disappearance of viral nucleoprotein (NP), which is comparable to translational inhibition of PIM1, a cellular kinase known to be affected by silvestrol (**8**) [79]. In another antiviral study, Slaine et al. examined the role of silvestrol (**8**) in blocking the replication of influenza A virus (IAV) [80]. They showed that silvestrol treatment during early IAV infection induced stress granule formation, inhibited viral protein synthesis, and blocked viral replication. Interestingly, the viral protein synthesis was "recovered" upon silvestrol (**8**) withdrawal, suggesting a reversible translation inhibition mode of action [80].

Several further evaluations of rocaglamide (**1**) and silvestrol (**8**) as potential antiviral agents have been performed against HEV [81, 82], corona- and picornaviruses [83], chikungunya virus [84], EBOV, Marburg virus [85], and zika virus [86]. All these studies were based on the assumption that efficient translation of the mRNAs of these viruses, which contain highly structured 5-UTRs, requires the DEAD-box RNA helicase eIF4A. (−)-CR-31-B (**26**), a synthesized rocaglate hydroxamate, was evaluated by Müller and colleagues for its antiviral activity against HEV, corona-, zika, Lassa, and Crimean Congo hemorrhagic fever viruses, in comparison with silvestrol [87]. It was found that (−)-CR-31-B (**26**) exhibited slightly more potent viral inhibition than silvestrol (**8**), with EC_{50} values in the low nanomolar range for most of the viruses examined. However, the inhibitory activity of (−)-CR-31-B (**26**) against HEV replication was somewhat weaker in comparison to silvestrol (**8**), suggesting a potential difference in the antiviral mode of action between these 2 rocaglates [87]. Recently, the synthetic rocaglate (−)-CR-1–31-B (**26**) was employed to show that eIF4A is a therapeutic target in PDA, and it suppressed tumor growth and extended the survival time in a genetically-engineered mouse PDA model [88].

Two additional mechanistic targets of rocaglates have been suggested, namely, KRAS [89], a member of the RAS family of small GTPases, and DDX3, a DEAD-box RNA helicase [90]. RAS proteins are imperative for triggering multiple signaling pathways required for cell proliferation and survival [91]. Mutations in *KRAS* have been frequently found in several types of cancer, including pancreatic, lung, and colon cancers, and NSCLC [92]. According to Yurugi et al., flavaglines, particularly rocaglamide (**1**), potently inactivate RAS by inhibiting its GTP loading and deterring its nanocluster formation at the phospholipid-enriched sites on the plasma membrane [89]. In turn, Chen et al. [90] focused on DDX3, a highly conserved DEAD-box helicase involved in cell-cycle regulation, differentiation, survival, and apoptosis [93]. Rocaglamide (**1**) was discerned to clamp DDX3 on its polypurine sequences in an ATP-independent manner, and the glutamine at position 360 was found to be a critical residue for DDX3 binding by this rocaglate [90].

Other Biological Properties of Rocaglate Derivatives

In 1985, Chiu published an initial report of the antifeedant activities against 3 agricultural pests of an acetone extract of *A. odorata* [94]. This was followed up in 1993 by the work of Ishibashi and colleagues showing that 2 CPBF constituents, rocaglamide (**1**) and methyl rocaglate (**2**), from this plant demonstrated potent insecticidal activities against the larvae of the variegated cutworm (*Peridroma saucia*) [16]. Subsequently, several studies have evaluated the potential insecticidal effects of rocaglamide and its analogs. Although the exact mechanism of action for the insecticidal property of CPBFs is as yet unknown, phytochemists and medicinal chemists have obtained several congeners to evaluate their structure-activity relationships. For instance, the free hydroxy groups at both C-1 (*R*) and C-8b were essential for mediation of the insecticidal activity of rocaglamide (**1**) (▶ **Fig. 1**), when evaluated against the pest insect *S. littoralis* [95, 96]. Moreover, favorable modifications by chemical synthesis at C-2 or C-4′ for insecticidal activity are a hydroxamide and halogen (Br or Cl) functional group, respectively. Such derivatives were well-tolerated compared to rocaglamide (**1**). They exhibited LC_{50} values ranging from 3 to 12.5 mg/L against an array of pests and beetles inclusive of *Diabrotia balteata, Heliothis vierescens, Plutella xylostella*, and *S. littoralis* [97].

Treatment of cerebral malaria, caused by infection of *Plasmodium falciparum*, has proven to be a continued challenge. Despite the widely available synthetic analogs of the plant-derived sesquiterpene lactone, artemisinin, resistance to this compound class by the causative organisms has been observed [98, 99]. Langlias and associates recently suggested the possibility of using rocaglates as potential therapeutic intervention agents for malaria. They showed the synthetic rocaglate derivative (−)-CR-31-B (**26**) to exhibit antiplasmodial activity. According to their report, owing to its potential to inhibit eIF4A, (−)-CR-31-B (**26**) not only inhibited *Plasmodium* protein synthesis at low nanomolar levels (ranging between 0.9 and 2.8 nM) *in vitro* but also showed similar effects in a dose-dependent manner in mice infected with *Plasmodium berghei* [100]. Additionally, their study highlighted the anti-inflammatory activity of (−)-CR-31-B (**26**) by suppressing the production of IRF1, a pro-inflammatory transcription factor essential for the expression of critical inflammatory factors, like GBP2 and CXCL10 [100]. Complemented by a previous study that established good pharmacokinetic properties of this synthetic rocaglate [101], Langlais et al. proposed that (−)-CR-31-B (**26**) warrants further evaluation as a potential therapy for cerebral malaria, either as a single agent or in combination with artemisinin [100].

In a recent publication, Wang et al. evaluated the potential neuroprotective effects of a 95% ethanol extract of *A. odorata* leaves [102]. This plant extract exhibited a neuroprotective effect in a middle cerebral artery occlusion (MCAO) rat model. Treatment with this extract reduced the number of apoptotic cells and increased mitochondrial membrane potential in oxygen-glucose deprivation/reperfusion (OGC/R)-induced PC12 cells. It was hypothesized that the extract exerts a neuroprotective effect against cerebral ischemia by suppressing the p53/Puma mediated signaling pathway [102]. While these biological results look interesting, the investigation was not supported by any detailed phytochemical work, but only with a preliminary chromatographic profiling method, indicating the presence of triterpenoids in the extract [102]. The actual active constituents may include rocaglate derivatives, as reported from *A. odorata* [16, 46].

Downloaded by: Ohio State University. Copyrighted material.

Conclusions

Unlike many other structural classes of specialized metabolites from higher plants that have long been known, the novel rocaglate (flavagline) derivative (−)-rocaglamide (**1**) was first reported in 1982 from the leaves of *A. elliptifolia* [12]. At the time of its isolation, the structure and absolute configuration of this CPBF were determined by single-crystal X-ray crystallographic analysis, and it was shown to exhibit antileukemic activity (T/C value of 156 %) in a P388 murine leukemia *in vivo* assay at a nontoxic dose (1.0 mg/kg) [12]. Likewise, the antileukemic activity of the dioxanyl-ring containing CPBF (−)-silvestrol (**8**) was reported in 2004 from *A. foveolata*, and its full structure and stereochemistry were also determined by X-ray diffraction analysis [21]. Dioxanyl ring-containing CPBFs are rare constituents in *Aglaia* species, and, at present, they have been found in only 3 of the approximately 120 members of this genus [8, 21, 47, 51, 53]. Subsequently, and particularly over the last decade, the key cellular mechanism inhibition of eIF4A [29, 30] and PHB1/2 [32] has made rocaglamide (**1**) and silvestrol (**8**) of great interest to the biomedical community as standard protein translation inhibitors. Both these compounds are now available commercially from fine-chemical scientific suppliers for research use. As a potential means of increasing their supply, rocaglamide [103–106] and silvestrol [107, 108] have been subjected to total chemical synthesis. In addition, methods have been developed for synthesizing rocaglate analogs to establish further structure-activity relationship information [109, 110]. However, it should be reiterated that while silvestrol has proven to be a useful pharmacological tool, it has suboptimal drug-like properties and can cause pulmonary toxicity [68]. Therefore, this dioxanyl ring-containing natural product must be modified structurally for further development as a bioactive molecule drug lead.

Several review articles have appeared recently by various groups on the pharmacological activities of rocaglates and have dealt, in particular, with their antineoplastic [14, 25, 111], antiviral [111, 112], and miscellaneous biological effects [14]. In terms of drug development, work on a synthetic derivative of rocaglamide (**1**), eFT-226 (**27**, Zotatifin), which was elucidated to have good pharmacokinetic properties and potent antitumor effects, like rocaglamide (**1**) and DDR (**3**), seems promising. The potent eIF4A inhibitor, Zotatifin, is the first compound with this mechanism of action to have entered into a clinical trial as a potential treatment for patients with advanced solid-tumor malignancies [113].

Contributors' Statement

Conception: A. D. Kinghorn, G. Agarwal, D. D. Soejarto, L. S. Chang; design of work: A. D. Kinghorn, G. Agarwal, D. D. Soejarto, L. S. Chang; drafting the manuscript: A. D. Kinghorn, G. Agarwal, L. S. Chang, D. D. Soejarto; critical revision of the manuscript: L. S. Chang, A. D. Kinghorn, G. Agarwal, D. D. Soejarto.

Acknowledgements

The plant collection and laboratory studies by our group mentioned in this article were supported by grants U19 CA52956 and P01 CA125066 from NCI to ADK, W81XWH-18-1-0547 from the U. S. Department of Defense to LSC, and P30CA16058 to The OSU Comprehensive Cancer Center. We are very grateful to many faculty colleagues, research staff, postdoctoral fellows, and graduate students who have contributed to this work.

Conflict of Interest

The authors declare that they have no conflict of interest.

References

[1] Shiengthong D, Verasarn A, NaNonggai-Suwanrath P. Constituents of Thai medicinal plants – I. Aglaiol. Tetrahedron 1965; 21: 914–924

[2] Ebada SS, Lajkiewicz N, Porco JA Jr., Li-Weber M, Proksch P. Chemistry and Biology of Rocaglamides (= Flavaglines) and Related Derivatives from *Aglaia* Species (Meliaceae). In: Kinghorn AD, Falk H, Kobayashi J, eds. Progress in the Chemistry of Organic Natural Products. Vienna: Springer; 2011: 1–58

[3] Zhang L, Wang LH, Yang YF, Yang SM, Zhang JH, Tan CH. Aglaianine, a new bisamide from *Aglaia abbreviata*. Nat Prod Res 2011; 25: 1676–1679

[4] Sianturi J, Purnamasari M, Darwati, Harneti D, Mayanti T, Supratman U, Awang K, Hayashi H. New bisamide compounds from the bark of *Aglaia eximia* (Meliaceae). Phytochem Lett 2015; 13: 297–301

[5] Zhang H, Song ZJ, Chen WQ, Wu XZ, Xu HH. Chemical constituents from *Aglaia odorata* Lour. Biochem Syst Ecol 2012; 41: 35–40

[6] Peng L, Fu WX, Zeng CX, Zhou L, Bao MF, Cai XH. Two new lignans from twigs of *Aglaia odorata*. J Asian Nat Prod Res 2016; 18: 147–152

[7] Joycharat N, Plodpai P, Panthong K, Yingyongnarongkul BE, Voravuthikunchai SP. Terpenoid constituents and antifungal activity of *Aglaia forbesii* seed against phytopathogens. Can J Chem 2010; 88: 937–944

[8] Pan L, Kardono LBS, Riswan S, Chai HB, Carcache de Blanco EJ, Pannell CM, Soejarto DD, McCloud TG, Newman DJ, Kinghorn AD. Isolation and characterization of minor analogues of silvestrol and other constituents from a large-scale re-collection of *Aglaia foveolata*. J Nat Prod 2010; 73: 1873–1878

[9] Harneti D, Supriadin A, Maharani R, Nurlelasari, Mayanti T, Hidayat AT, Anwar R, Supratman U, Awang K, Shiono Y. Triterpenoids from the bark of *Aglaia glabrata* and their *in vitro* effects on P-388 murine leukemia cells. Orient J Chem 2019; 35: 134–139

[10] Nugroho BW, Edrada RA, Wray V, Witte L, Bringmann G, Gehling M, Proksch P. An insecticidal rocaglamide derivative and related compounds from *Aglaia odorata* (Meliaceae). Phytochemistry 1999; 51: 367–376

[11] Bacher M, Hofer O, Brader G, Vajrodaya S, Greger H. Thapsakins: possible biogenetic intermediates towards insecticidal cyclopenta[*b*]benzofurans from *Aglaia edulis*. Phytochemistry 1999; 52: 253–263

[12] King ML, Chiang CC, Ling HC, Fujita E, Ochiai M, McPhail AT. X-Ray crystal structure of rocaglamide, a novel antileukemic 1*H*-cyclopenta[*b*]benzofuran from *Aglaia elliptifolia*. J Chem Soc, Chem Commun 1982; 1982: 1150–1151

[13] Pan L, Muñoz-Acuña U, Li J, Jena N, Ninh TN, Pannell CM, Chai HB, Fuchs JR, Carcache de Blanco EJ, Soejarto DD, Kinghorn AD. Bioactive flavaglines and other constituents isolated from *Aglaia perviridis*. J Nat Prod 2013; 76: 394–404

Downloaded by: Ohio State University. Copyrighted material.

[14] Harneti D, Supratman U. Phytochemistry and biological activities of *Aglaia* species. Phytochemistry 2021; 181: 112540

[15] Dumontet V, Thoison O, Omobuwajo OR, Martin MT, Perromat G, Chiaroni A, Riche C, Pais M, Sevenet T. New nitrogenous and aromatic derivatives from *Aglaia argentea* and *A. forbesii*. Tetrahedron 1996; 52: 6931–6942

[16] Ishibashi F, Satasook C, Ismant MB, Towers GHN. Insecticidal 1*H*-cyclopentatetrahydro[*b*]benzofurans from *Aglaia odorata*. Phytochemistry 1993; 32: 307–310

[17] Su BN, Chai HB, Mi Q, Riswan S, Kardono LBS, Afriastini JJ, Santarsiero BD, Mesecar AD, Farnsworth NR, Cordell GA, Swanson SM, Kinghorn AD. Activity-guided isolation of cytotoxic constituents from the bark of *Aglaia crassinervia* collected in Indonesia. Bioorg Med Chem 2006; 14: 960–972

[18] Kokpol U, Venaskulchai B, Simpson J, Weavers RT. Isolation and X-ray structure determination of a novel pyrimidinone from *Aglaia odorata*. J Chem Soc, Chem Commun 1994; 1994: 773–774

[19] Bringmann G, Mühlbacher J, Messer K, Dreyer M, Ebel R, Nugroho W, Wray V, Proksch P. Cyclorocaglamide, the first bridged cyclopentatetrahydrofuran, and a related "open chain" rocaglamide derivative from *Aglaia oligophylla*. J Nat Prod 2003; 66: 80–85

[20] Dreyer M, Nugroho BW, Bohnenstengel FI, Ebel R, Victor V, Witte L, Bringmann G, Mühlbacher J, Herold M, Hung P, Kiet LC, Proksch P. New insecticidal rocaglamide derivatives and related compounds from *Aglaia oligophylla*. J Nat Prod 2001; 64: 415–420

[21] Hwang BY, Su BN, Chai HB, Mi Q, Kardono LBS, Afriastini JJ, Riswan S, Santarsiero BD, Mesecar AD, Wild R, Fairchild CR, Vite GD, Rose WC, Farnsworth NR, Cordell GA, Pezzuto JM, Swanson SM, Kinghorn AD. Silvestrol and episilvestrol, potential anticancer rocaglate derivatives from *Aglaia silvestris*. J Org Chem 2004; 69: 3350–3358; ibid. 2004; 69: 6156

[22] Kim S, Salim AA, Swanson SM, Kinghorn AD. Potential of cyclopenta[*b*]benzofurans from *Aglaia* species in cancer chemotherapy. Anticancer Agents Med Chem 2006; 6: 319–345

[23] Pan L, Woodard JL, Lucas DM, Fuchs JR, Kinghorn AD. Rocaglamide, silvestrol and structurally related bioactive compounds from *Aglaia* species. Nat Prod Rep 2014; 31: 924–939

[24] Ribeiro N, Thuaud F, Bernard Y, Gaiddon C, Cresteil T, Hild A, Hirsch EC, Michel PP, Nebigil CG, Désaubry L. Flavaglines as potent anticancer and cytoprotective agents. J Med Chem 2012; 55: 10064–10073

[25] Ribeiro N, Thuaud F, Nebigil C, Désaubry L. Recent advances in the biology and chemistry of the flavaglines. Bioorg Med Chem 2012; 20: 1857–1864

[26] Chambers JM, Lindqvist LM, Webb A, Huang DCS, Savage GP, Rizzacasa MA. Synthesis of biotinylated episilvestrol: highly selective targeting of the translation factor eIF4AI/II. Org Lett 2013; 15: 1406–1409

[27] Basmadjian C, Zhao Q, de Gramont A, Serova M, Falvre S, Raymond E, Vagner S, Robert C, Nebigil CG, Désaubry L. Bioactive Flavaglines: Synthesis and Pharmacology. In: Brahmachari G, ed. Bioactive Natural Products. Weinheim: Wiley-VCH; 2015: 171–199

[28] Zhao Q, Abou-Hamdan H, Désaubry L. Recent advances in the synthesis of flavaglines, a family of potent bioactive natural compounds originating from traditional Chinese medicine. Eur J Org Chem 2016; 2016: 5908–5916

[29] Bordeleau ME, Robert F, Gerard B, Lindqvist L, Chen SM, Wendel HG, Brem B, Greger H, Lowe SW, Porco JA Jr., Pelletier J. Therapeutic suppression of translation initiation modulates chemosensitivity in a mouse lymphoma model. J Clin Invest 2008; 118: 2651–2660

[30] Cencic R, Carrier M, Galicia-Vázquez G, Bordeleau ME, Sukarieh R, Bourdeau A, Brem B, Teodoro JG, Greger H, Tremblay ML, Porco JA Jr., Pelletier J. Antitumor activity and mechanism of action of the cyclopenta[*b*]benzofuran, silvestrol. PLoS One 2009; 4: e5223

[31] Cencic R, Carrier M, Trnkus A, Porco JA Jr., Minden M, Pelletier J. Synergistic effect of inhibiting translation initiation in combination with cytotoxic agents in acute myelogenous leukemia cells. Leuk Res 2010; 34: 535–541

[32] Polier G, Neumann J, Thuaud F, Ribeiro N, Gelhaus C, Schmidt H, Giaisi M, Kohler R, Muller WW, Proksch P, Leippe M, Janssen O, Désaubry L, Krammer PH, Li-Weber M. The natural anticancer compounds rocaglamides inhibit the Raf-MEK-ERK pathway by targeting prohibitin 1 and 2. Chem Biol 2012; 19: 1093–1104

[33] Zhu JY, Lavrik IN, Mahlknecht U, Giaisi M, Proksch P, Krammer PH, Li-Weber M. The traditional Chinese herbal compound rocaglamide preferentially induces apoptosis in leukemia cells by modulation of mitogen-activated protein kinase activities. Int J Cancer 2007; 121: 1839–1846

[34] Alachkar H, Santhanam R, Harb JG, Lucas DM, Oaks JJ, Hickey CJ, Pan L, Kinghorn AD, Caligiuri MA, Perrotti D, Byrd JC, Garzon R, Grever MR, Marcucci G. Silvestrol exhibits significant *in vivo* and *in vitro* antileukemic activities and inhibits FLT3 and *miR-155* expressions in acute myeloid leukemia. J Hematol Oncol 2013; 6: 21

[35] Bueno Pérez L, Still PC, Naman CB, Ren Y, Pan L, Chai HB, Carcache de Blanco EJ, Ninh TN, Van Thanh B, Swanson SM, Soejarto DD, Kinghorn AD. Investigation of Vietnamese plants for potential anticancer agents. Phytochem Rev 2014; 13: 727–739

[36] Henkin JM, Sydara K, Xayvue M, Souliya O, Kinghorn AD, Burdette JE, Chen WL, Elkington BG, Soejarto DD. Revisiting the linkage between ethnomedical use and development of new medicines: A novel plant collection strategy towards the discovery of anticancer agents. J Med Plant Res 2017; 11: 621–634

[37] Henkin JM, Ren Y, Soejarto DD, Kinghorn AD. The Search for Anticancer Agents from Tropical Plants. In: Kinghorn AD, Falk H, Gibbons S, Kobayashi J, Asakawa Y, Liu J–K eds. Progress in the Chemistry of Organic Natural Products. Cham, Switzerland: Springer International 2018; 107: 1–94

[38] Pannell CM. A Taxonomic Monograph of the Genus *Aglaia* Lour. (Meliaceae). Richmond, Surrey, UK: HMSO Kew; 1992

[39] Brahms Online. Department of Plant Sciences, University of Oxford. Copyright © 1985–2020. Accessed October 6, 2020 at: https://herbaria.plants.ox.ac.uk/bol/aglaia

[40] Müellner AN, Samuel R, Chase MW, Pannell CM, Greger H. *Aglaia* (Meliaceae): An evaluation of taxonomic concepts based on DNA data and secondary metabolites. Am J Bot 2005; 92: 534–543

[41] IUCN. The IUCN Red List of Threatened Species. Version 2020. Accessed November 27, 2020 at: https://www.iucnredlist.org/

[42] Widodo SH. *Aglaia* (PROSEA Medicinal Plants). Plant Resources of Southeast Asia. Accessed October 8, 2020 at: https://uses.plantnet-project.org/en/Aglaia_(PROSEA_Medicinal_plants)#:~:text=Several%20Aglaia%20species%20are%20used,diseases%2C%20and%20bark%20against%20tumours

[43] Priya R, Sowmiya P, Muthuraman MS. An overview on the biological perspectives of *Aglaia* species. Asian J Pharm Clin Res 2018; 11: 42

[44] Stuart GU Jr. *Aglaia odorata*. Philippine Medicinal Plants. Accessed October 6, 2020 at: http://www.stuartxchange.com/Sinamomong-sungsong.html

[45] Hong Kong Baptist University. *Aglaia odorata*. Medicinal Plant Images Database. School of Chinese Medicine, Hong Kong Baptist Church. Accessed October 6, 2020 at: https://web.archive.org/web/20150510023028/http://libproject.hkbu.edu.hk/was40/detail?channelid=1288&lang=en&searchword=herb_id%3DD00922

[46] An FL, Wang JS, Wang H, Wang XB, Yang MH, Guo QL, Dai Y, Luo J, Kong LY. Cytotoxic flavonol-diamide [3 + 2] adducts from the leaves of *Aglaia odorata*. Tetrahedron 2015; 71: 2450–2457

[47] An FL, Wang XB, Wang H, Li ZR, Yang MH, Luo J, Kong LY. Cytotoxic rocaglate derivatives from leaves of *Aglaia perviridis*. Sci Rep 2016; 6: 20045

Downloaded by: Ohio State University. Copyrighted material.

[48] An FL, Xu WJ, Yang MH, Luo J, Kong LY. Anti-inflammatory flavagline glycosides and putrescine bisamides from *Aglaia perviridis* leaves. Tetrahedron 2020; 76: 131257

[49] Duong NT, Edrada-Ebel R, Ebel R, Lin W, Duong AT, Dang XQ, Nguyen NH, Proksch P. New rocaglamide derivatives from Vietnamese *Aglaia* species. Nat Prod Commun 2014; 9: 833–834

[50] Thuaud F, Ribeiro N, Gaiddon C, Cresteil T, Désaubry L. Novel flavaglines displaying improved cytotoxicity. J Med Chem 2011; 54: 411–415

[51] Othman N, Pan L, Mejin M, Voong JC, Chai HB, Pannell CM, Kinghorn AD, Yeo TC. Cyclopenta[*b*]benzofuran and secodammarane derivatives from the stems of *Aglaia stellatopilosa*. J Nat Prod 2016; 79: 784–791

[52] Meurer-Grimes BM, Yu J, Vairo GL. Therapeutic compounds and methods. U.S. Patent 6710075 B2, 2004

[53] Agarwal G, Wilson JR, Kurina SJ, Anaya-Eugenio GD, Ninh TN, Burdette JE, Soejarto DD, Cheng X, Carcache de Blanco EJ, Rakotondraibe LH, Kinghorn AD. Structurally modified cyclopenta[*b*]benzofuran analogues isolated from *Aglaia perviridis*. J Nat Prod 2019; 82: 2870–2877

[54] Lucas DM, Edwards RB, Lozanski G, West DA, Shin JD, Vargo MA, Davis ME, Rozewski DM, Johnson AJ, Su BN, Goettl VM, Heerema NA, Lin TS, Lehman A, Zhang X, Jarjoura D, Newman DJ, Byrd JC, Kinghorn AD, Grever MR. The novel plant-derived agent silvestrol has B-cell selective activity in chronic lymphocytic leukemia and acute lymphoblastic leukemia *in vitro* and *in vivo*. Blood 2009; 113: 4656–4666

[55] Callahan KP, Minhajuddin M, Corbett C, Lagadinou ED, Rossi RM, Grose V, Balys MM, Pan L, Jacob S, Frontier A, Grever MR, Lucas DM, Kinghorn AD, Liesveld JL, Becker MW, Jordan CT. Flavaglines target primitive leukemia cells and enhance anti-leukemia drug activity. Leukemia 2014; 28: 1960–1968

[56] Pillow T, Polson AG, Zheng B. Silvestrol antibody-drug conjugates and methods of use. US Pat Pub Appl 20170348422, December 7, 2017

[57] Chari RV. Targeted delivery of chemotherapeutics: tumor-activated prodrug therapy. Adv Drug Deliv Rev 1998; 31: 89–104

[58] Rautio J, Meanwell NA, Di L, Hageman MJ. The expanding role of prodrugs in contemporary drug design and development. Nat Rev Drug Discov 2018; 17: 559–587

[59] Agarwal G, Blanco Carcache PJ, Addo EM, Kinghorn AD. Current status and contemporary approaches to the discovery of antitumor agents from higher plants. Biotechnol Adv 2020; 38: 107337

[60] Grünweller A, Hartmann RK. Silvestrol: A potential future drug for acute Ebola and other viral infections. Future Virol 2017; 11: 243–245

[61] Parsyan A, Svitkin Y, Shahbazian D, Gkogkas C, Lasko P, Merrick WC, Sonenberg N. mRNA helicases: the tacticians of translational control. Nat Rev Mol Cell Biol 2011; 12: 235–245

[62] Thuaud F, Ribeiro N, Nebigil CG, Désaubry L. Prohibitin ligands in cell death and survival: mode of action and therapeutic potential. Chem Biol 2013; 20: 316–331

[63] Liu S, Wang W, Brown LE, Qiu C, Lajkiewicz N, Zhao T, Zhou J, Porco JA Jr., Wang TT. A novel class of small molecule compounds that inhibit hepatitis C virus infection by targeting the prohibitin-CRaf pathway. EBioMedicine 2015; 2: 1600–1606

[64] Oblinger JL, Burns SS, Akhmametyeva EM, Huang J, Pan L, Ren Y, Shen R, Miles-Markley B, Moberly AC, Kinghorn AD, Welling DB, Chang LS. Components of the eIF4F complex are potential therapeutic targets for malignant peripheral nerve sheath tumors and vestibular schwannomas. Neuro Oncol 2016; 18: 1265–1277

[65] Oblinger JL, Burns SS, Huang J, Pan L, Ren Y, Shen R, Kinghorn AD, Welling DB, Chang LS. Overexpression of eIF4F components in meningiomas and suppression of meningioma cell growth by inhibiting translation initiation. Exp Neurol 2018; 299: 299–307

[66] Sadlish H, Galicia-Vazquez G, Paris CG, Aust T, Bhullar B, Chang L, Helliwell SB, Hoepfner D, Knapp B, Riedl R, Roggo S, Schuierer S, Studer C, Porco JA Jr., Pelletier J, Movva NR. Evidence for a functionally relevant rocaglamide binding site on the eIF4A-RNA complex. ACS Chem Biol 2013; 8: 1519–1527

[67] Gupta SV, Sass EJ, Davis ME, Edwards RB, Lozanski G, Heerema NA, Lehman A, Zhang X, Jarjoura D, Byrd JC, Pan L, Chan KK, Kinghorn AD, Phelps MA, Grever MR, Lucas DM. Resistance to the translation initiation inhibitor silvestrol is mediated by ABCB1/P-glycoprotein overexpression in acute lymphoblastic leukemia cells. AAPS J 2011; 13: 357–364

[68] Chang LS, Oblinger JL, Burns SS, Huang J, Anderson LW, Hollingshead MG, Shen R, Pan L, Agarwal G, Ren Y, Roberts RD, O'Keefe BR, Kinghorn AD, Collins JM. Targeting protein translation by rocaglamide and didesmethylrocaglamide to treat MPNST and other sarcomas. Mol Cancer Ther 2020; 19: 731–741

[69] Chang LS, Oblinger JL, Agarwal G, Wilson TA, Roberts R, Fuchs J, O'Keefe BR, Kinghorn AD, Collins JM. The eIF4A inhibitors didesmethylrocaglamide and rocaglamide as effective treatments for pediatric bone and soft-tissue sarcomas. Cancer Res; 2020; 80 (Sup. 16): abs. no. 1950

[70] Chu J, Galicia-Vazquez G, Cencic R, Mills JR, Katigbak A, Porco JA, Jr., Pelletier J. CRISPR-mediated drug-target validation reveals selective pharmacological inhibition of the RNA helicase, eIF4A. Cell Rep 2016; 15: 2340–2347

[71] Iwasaki S, Floor SN, Ingolia NT. Rocaglates convert DEAD-box protein eIF4A into a sequence-selective translational repressor. Nature 2016; 534: 558–561

[72] Iwasaki S, Iwasaki W, Takahashi M, Sakamoto A, Watanabe C, Shichino Y, Floor SN, Fujiwara K, Mito M, Dodo K, Sodeoka M, Imataka H, Honma T, Fukuzawa K, Ito T, Ingolia NT. The translation inhibitor rocaglamide targets a bimolecular cavity between eIF4A and polypurine RNA. Mol Cell 2019; 73: 738–748

[73] Sridharan S, Robeson M, Bastihalli-Tukaramrao D, Howard CM, Subramaniyan B, Tilley AMC, Tiwari AK, Raman D. Targeting of the eukaryotic translation initiation factor 4A against breast cancer stemness. Front Oncol 2019; 9: 1311

[74] Sainz B Jr., Barretto N, Martin DN, Hiraga N, Imamura M, Hussain S, Marsh KA, Yu X, Chayama K, Alrefai WA, Uprichard SL. Identification of the Niemann-Pick C1-like 1 cholesterol absorption receptor as a new hepatitis C virus entry factor. Nat Med 2012; 18: 281–285

[75] Chiu CF, Ho MY, Peng JM, Hung SW, Lee WH, Liang CM, Liang SM. Raf activation by Ras and promotion of cellular metastasis require phosphorylation of prohibitin in the raft domain of the plasma membrane. Oncogene 2013; 32: 777–787

[76] Zhang W, Liu S, Maiga RI, Pelletier J, Brown LE, Wang TT, Porco JA Jr. Chemical synthesis enables structural reengineering of aglaroxin C leading to inhibition bias for hepatitis C viral infection. J Am Chem Soc 2019; 141: 1312–1323

[77] Porco JA Jr., Zhang W, Wang TT, Liu S. Preparation of rocaglates for inhibiting viral infection. US Patent Pub. Appl. 20200123170; 2020

[78] Too IHK, Bonne I, Tan EL, Chu JJH, Alonso S. Prohibitin plays a critical role in Enterovirus 71 neuropathogenesis. PLoS Pathog 2018; 14: e1006778

[79] Biedenkopf N, Lange-Grünweller K, Schulte FW, Weisser A, Müller C, Becker D, Becker S, Hartmann RK, Grünweller A. The natural compound silvestrol is a potent inhibitor of Ebola virus replication. Antiviral Res 2017; 137: 76–81

[80] Slaine PD, Kleer M, Smith NK, Khaperskyy DA, McCormick C. Stress granule-inducing eukaryotic translation initiation factor 4A inhibitors block influenza A virus replication. Viruses 2017; 9: 388

[81] Todt D, Moeller N, Praditya D, Kinast V, Friesland M, Engelmann M, Verhoye L, Sayed IM, Behrendt P, Dao Thi VL, Meuleman P, Steinmann E. The natural compound silvestrol inhibits hepatitis E virus (HEV) replication *in vitro* and *in vivo*. Antiviral Res 2018; 157: 151–158

[82] Glitscher M, Himmelsbach K, Woytinek K, Johne R, Reuter A, Spiric J, Schwaben L, Grünweller A, Hildt E. Inhibition of hepatitis E virus spread by the natural compound silvestrol. Viruses 2018; 10: 301

Downloaded by: Ohio State University. Copyrighted material.

[83] Müller C, Schulte FW, Lange-Grünweller K, Obermann W, Madhugiri R, Pleschka S, Ziebuhr J, Hartmann RK, Grünweller A. Broad-spectrum antiviral activity of the eIF4A inhibitor silvestrol against corona- and picornaviruses. Antiviral Res 2018; 150: 123–129

[84] Henss L, Scholz T, Grünweller A, Schnierle BS. Silvestrol inhibits chikungunya virus replication. Viruses 2018; 10: 592

[85] Grünweller A, Hartmann RK, Lange-Grünweller K, Schulte FW, Becker S, Biedenkopf N, Ziebuhr J, Müller C, Schlitzer M. Usage of silvestrol, episilvestrol analogs for the treatment of viral infections caused by viruses with cap-dependent translation. EP 33052889 A, 2018

[86] Elgner F, Sabino C, Basic M, Ploen D, Grünweller A, Hildt E. Inhibition of zika virus replication by silvestrol. Viruses 2018; 10: 149

[87] Müller C, Obermann W, Schulte FW, Lange-Grünweller K, Oestereich L, Elgner F, Glitscher M, Hildt E, Singh K, Wendel HG, Hartmann RK, Ziebuhr J, Grünweller A. Comparison of broad-spectrum antiviral activities of the synthetic rocaglate CR-31-B (−) and the eIF4A-inhibitor silvestrol. Antiviral Res 2020; 175: 104706

[88] Chan K, Robert F, Oertlin C, Kapeller-Libermann D, Avizonis D, Gutierrez J, Handly-Santana A, Doubrovin M, Park J, Schoepfer C, Da Silva B, Yao M, Gorton F, Shi J, Thomas CJ, Brown LE, Porco JA Jr., Pollak M, Larsson O, Pelletier J, Chio IIC. eIF4A supports an oncogenic translation program in pancreatic ductal adenocarcinoma. Nat Commun 2019; 10: 5151

[89] Yurugi H, Zhuang Y, Siddiqui FA, Liang H, Rosigkeit S, Zeng Y, Abou-Hamdan H, Bockamp E, Zhou Y, Abankwa D, Zhao W, Désaubry L, Rajalingam K. A subset of flavaglines inhibits KRAS nanoclustering and activation. J Cell Sci 2020; 133: jcs.244111

[90] Chen M, Asanuma M, Takahashi M, Shichino Y, Mito M, Fujiwara K, Saito H, Floor SN, Ingolia NT, Sodeoka M, Dodo K, Ito T, Iwasaki S. Dual targeting of DDX3 and eIF4A by the translation inhibitor rocaglamide A. Cell Chem Biol 2021; 28: 1–12. doi:10.1016/j.chembiol.2020.11.008

[91] Prior IA, Lewis PD, Mattos C. A comprehensive survey of Ras mutations in cancer. Cancer Res 2012; 72: 2457–2467

[92] Castagnola P, Giaretti W. Mutant KRAS, chromosomal instability and prognosis in colorectal cancer. Biochim Biophys Acta 2005; 1756: 115–125

[93] Bol GM, Xie M, Raman V. DDX3, a potential target for cancer treatment. Mol Cancer 2015; 14: 188

[94] Chiu SF. Recent research findings on Meliaceae and other promising botanical insecticides in China. J Plant Dis Prot 1985; 92: 310–319

[95] Chaidir, Hiort J, Nugroho BW, Bohnenstengel FI, Wray V, Witte L, Hung PD, Kiet LC, Sumaryono W, Proksch P. New insecticidal rocaglamide derivatives from flowers of *Aglaia duperreana*. Phytochemistry 1999; 52: 837–842

[96] Dreyer M, Nugroho BW, Bohnenstengel FI, Ebel R, Wray V, Witte L, Brigmann G, Muhlbacher J, Herold M, Hung PD, Kiet LC, Proksch P. New insecticidal rocaglamide derivatives and related compounds from *Aglaia oligophylla*. J Nat Prod 2001; 64: 415–420

[97] Hall RG, Bruce I, Cooke NG, Diorazio LJ, Cederbaum F, Dobler MR, Irving E. Investigating the structure-activity relationship of the insecticidal natural product rocaglamide. Chimia (Aarau) 2017; 71: 845–850

[98] Miller LH, Su X. Artemisinin: discovery from the Chinese herbal garden. Cell 2011; 146: 855–858

[99] Duru V, Witkowski B, Menard D. *Plasmodium falciparum* resistance to artemisinin derivatives and piperaquine: A major challenge for malaria elimination in Cambodia. Am J Trop Med Hyg 2016; 95: 1228–1238

[100] Langlais D, Cencic R, Moradin N, Kennedy JM, Ayi K, Brown LE, Crandall I, Tarry MJ, Schmeing M, Kain KC, Porco JA Jr., Pelletier J, Gros P. Rocaglates as dual-targeting agents for experimental cerebral malaria. Proc Natl Acad Sci U S A 2018; 115: E2366–E2375

[101] Rodrigo CM, Cencic R, Roche SP, Pelletier J, Porco JA. Synthesis of rocaglamide hydroxamates and related compounds as eukaryotic translation inhibitors: synthetic and biological studies. J Med Chem 2012; 55: 558–562

[102] Wang JK, Guo Q, Zhang XW, Wang LC, Liu Q, Tu PF, Jiang Y, Zeng KW. *Aglaia odorata* Lour. extract inhibit ischemic neuronal injury potentially via suppressing p53/Puma-mediated mitochondrial apoptosis pathway. J Ethnopharmacol 2020; 248: 112336

[103] Davey AE, Schaeffer MJ, Taylor RJK. Synthesis of the novel anti-leukaemic tetrahydrocyclopenta[*b*]benzofuran, rocaglamide. J Chem Soc Chem Commun 1991; 16: 1137–1139

[104] Davey AE, Schaeffer MJ, Taylor RJK. Synthesis of the novel antileukemic tetrahydrocyclopenta[*b*]benzofuran, rocaglamide and related synthetic studies. J Chem Soc, Perkin Trans 1 1992; 20: 2657–2666

[105] Gerard B, Jones G, Porco JA. A biomimetic approach to the rocaglamides employing photogeneration of oxidopyryliums derived from 3-hydroxyflavones. J Am Chem Soc 2004; 126: 13620–13621

[106] Zhou Z, Dixon DD, Jolit A, Tius MA. The evolution of the total synthesis of rocaglamide. Chem Eur J 2016; 22: 15929–15936

[107] Gerard B, Cencic R, Pelletier J, Porco JA Jr. Enantioselective synthesis of the complex rocaglate (−)-silvestrol. Angew Chem Int Ed 2007; 46: 7831–7834

[108] El Sous M, Khoo ML, Holloway G, Owen D, Scammells PJ, Rizzacasa MA. Total synthesis of (−)-episilvestrol and (−)-silvestrol. Angew Chem Int Ed 2007; 46: 7835–7838

[109] Hawkins BC, Lindqvist LM, Nhu D, Sharp PP, Segal D, Powell AK, Campbell M, Ryan E, Chambers JM, White JM, Rizzacasa MA, Lessene G, Huang DC, Burns CJ. Simplified silvestrol analogues with potent cytotoxic activity. ChemMedChem 2014; 9: 1556–1566

[110] Arai MA, Kofuji Y, Tanaka Y, Yanase N, Yamaku K, Fuentes RG, Karmakar UK, Ishibashi M. Synthesis of rocaglamide derivatives and evaluation of their Wnt signal inhibitory activities. Org Biomol Chem 2016; 14: 3061–3068

[111] Schulz G, Victoria C, Kirschning A, Steinmann E. Rocaglamide and silvestrol: a long story from anti-tumor to anti-coronavirus compounds. Nat Prod Rep 2021; 38: 18–23

[112] Nebigil CG, Moog C, Vagner S, Benkirane-Jessel N, Smith DR, Désaubry L. Flavaglines as natural products targeting eIF4A and prohibitins: From traditional Chinese medicine to antiviral activity against coronaviruses. Eur J Med Chem 2020; 203: 112653

[113] Ernst JT, Thompson PA, Nilewski C, Sprengeler PA, Sperry S, Packard G, Michels T, Xiang A, Tran C, Wegerski CJ, Eam B, Young NP, Fish S, Chen J, Howard H, Staunton J, Molter J, Clarine J, Nevarez A, Chiang GG, Appleman JR, Webster KR, Reich SH. Design of development candidate eFT226, a first in class inhibitor of eukaryotic initiation factor 4A RNA helicase. J Med Chem 2020; 63: 5879–5955

Downloaded by: Ohio State University. Copyrighted material.

frontiers in Oncology

REVIEW
published: 17 September 2021
doi: 10.3389/fonc.2021.698192

Neurofibromatosis: Molecular Pathogenesis and Natural Compounds as Potential Treatments

Anusha Amaravathi[1,2†], *Janet L. Oblinger*[1†], *D. Bradley Welling*[3], *A. Douglas Kinghorn*[4] *and Long-Sheng Chang*[1,5,6*]

[1] Center for Childhood Cancer and Blood Diseases, Abigail Wexner Research Institute at Nationwide Children's Hospital, Columbus, OH, United States, [2] Department of Medicine, University of Rochester School of Medicine and Dentistry, Rochester, NY, United States, [3] Department of Otolaryngology Head & Neck Surgery, Harvard Medical School, Massachusetts Eye and Ear, and Massachusetts General Hospital, Boston, MA, United States, [4] Division of Medicinal Chemistry and Pharmacognosy, The Ohio State University College of Pharmacy, Columbus, OH, United States, [5] Department of Pediatrics, The Ohio State University College of Medicine, Columbus, OH, United States, [6] Department of Otolaryngology-Head & Neck Surgery, The Ohio State University College of Medicine, Columbus, OH, United States

OPEN ACCESS

Edited by:
Fabrizio Martelli, National Institute of Health (ISS), Italy

Reviewed by:
Suresh Kumar Kalangi, Amity University Gurgaon, India
Christine Pratilas, Johns Hopkins University, United States

***Correspondence:**
Long-Sheng Chang
Long-Sheng.Chang@nationwidechildrens.org

[†]*These authors have contributed equally to this work*

Specialty section:
This article was submitted to Cancer Molecular Targets and Therapeutics, a section of the journal Frontiers in Oncology

Received: *20 April 2021*
Accepted: *01 September 2021*
Published: *17 September 2021*

Citation:
Amaravathi A, Oblinger JL, Welling DB, Kinghorn AD and Chang L-S (2021) Neurofibromatosis: Molecular Pathogenesis and Natural Compounds as Potential Treatments. Front. Oncol. 11:698192. doi: 10.3389/fonc.2021.698192

The neurofibromatosis syndromes, including NF1, NF2, and schwannomatosis, are tumor suppressor syndromes characterized by multiple nervous system tumors, particularly Schwann cell neoplasms. NF-related tumors are mainly treated by surgery, and some of them have been treated by but are refractory to conventional chemotherapy. Recent advances in molecular genetics and genomics alongside the development of multiple animal models have provided a better understanding of NF tumor biology and facilitated target identification and therapeutic evaluation. Many targeted therapies have been evaluated in preclinical models and patients with limited success. One major advance is the FDA approval of the MEK inhibitor selumetinib for the treatment of NF1-associated plexiform neurofibroma. Due to their anti-neoplastic, antioxidant, and anti-inflammatory properties, selected natural compounds could be useful as a primary therapy or as an adjuvant therapy prior to or following surgery and/or radiation for patients with tumor predisposition syndromes, as patients often take them as dietary supplements and for health enhancement purposes. Here we review the natural compounds that have been evaluated in NF models. Some have demonstrated potent anti-tumor effects and may become viable treatments in the future.

Keywords: neurofibromatosis (NF), signaling pathway, targeted therapy, natural compounds, eIF4A inhibitors, rocaglamide, didesmethylrocaglamide, protein translation

NEUROFIBROMATOSIS (NF) COMPRISES THREE DISTINCT GENETIC DISORDERS THAT CAUSE TUMORS TO GROW ALONG NERVES

As a group of slowly progressive autosomal-dominant syndromes, NF is classified into neurofibromatosis type 1 (NF1), neurofibromatosis type 2 (NF2), and schwannomatosis (1). These syndromes typically present with neural tumors, which manifest in different locations depending upon their genetic etiology. Although the tumors frequently remain benign, they incur severe patient morbidity and occasionally exhibit malignant progression.

NF1, previously known as von Recklinghausen disease, affects ~1 in 3,000 individuals (2) and is caused by mutations of the *NF1* gene on chromosome 17q11.2 (3–5). Although *NF1* mutations can be inherited, the *de novo* mutation rate is relatively high (~42%). With 100% penetrance, NF1 patients are symptomatic, but with variable expression. First presenting with hyperpigmentation-like café-au-lait macules and freckling in afflicted patients, the hallmark of NF1 is the development of neurofibromas, benign tumors composed of an admixture of dysplastic Schwann cells and stromal cells, including fibroblasts, mast cells, and perineural cells embedded in a collagenous extracellular matrix (ECM). Nearly all NF1 patients develop cutaneous neurofibromas (CNFs, or dermal neurofibroma), which arise along superficial nerves and are confined to the cutaneous tissues (6). CNFs can cause itching and pain. About half of NF1 patients also develop more serious plexiform neurofibromas (PNFs) (7). These tumors occur deeper within the body and are more extensive, surrounding multiple nerve roots and causing pain and disfigurement. PNFs can undergo malignant progression, and 8-13% of PNFs in NF1 patients develop into highly-aggressive malignant peripheral nerve sheath tumors (MPNSTs) (8).

A fraction (15-20%) of NF1 patients develop optic pathway gliomas (OPGs, astrocytomas of the optic tract) (9). Patients with OPGs may present with visual disturbances and progressive vision loss. NF1 patients are also predisposed to other types of tumors, including gliomas, gastrointestinal stromal tumors, juvenile myelomonocytic leukemia, and glomus tumors (10). Although most NF1-related gliomas are classified as benign pilocytic astrocytomas, adult NF1 patients are at ~50-fold increased risk of developing malignant glioblastomas.

For current NF1 treatment, surgical excision of CNFs can be performed when symptomatic (6). Surgical removal of PNFs is more challenging because they are more diffuse and involve multiple nerve roots. A recent exciting development is the FDA approval of the MEK inhibitor selumetinib (Koselugo™) for the treatment of children with symptomatic, inoperable PNF based on the trial (ClinicalTrials.gov Identifier: NCT01362803) which demonstrated a 72% response rate in tumor volume shrinkage by ≥20% in NF1 children with PNFs (11). However, this is not curative as no subjects had complete tumor disappearance and tumors regrew particularly after dose reduction or cessation due to toxic effects, including diarrhea, weight gain, paronychia, skin ulceration, and elevated creatinine level. Identification of other targeted agents that synergize with selumetinib in eliminating PNFs should be sought. Several other MEK inhibitors, such as trametinib (Mekinist®; ClinicalTrials.gov Identifiers: NCT02124772 and NCT03741101) and cobimetinib (NCT02639546), are also being evaluated in children and adults with PNFs. Mirdametinib was recently reported to shrink the sizes of PNFs in adults and reduce tumor-associated pain (NCT02096471) (12), and a larger trial of this drug in children and adults with NF1 is currently recruiting (NCT03962543). Additionally, a topical gel formulation of the MEK inhibitor NFX-179 is being tested in NF1 patients with CNFs (NCT04435665).

Children with OPGs are routinely monitored for clinical progression by neuroimaging and visual acuity tests (13). Slow-growing gliomas causing minimal symptoms are usually not treated, but if the disease progresses, chemotherapy and occasionally, surgery is used to stabilize and reduce tumor burden. Radiation is contraindicated in NF1 patients with benign tumors due to the heightened risk of secondary malignancies. In a phase 2 clinical trial of selumetinib for pediatric low-grade glioma, sustained responses were seen in ~40% of NF1 patients (14), leading to a phase 3 trial comparing selumetinib to chemotherapy (ClinicalTrials.gov Identifier: NCT03871257). Due to highly aggressive behavior, MPNSTs are excised with wide margins (8). Radiation may be used following resection of large (≥5cm) tumors, and chemotherapy can be applied in a primary or adjuvant setting to treat unresectable or metastatic tumors. Despite these efforts, the local recurrence rate remains high (~32-65%), suggesting an urgent need for additional effective treatments (8, 15).

NF2 has an incidence of ~1 in 30,000 and has nearly complete penetrance (16). It is caused by mutations in the *NF2* gene on chromosome 22q12.2 (17, 18). The hallmark of NF2 is bilateral vestibular schwannomas (*VS*). As the most common benign tumors of the cerebellopontine angle, 95% of *VS* are unilateral and occur sporadically. Occasionally, unilateral tumors are found in NF2 patients, especially when they are mosaic for *NF2* loss. Like NF2-related *VS*, sporadic unilateral *VS* harbor *NF2* mutations (19). Compared to sporadic *VS*, NF2-associated tumors display more aggressive behavior, with a propensity towards multifocal, rapid growth. Due to their intracranial location and proximity to cranial nerves, *VS* present with serious comorbidities, including hearing loss, tinnitus, balance dysfunction, facial weakness, and brainstem compression. NF2 is also associated with an increased incidence of cutaneous schwannomas.

Patients with NF2 also develop meningiomas and less commonly, spinal schwannomas, ependymomas, and astrocytomas (1, 16). Meningiomas are the most common brain tumors, and ~80% are benign (WHO grade I), whereas the remaining are atypical (grade II) and anaplastic (grade III) (20). In addition to NF2-related meningiomas, *NF2* mutations are found in ~50% of sporadic meningiomas. Up to 60% of NF2 patients develop meningiomas, mostly benign and often multiple, which are associated with disease severity and increased mortality (21). These tumors cause significant morbidity, including cranial nerve palsy, seizures, and brainstem compression, which may lead to paralysis, aspiration pneumonia, and death.

The current standard-of-care for NF2-related tumors is surgery (1, 16, 19). Radiosurgery, such as stereotactic γ-knife radiation, may be used, especially for unresectable tumors. However, it must be weighed against the risk of causing malignant transformation of benign tumors and inducing second-site malignancies. Also, surgery may not be recommended if the tumor is located in critical structures or if there is high tumor burden (21). Currently, an FDA-approved medical therapy is not available for NF2 patients, although a few

targeted therapies have been evaluated (1). Bevacizumab (Avastin®), a monoclonal antibody that neutralizes vascular endothelial growth factor (VEGF), is administered off-label to patients with NF2 and progressive *VS*, with ~36-41% of the patients experiencing durable hearing improvement and reduced tumor volume (22, 23). However, intravenous administration of bevacizumab is needed, and its adverse effect profile, including hypertension and proteinuria, may preclude long-term use for some patients. Also, meningiomas are unresponsive to bevacizumab (24). Another targeted drug, the kinase inhibitor brigatinib, is currently in a phase 2 clinical trial for NF2-related tumors (ClinicalTrials.gov Identifier: NCT04374305).

Schwannomatosis manifests as multiple schwannomas on nerves throughout the body but without involvement of vestibular nerves (1, 25). The true incidence of schwannomatosis is unknown but thought to be similar to NF2. Schwannomatosis usually occurs sporadically, although familial or mosaic cases occasionally occur. The most common familial mutations occur in either the *SNF5*/*SMARCB1*/*INI1* (Switch/Sucrose Non-Fermentable chromatin remodeling complex subunit-5/SWI/SNF-related, Matrix-associated, Actin-dependent Regulator of Chromatin, subfamily-B, member-1/INtegrase Interactor 1) gene on chromosome 22q11.23 or the *LZTR1* (Leucine Zipper-like Transcriptional Regulator 1) gene on chromosome 22q11.21; both are located near the *NF2* locus (26, 27). Interestingly, schwannomatosis-related schwannomas also exhibit *NF2* inactivation. It is currently thought that familial schwannomatosis is inherited through a "three-event, four-hit" process where inactivating mutations occur in the *NF2* gene located on the same chromosome as the germline-mutated *LZTR1* or *SMARCB1* allele. Loss of the remaining normal copy of chromosome 22q results in biallelic loss-of-heterozygosity (1, 16). However, some patients with schwannomatosis do not have *LZTR1* or *SNF5/SMARCB1/INI1* mutations, suggesting the presence of another tumor suppressor gene on chromosome 22q in schwannomatosis development.

Patients with schwannomatosis are often diagnosed at age over 30 and frequently present with chronic debilitating pain. As an FDA-approved drug is also not available, surgery is considered for symptomatic patients. As pain is the major symptom experienced by patients with schwannomatosis, the anti-nerve growth factor (NGF) neutralizing monoclonal antibody tanezumab is being tested in a phase 2 trial for pain alleviation (ClinicalTrials.gov Identifier: NCT04163419). Schwannomatosis is also associated with an increased risk of meningioma (1, 16). Unlike NF2, schwannomatosis patients with germline loss of *SMARCB1* have a higher risk of developing MPNSTs.

SIGNALING PATHWAYS AFFECTED IN NF-ASSOCIATED TUMORS

The *NF1* gene encodes neurofibromin, a Ras-GAP (GTPase-activating protein) which stimulates the intrinsic GTPase activity of Ras, converting it from the active GTP-bound to inactive GDP-bound state (9, 28). Therefore, *NF1*-deficient cells consistently exhibit excessive levels of Ras-GTP and activation of its downstream signaling, including the Raf/MEK/ERK mitogen-activated protein kinase (MAPK) and phosphoinositide-3-kinase (PI3K)/AKT/mammalian target of rapamycin (mTOR) pathways (**Figure 1**). Activated ERKs phosphorylate several effectors important for cell proliferation, including components of the protein translation apparatus, cell-cycle proteins, transcription factors, other kinases, and phosphatases. Activated AKT signals multiple downstream targets, promoting cell growth, survival, and motility (29). Through phosphorylation of mTOR, AKT also promotes protein translation. The mTOR protein functions as a component in two multi-protein complexes, mTORC1 and mTORC2, with overlapping protein compositions but distinct cellular functions (30). By integrating various extracellular and intracellular signals, including growth factor receptor signaling and the levels of ATP, oxygen, and nutrients, mTORC1 regulates ribosome biogenesis and protein translation. The mTORC2 complex is insensitive to nutrient levels but is responsive to growth factor-mediated activation of PI3K. Paradoxically, mTORC1 negatively regulates the activity of mTORC2 *via* direct inhibition or through S6-kinase. Acute inhibition of mTORC1 by rapamycin and rapalogs can cause feedback activation of mTORC2, which then phosphorylates AKT on serine-473, leading to restoration of PI3K/AKT signaling.

Neurofibromas express several RTK ligands, including neuregulin/heregulin, insulin-like growth factor-1 (IGF-1), and hepatocyte growth factor (HGF) (31). NF1-related PNFs can progress to atypical neurofibromatous neoplasms of uncertain biological potential (ANNUBP), which are hypothesized to be precursor lesions of MPNST. In addition to *NF1* loss, ANNUBP often harbor deletions of *CDKN2A/B* (Cyclin-Dependent Kinase Inhibitor 2A/B). Additionally, MPNSTs frequently acquire mutations in *SUZ12* or *EED*, subunits of the polycomb repressive complex 2 (PRC2) for chromatin remodeling. Loss of PRC2 enhances Ras-driven gene transcription (32). Also, MPNSTs often overexpress several RTKs, including epidermal growth factor receptor (EGFR), HGF receptor (HGFR or MET), platelet-derived growth factor receptor (PDGFR), and insulin-like growth factor-1 receptor (IGF-1R), potentially resulting in autocrine signaling. These aberrantly-activated RTKs can initiate Ras-independent survival signals through mediators, such as the STAT (signal transducers and activators of transcription) transcription factors (33).

The *NF2* gene encodes merlin for moesin, ezrin, and radixin-like protein (17, 18), which shares similarity to the protein 4.1, ezrin, radixin, and moesin (FERM) family of membrane-associated proteins that link cell-surface receptors to the actin cytoskeleton (34). Loss of merlin results in defective cell-cell adhesion *via* destabilizing adherens junctions, which correlates with abnormal activation of focal adhesion kinase (FAK), a downstream target of ECM-binding integrins and MET (35). Merlin negatively regulates ligand-induced internalization and recycling of multiple RTKs, such as EGFR and PDGFR (34) (**Figure 1A**). Cells lacking merlin also show elevated levels of several other RTKs, including IGF-1R, MET, and the EGFR

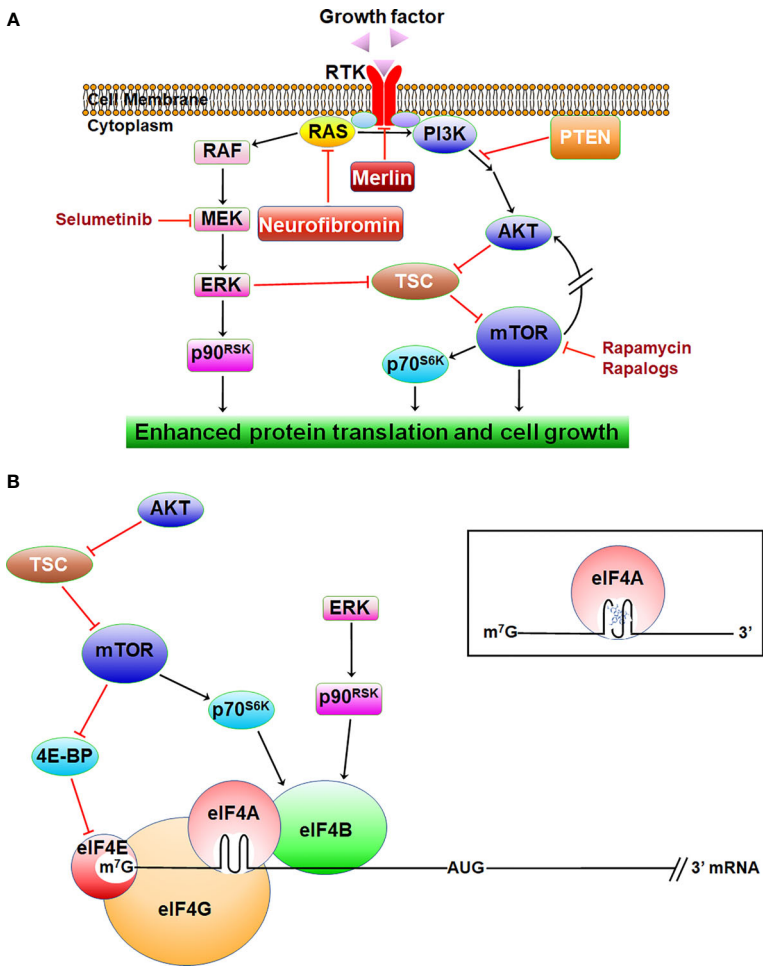

FIGURE 1 | The signaling pathways inhibited by neurofibromin and merlin. **(A)** NF-related tumors exhibit activated Ras/RAF/MEK/ERK and PI3K/AKT/mTOR, leading to enhanced protein translation and growth. **(B)** Activated ERK and AKT/mTOR enhance translation *via* eIF4B, which stimulates eIF4A activity. AKT/mTOR also promotes translation *via* eIF4E. Inset: rocaglamide locks eIF4A onto the structured 5'-UTR of mRNA.

family members ErbB2 and ErbB3 (36, 37). These RTKs activate ERKs and AKT/mTOR, promoting translation and cell growth. Through binding to angiomotin, merlin inhibits p21-activated kinases (PAKs), and PAKs reciprocally phosphorylate and inactivate merlin (38–40). Merlin-deficient cells display deregulated PAK and enhanced invasiveness.

Additionally, merlin suppresses the Hippo/large tumor suppressor kinase 1/2 (LATS1/2)/Yes-associated protein (YAP) pathway (41, 42). Merlin inhibits proteasomal degradation of LATS1/2 by interacting with the E3 ubiquitin ligase $CRL4^{DCAF1}$ in the nucleus (43). Therefore, merlin deficiency is associated with enhanced YAP-dependent gene transcription and cell proliferation. Further, loss of merlin resulted in mTORC1 activation, leading to phosphorylation of ribosomal protein S6 and enhanced cap-dependent protein synthesis *via* inhibition of the eIF4E-binding protein (4E-BP) (44, 45). *NF2*-deficient cells also display mTORC2 activation. Inhibition of mTORC1 by rapamycin amplifies AKT activation by mTORC2 (46, 47).

The molecular mechanisms by which inactivation of the *LZTR1* or *SMARCB1/INI1* gene in addition to the *NF2* gene causes schwannomatosis are not understood. Mutations in *LZTR1* also occur in several cancer types, including ~22% glioblastomas (48). Introducing LZTR1 to *LZTR1*-mutated glioblastoma cells decreases cyclin A and polo-like kinase 1 expression, indicating the importance of LZTR1 in cell cycle progression. As a member of the BTB-kelch superfamily, LZTR1 acts as an adaptor for cullin 3 (Cul3)-containing E3 ubiquitin ligases (27) and facilitates polyubiquitination and degradation of Ras (49). Cul3-containing ubiquitin ligases promote cell differentiation, and *LZTR1*-depleted Schwann cells have gene expression signatures consistent with a demyelinated proliferative phenotype. Additionally, recent evidence indicates that LZTR1-mutant schwannomatosis schwannomas exhibit deregulated VEGF receptor, ErbB3, and ERK signaling (25). SMARCB1 is a component of the SWI/SNF chromatin remodeling complex, which affects the accessibility of genes to

transcription factors and RNA polymerases (50). Loss of *SMARCB1* function is associated with deregulated Hedgehog/GLI and WNT/β-catenin signaling. Additionally, SWI/SNF antagonizes PRC function, and SMARCB1 deficiency results in PRC placing repressive histone methylation marks on other tumor suppressor genes, such as *CDKN2A (*51).

It should be emphasized that although NF1-, NF2-, and schwannomatosis-related tumors have distinct genetic origins, they share downstream activation of several molecular targets (1, 2, 6, 16, 25, 52). Collectively, these deregulated signaling pathways due to tumor suppressor loss in NF-associated tumors provide several targets for therapeutic development.

UNIQUE CHALLENGES FOR DEVELOPING MEDICAL THERAPIES FOR NF

Neurofibromatoses are systemic, life-long diseases with diverse manifestations. Drug safety and high efficacy must be carefully considered for these patients. Due to their anatomical locations, routine biopsies of NF-associated tumors may not be possible. Determination of appropriate endpoints and identification of noninvasive biomarkers to monitor drug pharmacodynamics and predict patient response are of great importance. Owing to their benign nature, NF-associated tumors exhibit variable growth patterns. NF1-related PNFs tend to rapidly expand during childhood but develop a more indolent growth pattern in adults. NF2-associated *VS* grow slowly at one-to-two millimeters per year with occasional increases in growth rates. Therefore, reduction in tumor volume may not be an ideal endpoint, and other metrics, such as time to progression, hearing loss, and pain, should be considered for drug efficacy (53–55). NF2 and schwannomatosis are rare diseases, and patients may be difficult to recruit to clinical trials unless the drugs are effective and well tolerated. For most NF-associated tumors, medication may need to be taken for years. The dosing regimen should be as simple as possible to aid in patient compliance, with a daily oral tablet being ideal. In addition, patients being recruited to clinical trials should be asked whether they are taking any drugs or supplements as there could be toxicities when combining over-the-counter (OTC) with investigational agents.

From identification of targets deregulated in NF-related tumors using traditional and systems biology approaches (56–59), it is anticipated that additional targeted compounds will be successful. The evaluation of these targeted drugs has been the focus of several recent reviews. Below, we summarize the current research on natural compounds in NF-associated tumors (**Table 1**).

NATURAL COMPOUNDS FOR PREVENTATIVE PURPOSES AND POTENTIAL TREATMENTS OF NF

Natural compounds from terrestrial microbes, higher plants, and marine organisms have been studied as cancer chemotherapeutic agents for several decades. Over the last 40 years, ~50% of FDA-approved drugs are natural products, natural product derivatives, or synthesized compounds based on pharmacophores originally identified in natural products (119). For example, the DNA-intercalating anti-neoplastic agents anthracyclines are made by *Streptomyces* bacteria. The microtubule-disruptor Taxol® (paclitaxel) was originally isolated from the bark of Pacific yew. Due to the slow-growing nature of this plant, Taxol is manufactured semi-synthetically from a precursor or produced by plant cell culture. The topoisomerase I inhibitor camptothecin was obtained from *Camptotheca acuminata* (happy tree). Several camptothecin analogs, including topotecan (Hycamtin®) and irinotecan (Camptosar®), have been synthesized. Trabectedin (Yondelis®, ecteinascidin 743, ET-743), which interferes with transcription and related processes, was discovered from extracts of the sea squirt *Ecteinascidia turbinata* and later found to come from *Candidatus Endoecteinascidia frumentensis*, a γ-proteobacterium living in symbiosis with the sea squirt. Since natural compounds tend to have diverse structural complexity and may inhibit molecules previously thought to be untargetable, the U.S. National Cancer Institute has divisions focused on drug discovery within the natural product space aiming to identify agents that inhibit difficult targets. Also, natural compounds have served valuable roles as probes to delineate the signaling pathways important for cell growth (103).

In addition to anti-neoplastic activity, natural compounds may possess antioxidant and anti-inflammatory properties and are particularly attractive as adjunct therapies for patients with tumor predisposition syndromes, including NF. Due to limited treatment options, NF patients often take them as dietary supplements for health enhancement purposes. Although much research has been conducted to evaluate anti-tumor activities of natural products, most studies only report their *in vitro* effects. Sometimes high doses are used, which may not be achievable or even desirable *in vivo*. At high concentrations, small molecules may cause off-target effects, unwanted redox activities, and anomalous plasma membrane permeability. Some natural dietary supplements are labeled as safe with health benefits, but these claims have not been validated. Many supplements are crude extracts, containing a mixture of compounds with the active components unknown, and lot-to-lot variability could contribute to irreproducible results. Compound sourcing may affect the activity of natural products. Also, some supplements may have dangerous contaminants, such as heavy metals, or may not contain the claimed ingredients. Therefore, dietary supplements should be carefully verified for overall chemical composition and safety (120). For purified single-chemical entity natural products that may be developed into new therapies for NF, it is important that their biological activities be carefully investigated and that they be treated as tractable hits, defined as compounds with rational structure-activity relationships. Here we summarize the natural compounds (**Figure 2**) that have been evaluated in NF-related tumor cell and animal models.

Phenolic Compounds

Characterized by the presence of one or more phenol functional groups, these compounds comprise flavonoids, usually found in herbs, citrus fruits, and other plants, and non-flavonoids, also

TABLE 1 | The natural compounds evaluated in NF-related models and their mechanisms of action, preclinical data, and human evaluation.

Natural compound			Preclinical data		Human data			References
Name	**Mode(s) of action**	**Availability**	**NF cell culture models**	**NF animal models**	**Pharmacokinetics**	**Efficacy studies**	**Toxicities**	
Curcumin	• Inhibits ERK1/2, AKT, NF-κB, and STAT3 • Induces caspase cleavage and MYPT1-pp1δ (merlin phosphatase)	• Turmeric-containing food/drink products • OTC supplements	• HPV-transformed *VS* cells HEI-193 IC_{50} ~10 μM • Primary *VS* IC_{50} 20 μM • *NF2*$^{-/-}$ Ben-Men-1 IC_{50} 7 μM • *NF1*$^{-/-}$, *NF1*$^{+/-}$, and *NF1*$^{+/+}$ MPNST IC_{50} 25-100 μM	ND	• $T_{1/2}$ < 5min • Poor absorption even after ingesting ~12 g/day	• Supplementation of a Mediterranean, but not Western, diet with curcumin was associated with 30-51% reduction in the number of cNFs	• 12 g/day well-tolerated • Relative lack of adverse effects may be due to poor absorption and short half-life	(60–67)
Calebin-A	• Inhibits ERK1/2, AKT, survivin, histone acetyltransferase	• Turmeric-containing food/drink products	• *NF1*$^{-/-}$, *NF1*$^{+/-}$, and *NF1*$^{+/+}$ MPNST IC_{50} 12.5-25 μM	• Reduces the growth of *NF1*$^{-/-}$ S462TY MPNST xenografts at 100 mg/kg	ND	ND	ND	(64)
Propolis constituents (CAPE and artepillin C)	• Inhibits PAK, NF-κB, and S-phase entry	• OTC supplements, including Bio30 extract	• HPV-transformed *VS* cells HEI-193 IC_{50} ~1.5 μg/mL (Bio30), ~36 μM (CAPE) • *NF1*$^{-/-}$ S462 MPNST IC_{50} ~8 μg/mL (Bio30) • Primary *VS* and *NF2*$^{-/-}$ Ben-Men-1 IC_{50} >20 μM (CAPE)	• Bio30 reduces the growth of HEI-193 xenografts and the growth and metastasis of *NF1*$^{-/-}$ S462 MPNST xenografts at 100 mg/kg	• CAPE: T_{max} ~ 2.7h and $T_{1/2}$ ~ 18.5h	• CAPE: Phase 1 safety clinical trial in healthy patients (NCT02050334)	• Allergic skin rash to CAPE	(63, 68, 69)
Honokiol	• Inhibits ERK1/2 and AKT	• OTC supplements	• HPV-transformed *VS* cells HEI-193 IC_{50} ~26 μM	ND	ND	ND	• Inhibits UDP-glucuronyltransferases • May inhibit the clearance of other drugs	(70, 71)
trans-Resveratrol	• Inhibits insulin/IGF1 signaling • Induces autophagy	• Fruits/vegetables • OTC supplements	• Primary *VS* IC_{50} ~20 μM • *NF2*$^{-/-}$ Ben-Men-1 IC50 >30 μM • *NF2*-positive HBL-52 IC_{50} >50 μM	ND	• C_{max} ~0.6 μM (5 mg dose); ~137 μM (1 g dose) • Extensively metabolized and rapidly degraded	ND	• Well-tolerated orally • High oral doses (>1g daily), associated with GI symptoms • Potential drug interactions, including tamoxifen, docetaxel, and imatinib	(63, 72–75)
Quercetin	• Stabilization of merlin	• Fruits/vegetables • OTC supplements	• HPV-transformed *VS* cells HEI-193 IC_{50} >25 μM • *NF2*$^{-/-}$ CH157-NM malignant meningioma transfected with mutant merlin protein, ~25 μM for merlin stabilization	ND	• C_{max} ~0.43-3.03 μM	ND	• Well-tolerated when consumed in foods • Mutagenic in the Ames test	(76–81

(Continued)

TABLE 1 | Continued

Natural compound			Preclinical data		Human data			References
Name	**Mode(s) of action**	**Availability**	**NF cell culture models**	**NF animal models**	**Pharmacokinetics**	**Efficacy studies**	**Toxicities**	
Sichuan pepper extracts	• Inhibits PAK1 and cyclin D1	• Spice and flavoring agents in various foods • OTC supplements	• *NF1*$^{-/-}$ S462 and S-805 MPNST IC_{50} ≥10 μg/mL	• Reduces the growth of *NF1*-deficient MDA-MB-231 breast cancer xenografts at 110 mg/kg	ND	ND	ND	(82)
Cucurbitacins	• Inhibits AKT, ERK1/2, and cyclins • Promotes p21^{Waf1} and tubulin disruption	• Low levels in edible plants and fungi • Higher amounts in bitter squash and melons	• Primary *VS* IC_{50} 250 nM (Cucurbitacin D) • *Nf2*$^{-/-}$ mouse schwannoma IC_{50} 750 nM • *NF2*$^{-/-}$ Ben-Men-1 IC_{50} 200 nM • Primary meningioma IC_{50} 200 nM • *NF1*$^{-/-}$ ST8814 MPNST ~50 nM (cucurbitacin I)	• Cucurbitacin I reduces the growth of *NF1*$^{-/-}$ ST8814 MPNST xenografts at 1 mg/kg	ND	ND	• Severe diarrhea and vomiting, possibly requiring intensive care.	(83–86)
Celastrol	• Inhibits proteasome and NF-κB • Promotes stabilization of merlin	• OTC *T. wilfordii* supplements	• *NF2*$^{-/-}$ CH157-NM malignant meningioma transfected with mutant merlin protein, ~800 nM for merlin stabilization	ND	ND	ND	• Hepatic, nephrotic, and cardiovascular toxicity • Inhibits CYP-450 enzymes with potential drug interactions • Impedes mitochondrial respiration	(77, 87, 88)
Goyazensolide	• Inhibits AKT, cyclins, and NF-κB	• Not commercially available for consumption	• Primary *VS* IC_{50} <4 μM • *Nf2*$^{-/-}$ mouse schwannoma cells, IC_{50} 0.9 μM • *NF2*$^{-/-}$ Ben-Men-1 IC_{50} 1 μM • Primary meningioma IC_{50} <4 μM	• Therapeutic doses toxic in mice	ND	ND	ND	(86, 89)
DAW22	• Inhibits AKT, ERK1/2, and β-catenin	• Not commercially available for consumption	• *NF1*$^{-/-}$, *NF1*$^{+/-}$, and *NF1*$^{+/+}$ MPNST IC_{50} ~30-47 μM	• Modestly reduces the growth of *NF1*$^{+/+}$ STS26T MPNST xenografts at 60 mg/kg	ND	ND	ND	(90)
Sulforaphane	• Inhibits NF-κB	• Plants and vegetables, including broccoli, cabbage, Brussels sprouts • OTC supplements	• HPV-transformed *VS* cells HEI-193 IC_{50} > 10 μM • Primary *VS* IC_{50} > 20 μM • *NF2*$^{-/-}$ Ben-Men-1 IC_{50} 8 μM	• Modest reduction in *Nf2*$^{-/-}$ SC4 mouse Schwann cell tumor weight at 25 mg/kg	• C_{max} ~200 nM	ND	• Well-tolerated orally	(63, 91–94)
Cannabidiol	• Binds to CB1 and CB2 • Modulates	• Oral suspension (Epidiolex) FDA-approved for epilepsy	ND	ND	• High volume of distribution (32 L/kg)	• Case study of NF1 patient with PNF: sublingual CBD oil	• Drowsiness, dizziness • Oral route	(95–99)

(Continued)

TABLE 1 | Continued

Natural compound			Preclinical data		Human data			References
Name	**Mode(s) of action**	**Availability**	**NF cell culture models**	**NF animal models**	**Pharmacokinetics**	**Efficacy studies**	**Toxicities**	
	other ion channels and neuroreceptors	• OTC supplements, e-cigarettes, and food/drink products			• C_{max}: ~2.2 μM (IV); ~0.008-0.011 μM (PO); ~0.35 μM (smoking); ~0.03 μM (nebulizer) • Bioavailability: ~6% (PO); ~31% (smoking)	appeared to help with chronic pain and mood control	associated with more psychoactive effects	
Ivermectin	• Inhibits PAK1 and Raf1	• Tablets/capsules prescribed for parasitic infections	• HPV-transformed *VS* cells HEI-193 IC_{50} ~ 5 μM	• CNS toxicity in mice with MDR1 knockout (topical spray) and in dog breeds with compromised MDR1 function (anti-parasitic medications)	• C_{max} <100 nM	ND	• Potential drug-drug and drug-food interactions through effects on CYP3A4 and MDR1	(100–102)
Silvestrol	• eIF4A inhibitor • Inhibits prohibitins	• Not commercially available for consumption • Source plants are endangered	• Primary *VS* IC_{50} 15 nM • *Nf2*$^{-/-}$ mouse schwannoma IC_{50} 70 nM • *NF2*$^{-/-}$ Ben-Men-1 IC_{50} 10 nM • Primary meningioma 25 nM • *NF1*$^{-/-}$ and *NF1*$^{+/+}$ MPNST IC50 ≤ 70 nM	• Suppresses the growth of mouse *Nf2*$^{-/-}$ schwannoma allografts and human meningioma and *NF1*$^{-/-}$ MPNST xenografts at 1.5 mg/kg • Bioavailability (mice): IP ~100%, oral ~1.7% • Lung toxicity in dogs (IV)	ND	ND	ND	(63, 103–110)
Roc and DDR	• eIF4A inhibitor • Inhibits Prohibitins	• Not commercially available for consumption • Source plants are endangered	• Primary *VS* IC_{50} 25 nM (Roc); 8 nM (DDR) (unpublished) • *Nf2*$^{-/-}$ mouse schwannoma IC_{50} 10 nM (DDR) • *NF2*$^{-/-}$ Ben-Men-1 IC_{50} 15 nM (Roc); 5 nM (DDR) • *NF1*$^{-/-}$, *NF1*$^{+/-}$, and *NF1*$^{-/-}$ MPNST IC_{50} 12-50 nM (Roc); 5-15 nM (DDR)	• Suppresses the growth of human *NF1*$^{-/-}$ ST8814 and patient-derived MPNST xenografts (IP at 3 mg/kg and PO at 1.2 mg/kg) • C_{max} of Roc in mice ~11 μM (IV); ~4 μM (IP); ~ 0.8 μM (PO) • Bioavailability (Roc in mice): ~100% (IP), ~ 1.7% (PO) • Well-tolerated in dogs (IV)	ND	ND	ND	(104, 106, 108, 110–113)
Annonacin	• Mitochondrial complex I inhibitor	• Fruits and leaves from soursop, custard apples, paw paws, and related plants in Annonaceae • OTC supplements	ND	ND	ND	ND	• Neurotoxicitiy to dopaminergic neurons • Atypical Parkinson's disease associated with high consumption of soursop	(114–118)

ND, Not determined; CBD, cannabidiol; CAPE, caffeic acid phenethyl ester; DDR, didesmethylrocaglamide; Roc, rocaglamide; HPV, human papillomavirus; OTC, over-the-counter; IP, intraperitoneal injection; IV, intravenous injection; PO, per oral; Cmax, maximum concentration; T1/2, half life; Tmax, time to Cmax; CNS, central nervous system; GI, gastrointestinal.

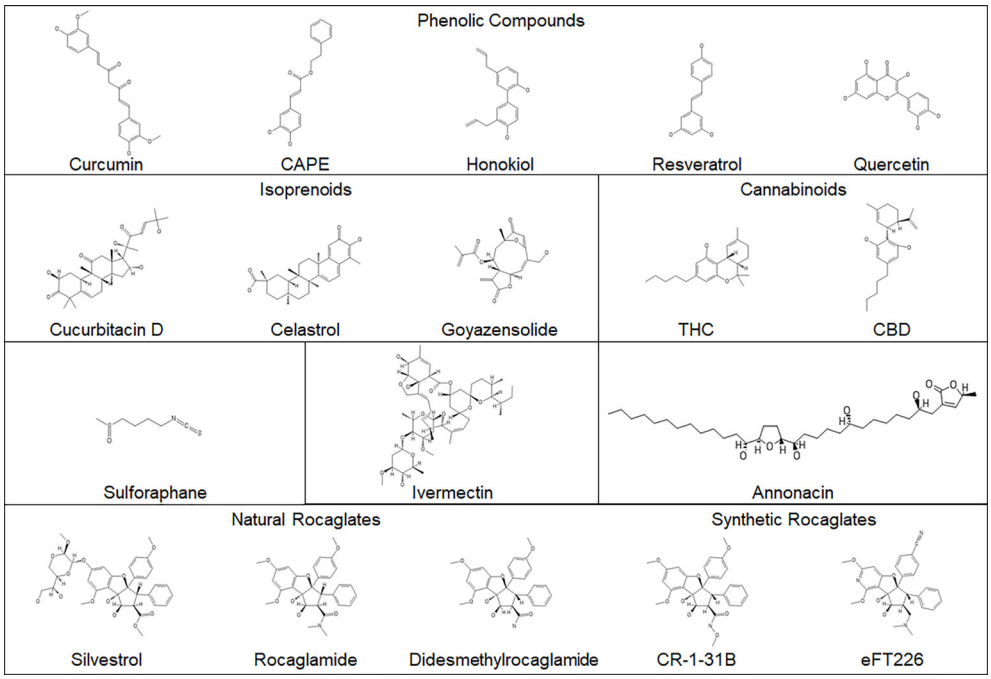

FIGURE 2 | The structures of the natural compounds evaluated in NF-associated disease. Synthetic rocaglates are included for comparison.

present in plants and including the curcuminoids in turmeric (121). However, phenolic compounds may be difficult to develop into drugs as many nonspecifically perturb cell membrane and alter protein function. The sections below summarize several phenolic compounds that have been evaluated in NF-related tumor models.

(i) ***Curcumin and other curcuminoids.*** The diarylheptanoid curcumin is isolated from turmeric (*Curcuma longa)* and comprises 2-5% of the plant rhizome. Turmeric is commonly used in Indian cooking and is a component in Ayurvedic medicine for treating infections, inflammation, and other chronic conditions. Curcumin possesses anti-inflammatory properties through inhibition of the NF-κB pathway and suppression of phospho-STAT3 in cancer cells at relatively high IC_{50} (50% inhibitory concentration; ~20μM) (60, 61). However, curcumin has also been shown to induce apoptosis by increasing pro-inflammatory oxidative damage. Using HEI-193, a human papillomavirus oncogene-transformed NF2-associated *VS* cell line, curcumin inhibits colony formation at ~10μM by downregulating the ERK, AKT, and NF-κB pathways while increasing free radical-mediated apoptosis (62) (**Table 1**). These results suggest cell context-dependent effects of curcumin. Also, curcumin enhances the expression of heat shock protein 70 (HSP70), a molecular chaperone associated with drug resistance. Combining curcumin with the pan-HSP inhibitor KNK437 yields synergistic growth inhibition in HEI-193 cells. The use of HEI-193 as an NF2-related cell model is of concern as viral oncogene transformation alters growth behavior of benign schwannoma cells. Other NF2-associated schwannoma models should be evaluated to confirm the findings.

Previously, we found that the IC_{50} value of curcumin was ~20μM in primary *VS* cells (63) and ~7μM in *NF2*-deficient Ben-Men-1 meningioma cells. Curcumin also inhibits proliferation of *NF1*-deficient MPNST cells at IC_{50} values of 25-100μM (64). A related curcuminoid, calebin-A, reduces cell growth at IC_{50} values ranging from 12.5-25μM and decreases the levels of phospho-AKT and survivin in the same MPNST cell lines. Calebin-A shows modest anti-tumor activity in an *NF1*-deficient MPNST xenograft model when dosed at 100mg/kg (**Table 1**). A dietary study in a small number of NF1 patients fed a Mediterranean diet supplemented with curcumin reported a 30-51% reduction in the number of CNFs, while a Western diet with the same supplement did not show any tumor inhibition (65). A larger study with well-defined objective outcomes is required to draw firm conclusions about the efficacy of curcumin in NF1 patients.

Curcumin has a short half-life in aqueous solution (<5 minutes), making it imperative that experiments be rigorously controlled to ensure the observed treatment effects are due to curcumin but not its degradation products (66). The instability of curcumin along with poor bioavailability may explain why many early trials did not show any clinical benefits. To increase bioavailability, alternative delivery approaches have been sought, including protein nanoparticles, liposomal formulations, and erythrocytes coated with porous nanoparticles (66, 67). It remains to be seen if these strategies could improve the efficacy of curcumin.

(ii) ***Propolis constituents.*** Also called bee glue, propolis is found in beehives and has been used since the ancient Egyptian civilization for its anti-inflammatory, anti-bacterial, and wound-healing properties. It comprises an admixture of different chemicals with wide variability in composition depending

upon factors, such as the regional flora, climate, and preparation method (68). Therefore, studies using crude propolis extracts are highly liable to lot-to-lot variabilities in their biological effects. Chinese red propolis inhibits VEGF expression and contains at least 12 components, including the phenolic ester, caffeic acid phenethyl ester (CAPE), and the flavonoid, kaempferol. Turkish propolis induces G_1 arrest and apoptosis in cancer cells and contains six major constituents, including caffeic acid and CAPE. Polish propolis inhibits S-phase entry, decreases cell viability, and contains multiple flavonoids. Bio30 is a water-miscible extract of New Zealand propolis, which contains multiple phenolic compounds including CAPE, and suppresses the growth of HEI-193 schwannoma and *NF1*-deficient S462 MPNST cells (69) (**Table 1**). Among these propolis specimens, a common constituent is CAPE. The IC_{50} of this compound in HEI-193 schwannoma cells was ~36 μM. We also found that CAPE has little growth-inhibitory activity in *VS* and meningioma cells at doses <=20μM (63). It is not known whether it is possible to achieve this high concentration of CAPE in humans.

(iii) ***Honokiol.*** As a biphenolic lignan from the bark of *Magnolia* trees, honokiol is commonly consumed as an ingredient in herbal tea preparations for treating anxiety in Asia and possesses anti-tumor activity (70). In HEI-193 schwannoma cells, honokiol inhibits proliferation by decreasing phospho-AKT and ERK1/2 at an IC_{50} of ~26μM (71) (**Table 1**). However, this compound has not been tested in other NF2- or NF1-related models. Also, honokiol crosses the blood-brain barrier, but its oral bioavailability and plasma half-life are low (70). Several approaches, including encapsulating honokiol in nanoparticles or liposomes, are being used to enhance these properties.

(iv) ***trans-Resveratrol.*** This stilbenoid was isolated originally from white hellebore, but is found widely in various fruits and nuts, including grapes, apples, and pistachios (72). It has beneficial metabolic effects in mouse models of diet-induced diabetes by negatively modulating insulin and IGF-1 signaling. It inhibits cell proliferation by reducing the levels of cyclin D, Hippo-YAP, and β-catenin. In addition, resveratrol at doses of 5mg or less per day reduces the number of adenomas by ~40% in a mouse model of high-fat diet-induced colorectal carcinoma by promoting autophagy, while a higher dose of ~1g per day shows less inhibitory effects. These results suggest that resveratrol may have chemo-preventive effects (73). Pharmacokinetic studies indicate that a single dose of resveratrol of 5mg or 1g reaches peak plasma concentrations of 0.6 and 137μM, respectively. It is generally accepted that resveratrol at doses ≤1g can be taken long-term, but higher doses (e.g., 2.5 and 5 g) can cause gastrointestinal symptoms (74). In human *VS* cells and *NF2*-deficient Ben-Men-1 cells, resveratrol exhibits moderate antiproliferative activity at doses up to 20μM (63). In *NF2*-expressing HBL-52 meningioma cells, the effective dose of resveratrol to induce apoptosis is >50μM (75). Therefore, additional studies in NF-related animal models are needed to determine if resveratrol exhibits anti-tumor effects at tolerable doses.

(v) ***Quercetin.*** The pigmented pentahydroxylated flavone quercetin is widely found in oaks (genus *Quercus*), herbs, fruits, and vegetables. It induces apoptosis at a relatively high dose and moderately reduces cancer cell growth (76). Quercetin inhibits the growth of HEI-193 schwannoma cells and stabilizes the expression of mutant merlin proteins in *NF2*-deficient CH157-NM malignant meningioma cells at doses ≥25μM (77); however, these doses are not possible to be reached in humans (**Table 1**). Additionally, it is known to aggregate and promiscuously bind to proteins, making it less therapeutically effective and potentially toxic (78–81). The known toxic effects of quercetin include mutagenicity, prooxidant activity, and mitochondrial toxicity.

(vi) ***Sichuan pepper extracts.*** The Sichuan peppercorns harvested from the seeds of the aromatic spiny shrub *Zanthoxylum piperitum* are used in East Asian cuisine and traditional Chinese medicine. Peppercorn extracts inhibit proliferation of *NF1*-deficient MPNST and MDA-MB-231 breast cancer cells by reducing PAK1 activation and cyclin D_1 levels (82) (**Table 1**). These extracts also suppress MDA-MB-231 xenografts, but resistant cell populations rapidly developed during treatment. Moreover, the constituents in Sichuan pepper extracts responsible for the antiproliferative effects have not been determined.

Isoprenoids

Terpenoids and steroids are isoprene-derived, with terpenes being a class of naturally-occurring hydrocarbons originally named for their discovery in turpentine, a resin distilled from conifer sap. Isoprenoids are the largest group of natural products. Although they are mainly found in plants, some classes, such as steroids, are common in animals. In plants, terpenoids are often found as aromatic compounds that play important roles in signal transduction and act as a defense against herbivores (122). With great structural diversity, terpenoids are made up of repeating units of the C_5-hydrocarbon isoprene and classified based on the number and structural organization of isoprene units. Although the words terpenes and terpenoids are often used interchangeably, terpenoids properly refer to modified terpenes with additional oxygenated functional groups.

(i) ***Cucurbitacin.*** Originally isolated from the squash family (Cucurbitaceae), cucurbitacins are tetracyclic triterpenoids with a steroidal skeleton (83). These compounds are also found in several other plants and mushrooms. They often have glycosidic linkages and are classified into multiple variants according to their side chains. Cucurbitacins are contained in traditional Asian remedies for treating viral diseases and inflammatory conditions. They exhibit antiproliferative effects by disrupting microtubule polymerization. Also, they inhibit cancer cell growth by decreasing phospho-AKT and phospho-ERK, increasing the levels of $p21^{WAF1}$, and promoting apoptosis (84). Cucurbitacin I effectively inhibits proliferation of *NF1*-null MPNST cells and induces apoptosis by decreasing STAT3 signaling (85) (**Table 1**). We showed that cucurbitacin D has growth-inhibitory activity against *Nf2*-null mouse schwannoma and human Ben-Men-1 cells at sub-micromolar IC_{50} concentrations by decreasing the expression of cyclins and phospho-AKT, leading to G_2/M arrest (86). Despite their anti-

tumor activity, cucurbitacins may cause gastrointestinal toxicity and have a low therapeutic index, which hamper their further clinical development (84).

(ii) *Celastrol.* Originally isolated from *Tripterygium wilfordii* (thunder god vine), celastrol (tripterine) is a pentacyclic triterpenoid, which exhibits anti-obesity, antioxidant, anti-inflammatory, and anti-tumor effects (87). It inhibits NF-κB signaling and multiple other pathways and reduces proliferation and invasion of cancer cells with an IC_{50} of ~2μM. Celastrol impedes degradation of the merlin protein in malignant meningioma cells carrying a missense mutation in the *NF2* gene at ~1μM (77) (**Table 1**). However, celastrol has a problematic *ortho*-quinone methide functional group that possesses redox activity and is reactive promiscuously with the sulfur nucleophiles present in the active sites of several enzymes, including metabolic coenzymes, needed by normal cells. These features may explain the serious adverse effects on hepatic, renal, reproductive, and cardiovascular systems reported after consuming *T. wilfordii* supplements (88).

(iii) *Goyazensolide.* Isolated from *Piptocoma rufescens* (velvetshrub) and other members of the sunflower family (Asteraceae), goyazensolide is a sesquiterpene lactone. It was identified initially as an anti-schistosomal agent and has antiproliferative activity by inhibiting NF-κB expression and inducing apoptosis (89). We found that goyazensolide suppresses proliferation of *Nf2*$^{-/-}$ mouse schwannoma cells and *NF2*-deficient human meningioma cells at IC_{50} doses of ~1μM and less effectively in primary human *VS* and meningioma cells (86) (**Table 1**). These growth-suppressive effects appear to be due to decreased expression of AKT and cyclins, followed by G_2/M arrest. Unfortunately, goyazensolide was too toxic in mice at therapeutic doses for further development.

(iv) *DAW22.* This sesquiterpene coumarin was isolated from the roots of *Ferula ferulaeoides*, a member of the carrot family (Apiaceae). It is antiproliferative and pro-apoptotic in sporadic and NF1-associated MPNST cells but at relatively high IC_{50} doses (30-47μM) (90) (**Table 1**). Also, it only modestly reduces tumor growth in *NF1*-expressing MPNST-bearing mice at the dose of 60mg/kg. The effects of DAW22 in NF2-related tumor cell and animal models have not been investigated.

Sulforaphane

Frequently found as a glycosidic precursor in cruciferous vegetables of the mustard family (Brassicaceae), sulforaphane is a sulfur-containing member of the isothiocyanate compound class (91). It has anti-inflammatory and anti-neoplastic activities in several types of cancer cells, partly *via* inhibiting NF-κB. In HEI-193 schwannoma cells, sulforaphane has growth-inhibitory effects at IC_{50} >10μM (92) (**Table 1**). We also found that it inhibited the growth of primary *VS* and meningioma cells at IC_{50} >20μM (63). Due to its short half life (93), the plasma concentrations of sulforaphane in humans peak at ~200nM (94). These results suggest that it may not be very potent against NF2-related tumors. However, sulforaphane is generally safe (93), improved formulation and delivery methods will be required to reach a therapeutic level.

Cannabinoids

Cannabis sativa, called marijuana or hemp, is used in traditional Chinese and Ayurvedic medicine, but in the West, more well-known for recreational purposes. Although *Cannabis sativa* varieties synthesize >100 different cannabinoids, two compounds, Δ^9-tetrahydrocannabinol (THC) and cannabidiol (CBD), are primarily studied for their clinical effects. *Cannabis* extracts and individual cannabinoids are increasingly used in patients suffering from glaucoma, neuropathic pain, and cancer (95, 96). THC is known for its appetite stimulation and psychoactive properties and is a Schedule 1-controlled substance. Dronabinol (Marinol®, Syndros™), a synthetic THC analog, is FDA-approved for treating HIV-induced appetite loss and chemotherapy-related nausea and vomiting. Nabiximols (Sativex®), a 1:1 THC : CBD extract, is approved in ~30 countries. for multiple sclerosis-related symptoms. Cannabinoids may have anti-neoplastic activity through their effects on endocannabinoid receptors (97). The synthetic THC analog, WIN-55212-2, is an endocannabinoid receptor agonist and induces G_1 cell cycle arrest (123). In some contexts, cannabinoids may be pro-tumorigenic as 100-300nM THC enhances DNA synthesis in cancer cells by endocannabinoid receptor-mediated EGFR transactivation (124). However, it should be noted that overdoses of THC may cause acute intoxication, tachycardia, aboulia, and psychosis. Also, THC and related analogs have not been assessed in NF-related cell and animal models.

In contrast, CBD is non-psychoactive and has analgesic, anxiolytic, and anticonvulsant properties (95, 96). In the U.S., chemically-synthesized CBD is legally sold as an over-the-counter supplement. Clinical trials suggest that CBD is overall well-tolerated with drowsiness and dizziness being the main adverse effects (96) (**Table 1**). The FDA approved Epidiolex®, a plant-derived CBD, to treat Lennox-Gastaut and Dravet syndromes, two rare forms of severe epilepsy. In addition, CBD may have helped control neuropathic pain and mood disorders in an NF1 patient with PNFs (98). A larger study is needed to confirm these findings. CBD preparations are sold in a wide variety of formulations, and the purity and safety of different products are unclear. Additional rigorous clinical examinations should be conducted to validate analgesic qualities, pharmacokinetics, and long-term safety (99).

Ivermectin

The anti-parasitic avermectins were originally isolated from *Streptomyces avermitilis*. Subsequently, a semi-synthetic derivative of avermectin, ivermectin, was developed for veterinary use to treat parasite infestations and was later approved by the FDA to treat river blindness and other nematode infections in humans (100, 101). Ivermectin is well tolerated and only causes mild toxicity even when taking ten times the FDA-approved dose. It has anti-tumor activity in various types of cancer. It inhibits proliferation of HEI-193 schwannoma cells at an IC_{50} of ~5μM by blocking PAK1 and decreasing phospho-Raf (102) (**Table 1**). However, the FDA-approved therapeutic dose of ivermectin in humans only reaches

plasma concentrations of <100nM (100). Also, ivermectin is a substrate for the multidrug resistance 1 (MDR1) transporter, which prevents the drug from reaching high concentrations in the brain (100, 101). Thus, this drug is not likely to be effective against NF2-related *VS* and meningiomas.

Silvestrol, Rocaglamide, and Didesmethylrocaglamide

Rocaglates, also called flavaglines, are a large family of cyclopenta [*b*]benzofurans synthesized by tropical trees of the *Aglaia* genus in the mahogany family (Meliaceae) (104). Among this group of natural compounds, rocaglamide (also known as rocaglamide A or RocA; **Figure 2**) was first found to possess antileukemic activity (111) but was not further characterized biologically for some years due to its scarcity. Subsequently, a few other rocaglates with anti-proliferative activity were identified, including silvestrol which was the first flavagline with an unusual sugar-like dioxanyl ring discovered in *Aglaia foveolata (*105). Silvestrol inhibits proliferation of a variety of cancer cell lines at low nanomolar concentrations similar to camptothecin and paclitaxel (104). Acting as inhibitors of the eukaryotic translation initiation factor 4A (eIF4A), an RNA helicase (106), silvestrol and rocaglamide bind eIF4A and lock it onto purine-rich sequences in the 5'-untranslated region (UTR) of certain mRNAs, leading to translation inhibition (107, 112) (**Figure 1B**). Rocaglates may also bind to prohibitins, resulting in inhibition Raf/ERK signaling (108).

We have shown that MPNST, *VS*, and meningioma tumors frequently overexpress the eIF4F components, including eIF4A (63, 109). Genetic depletion of eIF4A *via* RNA interference and pharmacological inhibition by silvestrol effectively suppress proliferation of *NF2*-deficient tumor and *NF1*-deficient MPNSTs cells (**Table 1**). As an eIF4A inhibitor, silvestrol reduces the protein levels of multiple cyclins and oncogenic kinases, including AKT, ERK, and FAK, leading to G_2/M arrest and apoptosis. Also, it profoundly suppresses tumor growth of $Nf2^{-/-}$ schwannomas and $NF1^{-/-}$ MPNSTs. However, a toxicology study in dogs revealed that silvestrol caused lung damage (https://dtp.cancer.gov/publications/silvestrol_rocaglamide_studies.pdf). Consequently, its further clinical development was suspended (103).

By side-by-side comparing 10 silvestrol-related rocaglates lacking the dioxanyl ring (110), we identified rocaglamide and didesmethylrocaglamide (also called RocB) with growth-inhibitory activity comparable to silvestrol in MPNST, schwannoma, and meningioma cells at low nanomolars (113) (**Table 1**). Both rocaglamide and didesmethylrocaglamide reduce expression of multiple oncogenic kinases IGF-1R, AKT, and ERKs while simultaneously inducing DNA damage response, caspase cleavage, and apoptosis. Interestingly, rocaglamide exhibited 50% oral bioavailability and was not susceptible to multi-drug resistance-1 efflux. When delivered by oral gavage or intraperitoneal injection, rocaglamide potently suppressed tumor growth in an orthotopic MPNST model. Most importantly, rocaglamide was well tolerated in mice and did not induce pulmonary toxicity in dogs. Furthermore, both rocaglamides exhibited strong anti-tumor effects against other sarcomas, including osteosarcoma, Ewing sarcoma, and rhabdomyosarcoma. These results warrant a clinical trial to evaluate these rocaglamides in patients with sarcomas and those afflicted by NF. It should also be mentioned that the synthetic rocaglates have also been developed that retain the core scaffold responsible for eIF4A inhibition, while incorporating side chain modifications to optimize pharmacokinetic and pharmacodynamic properties. One such compound, (-)-CR-1-31B prolongs survival of mice bearing pancreatic adenocarcinoma allografts (125). Another synthetic rocaglate-like compound, eFT226 (zotatifin), has anti-tumor activity against several fibroblast growth factor receptor- and ErbB2-driven cancers (126) and has recently entered a phase 1/2 clinical trial in patients with K-Ras- or RTK-driven advanced solid tumors (ClinicalTrials.gov Identifier: NCT04092673).

Annonacin

Also called guyabano or graviola, soursop is the fruit of *Annona muricata*, a member of the custard apple family (Annonaceae). With its pleasant aroma, soursop is used to make juices and as a flavoring agent (**Table 1**). Extracts from fruits and leaves of *Annona muricata* are reported to have anti-tumor activity against multiple tumor types, including anecdotally shrinking NF2-associated *VS* (114–116). One active component with anti-proliferative activity in soursop is annonacin, an acetogenin. However, this compound inhibits mitochondrial complex I, elicits severe neurotoxic effects, and excessive consumption of *Annona* plants and supplements are associated with atypical Parkinson's disease (117). These serious adverse effects prevent it from further development as an anti-tumor agent (118).

Additionally, several other natural compounds may be of interest to NF patients. Silibinin, the main flavonolignan component in the extract of milk thistle (*Silybum marianum*) seeds, is used to treat hepatotoxicity caused by poisoning from the death cap mushroom *Amanita phalloides*. It inhibits lung cancer cell proliferation by suppressing AKT and ERK activation (127). Gingerol, an alkylphenol found in ginger, decreases the growth of breast cancer cells by lowering the expression of EGFR and β1-integrin (128). Shikonin, a naphthoquinone pigment found in the root of *Lithospermum erythrorhizon* in the borage family (Boraginaceae), is used in traditional Chinese medicine for treating inflammatory diseases. It suppresses leukemia cell growth by decreasing phospho-AKT and ERKs (129). *Angelica sinensis*, commonly known as dong quai (danggui, dang'ui), is an herb in the carrot family (Apiaceae) used in traditional Asian medicine for reproductive disorders. An active component in dong quai is the γ-lactone *N*-butylidenephthalide, which inhibits proliferation of gastric carcinoma cells by increasing the levels of REDD1 (regulated in development and DNA damage responses 1), a negative regulator of the mTOR pathway (130). Genistein is an isoflavone found in soy-based foods, such as soymilk. It induces apoptosis, reduces tumor vascularity, and suppresses metastasis by inhibiting cyclins and AKT activation (131). Epigallocatechin gallate is the most abundant catechin ester in green tea (*Camellia sinensis*). It decreases phosphorylation of

PI3K and AKT and reduces IGF-1R levels in some cancer cells (132). Since these natural compounds inhibit the signaling pathways frequently activated in NF-associated tumors, it will be interesting to see whether they have anti-tumor effects in these tumors.

CONCLUSION

NF are characterized by multiple nervous system tumors and other non-tumoral manifestations. Surgery and/or radiation are the standard of care to control the tumor burden but often incur significant morbidities. The recent approval of the MEK inhibitor selumetinib to treat NF1-associated PNF suggests that medications targeting specific NF signaling pathways can be successful. However, combining selumetinib with other targeted agent(s) will be needed to achieve a cure. Although not FDA-approved, bevacizumab is used off-label for NF2 patients, with some of them experiencing tumor reduction and improved hearing. Recently, using traditional and systems biology approaches (56–59), several targeted compounds and compound combinations with anti-tumor effects in NF-related models have been identified, and some are being evaluated in humans.

Natural compounds have been investigated as potential cancer therapies for several decades, and many are on the WHO's List of Essential Medicines. Many patients with NF-related tumors take natural products as supplements in the hope of reducing tumor growth. While several natural compounds can inhibit signal transduction pathways deregulated in NF-associated tumors (**Figures 1** and **2**), most have only been tested in cell culture models and exhibit high IC_{50} values that may not be achievable *in vivo* (**Table 1**). In some cases, the cell culture and animal models used do not accurately reflect the pathogenesis of NF tumors. Therefore, the published data should be interpreted cautiously, with patients consulting their physicians before taking any natural compounds. Of the natural compounds that demonstrated potent anti-tumor activity in both NF-related models, the eIF4A inhibitors rocaglamide and didesmethylrocaglamide effectively block the expression multiple oncogenic kinases with good bioavailability and toxicity profiles and are expected to enter clinical trials in the future.

AUTHOR CONTRIBUTIONS

AA: project conception and manuscript writing. JO: project conception and manuscript writing, DW: project conception. AK: project conception, and L-SC: project conception and supervision and manuscript writing and authorship. All authors contributed to the article and approved the submitted version.

FUNDING

This study was supported by grants from the Galloway Family, Advocure NF2, CancerFree KIDS, Sunbeam Foundation, NF2 Biosolutions, Department of Defense W81XWH-18-1-0547, and National Institute of Neurological Disorders and Stroke R01NS113854 to L-SC, the Department of Defense W81XWH-14-1-0167 to DW, and National Cancer Institute P01CA125066 to AK and P30CA16058 to The OSU Comprehensive Cancer Center. The funder was not involved in the study design, collection, analysis, interpretation of data, the writing of this article or the decision to submit it for publication.

REFERENCES

1. Plotkin SR, Wick A. Neurofibromatosis and Schwannomatosis. *Semin Neurol* (2018) 38(1):73–85. doi: 10.1055/s-0038-1627471
2. Evans DGR, Salvador H, Chang VY, Erez A, Voss SD, Schneider KW, et al. Cancer and Central Nervous System Tumor Surveillance in Pediatric Neurofibromatosis 1. *Clin Cancer Res* (2017) 23(12):e46–53. doi: 10.1158/1078-0432.CCR-17-0589
3. Viskochil D, Buchberg AM, Xu G, Cawthon RM, Stevens J, Wolff RK, et al. Deletions and a Translocation Interrupt a Cloned Gene at the Neurofibromatosis Type 1 Locus. *Cell* (1990) 62(1):187–92. doi: 10.1016/0092-8674(90)90252-A
4. Wallace MR, Marchuk DA, Andersen LB, Letcher R, Odeh HM, Saulino AM, et al. Type 1 Neurofibromatosis Gene: Identification of a Large Transcript Disrupted in Three NF1 Patients. *Science* (1990) 249 (4965):181–6. doi: 10.1126/science.2134734
5. Xu GF, O'Connell P, Viskochil D, Cawthon R, Robertson M, Culver M, et al. The Neurofibromatosis Type 1 Gene Encodes a Protein Related to GAP. *Cell* (1990) 62(3):599–608. doi: 10.1016/0092-8674(90)90024-9
6. Chamseddin BH, Le LQ. Management of Cutaneous Neurofibroma: Current Therapy and Future Directions. *Neurooncol Adv* (2019) 2(Suppl 1):i107–16. doi: 10.1093/noajnl/vdz034
7. Staedtke V, Bai R-Y, Blakeley JO. Cancer of the Peripheral Nerve in Neurofibromatosis Type 1. *Neurotherapeutics* (2017) 14(2):298–306. doi: 10.1007/s13311-017-0518-y
8. Kim A, Stewart DR, Reilly KM, Viskochil D, Miettinen MM, Widemann BC. Malignant Peripheral Nerve Sheath Tumors State of the Science: Leveraging Clinical and Biological Insights Into Effective Therapies. *Sarcoma* (2017) 2017:7429697. doi: 10.1155/2017/7429697
9. Costa ADA, Gutmann DH. Brain Tumors in Neurofibromatosis Type 1. *Neurooncol Adv* (2020) 2(Supplement 1):i85–97. doi: 10.1093/noajnl/vdz040
10. Laycock-van Spyk S, Thomas N, Cooper DN, Upadhyaya M. Neurofibromatosis Type 1-Associated Tumours: Their Somatic Mutational Spectrum and Pathogenesis. *Hum Genomics* (2011) 5(6):623–90. doi: 10.1186/1479-7364-5-6-623
11. Gross AM, Wolters PL, Dombi E, Baldwin A, Whitcomb P, Fisher E, et al. Selumetinib in Children With Inoperable Plexiform Neurofibromas. *N Engl J Med* (2020) 382(15):1430–42. doi: 10.1056/NEJMoa1912735
12. Weiss BD, Wolters PL, Plotkin SR, Widemann B, Tonsgard JH, Blakeley J, et al. NF106: A Neurofibromatosis Clinical Trials Consortium Phase II Trial of the MEK Inhibitor Mirdametinib (PD-0325901) in Adolescents and Adults With NF1-Related Plexiform Neurofibromas. *J Clin Oncol* (2021) 39(7):797–806. doi: 10.1200/JCO.20.02220
13. de Blank PMK, Fisher MJ, Liu GT, Gutmann DH, Listernick R, Ferner RE, et al. Optic Pathway Gliomas in Neurofibromatosis Type 1: An Update: Surveillance, Treatment Indications, and Biomarkers of Vision. *J Neuroophthalmol* (2017) 37(Suppl 1):S23–32. doi: 10.1097/WNO.0000000000000550
14. Fangusaro J, Onar-Thomas A, Young Poussaint T, Wu S, Ligon AH, Lindeman N, et al. Selumetinib in Paediatric Patients With BRAF-

Aberrant or Neurofibromatosis Type 1-Associated Recurrent, Refractory, or Progressive Low-Grade Glioma: A Multicentre, Phase 2 Trial. *Lancet Oncol* (2019) 20(7):1011–22. doi: 10.1016/S1470-2045(19)30277-3
15. Wu LMN, Lu QR. Therapeutic Targets for Malignant Peripheral Nerve Sheath Tumors. *Future Neurol* (2019) 14(1):FNL7. doi: 10.2217/fnl-2018-0026
16. Evans DGR, Salvador H, Chang VY, Erez A, Voss SD, Druker H, et al. Cancer and Central Nervous System Tumor Surveillance in Pediatric Neurofibromatosis 2 and Related Disorders. *Clin Cancer Res* (2017) 23 (12):e54–61. doi: 10.1158/1078-0432.CCR-17-0590
17. Rouleau GA, Merel P, Lutchman M, Sanson M, Zucman J, Marineau C, et al. Alteration in a New Gene Encoding a Putative Membrane-Organizing Protein Causes Neuro-Fibromatosis Type 2. *Nature* (1993) 363(6429):515–21. doi: 10.1038/363515a0
18. Trofatter JA, MacCollin MM, Rutter JL, Murrell JR, Duyao MP, Parry DM, et al. A Novel Moesin-, Ezrin-, Radixin-Like Gene Is a Candidate for the Neurofibromatosis 2 Tumor Suppressor. *Cell* (1993) 72(5):791–800. doi: 10.1016/0092-8674(93)90406-G
19. Welling DB, Packer MD, Akhmametyeva EM, Chang L-S. The Biology and Genetics of Vestibular Schwannomas. In: Bambakidis N, Megerian C, Spetzler R, editors. *Surgery of the Cerebellopontine Angle*. Hamilton, Ontario, CA: B.C. Decker, Inc (2008). p. 119–34.
20. Kruchko C, Ostrom QT, Gittleman H, Barnholtz-Sloan JS. The CBTRUS Story: Providing Accurate Population-Based Statistics on Brain and Other Central Nervous System Tumors for Everyone. *Neuro Oncol* (2018) 20 (3):295–8. doi: 10.1093/neuonc/noy006
21. Goutagny S, Kalamarides M. Meningiomas and Neurofibromatosis. *J Neuro-Oncol* (2010) 99(3):341–7. doi: 10.1007/s11060-010-0339-x
22. Plotkin SR, Duda DG, Muzikansky A, Allen J, Blakeley J, Rosser T, et al. Multicenter, Prospective, Phase II and Biomarker Study of High-Dose Bevacizumab as Induction Therapy in Patients With Neurofibromatosis Type 2 and Progressive Vestibular Schwannoma. *J Clin Oncol* (2019) 37 (35):3446–54. doi: 10.1200/JCO.19.01367
23. Blakeley JO, Ye X, Duda DG, Halpin CF, Bergner AL, Muzikansky A, et al. Efficacy and Biomarker Study of Bevacizumab for Hearing Loss Resulting From Neurofibromatosis Type 2–Associated Vestibular Schwannomas. *J Clin Oncol* (2016) 34(14):1669–75. doi: 10.1200/JCO.2015.64.3817
24. Nunes FP, Merker VL, Jennings D, Caruso PA, di Tomaso E, Muzikansky A, et al. Bevacizumab Treatment for Meningiomas in NF2: A Retrospective Analysis of 15 Patients. *PloS One* (2013) 8(3):e59941. doi: 10.1371/journal.pone.0059941
25. Mansouri S, Suppiah S, Mamatjan Y, Paganini I, Liu JC, Karimi S, et al. Epigenomic, Genomic, and Transcriptomic Landscape of Schwannomatosis. *Acta Neuropathol.* (2021) 141(1):101–16. doi: 10.1007/s00401-020-02230-x
26. Smith MJ, Isidor B, Beetz C, Williams SG, Bhaskar SS, Richer WW, et al. Mutations in LZTR1 Add to the Complex Heterogeneity of Schwannomatosis. *Neurology* (2015) 84(2):141–7. doi: 10.1212/WNL.0000000000001129
27. Kehrer-Sawatzki H, Farschtschi S, Mautner V-F, Cooper DN. The Molecular Pathogenesis of Schwannomatosis, a Paradigm for the Co-Involvement of Multiple Tumour Suppressor Genes in Tumorigenesis. *Hum Genet* (2017) 136(2):129–48. doi: 10.1007/s00439-016-1753-8
28. Karnoub AE, Weinberg RA. Ras Oncogenes: Split Personalities. *Nat Rev Mol Cell Biol* (2008) 9(7):517–31. doi: 10.1038/nrm2438
29. Goncalves MD, Hopkins BD, Cantley LC. Phosphatidylinositol 3-Kinase, Growth Disorders, and Cancer. *N Engl J Med* (2018) 379(21):2052–62. doi: 10.1056/NEJMra1704560
30. Laplante M, Sabatini DM. mTOR Signaling in Growth Control and Disease. *Cell* (2012) 149(2):274–93. doi: 10.1016/j.cell.2012.03.017
31. Lemberg KM, Wang J, Pratilas CA. From Genes to -Omics: The Evolving Molecular Landscape of Malignant Peripheral Nerve Sheath Tumor. *Genes* (2020) 11(6):691. doi: 10.3390/genes11060691
32. De Raedt T, Beert E, Pasmant E, Luscan A, Brems H, Ortonne N, et al. PRC2 Loss Amplifies Ras-Driven Transcription and Confers Sensitivity to BRD4-Based Therapies. *Nature* (2014) 514(7521):247–51. doi: 10.1038/nature13561
33. Rad E, Tee AR. Neurofibromatosis Type 1: Fundamental Insights Into Cell Signalling and Cancer. *Semin Cell Dev Biol* (2016) 52:39–46. doi: 10.1016/j.semcdb.2016.02.007
34. Casaletto JB, McClatchey AI. Spatial Regulation of Receptor Tyrosine Kinases in Development and Cancer. *Nat Rev Cancer.* (2012) 12(6):387–400. doi: 10.1038/nrc3277
35. Fernandez-Valle C, Tang Y, Ricard J, Rodenas-Ruano A, Taylor A, Hackler E, et al. Paxillin Binds Schwannomin and Regulates Its Density-Dependent Localization and Effect on Cell Morphology. *Nat Genet* (2002) 31(4):354–62. doi: 10.1038/ng930
36. Lallemand D, Manent J, Couvelard A, Watilliaux A, Siena M, Chareyre F, et al. Merlin Regulates Transmembrane Receptor Accumulation and Signaling at the Plasma Membrane in Primary Mouse Schwann Cells and in Human Schwannomas. *Oncogene* (2009) 28(6):854–65. doi: 10.1038/onc.2008.427
37. Bush ML, Burns SS, Oblinger J, Davletova S, Chang L-S, Welling DB, et al. Treatment of Vestibular Schwannoma Cells With ErbB Inhibitors. *Otol Neurotol* (2012) 33(2):244–57. doi: 10.1097/MAO.0b013e31823e287f
38. Kissil JL, Wilker EW, Johnson KC, Eckman MS, Yaffe MB, Jacks T. Merlin, the Product of the Nf2 Tumor Suppressor Gene, Is an Inhibitor of the P21-Activated Kinase, Pak1. *Mol Cell* (2003) 12(4):841–9. doi: 10.1016/S1097-2765(03)00382-4
39. Morrison H, Sperka T, Manent J, Giovannini M, Ponta H, Herrlich P. Merlin/neurofibromatosis Type 2 Suppresses Growth by Inhibiting the Activation of Ras and Rac. *Cancer Res* (2007) 67(2):520–7. doi: 10.1158/0008-5472.CAN-06-1608
40. Yi C, Troutman S, Fera D, Stemmer-Rachamimov A, Avila JL, Christian N, et al. A Tight Junction-Associated Merlin-Angiomotin Complex Mediates Merlin's Regulation of Mitogenic Signaling and Tumor Suppressive Functions. *Cancer Cell* (2011) 19(4):527–40. doi: 10.1016/j.ccr.2011.02.017
41. Hamaratoglu F, Willecke M, Kango-Singh M, Nolo R, Hyun E, Tao C, et al. The Tumour-Suppressor Genes NF2/Merlin and Expanded Act Through Hippo Signalling to Regulate Cell Proliferation and Apoptosis. *Nat Cell Biol* (2006) 8(1):27–36. doi: 10.1038/ncb1339
42. Zhao B, Li L, Lei Q, Guan K-L. The Hippo–YAP Pathway in Organ Size Control and Tumorigenesis: An Updated Version. *Genes Dev* (2010) 24 (9):862–74. doi: 10.1101/gad.1909210
43. Li W, You L, Cooper J, Schiavon G, Pepe-Caprio A, Zhou L, et al. Merlin/NF2 Suppresses Tumorigenesis by Inhibiting the E3 Ubiquitin Ligase CRL4 (DCAF1) in the Nucleus. *Cell* (2010) 140(4):477–90. doi: 10.1016/j.cell.2010.01.029
44. James MF, Han S, Polizzano C, Plotkin SR, Manning BD, Stemmer-Rachamimov A, et al. NF2/merlin Is a Novel Negative Regulator of mTOR Complex 1, and Activation of Mtorc1 Is Associated With Meningioma and Schwannoma Growth. *Mol Cell Biol* (2009) 29(15):4250–61. doi: 10.1128/MCB.01581-08
45. López-Lago MA, Okada T, Murillo MM, Socci N, Giancotti FG. Loss of the Tumor Suppressor Gene NF2, Encoding Merlin, Constitutively Activates Integrin-Dependent Mtorc1 Signaling. *Mol Cell Biol* (2009) 29(15):4235–49. doi: 10.1128/MCB.01578-08
46. Beauchamp RL, James MF, DeSouza PA, Wagh V, Zhao W-N, Jordan JT, et al. A High-Throughput Kinome Screen Reveals Serum/Glucocorticoid-Regulated Kinase 1 as a Therapeutic Target for NF2-Deficient Meningiomas. *Oncotarget* (2015) 6(19):16981–97. doi: 10.18632/oncotarget.4858
47. Angus SP, Oblinger JL, Stuhlmiller TJ, DeSouza PA, Beauchamp RL, Witt L, et al. EPH Receptor Signaling as a Novel Therapeutic Target in NF2-Deficient Meningioma. *Neuro Oncol* (2018) 20(9):1185–96. doi: 10.1093/neuonc/noy046
48. Frattini V, Trifonov V, Chan JM, Castano A, Lia M, Abate F, et al. The Integrated Landscape of Driver Genomic Alterations in Glioblastoma. *Nat Genet* (2013) 45(10):1141–9. doi: 10.1038/ng.2734
49. Steklov M, Pandolfi S, Baietti MF, Batiuk A, Carai P, Najm P, et al. Mutations in LZTR1 Drive Human Disease by Dysregulating RAS Ubiquitination. *Science* (2018) 362(6419):1177–82. doi: 10.1126/science.aap7607
50. Hodges C, Kirkland JG, Crabtree GR. The Many Roles of BAF (mSWI/SNF) and PBAF Complexes in Cancer. *Cold Spring Harb Perspect Med* (2016) 6(8): a026930. doi: 10.1101/cshperspect.a026930
51. Mittal P, Roberts CWM. The SWI/SNF Complex in Cancer - Biology, Biomarkers and Therapy. *Nat Rev Clin Oncol* (2020) 17(7):435–48. doi: 10.1038/s41571-020-0357-3

52. Brosseau J-P, Liao C-P, Le LQ. Translating Current Basic Research Into Future Therapies for Neurofibromatosis Type 1. *Br J Cancer*. (2020) 123 (2):178–86. doi: 10.1038/s41416-020-0903-x
53. Widemann BC, Dombi E, Gillespie A, Wolters PL, Belasco J, Goldman S, et al. Phase 2 Randomized, Flexible Crossover, Double-Blinded, Placebo-Controlled Trial of the Farnesyltransferase Inhibitor Tipifarnib in Children and Young Adults With Neurofibromatosis Type 1 and Progressive Plexiform Neurofibromas. *Neuro Oncol* (2014) 16(5):707–18. doi: 10.1093/neuonc/nou004
54. Plotkin SR, Ardern-Holmes SL, Barker FG, Blakeley JO, Evans DG, Ferner RE, et al. Hearing and Facial Function Outcomes for Neurofibromatosis 2 Clinical Trials. *Neurology* (2013) 81(21 Suppl 1):S25–32. doi: 10.1212/01.wnl.0000435746.02780.f6
55. Wolters PL, Martin S, Merker VL, Tomsgard JH, Solomon SE, Baldwin A, et al. Patient-Reported Outcomes of Pain and Physical Functioning in Neurofibromatosis Clinical Trials. *Neurology* (2016) 87(7 Suppl 1):S4–12. doi: 10.1212/WNL.0000000000002927
56. Ferrer M, Gosline SJC, Stathis M, Zhang X, Guo X, Guha R, et al. Pharmacological and Genomic Profiling of Neurofibromatosis Type 1 Plexiform Neurofibroma-Derived Schwann Cells. *Sci Data* (2018) 5 (1):180106. doi: 10.1038/sdata.2018.106
57. Synodos for NF2 Consortium, Allaway R, Angus SP, Beauchamp RL, Blakeley JO, Bott M, et al. Traditional and Systems Biology Based Drug Discovery for the Rare Tumor Syndrome Neurofibromatosis Type 2. *PloS One* (2018) 13(6):e0197350. doi: 10.1371/journal.pone.0197350
58. Terribas E, Fernández M, Mazuelas H, Fernández-Rodríguez J, Biayna J, Blanco I, et al. KIF11 and KIF15 Mitotic Kinesins Are Potential Therapeutic Vulnerabilities for Malignant Peripheral Nerve Sheath Tumors. *Neurooncol Adv* (2020) 2(Suppl 1):i62–74. doi: 10.1093/noajnl/vdz061
59. Chang L-S, Oblinger JL, Smith AE, Ferrer M, Angus SP, Hawley E, et al. Brigatinib Causes Tumor Shrinkage in Both NF2-Deficient Meningioma and Schwannoma Through Inhibition of Multiple Tyrosine Kinases But Not ALK. *PloS One* (2021) 16(7):e0252048. doi: 10.1371/journal.pone.0252048
60. Peng Y, Zheng J, Zhou Y, Li J. Characterization of a Novel Curcumin Analog P1 as Potent Inhibitor of the NF-κb Signaling Pathway With Distinct Mechanisms. *Acta Pharmacol Sin* (2013) 34(7):939–50. doi: 10.1038/aps.2013.2
61. Siddiqui FA, Prakasam G, Chattopadhyay S, Rehman AU, Padder RA, Ansari MA, et al. Curcumin Decreases Warburg Effect in Cancer Cells by Down-Regulating Pyruvate Kinase M2 *via* mTOR-Hif1α Inhibition. *Sci Rep* (2018) 8(1):1–9. doi: 10.1038/s41598-018-25524-3
62. Angelo LS, Wu JY, Meng F, Sun M, Kopetz S, McCutcheon IA, et al. Combining Curcumin (Diferuloylmethane) and Heat Shock Protein Inhibition for Neurofibromatosis 2 Treatment: Analysis of Response and Resistance Pathways. *Mol Cancer Ther* (2011) 10(11):2094–103. doi: 10.1158/1535-7163.MCT-11-0243
63. Oblinger JL, Burns SS, Akhmametyeva EM, Huang J, Pan L, Ren Y, et al. Components of the Eif4f Complex Are Potential Therapeutic Targets for Malignant Peripheral Nerve Sheath Tumors and Vestibular Schwannomas. *Neuro Oncol* (2016) 18(9):1265–77. doi: 10.1093/neuonc/now032
64. Lee M-J, Tsai Y-J, Lin M-Y, You H-L, Kalyanam N, Ho C-T, et al. Calebin-A Induced Death of Malignant Peripheral Nerve Sheath Tumor Cells by Activation of Histone Acetyltransferase. *Phytomedicine* (2019) 57:377–84. doi: 10.1016/j.phymed.2019.01.001
65. Esposito T, Schettino C, Polverino P, Allocca S, Adelfi L, D-Amico A, et al. Synergistic Interplay Between Curcumin and Polyphenol-Rich Foods in the Mediterranean Diet: Therapeutic Prospects for Neurofibromatosis 1 Patients. *Nutrients* (2017) 9(7):783. doi: 10.3390/nu9070783
66. Nelson KM, Dahlin JL, Bisson J, Graham J, Pauli GF, Walters MA. The Essential Medicinal Chemistry of Curcumin. *J Med Chem* (2017) 60 (5):1620–37. doi: 10.1021/acs.jmedchem.6b00975
67. Xie X, Wang H, Williams GR, Yang Y, Zheng Y, Wu J, et al. Erythrocyte Membrane Cloaked Curcumin-Loaded Nanoparticles for Enhanced Chemotherapy. *Pharmaceutics* (2019) 11(9):429. doi: 10.3390/pharmaceutics11090429
68. Tran TD, Ogbourne SM, Brooks PR, Sánchez-Cruz N, Medina-Franco JL, Quinn RJ. Lessons From Exploring Chemical Space and Chemical Diversity of Propolis Components. *Int J Mol Sci* (2020) 21(14):4988. doi: 10.3390/ijms21144988
69. Demestre M, Messerli SM, Celli N, Shahhossini M, Kluwe L, Mautner V, et al. CAPE (Caffeic Acid Phenethyl Ester)-Based Propolis Extract (Bio 30) Suppresses the Growth of Human Neurofibromatosis (NF) Tumor Xenografts in Mice. *Phytother Res* (2009) 23(2):226–30. doi: 10.1002/ptr.2594
70. Ong CP, Lee WL, Tang YQ, Yap WH. Honokiol: A Review of Its Anticancer Potential and Mechanisms. *Cancers* (2020) 12(1):48. doi: 10.3390/cancers12010048
71. Lee JD, Lee JY, Baek BJ, Lee BD, Koh YW, Lee W-S, et al. The Inhibitory Effect of Honokiol, A Natural Plant Product, on Vestibular Schwannoma Cells. *Laryngoscope* (2012) 122(1):162–6. doi: 10.1002/lary.21781
72. Berretta M, Bignucolo A, Di Francia R, Cornello F, Facchini G, Ceccarelli M, et al. Resveratrol in Cancer Patients: From Bench to Bedside. *Int J Mol Sci* (2020) 21(8):2945. doi: 10.3390/ijms21082945
73. Cai H, Scott E, Kholghi A, Andreadi C, Rufini A, Karmokar A, et al. Cancer Chemoprevention: Evidence of a Nonlinear Dose Response for the Protective Effects of Resveratrol in Humans and Mice. *Sci Transl Med* (2015) 7(298):298ra117–298ra117. doi: 10.1126/scitranslmed.aaa7619
74. Brown VA, Patel KR, Viskaduraki M, Crowell JA, Perloff M, Booth TD, et al. Repeat Dose Study of the Cancer Chemopreventive Agent Resveratrol in Healthy Volunteers: Safety, Pharmacokinetics, and Effect on the Insulin-Like Growth Factor Axis. *Cancer Res* (2010) 70(22):9003–11. doi: 10.1158/0008-5472.CAN-10-2364
75. Hu S, Wei W, Yuan J, Cheng J. Resveratrol Inhibits Proliferation in HBL-52 Meningioma Cells. *Onco Targets Ther* (2019) 12:11579–86. doi: 10.2147/OTT.S228513
76. Hashemzaei M, Delarami Far A, Yari A, Heravi RE, Tabrizian K, Taghdisi SM, et al. Anticancer and Apoptosis–Inducing Effects of Quercetin *In Vitro* and *In Vivo*. *Oncol Rep* (2017) 38(2):819–28. doi: 10.3892/or.2017.5766
77. Yang C, Asthagiri AR, Iyer RR, Lu J, Xu DS, Ksendzovsky A, et al. Missense Mutations in the NF2 Gene Result in the Quantitative Loss of Merlin Protein and Minimally Affect Protein Intrinsic Function. *Proc Natl Acad Sci USA* (2011) 108(12):4980–5. doi: 10.1073/pnas.1102198108
78. McGovern SL, Shoichet BK. Kinase Inhibitors: Not Just for Kinases Anymore. *J Med Chem* (2003) 46(8):1478–83. doi: 10.1021/jm020427b
79. Guo Y, Mah E, Bruno RS. Quercetin Bioavailability Is Associated With Inadequate Plasma Vitamin C Status and Greater Plasma Endotoxin in Adults. *Nutrition* (2014) 30(11):1279–86. doi: 10.1016/j.nut.2014.03.032
80. Chen R, Lin J, Hong J, Han D, Zhang AD, Lan R, et al. Potential Toxicity of Quercetin: The Repression of Mitochondrial Copy Number *via* Decreased POLG Expression and Excessive TFAM Expression in Irradiated Murine Bone Marrow. *Toxicol Rep* (2014) 1:450–8. doi: 10.1016/j.toxrep.2014.07.014
81. Resende FA, Vilegas W, Dos Santos LC, Varanda EA. Mutagenicity of Flavonoids Assayed by Bacterial Reverse Mutation (Ames) Test. *Molecules* (2012) 17(5):5255–68. doi: 10.3390/molecules17055255
82. Hirokawa Y, Nheu T, Grimm K, Mautner V, Maeda S, Yoshida M, et al. Sichuan Pepper Extracts Block the PAK1/Cyclin D1 Pathway and the Growth of NF1-Deficient Cancer Xenograft in Mice. *Cancer Biol Ther* (2006) 5(3):305–9. doi: 10.4161/cbt.5.3.2404
83. Jing S, Zou H, Wu Z, Ren L, Zhang T, Zhang J, et al. Cucurbitacins: Bioactivities and Synergistic Effect With Small-Molecule Drugs. *J Func Foods*. (2020) 72:104042. doi: 10.1016/j.jff.2020.104042
84. Lee DH, Iwanski GB, Thoennissen NH. Cucurbitacin: Ancient Compound Shedding New Light on Cancer Treatment. *Sci World J* (2010) 10:413–8. doi: 10.1100/tsw.2010.44
85. Banerjee S, Byrd JN, Gianino SM, Harpstrite SM, Rodriguez FJ, Tuskan RG, et al. The Neurofibromatosis Type 1 Tumor Suppressor Controls Cell Growth by Regulating Signal Transducer and Activator of Transcription-3 Activity *In Vitro* and *In Vivo*. *Cancer Res* (2010) 70(4):1356–66. doi: 10.1158/0008-5472.CAN-09-2178
86. Spear SA, Burns SS, Oblinger JL, Ren Y, Pan L, Kinghorn AD, et al. Natural Compounds as Potential Treatments of NF2-Deficient Schwannoma and Meningioma: Cucurbitacin D and Goyazensolide. *Otol Neurotol* (2013) 34 (8):1519–27. doi: 10.1097/MAO.0b013e3182956169

87. Hou W, Liu B, Xu H. Celastrol: Progresses in Structure-Modifications, Structure-Activity Relationships, Pharmacology and Toxicology. *Eur J Med Chem* (2020) 189:112081. doi: 10.1016/j.ejmech.2020.112081
88. Du X, Nyagblordzro M, An L, Guo X, Du L, Wang Y, et al. Pharmacokinetic and Toxicological Characteristics of *Tripterigium* Glycosides and Their Derivatives. *Curr Drug Metab* (2018) 19(7):605–27. doi: 10.2174/1389200219666180302152752
89. Muñoz-Acuña U, Shen Q, Ren Y, Lantvit DD, Wittwer JA, Kinghorn AD, et al. Goyazensolide Induces Apoptosis in Cancer Cells *In Vitro* and *In Vivo*. *Int J Cancer Res* (2013) 9(2):36–53. doi: 10.3923/ijcr.2013.36.53
90. Li X-X, Zhang S-J, Chiu AP, Lo LH, Huang J, Rowlands DK, et al. Targeting of AKT/ERK/CTNNB1 by DAW22 as a Potential Therapeutic Compound for Malignant Peripheral Nerve Sheath Tumor. *Cancer Med* (2018) 7 (9):4791–800. doi: 10.1002/cam4.1732
91. Kamal MM, Akter S, Lin C-N, Nazzal S. Sulforaphane as an Anticancer Molecule: Mechanisms of Action, Synergistic Effects, Enhancement of Drug Safety, and Delivery Systems. *Arch Pharm Res* (2020) 43(4):371–84. doi: 10.1007/s12272-020-01225-2
92. Kim BG, Fujita T, Stankovic KM, Welling DB, Moon IS, Choi JY, et al. Sulforaphane, a Natural Component of Broccoli, Inhibits Vestibular Schwannoma Growth *In Vitro* and *In Vivo*. *Sci Rep* (2016) 6:1–10. doi: 10.1038/srep36215
93. Mangla B, Javed S, Sultan MH, Kumar P, Kohli K, Najmi A, et al. Sulforaphane: A Review of Its Therapeutic Potentials, Advances in Its Nanodelivery, Recent Patents, and Clinical Trials. *Phytother Res* (2021) 1–19. doi: 10.1002/ptr.7176
94. Langston-Cox A, Anderson D, Creek DJ, Palmer K, Wallace EM, Marshall SA. Measuring Sulforaphane and Its Metabolites in Human Plasma: A High Throughput Method. *Molecules* (2020) 25(4):829. doi: 10.3390/molecules25040829
95. Montero-Oleas N, Arevalo-Rodriguez I, Nuñez-González S, Viteri-García A, Simancas-Racines D. Therapeutic Use of Cannabis and Cannabinoids: An Evidence Mapping and Appraisal of Systematic Reviews. *BMC Complement Med Ther* (2020) 20(1):12. doi: 10.1186/s12906-019-2803-2
96. Urits I, Gress K, Charipova K, Habib K, Lee D, Lee C, et al. Use of Cannabidiol (CBD) for the Treatment of Chronic Pain. *Best Pract Res Clin Anaesthesiol.* (2020) 34(3):463–77. doi: 10.1016/j.bpa.2020.06.004
97. Kovalchuk O, Kovalchuk I. Cannabinoids as Anticancer Therapeutic Agents. *Cell Cycle* (2020) 19(9):961–89. doi: 10.1080/15384101.2020.1742952
98. Hegazy O, Platnick H. Cannabidiol (CBD) for Treatment of Neurofibromatosis-Related Pain and Concomitant Mood Disorder: A Case Report. *Cureus* (2019) 11(12):e6312. doi: 10.7759/cureus.6312
99. Millar SA, Stone NL, Yates AS, O'Sullivan SE. A Systematic Review on the Pharmacokinetics of Cannabidiol in Humans. *Front Pharmacol* (2018) 9:1365. doi: 10.3389/fphar.2018.01365
100. González Canga A, Sahagún Prieto AM, Diez Liébana MJ, Fernández Martínez N, Sierra Vega M, García Vieitez JJ. The Pharmacokinetics and Interactions of Ivermectin in Humans—A Mini-Review. *AAPS J* (2008) 10 (1):42–6. doi: 10.1208/s12248-007-9000-9
101. Dowling P. Pharmacogenetics: It's Not Just About Ivermectin in Collies. *Can Vet J* (2006) 47(12):1165–8.
102. Hashimoto H, Messerli SM, Sudo T, Maruta H. Ivermectin Inactivates the Kinase PAK1 and Blocks the PAK1-Dependent Growth of Human Ovarian Cancer and NF2 Tumor Cell Lines. *Drug Discov Ther* (2009) 3(6):243–6.
103. Kinghorn AD, Blanco EJC DE, Lucas DM, Rakotondraibe HL, Orjala J, Soejarto DD, et al. Discovery of Anticancer Agents of Diverse Natural Origin. *Anticancer Res* (2016) 36(11):5623–37. doi: 10.21873/anticanres.11146
104. Pan L, Woodard JL, Lucas DM, Fuchs JR, Kinghorn AD. Rocaglamide, Silvestrol and Structurally Related Bioactive Compounds From *Aglaia* Species. *Nat Prod Rep* (2014) 31(7):924–39. doi: 10.1039/C4NP00006D
105. Hwang BY, Su B-N, Chai H, Mi Q, Kardono LBS, Afriastini JJ, et al. Silvestrol and Episilvestrol, Potential Anticancer Rocaglate Derivatives From *Aglaia Silvestris*. *J Org Chem* (2004) 69(10):3350–8. doi: 10.1021/jo040120f
106. Sadlish H, Galicia-Vazquez G, Paris CG, Aust T, Bhullar B, Chang L, et al. Evidence for a Functionally Relevant Rocaglamide Binding Site on the Eif4a-RNA Complex. *ACS Chem Biol* (2013) 8(7):1519–27. doi: 10.1021/cb400158t
107. Wolfe AL, Singh K, Zhong Y, Drewe P, Rajasekhar VK, Sanghvi VR, et al. RNA G-Quadruplexes Cause Eif4a-Dependent Oncogene Translation in Cancer. *Nature* (2014) 513(7516):65–70. doi: 10.1038/nature13485
108. Thuaud F, Ribeiro N, Nebigil CG, Désaubry L. Prohibitin Ligands in Cell Death and Survival: Mode of Action and Therapeutic Potential. *Chem Biol* (2013) 20(3):316–31. doi: 10.1016/j.chembiol.2013.02.006
109. Oblinger JL, Burns SS, Huang J, Pan L, Ren Y, Shen R, et al. Overexpression of Eif4f Components in Meningiomas and Suppression of Meningioma Cell Growth by Inhibiting Translation Initiation. *Exp Neurol* (2018) 299(Pt B):299–307. doi: 10.1016/j.expneurol.2017.06.015
110. Pan L, Acuña UM, Li J, Jena N, Ninh TN, Pannell CM, et al. Bioactive Flavaglines and Other Constituents Isolated From *Aglaia Perviridis*. *J Nat Prod* (2013) 76(3):394–404. doi: 10.1021/np3007588
111. King ML, Chiang C-C, Ling H-C, Fujita E, Ochiai M, McPhail AT. X-Ray Crystal Structure of Rocaglamide, a Novel Antileukemic 1*h*-Cyclopenta[*B*] Benzofuran From *Aglaia Elliptifolia*. *J Chem Soc Chem Commun* (1982) 20):1150–1. doi: 10.1039/c39820001150
112. Iwasaki S, Iwasaki W, Takahashi M, Sakamoto A, Watanabe C, Shichino Y, et al. The Translation Inhibitor Rocaglamide Targets a Bimolecular Cavity Between Eif4a and Polypurine RNA. *Mol Cell* (2019) 73(4):738–48.e9. doi: 10.1016/j.molcel.2018.11.026
113. Chang L-S, Oblinger JL, Burns SS, Huang J, Anderson LW, Hollingshead MG, et al. Targeting Protein Translation by Rocaglamide and Didesmethylrocaglamide to Treat MPNST and Other Sarcomas. *Mol Cancer Ther* (2020) 19(3):731–41. doi: 10.1158/1535-7163.MCT-19-0809
114. Ecosystems Research and Development Bureau. Guyabano (*Annona Muricata* Linnaeus). *Department Environ Natural Resources Res Inf Ser Ecosystems* (2014) 26(3):1–13. Available at: http://erdb.denr.gov.ph/files/publications/rise/r_v26n3.pdf.
115. Moghadamtousi SZ, Fadaeinasab M, Nikzad S, Mohan G, Ali HM, Kadir HA. *Annona Muricata* (Annonaceae): A Review of Its Traditional Uses, Isolated Acetogenins and Biological Activities. *Int J Mol Sci* (2015) 16(7):15625–58. doi: 10.3390/ijms160715625
116. GoodByeNf. Neurofibromatosis Network, Inspire. In: *Good Bye NF - Neurofibromatosis* (2014). Available at: https://www.inspire.com/groups/neurofibromatosis-network/discussion/good-bye-nf/ (Accessed 2/12/2021).
117. Lannuzel A, Höglinger GU, Champy P, Michel PP, Hirsch EC, Ruberg M. Is Atypical Parkinsonism in the Caribbean Caused by the Consumption of Annonacae? *J Neural Transm Suppl* (2006) 70):153–7. doi: 10.1007/978-3-211-45295-0_24
118. Cancer Research UK. *Graviola (Soursop)* (2018). Available at: https://www.cancerresearchuk.org/about-cancer/cancer-in-general/treatment/complementary-alternative-therapies/individual-therapies/graviola (Accessed 2/12/2021).
119. Newman DJ, Cragg GM. Natural Products as Sources of New Drugs Over the Nearly Four Decades From 01/1981 to 09/2019. *J Nat Prod* (2020) 83(3):770–803. doi: 10.1021/acs.jnatprod.9b01285
120. Shipkowski KA, Betz JM, Birnbaum LS, Bucher JR, Coates PM, Hopp DC, et al. Naturally Complex: Perspectives and Challenges Associated With Botanical Dietary Supplement Safety Assessment. *Food Chem Toxicol* (2018) 118:963–71. doi: 10.1016/j.fct.2018.04.007
121. Perrone L, Sampaolo S, Melone MAB. Bioactive Phenolic Compounds in the Modulation of Central and Peripheral Nervous System Cancers: Facts and Misdeeds. *Cancers* (2020) 12(2):454. doi: 10.3390/cancers12020454
122. Pichersky E, Raguso RA. Why do Plants Produce So Many Terpenoid Compounds? *New Phytol* (2018) 220(3):692–702. doi: 10.1111/nph.14178
123. Sarfaraz S, Afaq F, Adhami VM, Malik A, Mukhtar H. Cannabinoid Receptor Agonist-Induced Apoptosis of Human Prostate Cancer Cells LNCaP Proceeds Through Sustained Activation of ERK1/2 Leading to G1 Cell Cycle Arrest. *J Biol Chem* (2006) 281(51):39480–91. doi: 10.1074/jbc.M603495200
124. Hart S, Fischer OM, Ullrich A. Cannabinoids Induce Cancer Cell Proliferation *via* Tumor Necrosis Factor α-Converting Enzyme (TACE/ADAM17)-Mediated Transactivation of the Epidermal Growth Factor Receptor. *Cancer Res* (2004) 64(6):1943–50. doi: 10.1158/0008-5472.CAN-03-3720
125. Chan K, Robert F, Oertlin C, Kapeller-Libermann D, Avizonis D, Gutierrez J, et al. Eif4a Supports an Oncogenic Translation Program in Pancreatic Ductal Adenocarcinoma. *Nat Commun* (2019) 10(1):5151. doi: 10.1038/s41467-019-13086-5

126. Ernst JT, Thompson PA, Nilewski C, Sprengeler PA, Sperry S, Packard G, et al. Design of Development Candidate Eft226, A First in Class Inhibitor of Eukaryotic Initiation Factor 4a RNA Helicase. *J Med Chem* (2020) 63 (11):5879–955. doi: 10.1021/acs.jmedchem.0c00182
127. Chen P-N, Hsieh Y-S, Chiou H-L, Chu S-C. Silibinin Inhibits Cell Invasion Through Inactivation of Both PI3K-Akt and MAPK Signaling Pathways. *Chem Biol Interact* (2005) 156(2-3):141–50. doi: 10.1016/j.cbi.2005.08.005
128. Martin ACBM, Fuzer AM, Becceneri AB, da Silva JA, Tomasin R, Denoyer D, et al. [10]-Gingerol Induces Apoptosis and Inhibits Metastatic Dissemination of Triple Negative Breast Cancer In Vivo. *Oncotarget* (2017) 8(42):72260–71. doi: 10.18632/oncotarget.20139
129. Zhao Q, Assimopoulou AN, Klauck SM, Damianakos H, Chinou I, Kretschmer N, et al. Inhibition of C-MYC With Involvement of ERK/JNK/MAPK and AKT Pathways as a Novel Mechanism for Shikonin and Its Derivatives in Killing Leukemia Cells. *Oncotarget* (2015) 6(36):38934–51. doi: 10.18632/oncotarget.5380
130. Liao K-F, Chiu T-L, Huang S-Y, Hsieh T-F, Chang S-F, Ruan S-P, et al. Anti-Cancer Effects of Radix *Angelica Sinensis* (Danggui) and N-Butylidenephthalide on Gastric Cancer: Implications for REDD1 Activation and mTOR Inhibition. *CPB* (2018) 48(6):2231–46. doi: 10.1159/000492641
131. Spagnuolo C, Russo GL, Orhan IE, Habtemariam S, Daglia M, Sureda A, et al. Genistein and Cancer: Current Status, Challenges, and Future Directions. *Adv Nutr* (2015) 6(4):408–19. doi: 10.3945/an.114.008052
132. Luo K-W, Lung W-Y, Chun-Xie, Luo X-L, Huang W-R. EGCG Inhibited Bladder Cancer T24 and 5637 Cell Proliferation and Migration *via* PI3K/AKT Pathway. *Oncotarget* (2018) 9(15):12261–72. doi: 10.18632/oncotarget.24301

Conflict of Interest: L-SC and AK: Patent: U.S. Provisional Application No. 19/55304 Anticancer rocaglamide derivatives. DW: Consultant: CereXis.

The remaining authors declare that the research was conducted in the absence of any commercial or financial relationships that could be construed as a potential conflict of interest.

Publisher's Note: All claims expressed in this article are solely those of the authors and do not necessarily represent those of their affiliated organizations, or those of the publisher, the editors and the reviewers. Any product that may be evaluated in this article, or claim that may be made by its manufacturer, is not guaranteed or endorsed by the publisher.

Copyright © 2021 Amaravathi, Oblinger, Welling, Kinghorn and Chang. This is an open-access article distributed under the terms of the Creative Commons Attribution License (CC BY). The use, distribution or reproduction in other forums is permitted, provided the original author(s) and the copyright owner(s) are credited and that the original publication in this journal is cited, in accordance with accepted academic practice. No use, distribution or reproduction is permitted which does not comply with these terms.

Check for updates

Received: 10 April 2021 | Revised: 16 July 2021 | Accepted: 10 August 2021

DOI: 10.1002/lio2.643

ORIGINAL RESEARCH

Laryngoscope Investigative Otolaryngology

Early phase clinical studies of AR-42, a histone deacetylase inhibitor, for neurofibromatosis type 2-associated vestibular schwannomas and meningiomas

D. Bradley Welling MD, PhD[1] | Katharine A. Collier MD[2] | Sarah S. Burns BS[3,4] | Janet L. Oblinger PhD[3,4] | Edina Shu BS[1] | Beth A. Miles-Markley MS[5] | Craig C. Hofmeister MD[6] | Mina S. Makary MD[7] | H. Wayne Slone MD[7] | Jaishri O. Blakeley MD[8] | S. Alireza Mansouri MD[8] | Brian A. Neff MD[9] | Robert K. Jackler MD[10] | Amir Mortazavi MD[2] | Long-Sheng Chang PhD[3,4,5]

[1]Department of Otolaryngology Head and Neck Surgery, Harvard Medical School, Massachusetts Eye and Ear Infirmary, Massachusetts General Hospital, Boston, Massachusetts, USA

[2]Division of Medical Oncology, Department of Internal Medicine, The Ohio State University College of Medicine and the Comprehensive Cancer Center, Columbus, Ohio, USA

[3]Center for Childhood Cancer and Blood diseases, Abigail Wexner Research Institute at Nationwide Children's Hospital, Columbus, Ohio, USA

[4]Department of Pediatrics, The Ohio State University College of Medicine, Columbus, Ohio, USA

[5]Department of Otolaryngology-Head and Neck Surgery, The Ohio State University College of Medicine, Columbus, Ohio, USA

[6]Department of Hematology & Oncology, Winship Cancer Institute of Emory University, Atlanta, Georgia, USA

[7]Department of Radiology, The Ohio State University College of Medicine, Columbus, Ohio, USA

[8]Departments of Neurology, Neurosurgery, & Oncology, Johns Hopkins University, Baltimore, Maryland, USA

[9]Department of Otolaryngology Head and Neck Surgery, Mayo Clinic, Rochester, Minnesota, USA

[10]Department of Otolaryngology Head and Neck Surgery, Stanford University, Palo Alto, California, USA

Correspondence
D. Bradley Welling, Department of Otolaryngology Head and Neck Surgery, Harvard Medical School, Massachusetts Eye and Ear and Massachusetts General Hospital, 243 Charles Street, Boston, MA 20114, USA.
Email: brad_welling@meei.harvard.edu

Abstract

Objectives: Two pilot studies of AR-42, a pan-histone deacetylase inhibitor, in human neurofibromatosis type 2 (NF2), vestibular schwannomas (VS), and meningiomas are presented. Primary endpoints included safety, and intra-tumoral pharmacokinetics (PK) and pharmacodynamics (PD).

Methods: Pilot 1 is a subset analysis of a phase 1 study of AR-42 in solid tumors, which included NF2 or sporadic meningiomas. Tumor volumes and treatment-related adverse events (TRAEs) are reported (NCT01129193).

Pilot 2 is a phase 0 surgical study of AR-42 assessing intra-tumoral PK and PD. AR-42 was administered for 3 weeks pre-operatively. Plasma and tumor drug concentrations and p-AKT expression were measured (NCT02282917).

D. Bradley Welling, Katharine A. Collier, Sarah S. Burns, Amir Mortazavi, and Long-Sheng Chang contributed equally.

Results from this study were presented in part at the American Society of Clinical Oncology Annual Meeting, May 2016 in Chicago, Illinois and at the 2018 Joint Global Neurofibromatosis Conference, Paris, France, November 2018.

This is an open access article under the terms of the Creative Commons Attribution-NonCommercial-NoDerivs License, which permits use and distribution in any medium, provided the original work is properly cited, the use is non-commercial and no modifications or adaptations are made.
© 2021 The Authors. *Laryngoscope Investigative Otolaryngology* published by Wiley Periodicals LLC on behalf of The Triological Society.

Funding information
Advocure NF2; National Cancer Institute, Grant/Award Numbers: R01CA201382, U01CA076576; The Galloway Family; The Ohio State University Center for Clinical and Translational Science; The Ohio State University Comprehensive Cancer Center, Grant/Award Number: P30CA16058; U.S. Department of Defense, Grant/Award Numbers: W81XWH-14-1-0167, W81XWH-18-1-0547

Results: Pilot 1: Five patients with NF2 and two with sporadic meningiomas experienced a similar incidence of TRAEs to the overall phase I trial. The six evaluable patients had 15 tumors (8 VS, 7 meningiomas). On AR-42, tumor volume increased in six, remained stable in eight, and decreased in one tumor. The annual percent growth rate decreased in eight, remained stable in three, and increased in four tumors. Pilot 2: Four patients with sporadic VS and one patient with meningioma experienced no grade 3/4 toxicities. Expression of p-AKT decreased in three of four VS. All tumors had higher AR-42 concentrations than plasma.

Conclusions: AR-42 is safe. Tumor volumes showed a mixed response, but most slowed growth. On a 40-mg regimen, drug concentrated in tumors and growth pathways were suppressed in most tumors, suggesting this may be a well-tolerated and effective dose. A phase 2 study of AR-42 for NF2-associated tumors appears warranted.

Level of Evidence: 1b, 4.

KEYWORDS
AR-42, histone deacetylase inhibitor, meningioma, neurofibromatosis type 2, vestibular schwannoma

1 | INTRODUCTION

1.1 | Neurofibromatosis type 2 is a debilitating disease

Neurofibromatosis type 2 (NF2) is a highly penetrant, autosomal dominant disorder with an incidence of approximately 1/40 000.[1,2] The mean age at presentation is 20-21 years.[3] Patients develop multiple nervous-system tumors, primarily bilateral vestibular schwannomas (VS), but up to 60% also develop meningiomas.[4] Mutations in the *NF2* tumor suppressor gene cause schwannomas and meningiomas to arise from Schwann cells, and meningothelial or arachnoid cap cells, respectively.

VS disrupt cranial nerve VIII resulting in tinnitus, hearing loss, and vestibular disequilibrium. Deafness and facial nerve paralysis lead to social isolation and communication challenges. Meningiomas or lower cranial nerve schwannomas can cause aspiration, cranial nerve paralysis, and brainstem compression. NF2 shortens life expectancy, particularly in patients with truncating *NF2* mutations or meningiomas.[5,6] Sporadic VS and meningiomas may cause similar debilitating symptoms. Meningiomas are the most common intracranial tumor, constituting 38.2% of all primary intracranial tumors.[4]

1.2 | Improved therapy for VS and meningiomas is urgently needed

Current treatment options for NF2-associated tumors are limited to observation, surgery, or stereotactic radiation.[7] Given the risk of secondary malignancy, radiation is seldom used first-line in children,[8,9] but may be considered in adults. Meningiomas are less radiosensitive than VS, but radiation is still utilized when surgical resection is incomplete or impractical.[10] If tumors grow following radiation, surgical tumor removal from cranial nerves and the brainstem may be complicated by adhesion to adjacent neural structures.

Surgical resection of VS and meningiomas may be necessary to relieve brainstem compression and threat of acute hydrocephalus. Hearing and facial nerve preservation may not be possible. Complications can also include brainstem injury, cerebrospinal fluid (CSF) leak, meningitis, hemorrhage, pneumocephalus, and death. Lower cranial nerve palsies and shared blood supply to the brainstem are especially hazardous. Up to 30% of patients have recurrence following resection of meningiomas.[10] Surgical intervention in a genetic disease is, at best, a temporizing treatment.

No FDA-approved drugs are available for the treatment of NF2-associated tumors despite numerous trials.[11-21] Off-label, bevacizumab has been most widely used, showing decreased VS volumes and hearing improvement in 30%-50% of patients,[14,22] but toxicities prevent long term use. Additionally, meningiomas do not respond to bevacizumab.[23] It is evident that current treatment options for NF2-associated tumors are inadequate.

1.3 | Development of new therapies for NF2 has been difficult

Development of targeted treatments for NF2-associated VS and meningiomas has been challenging in both preclinical and clinical studies. Primary VS and meningioma cells in culture have a limited lifespan and mouse xenograft models of VS do not show consistent

growth.[24,25] Genetically engineered mice with *Nf2*-knockout in Schwann cells do not consistently produce VS.[26,27] Two meningioma mouse models have been successful. *Nf2* inactivation in arachnoidal cells or meningeal precursor cells leads to meningioma in mice[28,29] and *NF2*-deficient Ben-Men-1 cells expressing luciferase have been successfully implanted into the inner table of SCID mice crania.[30]

Clinical trials are difficult to perform because there are relatively few patients with NF2, endpoints must be selected carefully, and any drug candidate must be well tolerated to be considered for long courses of suppressive treatment in this slowly progressive disease in a young patient population.

1.4 | Histone deacetylase inhibitors suppress tumor growth

To assess the activity of 19 small molecules in NF2, isogenic VS- and meningioma-related cell lines with or without *NF2* expression were used. Two of the agents with greatest activity across schwannoma and meningioma cell models were HDAC inhibitors (HDACis): panobinostat, a pan-HDACi, and CUDC-907, a PI3K and HDAC inhibitor.[31]

The PI3K/AKT pathway is activated in human VS and meningiomas.[32-37] Since it is a convergence point for many growth stimuli, and it controls downstream cellular processes such as cell survival, cell proliferation, insulin response, stress response, and differentiation,[38] the PI3K/AKT pathway is an attractive therapeutic target for VS.

AR-42 is an orally bioavailable pan-histone deacetylase inhibitor (HDACi) with tumor inhibitory effects on schwannomas and meningiomas in vitro and in vivo.[39,40] AR-42, also known as REC-2282 or OSU-HDAC42, was formerly licensed by Arno Therapeutics, Parsippany, NJ and now is licensed by Recursion Therapeutics, Salt Lake City, UT. AR-42 was shown to inhibit the growth of human VS and *Nf2*-deficient mouse schwannoma cells with a half-maximal inhibitory concentration (IC_{50}) of 500 nM and 250-350 nM, respectively.[39] It also inhibited primary meningioma cells and *NF2*-deficient benign meningioma Ben-Men-1 cells with IC_{50} values of 1.5 and 1.0 μM, respectively. AR-42 induced cell-cycle arrest at G_2/M, triggered apoptosis, and decreased p-AKT levels in both VS and meningioma cells. In vivo AR-42 inhibited the growth of schwannoma xenografts, induced apoptosis, and decreased AKT activation. Additionally, AR-42 markedly diminished meningioma tumor volumes in a Ben-Men-1 xenograft mouse model[40] and tumors did not return when followed 6 months post-treatment. Collectively, these results demonstrate a high potency of AR-42 against NF2-associated VS and meningiomas.

In a first-in-human, phase I, open-label, 3 + 3 dose-escalation study, AR-42 was investigated for safety and tolerability in patients with multiple myeloma, and T- and B-cell lymphomas.[41] The maximum tolerated dose (MTD) was 40 mg three times weekly for 3 weeks of a 28-day cycle. Subsequently, a phase I, 3 + 3 dose-escalation study was performed with single-agent AR-42 in a cohort of patients with advanced solid tumors to evaluate safety, the MTD, pharmacokinetics (PK), and preliminary clinical activity.[1] The study enrolled 5 patients with NF2, 2 patients with sporadic non-NF2 meningiomas, and 10 patients with various solid tumor malignancies. Patients received AR-42 30, 60, or 80 mg orally three times weekly for 3 weeks of a 28-day cycle. The two dose-limiting toxicities (DLTs) were grade 3 thrombocytopenia and grade 4 psychosis. The recommended phase II dose was 60 mg daily, three times weekly for 3 weeks of a 28-day cycle. The most common treatment-related adverse events (TRAEs) were cytopenias, fatigue, and nausea. The best response was stable disease in 53% of patients (95% CI: 26.6-78.7). A post-hoc subset analysis of the patients with NF2 and non-NF2 meningiomas showed a median progression-free survival of 9.1 months (95% CI: 1.9—not reached) by RECIST criteria. It was concluded that AR-42 was safe and well tolerated, and that further studies may be considered in combination with other agents in advanced solid tumors.[1]

Here, we present two early-phase in-human clinical studies of AR-42 in patients with NF2 and sporadic meningiomas and VS. Pilot 1 is a post-hoc subset analysis of the patients with NF2-associated tumors and sporadic meningiomas from Collier et al.[1] Pilot 2 is a phase 0 surgical study to determine intra-tumoral PK and pharmacodynamics (PD) based on blood samples and surgically resected meningiomas and VS.

2 | MATERIALS AND METHODS

2.1 | Pilot 1

2.1.1 | Study design

Pilot 1 is a post-hoc subset analysis of the open label phase I trial noted above of AR-42 in patients with advanced solid tumors, including NF2-associated VS and meningiomas, to determine safety and tolerability of AR-42 in this patient population.[1] The secondary objective was to analyze change in tumor volumes with AR-42. This was a 3 + 3 dose escalation study starting at 30 mg orally three times weekly for 3 weeks followed by 1 week off every 28-day cycle, as previously published. Toxicities were graded based on the Common Terminology Criteria for Adverse Events v4.0. AR-42 was provided by Arno Therapeutics (Parsippany, NJ). The study was approved by the Ohio State University Institutional Review Board (Protocol 2010C0006, approved 3/24/2010) and conducted in accordance with the Declaration of Helsinki. Written informed consent was obtained from all patients.

2.1.2 | Eligibility criteria

To enroll, patients with CNS tumors had to be at least 18 years old and have NF2-associated or sporadic VS or meningiomas with ≥15% volumetric growth of at least one tumor on pre-enrollment MRI. Additional requirements were an Eastern Cooperative Oncology Group (ECOG) performance status 0-1, normal organ function, and life expectancy >12 months. Exclusion criteria included chemotherapeutic intervention within 4 weeks, major surgery within 3 weeks, malabsorption, or pregnancy.

2.1.3 | Tumor volumetric measurement

Response was monitored with magnetic resonance imaging (MRI). Three-dimensional tumor volumes were measured at least as frequently as (a) within 2 years prior to study entry; (b) at the time of study entry; (c) at end of study; and (d) post-treatment up to 2 years. Volumetric measures were created using Visage 7 Enterprise Imaging software (version 7.1.15; San Diego, CA) with manual and auto-segmentation. Additional contouring in the axial, sagittal, and coronal planes and 3-D image overlay for verification of segmentation accuracy were performed.

Percent tumor volume change was calculated between the start and end of treatment. By the Response Evaluation in Neurofibromatosis and Schwannomatosis (REiNS)[42] criteria for tumor assessment with MRI and volumetric analysis, a 20% volume decrease indicates a partial response, and a 20% volume increase indicates progressive disease. Estimated annual percent growth rates were calculated by dividing the percent volume change by the time between measurements in years. The pre-treatment, on-treatment, and post-treatment annual percent growth rates were compared with a Wilcoxon matched-pairs signed-rank test using R version 3.6.0. A nominal *P*-value ≤.05 was considered statistically significant.

2.2 | Pilot 2

2.2.1 | Study design

Pilot 2 is a phase 0 study of subjects undergoing planned surgical resection of VS or meningioma to evaluate tumor penetration by drug and intra-tumoral growth pathway suppression. The primary objective was to measure expression levels of p-AKT in VS and meningiomas compared with control untreated VS and meningioma tissue samples from our tissue bank. Secondary objectives included measurement of plasma and intra-tumor AR-42 concentrations. Subjects took AR-42 40 mg orally three times per week for 3 weeks prior to tumor resection. The study was started prior to completion of the solid tumor phase I trial; therefore, 40 mg was selected based on the MTD in the phase 1 study of AR-42 for hematologic malignancies.[41] Study drug was provided by Arno Therapeutics. The study was approved by the Massachusetts Eye and Ear Institutional Review Board (Protocol 2018A019856, approved 10/01/2014) and was conducted in accordance with the Declaration of Helsinki. Written informed consent was obtained from all patients.

2.2.2 | Eligibility criteria

To enroll, patients with a VS and/or meningioma diagnosed by MRI with planned surgical resection had to be greater than 18 years of age and have normal organ and bone marrow function. ECOG performance status of 0-1 and the ability to swallow capsules were required. Females of childbearing potential were required to have a negative serum or urine pregnancy test and be willing to comply with contraception. Exclusion criteria included pregnancy, breastfeeding, malabsorption, chronic corticosteroid use, second malignancy, prolonged QT, active infection, anti-neoplastic systemic therapy, or concomitant radiotherapy.

2.2.3 | Pharmacokinetics and pharmacodynamics

Venous blood samples were collected at the time of induction of anesthesia and again at tumor removal, about 3-4 hours from surgery start. Plasma samples were prepared by centrifugation at 4°C. Upon tumor removal, each VS was divided into a peripheral capsule (P) and a tumor center (C). Plasma and tumor samples were rapidly frozen and kept at −70°C until PK analysis by liquid chromatography-tandem mass spectrometry (LC-MS/MS) at The Ohio State University Comprehensive Cancer Center Pharmaco-analytical Shared Resource, as previously described.[25] Plasma and tumor AR-42 concentrations were estimated by comparison to a standard curve of known drug concentrations. Serum levels were compared using a *t*-test with $P \leq .05$ considered statistically significant.

The Supplementary Methods describe in detail the preparation of tumor tissue lysates and quantitation of pAKT, total AKT, p-S6, total S6, p-ERK, and total ERK using fluorescent Western blotting.

3 | RESULTS

3.1 | Pilot 1

3.1.1 | Patients

Five patients with NF2 and two patients with sporadic meningiomas were enrolled between June 2012 and November 2013. Demographics are shown in Table 1. Only one patient (Patient 1.5) had previously received radiation. Enrolled patients received AR-42 either 60 mg (n = 6) or 80 mg (n = 1) orally three times weekly for 3 weeks followed by 1-week off every 28-day cycle. Median duration of treatment was 109 days (range 11-838), about 4 cycles. Patient 1.3 was non-compliant and was dismissed from the study after only six doses, and thus was not evaluable for tumor volume change. Patient 1.5 withdrew consent for mild toxicities after 3 months. Patient 1.7 did not complete cycle 1 due to a DLT and was included only in the safety analysis of the reported phase 1 trial, though tumor volumetric analysis is presented here. The remaining four patients discontinued due to progression.

3.1.2 | Safety and tolerability

Seven patients with NF2 or sporadic meningioma were evaluable for toxicity. Collier et al previously reported the adverse events for the full phase I trial.[1] Table 2 shows the TRAEs for only the subset of

TABLE 1 Patient demographics

Pilot	Patient #	Age	Sex	Weight (kg)	Ethnicity	Diagnosis	Dose (mg)	Days on AR-42	Number of doses
1	1.1	33	F	76.2	Caucasian	NF2	60	838	234
	1.2	48	F	78.5	Caucasian	NF2	60	85	26
	1.4	28	M	76.2	Caucasian	NF2	60	276	89
	1.5	59	F	55.8	Caucasian	Sporadic meningioma	60	133	33
	1.6	20	F	62.2	Caucasian	NF2	60	59	18
	1.7	20	F	47.6	Asian	NF2	80	11	5
2	2.1	69	F	97.1	Caucasian	Sporadic VS	40	21	9
	2.2	40	M	120	Caucasian	Sporadic VS	40	21	11
	2.3	64	M	100.7	Caucasian	Sporadic VS	40	21	9
	2.5	30	M	90.7	Caucasian	Sporadic VS	40	21	8
	2.7	64	M	82.6	Caucasian	Sporadic meningioma	40	21	8

Abbreviations: NF2, neurofibromatosis type 2; VS, vestibular schwannomas.

patients with NF2 and sporadic meningioma. The most common TRAEs of any grade were thrombocytopenia (n = 7), nausea (n = 6), fatigue (n = 6), and diarrhea (n = 6). One of the two DLTs in the phase I study was a grade 4 psychiatric disorder, possibly related to AR-42, at the 80 mg dose level in Patient 1.7 with NF2. This DLT occurred after 10 days of treatment, or 5 doses. Drug was terminated and she came off study. Her psychosis resolved with termination of AR-42, initiation of an anti-psychotic and a benzodiazepine, and treatment of a urinary tract infection. One patient (Patient 1.5) required a dose reduction for fatigue, which was ultimately attributed to hypophysitis from previous cranial irradiation. There were no reported arrhythmias or QT prolongations of any grade. AR-42 was generally well tolerated at 60 mg among the patients with NF2 or sporadic meningioma, though the incidence of toxicities may not be acceptable for chronic use in this young patient population.

3.2 | Efficacy

Tumor volumes and annual percent growth rates prior to entry on study, while on study, and following drug termination are demonstrated in Figure 1. Six patients were evaluable for response and together had 15 evaluable tumors (8 VS and 7 meningiomas). Pre-treatment, 13 of 15 tumors demonstrated volumetric growth of 20% or more as shown in Table S1. As shown in Table 3 and Figure S1, while on AR-42, six tumors showed volume growth of 20% or greater, eight showed stable disease, and one showed a partial response with a 24% decrease in volume. There was no appreciable difference between the response of VS and meningiomas to AR-42. Five VS were stable and three progressed. Four meningiomas were stable or regressed, and three progressed. Analysis of the change in the estimated annual rate of tumor growth from pre-treatment to on-treatment showed that eight tumors had reduced growth rates (>20% decrease in growth rate), three had stable growth rates (± <20% change in growth rate) and four had increased growth rates (>20% increase in growth rate). The median reduction in annual growth rate was −54%, but the pre-treatment and on-treatment growth rates were not significantly different ($P = 0.259$).

After termination of AR-42, four tumors were not available, two because of surgery and two because long-term follow-up was not available. Two patients had progression requiring a tumor to be excised shortly after coming off study. The tumor excised from Subject 1.6 was a WHO-grade II meningioma. Subject 1.4 had his left VS re-excised and the adjacent stable posterior fossa meningioma was also removed, found to be WHO-grade I. Of the 11 remaining evaluable lesions, when compared to growth rates on AR-42, 4 tumors rebounded in growth rate (increased more than 20%), 4 were not changed, and 3 decreased. Pre-treatment (median = 60%) to post-treatment (median = 10%) estimated annual growth rates were not statistically different ($P = .083$). Nor did on-treatment (median = 22%) to post-treatment estimated growth rates differ ($P = .760$).

Though preservation of hearing was not a prespecified endpoint, standard of care audiograms were monitored for the five patients with NF2. The two patients with meningiomas did not have involvement of the eighth cranial nerve and were not monitored with audiograms. Audiometric results are summarized in Table S2. Subject 1.2 was profoundly deaf in both ears prior to study initiation and no change was noted with treatment. Three patients (1.1, 1.4, and 1.7) had profound deafness in one ear with measurable hearing in the contralateral ear that remained stable on AR-42. Of note, Patients 1.1 and 1.4 had radiographically stable disease on AR-42 and remained on treatment for approximately 27.5 and 9 months, respectively. Patient 1.7 only received AR-42 briefly prior to experiencing a DLT in cycle 1. Conversely, Patient 1.6, who had radiographic progression after 2 months on AR-42, also had a decline in hearing while on treatment from good hearing in both ears at initiation of the study with 17 db pure tone average (PTA) to 55 db PTA with a loss of discrimination from 100% to 0%. Though the numbers are small in this post hoc analysis, it appears that preservation of hearing was associated with radiographic assessment.

TABLE 2 Treatment-related adverse events

	Pilot 1 (60-80 mg)					Pilot 2 (40 mg)				
Adverse event	Grade 1	Grade 2	Grade 3	Grade 4	Total	Grade 1	Grade 2	Grade 3	Grade 4	Total
Thrombocytopenia	1	5	1		7	3				3
Fatigue	2	3	1		6	3				3
Nausea	5		1		6	2				2
Diarrhea	5		1		6	1				1
Anemia	3	2			5	2				2
Increased creatinine	3	2			5					
Leukopenia	4				4	2	1			3
Neutropenia	2	2			4	1				1
Anorexia	2	1	1		4					
Confusion	3				3	4				4
Lymphopenia		2	1		3	1				1
Myalgia	3				3	1				1
Hypoalbuminemia	2	1			3					
Low serum phosphate	1	1	1		3					
Taste change	2				2	1				1
Hypocalcemia	2				2					
High alanine aminotransferase (ALT)	2				2					
Increased INR	1		1		2					
Weight loss	1		1		2					
Emesis	2				2					
Constipation	2				2					
Urinary frequency	2				2					
Hypernatremia	2				2					
Headache		1			1	1	2			3
Dyspepsia	1				1	2				2
Facial weakness	1				1	2				2
Rash	1				1	1				1
Hypokalemia	1				1					
High aspartate aminotransferase (AST)	1				1					
Psychotic disorder				1	1					
Vestibular disorder		1			1					
Hematuria	1				1					
Urinary tract infection		1			1					
Upper respiratory infection		1			1					
Thrombotic event			1		1					
Leukocytosis						2				2
Non-cardiac chest pain						2				2
CSF leak							2			2
Lymphocytosis							1			1
Tremor						1				1
Scleral disorder						1				1

3.3 | Pilot 2

3.3.1 | Patients and tolerability

Six patients with sporadic VS and one patient with sporadic meningioma enrolled between 2014 and 2017. Two patients with VS (2.4 and 2.6) withdrew prior to beginning AR-42 treatment. Demographics are shown in Table 1, and TRAEs are illustrated in Table 2. Two patients (2.5 and 2.7) had thrombocytopenia (<100K platelets) preoperatively, but withholding the last dose of AR-42 prior to surgery resulted in rapid recovery to a normal platelet count, and surgery proceeded as scheduled. Two subjects had postoperative CSF leaks. There were no arrhythmias or QT changes.

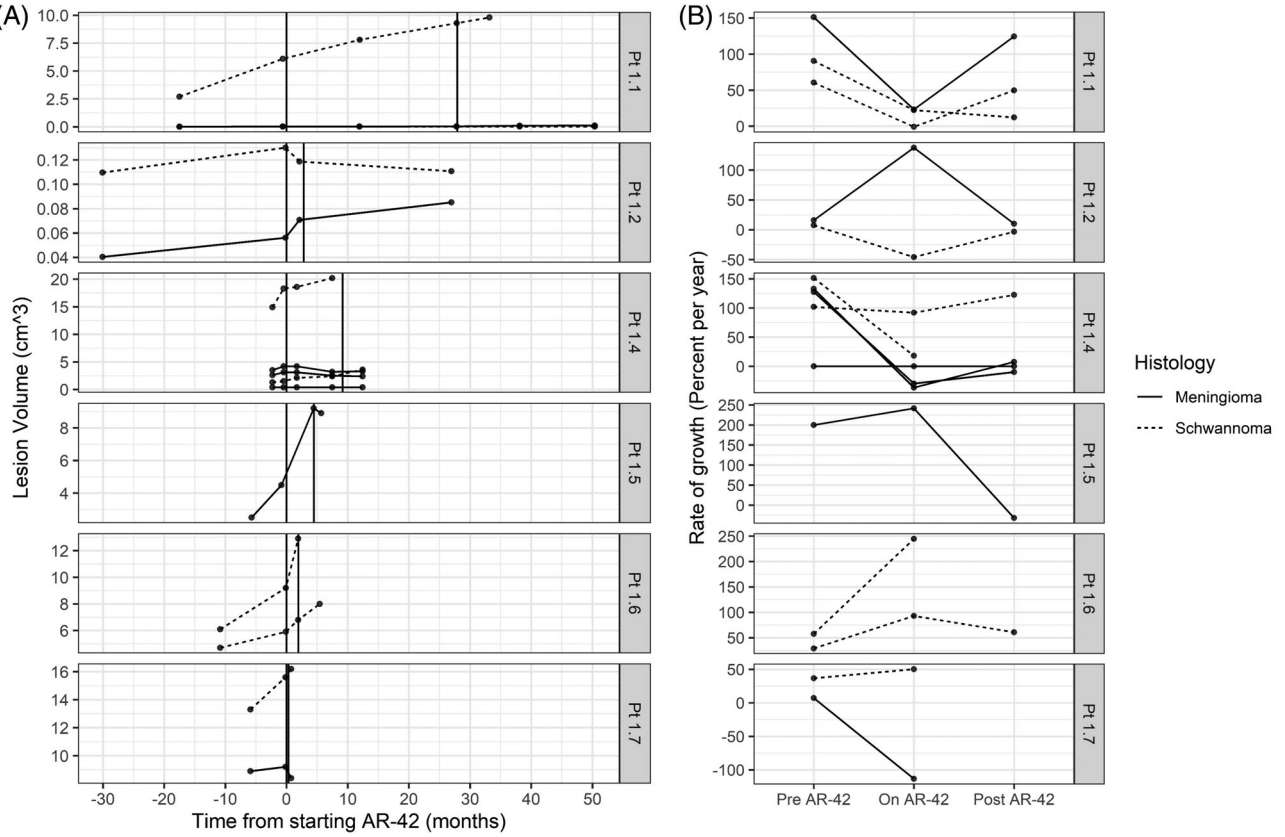

FIGURE 1 Pilot 1—Change in tumor volumes and annual rate of tumor growth. A, Change in 3-D tumor volume in cm^3 over time. Vertical black lines indicate initiation and discontinuation of AR-42. B, Annual estimated rate of growth, in percent per year, pre-treatment, on AR-42, and post-treatment

TABLE 3 Pilot 1—Summary of volumetric tumor growth and annual estimated growth rates

Patient	Days on AR-42	Tumor location	Histology	% Volume growth on Rx	On Rx response	Est. annual growth rate			Change in GR Pre to On Rx (%)	Change in GR Pre to post Rx
						Pre Rx (%)	On Rx (%)	Post Rx		
1.1	837	Right IAC	Schwannoma	−2	SD	60	−1	50%	−61	−10%
		Left parieto-occipital	Meningioma	54	PD	151	23	125%	−128	−26%
		Right neck	Schwannoma	52	PD	91	22	12%	−69	−79%
1.2	84	Left trigeminal	Schwannoma	−9	SD	8	−46	−3%	−54	−11%
		Right intradural C1	Meningioma	26	PD	16	138	10%	122	−6%
1.4	275	Left IAC	Schwannoma	60	PD	102	92	122%	−10	20%
		Left posterior fossa	Meningioma	−24	PR	133	−37	8%	−170	−125%
		Let foramen magnum	Meningioma	−19	SD	128	−30	−10%	−158	−138%
		Right IAC	Schwannoma	9	SD	151	18	Surgery	−133	N/A
		Right anterior falx	Meningioma	0	SD	0	0	0%	0	0%
1.5	134	Right petroclinoid	Meningioma	104	PD	200	241	−32%	41	−232%
1.6	58	Left IAC	Schwannoma	15	SD	29	93	61%	64	32%
		Right IAC	Schwannoma	40	PD	58	245	Surgery	187	N/A
1.7	10	Left IAC	Schwannoma	4	SD	37	50	N/A	13	N/A
		Left prepontine cistern	Meningioma	−9	SD	7	−113	N/A	−120	N/A

Abbreviations: C1, cervical level 1; Est., estimated; GR, growth rate; IAC, internal auditory canal; NA, not applicable; PD, progressive disease (>20% increase in volume); PR, partial response (>20% decrease in volume); Rx, AR-42; SD, stable disease.

TABLE 4 Pilot 2—Plasma and tumor concentrations of AR-42

AR-42	Concentration in plasma (nM)				
Patient #	2.1	2.2	2.4	2.6	2.7
Before surgery	362.3	224.2	61.8	3.5	99.1
At tumor removal	303.7	121.1	36.8	3.4	72.9
	Concentration in tumors (nM)				
Capsule	624.2	429.4	230.6	16.2	5296.6
Center	577.0	586.6	289.0	7.1	1766.2
Capsule/plasma	1.72	1.87	3.73	4.67	53.4
Center/plasma	1.59	2.62	4.68	2.05	17.8

Note: Nanomolar (nM) drug concentrations were measured in plasma pre-operatively before anesthesia and at tumor removal. AR-42 concentration was measured in the peripheral capsule and center of each tumor. The tumor to plasma ratios of AR-42 were calculated by dividing the drug concentration for the tumor capsule or center by the corresponding pre-anesthesia plasma concentration. Plasma and tumor concentrations listed are the mean of three trials. The VS and meningioma exhibited higher concentrations of AR-42 than did the plasma samples.

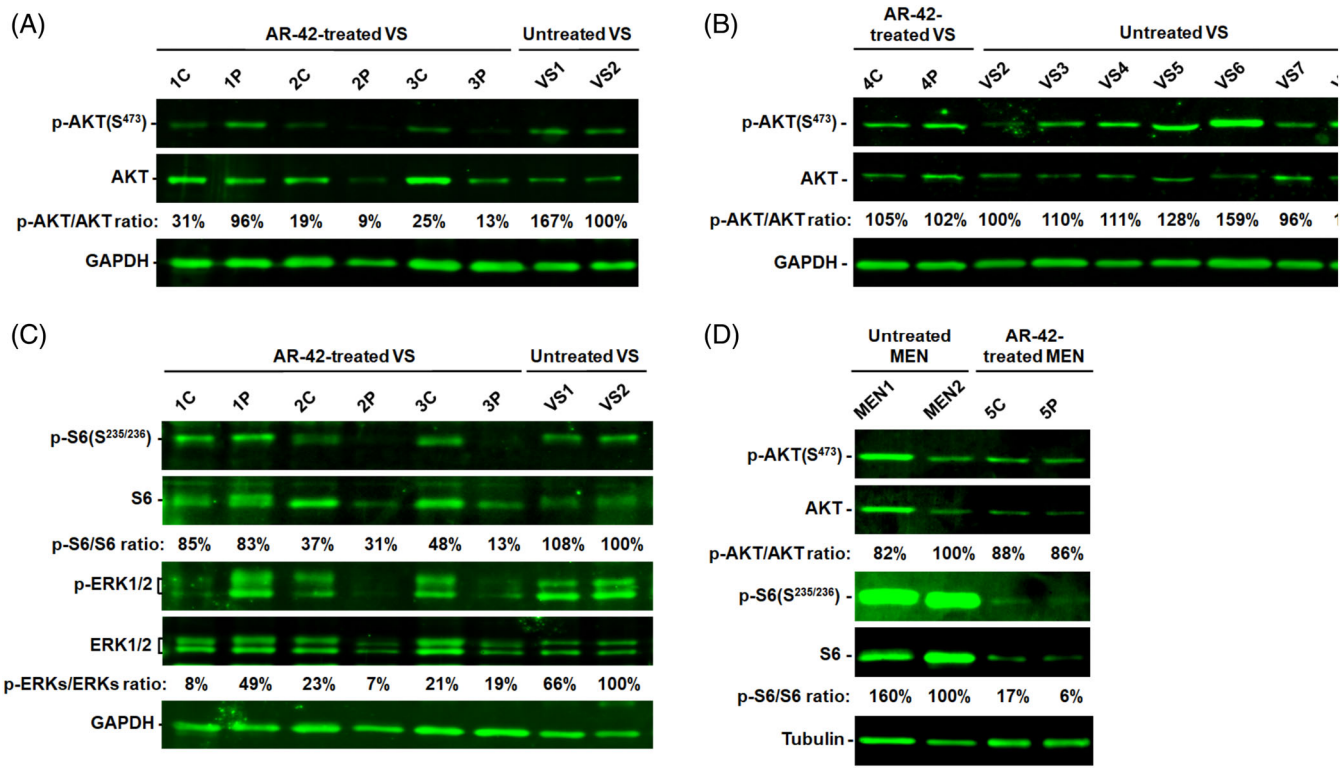

FIGURE 2 Pilot 2—AR-42 suppressed the AKT and ERK pathways in VS. A, AR-42 (or REC-2282) decreased p-AKT levels in three of four treated VS compared to untreated tumors VS1 and VS2. B, Patient 2.4 did not have reduced p-AKT in the tumor, compared with seven untreated VS controls. Quantitation of the normalized p-AKT/AKT ratio is depicted as percentage relative to the untreated VS2 set as 100%. C, AR-42-treated VS also showed reduced levels of p-S6, downstream of the AKT/mTOR pathway, as well as p-ERKs. Quantitation shown is a percentage of p-S6/S6 or p-ERKs/ERKs relative to VS2 set as 100%. D, Suppression of p-S6 was also observed in an AR-42-treated meningioma compared to untreated tumors (MEN1 and MEN2); however, reduction of p-AKT was not detected. Shown below the blot is the relative percentage of p-AKT/AKT or p-S6/S6 relative to the untreated MEN2 set as 100%. C, core of tumor; MEN, meningioma; P, periphery of tumor; VS, vestibular schwannoma

3.3.2 | Plasma and tumor PK/PD

Table 4 shows plasma drug concentrations before and at the time of tumor removal. For PK analysis, AR-42 was stable in blood kept on ice for more than 4 hours (Table S3). In the first three patients with VS, the plasma concentration of AR-42 ranged from 0.062 to 0.36 μM and remained stable before and at the time of tumor removal. There was no statistically significant difference between the preoperative serum levels and serum levels at the time of tumor removal by paired *t* test with $P = .07$. The concentrations of AR-42 in VS ranged from

0.23 to 0.62 μM. AR-42 appeared to concentrate in three of the four VS tumors, with similar drug levels observed in the center and capsule of each tumor. A fourth patient with VS exhibited very low plasma levels of AR-42. This patient had withheld the final dose of AR-42 prior to surgery to allow recovery of thrombocytopenia. The plasma levels of AR-42 in the patient with meningioma were 0.099 and 0.073 μM before and after anesthesia, respectively. Interestingly, the concentrations of AR-42 in the meningioma reached high concentrations in the tumor center (1.8 μM) and capsule (5.3 μM). This analysis was repeated in triplicate to verify the unexpectedly high AR-42 levels compared to VS tumors. The results indicate that AR-42 may concentrate in VS and meningioma tumors. In our previous in vitro studies, we had found an IC_{50} of ~0.5 μM for schwannomas and ~1 μM for meningiomas.[39,40] Thus, the tumor concentrations of AR-42 reached likely effective doses in three of four VS and the meningioma.

In line with these results, we observed decreased p-AKT levels in three of four AR-42-treated VS tumors, particularly in the center of tumors (Figure 2A,B). The levels of p-ERKs and the downstream target of the AKT/mTOR pathway, p-S6, were also substantially reduced in three of four AR-42-treated VS (Figure 2C). However, the VS in the fourth AR-42-treated patient did not show reduction in p-AKT, which is consistent with the observed low concentrations of drug in the plasma. Drug logs indicate that this patient took 8 of 10 planned doses. Similarly, the meningioma from Patient 2.7 also showed reduction in p-S6 (Figure 2D). Surprisingly, p-AKT was not reduced in this tumor compared with untreated meningioma tumors, despite high tumor drug concentrations. AR-42 also reduced AKT phosphorylation in primary human VS cells (Figure S2). Taken together with the PK data, these results suggest that AR-42 decreases p-AKT, p-ERK, and p-S6 in the majority of treated tumors.

4 | DISCUSSION

These pilot studies found AR-42 had a tolerable profile for patients with NF2 and NF2-related tumors. Overall toxicity was not different from other patients with solid tumors in the parent study. The most common TRAEs of any grade in the two pilot studies combined were thrombocytopenia, fatigue, and nausea. This is consistent with the phase I study of AR-42 in hematologic malignancies, where the most common adverse events were cytopenias.[41] Thrombocytopenia occurred in all Pilot 1 subjects and 2 of our 5 Pilot 2 subjects. Only one patient (1.7) reached grade 3 thrombocytopenia and no bleeding episodes occurred. Two patients in Pilot 2 had mild pre-operative thrombocytopenia that improved with dose hold. One patient in Pilot 1 required a dose reduction for fatigue, ultimately not attributed to AR-42. The only adverse event leading to discontinuation of treatment was grade 4 psychosis in one patient in Pilot 1, which may have been attributable to AR-42, steroids, anti-emetics, or an underlying mood disorder. Notably, this patient received the highest dose of 80 mg, and also had the smallest body weight. Collier et al noted that higher maximum serum concentrations of AR-42 and median area-under-the-curve (AUC) were associated with an increase in grade 3 and 4 toxicities.[1] The mean maximal plasma concentration of AR-42 for patients who received the 60 mg dose on day one was 1.48 (±0.38) μM, but for Patient 1.7, who received the 80 mg dose on day one, the maximum plasma concentration was 3.25 μM.[1] However, since only two patients in the phase I study received 80 mg, no conclusions can be drawn. Notably, in Pilot 2 where patients only received 3 weeks of AR-42 at 40 mg, there were no grade 3 or 4 toxicities.

In Pilot 2, two subjects had postoperative CSF leaks, which is higher than the usual rate of 5%. This is of uncertain significance and was not thought to be related to AR-42. If a phase 2 study is initiated, consideration should be given for a pre-operative washout period. There were no other surgical side effects seen; in particular, no intra- or post-operative bleeding was noted. No QT prolongation or cardiac toxicity occurred in any patient in either pilot. Early concerns of QT prolongation and cardiac toxicity from HDACis[43] have failed to show clinically relevant drug-induced QTc changes.[44,45] Nonetheless, further due diligence with QT monitoring is warranted with AR-42.

Overall, there was variable volumetric response of tumors, even within patients. Of note, the volumetric measurements are from a post-hoc, subset analysis of a phase I trial, which was not designed or powered to show efficacy. Although tumor volumes showed that only one tumor (7%) had a partial response, eight others (53%) remained stable. The partial response, which was the posterior fossa meningioma of Patient 1.4, was durable, lasting 3 years. Looking at estimated percent annual growth rates, eight tumors (53%) slowed their growth and three (20%) had stable growth. Overall, this suggests possible anti-tumor activity. There was no appreciable difference between the response of VS and meningiomas. A larger phase II trial of AR-42 for sporadic or NF2-associated VS and meningiomas is needed to adequately evaluate efficacy. In Pilot 1, three patients had initially stable disease, then had progression months later, suggesting that they developed resistance to AR-42. The mechanism of resistance to AR-42 in NF2 or sporadic meningioma is not known. The variability of response and developed resistance to AR-42 may occur at a genomic, expression, epigenetic, or microenvironment level, or may be due to variability of drug delivery, and needs further exploration.

In Pilot 2, AR-42 given at 40 mg for 3 weeks pre-operatively appeared to concentrate in tumors at levels sufficient to suppress the AKT/PI3K pathway in most tumors. Intra-tumoral drug concentrations at or about the IC_{50} were reached. Subjects 2.6 and 2.7 are noteworthy, both who held the last dose for thrombocytopenia. Subject 2.6 had plasma and tumor levels of AR-42 which were 10 to 100-fold less than tumor levels in the other four subjects; however, the ratios of drug in tumor to plasma were similar to the other subjects with VS. Interestingly, the WHO grade I meningioma in subject 2.7 concentrated AR-42 at levels 10-fold higher than the VS. Although AR-42-treated VS exhibited reduced levels of p-AKT and p-S6, the treated meningioma only showed decreased p-S6. One possible explanation could be feedback signaling, resulting in the reactivation

of p-AKT.[46-48] Alternatively, p-AKT may be more liable to dephosphorylation in meningioma than VS tissues during biopsy specimen storage. Although *NF2* mutations disrupt the merlin pathway in both tumor types, the mechanism of tumor growth appears to be different by kinome analysis.[31] Drug combinations will likely be necessary to suppress alternative growth pathways and adequately treat both NF2-associated tumor types. Further, preclinical studies and early phase clinical trials (NCT00731731, NCT00302159) support combination of HDACis with radiation.[49-55] Future studies for NF2 or sporadic meningioma may consider the use of AR-42 as a radiosensitizing agent.

We acknowledge the limitations of these pilot studies. Pilot 1 is a post-hoc subset analysis of a larger phase I study, which was not designed to evaluate efficacy. For Pilot 2, the supplier of AR-42 was unfortunately unable to continue to supply drugs after 2017. We elected to present the data on five of the originally planned 20 patients hoping to expedite further drug availability. Accrual to Pilot 2 was also limited by patient willingness to accept potential additional perioperative risk without a reasonable likelihood of benefit from only 3 weeks of therapy with AR-42. Other limitations inherent in small pilot studies include possible selection bias, lack of control subjects, and the inability to perform meaningful statistical analysis. Despite these limitations, we feel that the presented pilot studies are valuable to the field.

5 | CONCLUSION

In summary, AR-42 was safe and well tolerated in both pilots, but no grade 3-4 toxicities were seen at the lower dose in Pilot 2: 40 mg three times weekly for 3 weeks of a 28-day cycle. Importantly, this lower dose was sufficient to concentrate in tumors at levels sufficient to suppress the intended AKT/PI3K pathway in most tumors, indicating that the 40 mg regimen may be a biologically active, well-tolerated dose of AR-42 for future clinical trials for NF2-associated tumors. Preliminary evidence of possible anti-tumor activity based on volumetric measurements is suggested. A phase II trial of AR-42 for sporadic or NF2-associated VS and meningiomas is needed to adequately evaluate efficacy. Consideration should be given to combination therapy with other medications or radiation.

ACKNOWLEDGMENTS

The authors thank our patients who participated. We also thank the OSUCCC PhASR core for PK analysis. We express appreciation to Edwin M. Choy, MD, PhD, Dominic J. Reda, PhD, and Christopher Moertel, MD, our Data Safety & Monitoring Board; Christine Finn, PharmD consultant; and Arno Therapeutics. This work was supported by the U.S. Department of Defense (W81XWH-14-1-0167 to D. Bradley Welling, W81XWH-18-1-0547 to Long-Sheng Chang); National Cancer Institute of the National Institutes of Health (U01CA076576, R01CA201382 to Amir Mortazavi and Craig C. Hofmeister); the Galloway Family; Advocure NF2; The Ohio State University Comprehensive Cancer Center (P30CA16058); and The Ohio State University Center for Clinical and Translational Science to Long-Sheng Chang. The content is solely the responsibility of the authors and does not represent official views of the sponsors.

CONFLICT OF INTEREST

D. Bradley Welling is a consultant for CereXis, Science 24/7, NFBio, NF2 Biosolutions, and Mulberry Bio. Craig C. Hofmeister has received research grants from Takeda and Oncolytics Biotech; research and personal grants from Janssen, BMS, Sanofi, Nektar, Karyopharm, Imbrium, and Oncopeptides, all outside the submitted work. Amir Mortazavi is on the advisory board for Seattle Genetics and Pfizer and is on the scientific advisory board for Debiopharm Group. His institution (but not him) has received research funding from Acerta Pharma, Genentech, Roche, Merck, Novartis, Seattle Genetics, Astellas Pharma, Mirati Therapeutics, and Bristol-Myers Squibb. The other authors declare no potential conflict of interest. The Ohio State University (OSU) holds the patent on the investigational drug AR-42 (US 10/597022). The Technology Commercialization Office has licensed AR-42 (now called REC-2282) to Recursion Pharmaceuticals using the institution's standard terms, conditions, and approval process, in which no author participated. To assure absence of institutional conflict of interest in assessment of response and attribution of toxicity, both were reviewed by the Cancer Therapy Evaluation Program of the National Cancer Institute prior to reporting results for the phase I study. Safety issues related to dose increases and attribution of response were monitored by The OSU Data Safety Monitoring Committee and The OSU Cancer Center Institutional Review Board for the phase 1 pilot. A separate Data Safety and Monitoring Board of Massachusetts Eye and Ear oversaw pilot study 2.

AUTHOR CONTRIBUTIONS

Conceived the study: D. Bradley Welling, Amir Mortazavi, Craig C. Hofmeister. Performed experiments: Long-Sheng Chang, Janet L. Oblinger, Sarah S. Burns. Provided patient care: D. Bradley Welling, S. Alireza Mansouri, Brian A. Neff, Janet L. Oblinger, Robert K. Jackler, Amir Mortazavi. Analyzed the data: D. Bradley Welling, Katharine A. Collier, Beth A. Miles-Markley, Mina S. Makary, H. Wayne Slone. Prepared the manuscript: D. Bradley Welling, Katharine A. Collier, Long-Sheng Chang, Amir Mortazavi, Edina Shu. Supervised project: D. Bradley Welling, Amir Mortazavi, Long-Sheng Chang. All authors contributed to and approved the manuscript.

ORCID

D. Bradley Welling https://orcid.org/0000-0002-9963-469X
Katharine A. Collier https://orcid.org/0000-0003-0485-8031
Robert K. Jackler https://orcid.org/0000-0003-2525-8377

REFERENCES

1. Collier KA, Valencia H, Newton H, et al. A Phase 1 trial of the histone deacetylase inhibitor AR-42 in patients with neurofibromatosis type 2-associated tumors and advanced solid malignancies. *Cancer Chemother Pharmacol*. 2021;87:599-611.
2. Evans DG. Neurofibromatosis type 2. *Handb Clin Neurol*. 2015;132:87-96.
3. Evans DG, Huson SM, Donnai D, et al. A clinical study of type 2 neurofibromatosis. *Q J Med*. 1992;84(304):603-618.

4. Ostrom QT, Patil N, Cioffi G, Waite K, Kruchko C, Barnholtz-Sloan JS. CBTRUS statistical report: primary brain and other central nervous system tumors diagnosed in the United States in 2013-2017. *Neuro Oncol*. 2020;22(12 Suppl 2):iv1-iv96.
5. Evans DGR, Salvador H, Chang VY, et al. Cancer and central nervous system tumor surveillance in pediatric neurofibromatosis 1. *Clin Cancer Res*. 2017;23(12):e46-e53.
6. Goutagny S, Kalamarides M. Medical treatment in neurofibromatosis type 2. Review of the literature and presentation of clinical reports. *Neurochirurgie*. 2018;64(5):370-374.
7. Mathieu D, Kondziolka D, Flickinger JC, et al. Stereotactic radiosurgery for vestibular schwannomas in patients with neurofibromatosis type 2: an analysis of tumor control, complications, and hearing preservation rates. *Neurosurgery*. 2007;60(3):460-468; discussion 468-470.
8. Evans DG. Neurofibromatosis type 2 (NF2): a clinical and molecular review. *Orphanet J Rare Dis*. 2009;4:16.
9. Balasubramaniam A, Shannon P, Hodaie M, Laperriere N, Michaels H, Guha A. Glioblastoma multiforme after stereotactic radiotherapy for acoustic neuroma: case report and review of the literature. *Neuro Oncol*. 2007;9(4):447-453.
10. Jordan JT, Plotkin SR. Benign intracranial tumors. *Neurol Clin*. 2018;36(3):501-516.
11. Plotkin SR, Halpin C, McKenna MJ, Loeffler JS, Batchelor TT, Barker FG II. Erlotinib for progressive vestibular schwannoma in neurofibromatosis 2 patients. *Otol Neurotol*. 2010;31(7):1135-1143.
12. Ammoun S, Cunliffe CH, Allen JC, et al. ErbB/HER receptor activation and preclinical efficacy of lapatinib in vestibular schwannoma. *Neuro Oncol*. 2010;12(8):834-843.
13. Karajannis MA, Legault G, Hagiwara M, et al. Phase II trial of lapatinib in adult and pediatric patients with neurofibromatosis type 2 and progressive vestibular schwannomas. *Neuro Oncol*. 2012;14(9):1163-1170.
14. Blakeley JO, Ye X, Duda DG, et al. Efficacy and biomarker study of bevacizumab for hearing loss resulting from neurofibromatosis type 2-associated vestibular schwannomas. *J Clin Oncol*. 2016;34(14):1669-1675.
15. Plotkin SR, Duda DG, Muzikansky A, et al. Multicenter, prospective, phase II and biomarker study of high-dose bevacizumab as induction therapy in patients with neurofibromatosis type 2 and progressive vestibular schwannoma. *J Clin Oncol*. 2019;37(35):3446-3454.
16. Goutagny S, Raymond E, Esposito-Farese M, et al. Phase II study of mTORC1 inhibition by everolimus in neurofibromatosis type 2 patients with growing vestibular schwannomas. *J Neurooncol*. 2015;122(2):313-320.
17. Karajannis MA, Legault G, Hagiwara M, et al. Phase II study of everolimus in children and adults with neurofibromatosis type 2 and progressive vestibular schwannomas. *Neuro Oncol*. 2014;16(2):292-297.
18. Angus SP, Oblinger JL, Stuhlmiller TJ, et al. EPH receptor signaling as a novel therapeutic target in NF2-deficient meningioma. *Neuro Oncol*. 2018;20(9):1185-1196.
19. Fong B, Barkhoudarian G, Pezeshkian P, Parsa AT, Gopen Q, Yang I. The molecular biology and novel treatments of vestibular schwannomas. *J Neurosurg*. 2011;115(5):906-914.
20. Troutman S, Moleirinho S, Kota S, et al. Crizotinib inhibits NF2-associated schwannoma through inhibition of focal adhesion kinase 1. *Oncotarget*. 2016;7(34):54515-54525.
21. Ammoun S, Evans DG, Hilton DA, Streeter A, Hayward C, Hanemann CO. Phase 0 trial investigating the intratumoural concentration and activity of sorafenib in neurofibromatosis type 2. *J Neurol Neurosurg Psychiatry*. 2019;90(10):1184-1187.
22. Plotkin SR, Merker VL, Halpin C, et al. Bevacizumab for progressive vestibular schwannoma in neurofibromatosis type 2: a retrospective review of 31 patients. *Otol Neurotol*. 2012;33(6):1046-1052.
23. Nunes FP, Merker VL, Jennings D, et al. Bevacizumab treatment for meningiomas in NF2: a retrospective analysis of 15 patients. *PLoS One*. 2013;8(3):e59941.
24. Chang LS, Jacob A, Lorenz M, et al. Growth of benign and malignant schwannoma xenografts in severe combined immunodeficiency mice. *Laryngoscope*. 2006;116(11):2018-2026.
25. Jacob A, Oblinger J, Bush ML, et al. Preclinical validation of AR42, a novel histone deacetylase inhibitor, as treatment for vestibular schwannomas. *Laryngoscope*. 2012;122(1):174-189.
26. Giovannini M, Robanus-Maandag E, van der Valk M, et al. Conditional biallelic Nf2 mutation in the mouse promotes manifestations of human neurofibromatosis type 2. *Genes Dev*. 2000;14(13):1617-1630.
27. Gehlhausen JR, Park SJ, Hickox AE, et al. A murine model of neurofibromatosis type 2 that accurately phenocopies human schwannoma formation. *Hum Mol Genet*. 2015;24(1):1-8.
28. Kalamarides M, Niwa-Kawakita M, Leblois H, et al. Nf2 gene inactivation in arachnoidal cells is rate-limiting for meningioma development in the mouse. *Genes Dev*. 2002;16(9):1060-1065.
29. Kalamarides M, Peyre M, Giovannini M. Meningioma mouse models. *J Neurooncol*. 2010;99(3):325-331.
30. Burns SS, Chang LS. Generation of noninvasive, quantifiable, orthotopic animal models for NF2-associated schwannoma and meningioma. *Methods Mol Biol*. 2016;1427:59-72.
31. Synodos for NFC, Allaway R, Angus SP, et al. Traditional and systems biology based drug discovery for the rare tumor syndrome neurofibromatosis type 2. *PLoS One*. 2018;13(6):e0197350.
32. Welling DB, Lasak JM, Akhmametyeva E, Ghaheri B, Chang LS. cDNA microarray analysis of vestibular schwannomas. *Otol Neurotol*. 2002;23(5):736-748.
33. Lasak JM, Welling DB, Akhmametyeva EM, Salloum M, Chang LS. Retinoblastoma-cyclin-dependent kinase pathway deregulation in vestibular schwannomas. *Laryngoscope*. 2002;112(9):1555-1561.
34. Jacob A, Lee TX, Neff BA, Miller S, Welling B, Chang LS. Phosphatidylinositol 3-kinase/AKT pathway activation in human vestibular schwannoma. *Otol Neurotol*. 2008;29(1):58-68.
35. Hilton DA, Ristic N, Hanemann CO. Activation of ERK, AKT and JNK signalling pathways in human schwannomas in situ. *Histopathology*. 2009;55(6):744-749.
36. Okada M, Wang Y, Jang SW, Tang X, Neri LM, Ye K. Akt phosphorylation of merlin enhances its binding to phosphatidylinositols and inhibits the tumor-suppressive activities of merlin. *Cancer Res*. 2009;69(9):4043-4051.
37. Blair KJ, Kiang A, Wang-Rodriguez J, Yu MA, Doherty JK, Ongkeko WM. EGF and bFGF promote invasion that is modulated by PI3/Akt kinase and Erk in vestibular schwannoma. *Otol Neurotol*. 2011;32(2):308-314.
38. LoPiccolo J, Blumenthal GM, Bernstein WB, Dennis PA. Targeting the PI3K/Akt/mTOR pathway: effective combinations and clinical considerations. *Drug Resist Updat*. 2008;11(1-2):32-50.
39. Bush ML, Oblinger J, Brendel V, et al. AR42, a novel histone deacetylase inhibitor, as a potential therapy for vestibular schwannomas and meningiomas. *Neuro Oncol*. 2011;13(9):983-999.
40. Burns SS, Akhmametyeva EM, Oblinger JL, et al. Histone deacetylase inhibitor AR-42 differentially affects cell-cycle transit in meningeal and meningioma cells, potently inhibiting NF2-deficient meningioma growth. *Cancer Res*. 2013;73(2):792-803.
41. Sborov DW, Canella A, Hade EM, et al. A phase 1 trial of the HDAC inhibitor AR-42 in patients with multiple myeloma and T- and B-cell lymphomas. *Leuk Lymphoma*. 2017;58(10):2310-2318.
42. Dombi E, Ardern-Holmes SL, Babovic-Vuksanovic D, et al. Recommendations for imaging tumor response in neurofibromatosis clinical trials. *Neurology*. 2013;81(21 Suppl 1):S33-S40.
43. Sager PT, Balser B, Wolfson J, et al. Electrocardiographic effects of class 1 selective histone deacetylase inhibitor romidepsin. *Cancer Med*. 2015;4(8):1178-1185.

44. Iyer SP, Foss FF. Romidepsin for the treatment of peripheral T-cell lymphoma. *Oncologist*. 2015;20(9):1084-1091.
45. Molife R, Fong P, Scurr M, Judson I, Kaye S, de Bono J. HDAC inhibitors and cardiac safety. *Clin Cancer Res*. 2007;13(3):1068; author reply 1068-1069.
46. James MF, Stivison E, Beauchamp R, et al. Regulation of mTOR complex 2 signaling in neurofibromatosis 2-deficient target cell types. *Mol Cancer Res*. 2012;10(5):649-659.
47. Makarevic J, Tawanaie N, Juengel E, et al. Cross-communication between histone H3 and H4 acetylation and Akt-mTOR signalling in prostate cancer cells. *J Cell Mol Med*. 2014;18(7):1460-1466.
48. Rodrik-Outmezguine VS, Chandarlapaty S, Pagano NC, et al. mTOR kinase inhibition causes feedback-dependent biphasic regulation of AKT signaling. *Cancer Discov*. 2011;1(3):248-259.
49. Camphausen K, Burgan W, Cerra M, et al. Enhanced radiation-induced cell killing and prolongation of gammaH2AX foci expression by the histone deacetylase inhibitor MS-275. *Cancer Res*. 2004;64(1):316-321.
50. Shabason JE, Tofilon PJ, Camphausen K. Grand rounds at the National Institutes of Health: HDAC inhibitors as radiation modifiers, from bench to clinic. *J Cell Mol Med*. 2011;15(12):2735-2744.
51. Lu YS, Chou CH, Tzen KY, et al. Radiosensitizing effect of a phenylbutyrate-derived histone deacetylase inhibitor in hepatocellular carcinoma. *Int J Radiat Oncol Biol Phys*. 2012;83(2):e181-e189.
52. Mueller S, Yang X, Sottero TL, et al. Cooperation of the HDAC inhibitor vorinostat and radiation in metastatic neuroblastoma: efficacy and underlying mechanisms. *Cancer Letters*. 2011;306(2):223-229.
53. Chinnaiyan P, Vallabhaneni G, Armstrong E, Huang SM, Harari PM. Modulation of radiation response by histone deacetylase inhibition. *Int J Radiat Oncol Biol Phys*. 2005;62(1):223-229.
54. Camphausen K, Cerna D, Scott T, et al. Enhancement of in vitro and in vivo tumor cell radiosensitivity by valproic acid. *Int J Cancer*. 2005;114(3):380-386.
55. Kim JH, Shin JH, Kim IH. Susceptibility and radiosensitization of human glioblastoma cells to trichostatin A, a histone deacetylase inhibitor. *Int J Radiat Oncol Biol Phys*. 2004;59(4):1174-1180.

SUPPORTING INFORMATION

Additional supporting information may be found in the online version of the article at the publisher's website.

How to cite this article: Welling DB, Collier KA, Burns SS, et al. Early phase clinical studies of AR-42, a histone deacetylase inhibitor, for neurofibromatosis type 2-associated vestibular schwannomas and meningiomas. *Laryngoscope Investigative Otolaryngology*. 2021;1-12. doi:10.1002/lio2.643

Abstract Submission

Basic and translational research

NF2/Schwannomatosis

NF2018/ABS-184

Novel drug discovery for NF2-deficient meningiomas: Brigatinib causes tumor shrinkage in NF2-deficient meningiomas

Long-Sheng Chang[*1], Sarah S Burns[1], Janet L Oblinger[1], Marc Ferrer[2], Jie Huang[1], Ming Poi[3], Vijaya Ramesh[4], On behalf of the Synodos for NF2 Consortium[5] and Full list of Investigators of the Children's Tumor Foundation (CTF)-supported Synodos for NF2 Consortium: https://www.synapse.org/#!Synapse:syn2343195/wiki/62126

[1]Center for Childhood Cancer & Blood Diseases/Department of Pediatrics, The Res Inst at Nationwide Children's Hosp/The Ohio State Univ College of Medicine, Columbus, OH, [2]National Center for Advancing Translational Sciences, NIH, Bethesda, MD, [3]Division of Pharmacy Practice & Science , The Ohio State Univ College of Pharmacy, Columbus, OH, [4]Center for Genomic Medicine and Department of Neurology, Massachusetts General Hospital, Boston, MA, [5]The CTF-supported Synodos for NF2 Consortium, NY, United States

Select your prefered type of presentation: Platform presentation

Background: Originating from meningothelial cells of the arachnoid layer lining the brain, meningiomas cause significant morbidities by compressing adjacent brain tissues, cranial nerves, and blood vessels. Meningiomas can occur spontaneously or are frequently found in NF2 patients carrying *NF2* mutations. As an FDA-approved drug is presently not available for *NF2*-deficient meningioma, we aimed to identify novel targeted drugs that delay tumor progression or cause tumor shrinkage.

Methods: A panel of isogenic *NF2*$^-$ and *NF2*$^+$ arachnoidal cells and *NF2*$^-$ meningioma cells was used to screen ~2000 compounds of diverse mechanisms of action. The anti-tumor activity of the selected drug combination, pharmacokinetic (PK) analysis, PathScan RTK Signaling Antibody Arrays, and Western blots were performed.

Results: From the single agent screen, 45 potent compounds were selected for further combination screening, and 33 drug combinations, including the combination of brigatinib, an inhibitor of multi-RTKs including ALK, and MK2206, an AKT inhibitor, were identified that exhibited a greater synergistic growth inhibition in *NF2*$^-$ cells versus *NF2*$^+$ cells. As a single agent, brigatinib effectively blocked tumor growth and reduced tumor size in the intracranial *NF2*-deficient Ben-Men-1-LucB meningioma model, while MK2206 only modestly suppressed tumor growth. Combined treatment with brigatinib and MK2206 further reduced tumor size. Upon cessation of treatment, the tumors treated with brigatinib or the brigatinib/MK2206 combination regrew. Importantly, these regrown tumors were responsive to these drugs when retreated again. PK analysis revealed that both brigatinib and MK2206 crossed the blood-brain barrier and accumulated in tumor-containing brain tissues. Intriguingly, Ben-Men-1 cells did not express ALK but expressed several phospho-RTKs (p-RTKs) with strong expression of p-ErbB2, ErbB3, FGFR1, TrkA, and VEGFR2. Brigatinib treatment reduced the levels of most of these p-RTKs with the most significant reduction in EGFR, ErbB2, ErbB3, VEGFR2, several Eph receptor members, as well as FAK. In addition, brigatinib treatment attenuated the downstream signals of these kinases, including p-AKT and p-ERKs.

Conclusions: The anti-tumor effects of brigatinib in *NF2*-deficient meningiomas are mediated through inhibition of multiple growth-promoting RTKs but not ALK. Brigatinib and its combination with an AKT inhibitor should be further evaluated in patients with *NF2*-deficient meningiomas (Support: the CTF and US Department of Defense)

Disclosure of Interest: None Declared

Keywords: None

Abstract Submission

Basic and translational research

NF1

NF2018/ABS-185

Identification of silvestrol-related rocaglates with better bioavailability and high potency against malignant peripheral nerve sheath tumors

Long-Sheng Chang[*1], Janet L Oblinger[1], Sarah S Burns[1], Jie Huang[1], Larry Anderson[2], Rulong Shen[3], Li Pan[4], Yulin Ren[4], Barry R O'Keefe[5], A Douglas Kinghorn[4], Jerry M Collins[2]

[1]Center for Childhood Cancer & Blood Diseases/Department of Pediatrics, The Research Institute at Nationwide Children's Hospital/The Ohio State University College of Medicine, Columbus, OH, [2]Division of Cancer Treatment and Diagnosis, National Cancer Institute, NIH, Bethesda, MD, [3]Department of Pathology, The Ohio State University College of Medicine, [4]Division of Medicinal Chemistry and Pharmacognosy, The Ohio State University College of Pharmacy, Columbus, OH, [5]Division of Cancer Treatment and Diagnosis and Molecular Targets Program, Center for Cancer Research, National Cancer Institute, NIH, Bethesda, MD, United States

Select your prefered type of presentation: Platform presentation

Background: Malignant peripheral nerve sheath tumors (MPNSTs) frequently overexpress eIF4F components, and the eIF4A inhibitor silvestrol effectively suppresses MPNST growth. However, silvestrol has suboptimal drug-like properties, including a bulky structure and poor oral bioavailability. Our objectives are to identify potent silvestrol-related rocaglates and to determine their bioavailability, anti-tumor effects, and mechanisms of action.

Methods: *NF1*$^{+/+}$ STS26T and *NF1*$^{-/-}$ ST8814 MPNST and 697 and silvestrol-resistant 697-R leukemic cells were treated with various concentrations of each rocaglate. Cell proliferation assays, flow cytometry, Western blots, and pharmacokinetic (PK) analysis were performed. A quantifiable, orthotopic *NF1*-deficient MPNST mouse model and immunohistochemistry were conducted to assess antitumor effects.

Results: Among 10 silvestrol-related rocaglates lacking the dioxanyl ring examined, didesmethylrocaglamide (DDR) and rocaglamide (ROC) had potent growth-inhibitory activity comparable to silvestrol in MPNST cells. Structure-activity relationship analysis revealed that the dioxanyl ring in silvestrol was dispensable while the C-8b hydroxyl group was essential for cytotoxicity. DDR and ROC arrested MPNST cells at G_2/M and significantly increased the sub-G_1 fraction. Accordingly, these rocaglamides induced cleavage of caspases 3 and 7 and poly(ADP-ribose) polymerase, while decreasing total protein levels of these apoptotic markers, consistent with translation inhibition. Additionally, DDR and ROC reduced the levels of mitogenic kinases AKT and ERK1/2. Unlike silvestrol, DDR and ROC inhibited proliferation of silvestrol-resistant 697-R leukemic cells, which over-express the MDR1 multidrug transporter, at IC_{50} values similar to silvestrol-sensitive 697 cells, suggesting that these rocaglamides may be more bioavailable. PK analysis confirmed that ROC had 50% oral bioavailability. Importantly, ROC, when administered intraperitoneally or orally, potently suppressed the growth of luciferase-expressing *NF1*$^{-/-}$ ST8814-Luc MPNST xenografts with no overt toxicity. Treated tumors had abundant phospho-histone H3 labeling and more cleaved caspase 3-positive cells, consistent with G_2/M arrest and indicative of increased apoptosis, respectively.

Conclusions: The more favorable drug-like properties and potent anti-tumor effects suggest that ROC and DDR have potential to become viable MPNST treatments. (Support: CancerFree Kids, the US Department of Defense, and National Cancer Institute, NIH)

Disclosure of Interest: None Declared

Keywords: None

Abstract Submission

Basic and translational research

NF2/Schwannomatosis

NF2018/ABS-151

Preclinical Assessment of MEK1/2 Inhibitors for Neurofibromatosis Type 2-Associated Schwannomas Reveals Differences in Efficacy and Drug Resistance Development.

Cristina Fernandez-Valle[*1], Marisa Fuse[1], Christine Dinh[2], Jeremie Vitte[3], Joanna Kirkpatrick[4], Thomas Mindos[4], Stephani Campion[5], Konstantin Brnjos[1], Maria Clara Franco[6], Jie Huang[7], Juan Young[2], Alejandra Petrilli[1], Denise Yan[2], Rahul Mittal[2], Rulong Shen[8], Fred Telischi[2], Long-Sheng Chang[7], Helen Morrison[4], Marco Giovannini[3], Xue-Zhong Liu[2]

[1]University of Central Florida, Orlando, [2]University of Miami Miller School of Medicine, Miami, [3]David Geffen School of Medicine, UCLA, Los Angeles, United States, [4]Leibniz Institute on Aging, Jena, Germany, [5]Orlando Health , Orlando, [6] Oregon State University, Corvallis, [7]Nationwide Children's Hospital, [8]Ohio State University, Columbus, United States

Select your prefered type of presentation: Platform presentation

Background: Neurofibromatosis type 2 (NF2) is a genetic tumor disorder caused by loss of function of the *NF2*/merlin tumor suppressor gene. A hallmark of NF2 is formation of bilateral vestibular schwannomas (VS) for which no FDA-approved drug is presently available. Because merlin modulates activity of the Ras/Raf/MEK/ERK pathway, we investigated repurposing drugs targeting MEK1/2 to treat NF2-associated schwannomas.

Methods: Mouse and human merlin-deficient Schwann cell (MD-MSC/HSC) lines were screened against six MEK1/2 inhibitors. Efficacious drugs were tested in orthotopic allograft and *NF2* transgenic mouse models. Proteome and pathway analyses were conducted. Drug efficacy was examined in primary human VS cells with *NF2* mutations and correlated with differential DNA methylation patterns.

Results: Trametinib, PD0325901, and cobimetinib were the most potent in reducing MD-MSC/HSC viability. Each decreased pERK1/2 and cyclin $D_{1,}$ increased p27, and induced caspase 3 cleavage in MD-MSCs. Proteome analysis was consistent with cell cycle arrest and activation of pro-apoptotic pathways in trametinib-treated MD-MSCs. The three inhibitors slowed the growth of MD-MSC allografts compared to controls. However, decreased pERK1/2, cyclin $D_{1,}$ and Ki67 levels were observed in PD0325901 and cobimetinib, but not trametinib treated grafts. Eight weeks of trametinib treatment reduced tumor burden and average tumor size compared to controls in the *NF2* transgenic mouse model; tumors did not exhibit reduced pERK1/2 staining compared to control. Both trametinib and PD0325901 modestly reduced viability of several primary human VS cells with *NF2* mutations. DNA methylation analysis of PD0325901-resistant versus -susceptible VS identified differentially methylated regions in genes that could contribute to drug-resistance.

Conclusions: This comprehensive pre-clinical study demonstrates efficacy differences and possible emergence of drug resistance among MEK inhibitors in schwannoma models and supports further investigation of MEK inhibitors alone and in combination with other targeted drugs as treatments for NF2-associated schwannomas.

Disclosure of Interest: None Declared

Keywords: None

Abstract Submission

Clinical research

NF2/Schwannomatosis

NF2018/ABS-215

Phase 1 and Phase 0 studies of AR-42, a pan histone deacetylase inhibitor, in subjects with neurofibromatosis type 2 (NF2)-associated vestibular schwannomas and meningiomas

D. Bradley Welling[*1], Sarah Burns[2], Janet Oblinger[3], Beth Miles-Markley[4], Amir Mortazavi[5], Amy Quinkert[6], Jaishri Blakeley[7], S. Alireza Monsouri[8], Brian Neff[9], Robert Jackler[10], Long-Sheng Chang[2,3,4]

[1]Otolaryngology, Harvard Medical School, Massachusetts Eye and Ear, Massachusetts General Hospital, Boston, [2]Departments of Pediatrics, [3]Center for Childhood Cancer, Nationwide Children's Hospital, [4]Otolaryngology Head & Neck Surgery, [5]Internal Medicine, The Ohio State University, Columbus, [6]Otolaryngology, Harvard University/MEEI, Boston, [7]Departments of Neurology, Neurosurgery and Oncology, [8]Neurosurgery, Johns Hopkins University, Baltimore, [9]Department of Otolaryngology, Mayo Clinic, Rochester, [10]Department of Otolaryngology, Stanford University, Palo Alto, United States

Select your prefered type of presentation: Platform presentation

Background: Patients with NF2 frequently develop bilateral vestibular schwannomas (VS) and multiple meningiomas. Presently, an FDA-approved medical therapy is not available. The histone deacetylase inhibitor AR-42 suppresses schwannoma growth and causes tumor shrinkage in meningiomas in preclinical models.

Methods: As part of a phase I trial of AR-42 in patients with advanced or recurrent solid tumors for which no standard therapy is available or patients who decline available standard treatment options, patients with NF2-associated VS and meningiomas were enrolled and received AR-42 treatment 3 times weekly for 3 weeks followed by 1-week break. Subsequently, a phase 0 exploratory evaluation of AR-42 for intratumoral pharmacodynamics and pharmacokinetics in VS and meningiomas was performed.

Results: In the phase I trial, 5 NF2 patients were recruited. AR-42 was overall well-tolerated, and the maximum tolerated dose (MTD) was defined at 60 mg. AR-42 demonstrated anti-tumor activity mostly in the form of tumor stability. In one NF2 patient treated for 10 months, AR-42 significantly reduced tumor size in meningiomas and slowed VS growth rates. After cessation of treatment, meningiomas remained small, but VS quickly resumed growth. Tissue samples including bilateral right and left VS, a skull base meningioma, and an optic meningioma from this patient as well as a VS from a second person with NF2 were collected. These 5 tumors underwent comprehensive genomic profiling via FoundationOne. Mutations in *NF2* and *NUP98* were found. A phase 0 study with the primary objective to estimate p-AKT and $p16^{INK4A}$ levels after 3 weeks of oral AR-42 at 40 mg every other day, 3 times a week for 3 weeks preceding surgery, in NF2-related and sporadic VS and meningiomas, as well as control tumor samples from a tissue bank is ongoing. The secondary objectives include assessment of audiometric changes and volumetric tumor reduction and determination of plasma and intra-tumoral AR-42 concentrations. So far, 5 patients were studied. AR-42 concentrations in the plasma and VS of treated patients reached levels around the IC_{50} value determined *in vitro* and was more preferentially concentrated in the tumors. AR-42 decreased the levels of p-AKT, pERK1/2, p-PRAS40, and p-S6 in treated VS.

Conclusions: **Conclusions:**AR-42 achieves therapeutic concentrations in the tumors and hits its targets. Further investigation of AR-42 as an NF2 treatment is ongoing.

(Funding: The US Department of Defense, The Galloway Family, and Advocure NF2)

Disclosure of Interest: None Declared

Keywords: None

revealed by flow cytometry analysis. Overall, we demonstrated that gp120 triggers activation of ERK and Akt signaling in glioma cells, resulting in increased protein synthesis and cell growth. This research was made possible by NIH grant number 1SC1GM122691 and Puerto Rico Science, Technology, and Research Trust grant 2016-00157.

CSIG-40. HETEROZYGOUS IDH1$^{R132H/WT}$ CREATED BY "SINGLE BASE EDITING" INHIBITS HUMAN ASTROGLIAL CELL GROWTH AND PROMOTES CELL MIGRATION

Shuang Wei[1], Jie Wang[2], Olutobi Oyinlade[1], Ding Ma[1], Shuyan Wang[1], Jiang Qian[2] and Shuli Xia[1]; [1]Kennedy Krieger Institute, Baltimore, MD, USA, [2]Johns Hopkins University, Baltimore, MD, USA

Mutations in the isocitrate dehydrogenase 1 (*IDH1*) gene have been identified in a number of cancer types, including brain cancer. The Cancer Genome Atlas project has revealed that *IDH1* mutations occur in 70–80% of grade II and grade III gliomas. Until recently, most of the functional studies of *IDH1* mutations in cellular models have been conducted in overexpression systems with the IDH1 wild type background. In this study, we employed a modified CRISPR/Cas9 genome editing technique called "single base editing", and efficiently introduced heterozygous IDH1 R132H mutation (*IDH1R132H/WT*) in human astroglial cells. Global DNA methylation profiling revealed hypermethylation as well as hypomethylation induced by *IDH1R132H/WT*. Global gene expression analysis identified molecular targets and pathways altered by *IDH1R132H/WT*, including cell proliferation, extracellular matrix, and cell migration. Our phenotype analysis indicated that compared with IDH1 wild type cells, *IDH1R132H/WT* promoted cell migration by up-regulating integrin b4 (ITGB4), and significantly inhibited cell proliferation. All these genotype and phenotype changes were reversed by mutant IDH1 inhibitor AGI-5198. Using our mutated *IDH1* models generated by genome editing, we identified novel molecular targets of *IDH1R132H/WT*, namely Yes-associated protein (YAP) and its downstream signaling pathway Notch, to mediate the cell growth-inhibiting effect of *IDH1R132H/WT*. In summary, the "single base editing" strategy has successfully created heterozygous *IDH1* R132H mutation that recapitulates the naturally occurring IDH1 mutation. Our isogenic cellular systems that differ in a single nucleotide in one allele of the *IDH1* gene provide a valuable model for novel discoveries of *IDH1R132H/WT*-driven biological events.

CSIG-41. ONCOGENE ADDICTION SWITCH FROM NOTCH TO PI3K REQUIRE SIMULTANEOUS TARGETING OF DUAL PATHWAY INHIBITION IN GLIOBLASTOMA

Norihiko Saito, Kazuya Aoki, Nozomi Hirai, Ryo Suzuki, Satoshi Fujita, Haruo Nakayama, Morito Hayashi, Takatoshi Sakurai and Satoshi Iwabuchi; Toho University Ohashi Medical Center, Tokyo, Japan

Notch signaling pathway regulates normal stem cells in the brain and glioma stem cells (GSCs). However, blocking the proteolytic activation of NOTCH with γ-secretase inhibitors (GSIs) fails to alter the growth of some GSCs as GSIs seem to be active in only a fraction of GSCs lines with constitutive NOTCH activity. Here we report loss of PTEN as a critical event leading to resistance to NOTCH inhibition, which causes the transfer of "oncogene addiction" from the NOTCH to the phosphoinositol-3 kinase (PI3K) pathway. We investigated the effects of Notch inhibition in GSC using GSI. Drug cytotoxicity test on 16 GSCs show differential growth response to GSI stratifying GSCs into two groups: responders vs non-responders. Active Notch signaling seems to be important features for the GSC as Notch inhibition only affected GSCs defined as having increased Notch activity. However in the responder group GSCs with the PTEN mutation seems to be less sensitive to GSI treatment. Here we show that NOTCH regulates the expression of PTEN and the activity of the PI3K signaling pathway in GSCs since treatment with GSI attenuated Notch signaling and increases PTEN expression. NOTCH regulates PTEN expression via Hes-1 as knockdown of either Notch or Hes1 led to increase expression of PTEN.This novel observation suggests the need to simultaneous inhibition of both pathways as a means to improve therapeutic efficacy in human glioblastoma.

CSIG-42. HIGH THROUGHPUT KINOME AND TRANSCRIPTOME ANALYSES REVEAL NOVEL THERAPEUTIC TARGETS IN NF2-DEFICIENT MENINGIOMA

Roberta Beauchamp[1], Serkan Erdin[1], Steven Angus[2], Timothy Stuhlmiller[2], Janet Oblinger[3], Justin Jordan[4], Stephen J. Haggarty[1], Scott R. Plotkin[4], Long-Sheng Chang[3], Gary L. Johnson[2], James F. Gusella[1] and Vijaya Ramesh[1]; [1]Massachusetts General Hospital, Center for Genomic Medicine, Boston, MA, USA, [2]University of North Carolina School of Medicine, Department of Pharmacology, Chapel Hill, NC, USA, [3]The Ohio State University College of Medicine, Center for Childhood Cancer and Blood Diseases, Columbus, OH, USA, [4]Massachusetts General Hospital, Department of Neurology, Boston, MA, USA

Meningiomas (MN), the most common adult primary intracranial tumor, arise from the arachnoid/meninges and are non-responsive to chemotherapies with a high recurrence rate despite surgery, necessitating effective non-invasive therapies. Our previous work showed that *NF2* loss activates mechanistic target of rapamycin complex 1 (mTORC1) and mTORC2 signaling, which led to past NF2 clinical trials using rapalogs (RAD001/everolimus), and current meningioma clinical trials with dual mTORC1/mTORC2 inhibitor (mTORi) AZD2014. To understand additional dysregulated, potentially druggable pathways, we undertook an 'omics approach of large-scale kinomics and RNA-sequencing employing CRISPR-modified human arachnoidal cells (ACs), *NF2*-expressing vs *NF2*-null. In *NF2*-null ACs, several kinases were elevated including erythropoietin-producing hepatocellular (EPH)-receptor tyrosine kinase (RTK) family members, Src family kinase (SFK) members, and c-KIT, all targets of dasatinib. *In vitro* treatment of MN cells using mTORi (AZD2014 or INK128) and dasatinib enhanced growth inhibition upon combination mTORi+dasatinib. *In vivo* treatment of an orthotopic mouse MN model showed moderate response to dasatinib with stronger response using INK128 or INK128+dasatinib (e-published in Neuro-Oncology). Our transcriptomic data also revealed increased expression of several ligands/growth factors, particularly NRG1/neuregulin. Expanding these results, we have confirmed increased expression of NRG1 in human *NF2*-null ACs. We also find *NF2*-null ACs secrete NRG1, and in conditioned-media experiments we observe stimulation of ErbB3, EPHA2 and mTOR pathways, suggesting an autocrine signaling mechanism. *NF2*-null AC or MN cells, when stimulated with exogenous NRG1, show enhanced activation of mTOR and EPH pathways besides ErbB3 signaling. Further, lapatinib (multi-ErbB inhibitor) but not erlotinib (EGFR inhibitor) attenuates the NRG1-stimulated activation of ErbB3, EPHA2 and mTOR, suggesting that NRG1-induced activation is EGFR-independent. Taken together, our results support a mechanistic link where NF2 loss increases NRG1/ErbB signaling to EPH/SFK and mTOR pathways, which may be a critical driver of tumorigenesis, thus providing a therapeutic opportunity to co-target these pathways in *NF2*-deficient meningiomas.

CSIG-43. THE TYROSINE PHOSPHATASE PTPN12/PTP-PEST REGULATES PHOSPHORYLATION-DEPENDENT UBIQUITINATION AND STABILITY OF FOCAL ADHESION SUBSTRATES IN INVASIVE GLIOBLASTOMA CELLS

Joseph McCarty, John Morales, Paola Guerrero and Zhihua Chen; MD Anderson Cancer Center, Houston, TX, USA

Glioblastoma (GBM) is an invasive brain cancer with tumor cells that disperse from the primary mass escaping surgical resection, displaying resistance to chemotherapy and radiation, and invariably giving rise to lethal recurrent lesions. Targeted therapies such as the anti-vascular endothelial growth factor (VEGF) blocking antibody bevacizumab have yielded disappointing results in GBM clinical trials, with no improvements in overall patient survival. Many patients treated with bevacizumab develop acquired resistance leading to lethal recurrent lesions associated with robust tumor cell invasion. While a great deal is known about genes and pathways that promote GBM proliferation and neovascularization, relatively little is understood about mechanisms that drive GBM cell invasion during progression or following anti-angiogenic therapy. Here, we report that PTP-PEST, a cytoplasmic protein tyrosine phosphatase encoded by the PTPN12 gene, controls GBM cell invasion by physically bridging the focal adhesion protein Crk-associated substrate (Cas) to valosin containing protein (Vcp), an ATP-dependent protein segregase that selectively extracts ubiquitinated proteins from multiprotein complexes and targets them for degradation via the ubiquitin proteasome system. Both Cas and Vcp are substrates for PTP-PEST, with the phosphorylation status of tyrosine 805 (Y805) in Vcp impacting affinity for Cas in focal adhesions and controlling ubiquitination levels and protein stability. Perturbing PTP-PEST-mediated phosphorylation of Cas and Vcp led to alterations in GBM cell invasive growth in vitro and in pre-clinical mouse models generated with GBM stem cells. Furthermore, acquired resistance to bevacizumab correlates with reduced expression of PTP-PEST in invasive GBM cells. Collectively, these data reveal a novel regulatory mechanism involving PTP-PEST, Vcp, and Cas that dynamically balances phosphorylation-dependent ubiquitination of key focal proteins involved in GBM cell invasion.

CSIG-44. TREATMENT WITH THE CASEIN KINASE 2 INHIBITOR, CX-4945, SENSITIZES MEDULLOBLASTOMA TO TEMOZOLOMIDE

Ryan Nitta[1] and Gordon Li[2]; [1]Stanford University, Stanford, CA, USA, [2]Stanford University, Palo Alto, CA, USA

Medulloblastoma (MB) is the most common malignant pediatric brain tumor, accounting for ~20% of all cases. While current treatments result in

Downloaded from https://academic.oup.com/neuro-oncology/article/20/suppl_6/vi52/5153857 by Serials Division user on 12 October 2020

Abstract presented at the 2019 NF Conference, San Francisco, CA. (Sept. 2019)

Brigatinib as a potential therapy for malignant peripheral nerve sheath tumors

Janet Oblinger, Ph.D.
Nationwide Children's Hospital & The Ohio State University

MPNSTs are highly aggressive soft-tissue sarcomas that have a high risk of recurrence and metastasis and are refractory to current treatment. These tumors can arise spontaneously or from pre-existing plexiform neurofibromas in patients with neurofibromatosis type 1 (NF1), a tumor predisposition syndrome caused by inactivating mutations in the *NF1* tumor suppressor gene which encodes a Ras-GTPase-activating protein. Importantly, even sporadic tumors often incur mutations in the *NF1* gene or the Ras pathway. As a consequence, MPNSTs exhibit upregulation of Ras downstream kinase signaling, including the phosphatidylinositol 3-kinase (PI3K)-AKT-mammalian target of rapamycin (mTOR) and Raf-MEK-ERK mitogen-activated protein kinases. MPNSTs also harbor other genetic alterations, such as aberrant activation of epidermal growth factor receptor (EGFR) and insulin-like growth factor-1 receptor (IGF-1R), suggesting that these receptor tyrosine kinases (RTKs) may be therapeutic targets. Previously we showed that the FDA-approved ALK inhibitor brigatinib (ALUNBRIG™) suppresses multiple RTKs and non-RTKs, including focal adhesion kinase (FAK). Here we demonstrate that brigatinib exhibited growth-inhibitory activity in *NF1*-deficient ST8814 and *NF1*-expressing STS26T MPNST cells. Combination of brigatinib with the dual mTORC1/2 inhibitor INK128 (sapanisertib) yielded enhanced anti-proliferative effects. Treatment of ST8814 cells with brigatinib decreased p-EGFR and p-IGF-1R and their downstream p-AKT and p-S6. Treatment with INK128 also profoundly inhibited p-AKT and p-S6. Interestingly, combination of brigatinib and INK128 further reduced the phosphorylation of these signaling mediators and p-FAK compared to either monotherapy, suggesting cooperation in suppressing the AKT-mTOR pathway. However, we did not detect ALK expression in ST8814 and STS26T cells, indicating that brigatinib mediates growth inhibition via targeting of other tyrosine kinases. Experiments are in progress to investigate the anti-tumor activity of brigatinib in patient-derived xenograft (PDX) models for MPNST. Collectively, our data suggest that brigatinib should be further evaluated as a potential treatment for MPNST.

Full List Authors: Janet Oblinger[1,2] and Long-Sheng Chang[1,2,3]

[1]Center for Childhood Cancer and Blood Diseases, Abigail Wexner Research Institute at Nationwide Children's Hospital and Depts of [2]Pediatrics & [3]Otolaryngology-Head & Neck Surgery, The Ohio State University

Funding: CancerFree KIDS, Department of Defense

Abstract presented at the 2019 NF Conference, San Francisco, CA. (Sept. 2019)

Targeting protein translation with rocaglamide and didesmethylrocaglamide to treat NF1 and NF2 tumors

Long-Sheng Chang
Nationwide Children's Hospital & The Ohio State University

To sustain uncontrolled growth, cancer cells exhibit enhanced protein synthesis by upregulation of the protein translation machinery. Previously we reported that NF1-associated malignant peripheral nerve sheath tumors (MPNSTs) and NF2-related vestibular schwannomas and meningiomas exhibit elevated expression of eIF4A, eIF4E, and eIF4G, components of the eIF4F translation initiation complex, and that the eIF4A inhibitor silvestrol potently suppresses the growth of these tumor cells. Studies by others also show strong anti-tumor activity of silvestrol in several other cancer models, suggesting that it may be a potential cancer treatment. However, silvestrol has suboptimal drug-like properties, including a bulky structure, sensitivity to inhibition by the MDR1 multidrug-resistant transporter, and poor oral bioavailability. By screening 10 silvestrol-related rocaglates lacking the dioxanyl ring, we identified rocaglamide (Roc) and didesmethylrocaglamide (DDR) with potent growth-inhibitory activity comparable to silvestrol in MPNST cells. Structure-activity relationship analysis revealed that the dioxanyl ring present in silvestrol was dispensable for, but may enhance, cytotoxicity. Both Roc and DDR arrested MPNST cells at G_2/M, significantly increased the sub-G_1 fraction, and induced cleavage of caspases 3 and 7 and poly(ADP-ribose) polymerase, while decreasing total protein levels of these apoptotic markers and mitogenic kinases AKT and ERK1/2, consistent with translation inhibition. Additionally, these rocaglamides elevated the levels of γH2AX, a marker of the DNA damage response. Unlike silvestrol, Roc and DDR were not sensitive to MDR1 inhibition. Pharmacokinetic analysis confirmed that Roc had 50% oral bioavailability. Importantly, Roc, when administered intraperitoneally or orally, potently suppressed the growth of orthotopic *NF1*-deficient MPNST xenografts with no overt toxicity. Treated MPNSTs had abundant phospho-histone H3 labeling and more cleaved caspase 3-positive cells, consistent with G_2/M arrest and indicative of increased apoptosis, respectively. In addition, Roc exhibited anti-tumor effects in patient-derived xenograft models for several types of sarcomas, including Ewing sarcoma, osteosarcoma, and rhabdomyosarcoma. Western blot analysis revealed that Roc and DDR decreased multiple oncogenic kinases, including IGF-1R, in sarcoma cells. Further, these rocaglamides potently inhibited proliferation of *NF2*-deficient schwannoma and meningioma cells. The more favorable drug-like properties and potent anti-tumor effects of Roc and DDR suggest that these rocaglamides have potential to become viable treatments for NF1- and NF2-associated tumors, including MPNST, as well as other sarcomas.

Full List Authors: Long-Sheng Chang[1], Janet L Oblinger[1], Sarah S Burns[1], Jie Huang[1], Larry Anderson[2], Rulong Shen[3], Li Pan[4], Yulin Ren[4], Ryan Roberts[1], Barry R O'Keefe[5], A Douglas Kinghorn[4], Jerry M Collins[2]

[1]Ctr for Childhood Cancer & Blood Diseases, Nationwide Children's Hospital/Dept of Pediatrics, The Ohio State Univ, [2]Div of Cancer Treatment and Diagnosis, National Cancer Institute, NIH, [3]Dept of Pathology, The Ohio State Univ, [4]Div of Medicinal Chemistry and Pharmacognosy, The Ohio State Univ Coll of Pharmacy, [5]Div of Cancer Treatment and Diagnosis and Molecular Targets Program, Ctr for Cancer Research, National Cancer Institute, NIH

Funding: CancerFree KIDS, Sunbeam Foundation, Department of Defense

Join us for a day of learning and sharing at our 2019 NF Symposium and iNFo Fair. There will be plenty of opportunities to meet others. Plus, we will have special tables for extra iNFormation and questions.

TOPICS AND AGENDA*

8:00 – 9:00 am Registration, Continental Breakfast, and Socializing
CART (Captioning will be provided for MOST sessions. Email us for more info at info@nfmidwest.org.
Speakers may be added or changed. Look for updated information at www.nfmidwest.org/symposium.

SCHEDULED PRESENTATIONS

(Topics are NOT in order of the actual schedule or in any order of importance and may be subject to change)

- **New NF1, NF2, and Schwannomatosis New Diagnostic Criteria**
- **Regional Clinic Info and Trial Updates**
- **Encouraging Social Connections and Adaptive Behaviors. How Parents Can Help!**—Sandra Cushner-Weinstein LICSW, Children's National Medical Center in Washington, DC; Director of Brainy Camps and Camp New Friends
- **Gene Therapy/Gene Editing**—Robert Kesterson, PhD, University of Alabama, Department of Genetics

NF Type 1 Topics

- **Surgical Management of Cutaneous Neurofibroma: Current Therapy and Future Directions** – Lu Le, MD PhD, University of Texas Southwestern Medical Center
- **Drug Treatment of Cutaneous Neurofibromas: Past, Present, and Future**—Ashley Cannon, MS, CGC, PhD, University of Alabama
- **Translational Research Update on Cutaneous Neurofibromas**—Matt Steensma, MD, Spectrum Health, Francis S Collins Scholar
- **Research Update: Photodynamic Therapy on Cutaneous Neurofibromas**—Medical College of Wisconsin
- **Optic Gliomas/Research and Treatment Update**—Robert Listernick, MD, Lurie Children's Hospital and NF Clinic, Chicago, IL

NF Type 2 Topics

- **Hearing Rehabilitation in NF2: Auditory Brainstem and Cochlear Implantation**—Kevin Peng, MD, Otologist/Neurotologist, House Clinic. Los Angeles, CA
- **Discoveries from Synodos for NF2**—Long-Sheng Chang, PhD, Nationwide Children's Hospital and The Ohio State University College of Medicine
- **NF2 BioSolutions: Accelerating Gene Therapy Research for Neurofibromatosis Type 2**—John Manth, NF2 BioSolutions Board Member

INFORMATION TABLES

We will have tables of various iNFormation on topics related to NF, plus opportunities to visit with our presenters to ask more questions. We will be bringing virtually all the material we have available, with copies for you to take. Examples of iNFormation provided includes (there will be much more!)...

- NF Clinics and their clinical trials
- New Health Supervision Guidelines for Children with NF1
- Care Guideline for Adults with NF1
- Participating in Research
- Learning Disabilities and School Issues
- Medical Imaging for NF1: Radiation Exposure
- Autism Spectrum Disorder Symptomatology in Children with NF1
- Insurance Coverage for Neurofibroma Removal by NF Midwest
- Procedure Codes for Removing a High Quantity of Neurofibromas
- Info on Various Complications in NF1 including…
  - Optic gliomas, seizures, scoliosis, pain, vascular disease, brainstem tumors
- Making a Difference—Raising Funds and Awareness

KIDS GROUPS

CHILDRENS GROUP (Ages 5-12) A fun day is provided for children ages 5-11. This childcare will be provided FREE of charge, but you MUST make a reservation.

TEEN GROUP (Ages 13-18) Bring the older kids for a day of fun, games, and just hanging out. This is a great chance for your kids to meet others with NF. Siblings are also welcome! We ask that you donate $10 per child, if possible. Reservations required.

The kids will be served pizza for lunch.

Please let us know if your children have any special needs so that we can accommodate them better.

SPECIAL NEEDS

- The NF Midwest Symposium will have CART services for the hearing impaired that **will follow the shared and NF2 sessions only.** If you need CART services for the NF1 sessions, please let us know.
- Financial assistance is available from NF Midwest for people from our region who are in need and we waive the registration fee for people traveling more than 90 miles. Our region includes Illinois, Wisconsin, Indiana, Iowa, Kentucky and the eastern half of Missouri. If you are not from our area, you will have to contact your local NF organization or another institution that may be able to assist you. Please, call us if you need assistance from us or in reaching another organization.
- If you have any other special needs, please let us know as soon as possible.

ACCOMMODATIONS AND TRANSPORTATION

HOTELS A block of rooms is available at the Chicago Marriott Northwest/Hoffman Estates for $89 a night. A shuttle can take you to and from the venue if needed. Make a reservation at www.nfmidwest.org/hotel or call (847) 645-9500 and ask for the NF Midwest group rate. There are also many other hotels in the area.

TRAVEL BY CAR See map in this brochure for directions.

TRAVEL BY AIR NIU is 20 miles from O'Hare International Airport; 40 miles from Midway Airport.

TRAVEL FROM CHICAGO We would like to try to help people who may not have cars travel to the symposium from the city. If you are traveling from the city and need help please contact us so we can see if special arrangements can be made.

TRAVELING MORE THAN 90 MILES If you are traveling more than 90 miles and are in our region, or NF Upper Midwest's region, (this includes Illinois, Indiana, Iowa, Kentucky, Minnesota, Missouri, North Dakota, South Dakota, or Wisconsin) as a service to both of our communities we will waive your fees. Use the coupon code "90miles".

ADDRESS AND DIRECTIONS

Northern Illinois University (NIU)—Hoffman Estates
5555 Trillium Blvd.
Hoffman Estates, IL 60192
Phone: (847) 645-3000

From I-90 Eastbound
Exit Route 59 north (left) to Higgins Road (IL Rt. 72). Turn west (left) onto Higgins Road. Turn south (left) onto Beverly Road. Turn east (left) onto Trillium Boulevard. The NIU Hoffman-Estates is on the right, across from the Sears Merchandising Group Headquarters.

From I-90 Westbound
Exit Beverly Road north (right) to Trillium Boulevard. Turn east (right) onto Trillium Boulevard. The NIU Hoffman-Estates is on the right, across from the Sears Merchandising Group Headquarters.

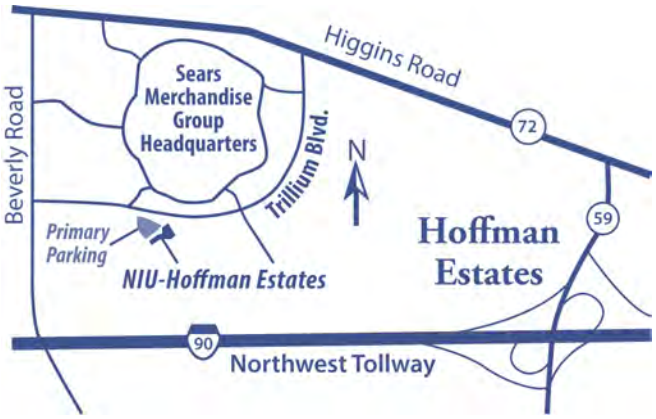

Note: You cannot turn left into the NIU lot from Trillium Blvd. You will have to make a U-turn or come in from Beverly Road.

FRIDAY NIGHT GATHERING!

This year we are holding a special social event on Friday night before the symposium!

Details are still in the works, but the event will be free and probably at the hotel. Please, mark during registration whether or no you are interested in attending.

REGISTER ONLINE!

Please register online at
www.nfmidwest.org/symposium
or
call the office at 630-945-3562.

Registration deadline is November 6, 2018

Please register as early as possible!

Symposium Registration Fees include Continental Breakfast, Lunch, & Snack

$25.00—per adult over 18
$10—Teens ages 13-18
FREE—Children ages 5-12
Bowling—$15

Children under 5 are not allowed, though we MAY make an exception for 4 year olds (please call).

Note: The cost for the symposium and bowling are well below our actual costs. We do all we can to make this event affordable for the NF Midwest community. If you'd like to help defray the costs, please make a donation at www.nfmidwest.org/donate.

Help NF Education by donating at www.nfmidwest.org/donate

Neurofibromatosis Midwest
473 Dunham Road, Suite 3
St. Charles, IL 60174

630-945-3562
info@nfmidwest.org
www.nfmidwest.org

Register Now!

...Or donate to support the symposium and future educational events for NF!

Neurofibromatosis Symposium & iNFo Fair!

Presented by NF Midwest

November 9th

Saturday, 8:00 am to 4:30 pm
Northern Illinois Building
Hoffman Estates, IL

Plus Friday Night Gathering!

Socialize, strengthen and learn from Leading experts and each other.

Don't miss it!

Drug Discoveries from Synodos for NF2 and Identification of Natural Compounds to Treat NF1 and NF2 Tumors

Long-Sheng Chang

OSU Dept of Pediatrics, Biol Chem & Pharmacol, Otolaryngology-Head & Neck Surgery, and Pathology and Ctr for Childhood Cancer & Blood Diseases, Abigail Wexner Res Inst at Nationwide Children's Hosp

Long-Sheng.Chang@nationwidechildrens.org

NF Midwest – Neurofibromatosis Symposium & iNFo Fair 2019

Targeting protein translation via eIF4A inhibition with didesmethylrocaglamide (DDR) and rocaglamide (Roc) to treat pediatric osteosarcoma

Long-Sheng Chang
Long-Sheng.Chang@nationwidechildrens.org

Ctr for Childhood Cancer & Blood Diseases, Nationwide Children's Hosp & Dept of Pediatrics, The Ohio State Univ College of Medicine

Kids Beating Cancer – Science Is the Cure Symposium 2020

Print this Page for Your Records Close Window

Control/Tracking Number: 20-A-7875-AACR
Activity: Abstract Submission
Current Date/Time: 12/5/2019 9:00:29 PM

The eIF4A inhibitors didesmethylrocaglamide and rocaglamide as effective treatments for pediatric bone and soft-tissue sarcomas

Short Title:
Rocaglamides to treat bone sarcomas

Author Block: Long-Sheng Chang[1], Janet L. Oblinger[1], Garima Agarwal[2], Tyler A. Wilson[2], Ryan Roberts[1], James Fuchs[2], Barry R. O'Keefe[3], A. Douglas Kinghorn[2], Jerry M. Collins[3]. [1]Nationwide Children's Hospital and The Ohio State University Wexner Medical Center, Columbus, OH; [2]The Ohio State University College of Pharmacy, Columbus, OH; [3]Center for Cancer Research, National Cancer Institute, NIH, Frederick, MD

Abstract:
Background: Development of an effective medical therapy for osteosarcoma and Ewing sarcoma, the two most common aggressive forms of pediatric bone and soft-tissue sarcomas, is urgently needed as current treatments are inadequate particularly for those with recurrent or metastatic diseases. To achieve this goal, we have identified two natural eIF4A inhibitors, rocaglamide (Roc) and didesmethylrocaglamide (DDR), which potently inhibit proliferation of a series of commonly-used osteosarcoma and Ewing sarcoma cell lines. We also demonstrated that Roc effectively suppresses tumor growth in patient-derived xenograft (PDX) models of osteosarcoma and Ewing sarcoma. Both Roc- and DDR-treated sarcoma cells show decreased levels of multiple oncogenic kinases, including insulin-like growth factor-1 receptor (IGF-1R). Importantly, these rocaglamides are not sensitive to multidrug resistance 1 (MDR1) efflux. In addition, Roc exhibits 50% oral bioavailability, is well-tolerated in mice, and does not induce pulmonary toxicity in dogs as found with another eIF4A inhibitor silvestrol (Chang et al. Mol Cancer Ther. 2019; In Revision). **Methods**: Various osteosarcoma and Ewing sarcoma cell lines were treated with DDR and Roc, followed by cell proliferation assay, flow cytometry, and immunoblotting. Mesenchymal stem cells (MSCs) were used as a control for comparing the expression levels of the eIF4F components important for translation initiation. RNA interference (RNAi) and CRISPR/Cas9 techniques were used to verify eIF4A dependency. An orthotopic cell line-derived xenograft (CDX), a metastatic xenograft, and a PDX models for osteosarcoma and immunohistochemistry were used to assess antitumor efficacy. **Results**: We hypothesize that osteosarcoma and Ewing sarcoma cells are highly addicted to active protein synthesis and that Roc and DDR, by acting as potent eIF4A inhibitors with an ability to induce apoptosis and the DNA damage response, effectively eliminate these malignant sarcomas. We found that various osteosarcoma and Ewing sarcoma cell lines expressed higher levels of eIF4A2, but not eIF4A1, eIF4E, and eIF4G, than MSCs, suggesting a role of eIF4A2 in enhancing protein translation in these sarcoma cells. RNAi knockdown and CRISPR/Cas9 knockout experiments are being evaluated to verify this finding. Both DDR and Roc effectively blocked tumor growth in an orthotopic CDX model. As found with Roc previously, DDR also potently inhibited the growth of an osteosarcoma PDX model. Both rocaglamides were well tolerated at 3 mg/kg by IP every other day and did not cause any significant changes in body weight, compared with vehicle-treated controls. We are presently determining the effects of Roc and DDR on osteosarcoma metastasis. **Conclusions**: The potent anti-tumor activity and favorable toxicity profile of Roc and DDR suggest that these rocaglamides should be further evaluated as potential treatments for osteosarcomas and Ewing sarcomas.
:

Author Disclosure Information:

L. Chang: None. **J.L. Oblinger:** None. **G. Agarwal:** None. **T.A. Wilson:** None. **R. Roberts:** None. **J. Fuchs:** None. **B.R. O'Keefe:** None. **A.D. Kinghorn:** None. **J.M. Collins:** None.
Sponsor (Complete):
Category and Subclass (Complete): ET06-04 Novel antitumor agents
Research Type (Complete): Translational research
Organ Site/Structures (Complete):
***Primary Organ Site:** Pediatric cancers
***Choose Chemical Structure Disclosure Option:**
YES, and I WILL DISCLOSE. Compounds with defined structures were used, and I WILL DISCLOSE them in my presentation.
***Please explain reason for not disclosing (maximum 250 characters with spaces):** : NA
***Reference or patent application number** : NA

Manuscript Publication (Complete):
Manuscript Publication Options: YES, I INTEND to submit a manuscript to be peer-reviewed for AACR journal publication simultaneously with presentation of the abstract (if selected).
Journal Preference : Mol Cancer Ther
Is this study/trial supported in whole or in part by an AACR grant?: No
Is this study/trial sponsored in whole or in part by the pharmaceutical industry?: No

Submission Fee (Complete): Your credit card order has been processed on Thursday 5 December 2019 at 8:57 PM.
Status: Complete

***To log out, simply close your browser window. All information will be saved if you hit the Continue button after each step.

For all log-in problems or technical questions, please contact the OASIS Helpdesk or call (217) 398-1792.
If you have any policy questions related to the AACR Annual Meeting 2020,
please contact the AACR [E-mail: abstract@aacr.org; Phone: (215) 440-9300 or (866) 423-3965].

Feedback

Powered by cOASIS, The Online Abstract Submission and Invitation System SM
© 1996 - 2019 CTI Meeting Technology. All rights reserved. Privacy Policy

Novel drug discovery for NF2-deficient tumors: Brigatinib causes tumor shrinkage in NF2-deficient meningioma and schwannoma

Long-Sheng Chang, Janet L Oblinger, Eric Hawley, Abbi Smith, Marc Ferrer, Steven P Angus, Alejandra M Petrilli, Roberta Beauchamp, Lars Björn Riecken, Serkan Erdin, Ming Poi, Jie Huang, Waylan K Bessler, Xiaohu Zhang, Rajarshi Guha, Craig Thomas, Sarah S Burns, Li Jang, Xiaohong Li, Qingbo Lu, Jin Yuan, Yongzheng He, Andrea Masters, David R Jones, Charles W Yates, Stephen J Haggarty, Salvatore La Rosa, D Bradley Welling, Anat O Stemmer-Rachamimov, Scott Plotkin, James F Gusella, Helen Morrison, Vijaya Ramesh, Cristina Fernandez-Valle, Gary L Johnson, Jaishri Blakeley, D Wade Clapp, on behalf of the Synodos for NF2 Consortium

Children's Tumor Foundation – NF2 Virtual Meeting 2020

Abstract presented at the 2021 Virtual NF Conference (June 14-16, 2021)

Targeting Protein Translation in Combination with MEK Inhibition as an Effective Treatment for NF1, NF2, and Schwannomatosis-Related Tumors

Long-Sheng Chang
Nationwide Children's Hospital & The Ohio State University

Previously, we showed that NF1-associated malignant peripheral nerve sheath tumors (MPNSTs) and NF2-related vestibular schwannomas and meningiomas frequently exhibit elevated expression of the components of the eIF4F translation initiation complex, including eIF4A. We also identified two silvestrol-related eIF4A inhibitors, rocaglamide (Roc) and didesmethylrocaglamide (DDR), with potent growth-inhibitory activities in both NF1 and NF2-associated tumor cells comparable to silvestrol but having better drug-like properties. Both Roc and DDR arrest these tumor cells at G_2/M and induce DNA damage response and apoptosis, while decreasing the levels of multiple oncogenic kinases IGF-1R, AKT, and ERK1/2, consistent with translation inhibition. Unlike silvestrol, Roc and DDR are not sensitive to multi-drug resistance 1 efflux. Roc exhibits 50% oral bioavailability, is well-tolerated in mice, and does not induce pulmonary toxicity in dogs as found with silvestrol. Importantly, Roc, when administered intraperitoneally or orally, potently suppress orthotopic *NF1*-deficient MPNST cell line-derived xenografts. Treated MPNSTs have more cleaved caspase 3-positive cells, indicative of increased apoptosis *in vivo*. We now showed that like Roc, DDR was also well-tolerated and exhibited oral bioavailability better than silvestrol. Both DDR and Roc effectively inhibited the growth of patient-derived xenografts of MPNST. Using mouse *Nf1*$^{-/-}$ plexiform neurofibroma (PNF)-derived sphere cultures, Roc reduced sphere numbers in a dose-dependent manner, decreased ERK protein levels, and induced apoptosis as evidenced by increased PARP cleavage. In addition, like NF2-related tumor cells, Roc effectively decreased the viability of schwannoma cells from a schwannomatosis patient. However, while Roc and DDR potently suppressed the growth of NF-related tumor cells, they did not completely eliminate them. By conducting a high-throughput screening of the MIPE oncology compound library, which contains ~3,000 compounds with diverse mechanisms of action, for agents that synergized with DDR in killing MPNST cells, several targeted agents were identified. Interestingly, among them were MEK inhibitors, including selumetinib which was recently approved by the FDA for treating NF1 children with inoperable PNFs. Collectively, our results imply that targeting protein translation via eIF4A inhibition may simultaneously block the expression of many aberrantly expressed oncogenic signaling molecules necessary for the growth of NF1-, NF2-, and schwannomatosis-associated tumors. Combination of eIF4A inhibitors with selected targeted drugs, such as MEK inhibitors, may further eradicate these tumor cells.

Full List Authors: Long-Sheng Chang[1,2], Janet L Oblinger[1], Xiaohu Zhang[3], Jianqiang Wu[4], Cristina Fernandez-Valle[5], Larry W Anderson[6], Marc Ferrer[3], Nancy Ratner[4], A Douglas Kinghorn[8], Barry R O'Keefe[6,7], Jerry M Collins[6]

[1]Ctr for Childhood Cancer & Blood Dis, Nationwide Children's Hosp, [2]OSU Dept of Pediatrics, [3]Nat'l Ctr for Advancing Translational Sci, NIH, [4]Cancer Biol & Neural Tumors Prog, Cincinnati Children's Hosp Med Ctr and UC Dept of Pediatrics, [5]Neuroscience Div, Univ of Central Florida, [6]Div of Cancer Treatment & Diagnosis and [7]Ctr for Cancer Research, NCI, NIH, [8]Div of Medicinal Chemistry & Pharmacognosy, OSU Coll of Pharmacy

Funding: CancerFree KIDS, Sunbeam Foundation, Department of Defense

Targeting protein translation in combination with nuclear export inhibition to eliminate pediatric and adult sarcomas

Long-Sheng Chang

Center for Childhood Cancer & Blood Diseases, Nationwide Children's Hospital and Department of Pediatrics, The Ohio State University College of Medicine

National Pediatric Cancer Foundation/Sunshine Project Summit 2021

Abstract Title: TARGETING INHIBITION OF EIF4A AND A HIGH THROUGHPUT SCREENING TO IDENTIFY SYNERGISTIC DRUG COMBINATIONS TO TREAT PEDIATRIC AND ADULT SARCOMAS

ABSTRACT PREVIEW: TARGETING INHIBITION OF EIF4A AND A HIGH THROUGHPUT SCREENING TO IDENTIFY SYNERGISTIC DRUG COMBINATIONS TO TREAT PEDIATRIC AND ADULT SARCOMAS

TARGETING INHIBITION OF EIF4A AND A HIGH THROUGHPUT SCREENING TO IDENTIFY SYNERGISTIC DRUG COMBINATIONS TO TREAT PEDIATRIC AND ADULT SARCOMAS

Abstract ID: **1078974**

Presentation Type: **Oral**

Abstract Status: **Complete**

Co-Author(s)

LC

Long-Sheng Chang, PhD

Position:
Professort

Organization:
Nationwide Children's Hospital and The Ohio State University

Role:
Author

CTOS Membership
Not Sure

JO

Janet L. Oblinger, PhD

Position:
Research Associate

Organization:
Center for Childhood Cancer & Blood Diseases, Nationwide Children's Hospital

Role:
Co-Author

CTOS Membership
No

XZ

Xiaohu Zhang, PhD

Organization:
National Center for Advancing Translational Sciences, NIH

Role:

Co-Author

CTOS Membership
No

hA

hyndavi Anksapuram, BA

Position:
Student

Organization:
Nationwide Children's Hospital and The Ohio State University

Role:

Co-Author

CTOS Membership
No

MF

Marc Ferrer, PhD

Position:
Leader, Biomol Screening & Probe Dev

Organization:
National Center for Advancing Translational Sciences, NIH

Role:

Co-Author

CTOS Membership
No

RR

Ryan D. Roberts, MD, PhD

Position:
Assistant Professor

Organization:
Nationwide Children's Hospital and The Ohio State University

Role:

Co-Author

CTOS Membership
Yes

AK

A Douglas Kinghorn, DSc, PhD

Position:
Professor

Organization:
Division of Medicinal Chemistry & Pharmacognosy, The Ohio State University College of Pharmacy

Role:

Co-Author

CTOS Membership
No

Abstract Information

Category

Basic Science | Preclinical Models

Permission to Use

- Yes

Attendance

- Yes

Objective

To sustain uncontrolled growth, cancer cells enhance protein translation by upregulating the translation machinery. We have shown over-expression of the eukaryotic initiation factor 4A (eIF4A) in several types of sarcomas, including malignant peripheral nerve sheath tumors (MPNSTs). Genetic depletion of eIF4A and pharmacological inhibition using the natural eIF4A inhibitor silvestrol reduce multiple oncogenic signaling molecules and effectively suppress tumor growth in vitro and in vivo. We also identified two silvestrol-related eIF4A inhibitors, rocaglamide (Roc) and didesmethylrocaglamide (DDR), with potent growth-inhibitory activities comparable to silvestrol but having better drug-like properties. Both Roc and DDR arrest tumor cells at G2/M and induce DNA damage response and apoptosis, while decreasing the levels of multiple oncogenic kinases including IGF-1R, AKT, and ERK1/2, consistent with translation inhibition. Unlike silvestrol, Roc and DDR are not sensitive to multi-drug resistance 1 (MDR1) efflux, and Roc does not cause pulmonary toxicity in dogs as found with silvestrol. Importantly, Roc has oral bioavailability and, when administered intraperitoneally or orally, potently suppresses the growth of orthotopic MPNST xenografts. Treated tumors have more cleaved caspase 3-positive cells, indicative of increased apoptosis in vivo. These results indicate that these eIF4A inhibitors merit further investigation as sarcoma treatments. The objective of this study is to evaluate the potential of using Roc and DDR to treat multiple types of pediatric and adult sarcomas and to identify other targeted agents that synergize with these eIF4A inhibitors to completely eradicate sarcoma cells.

Methods

Various types of bone and soft-tissue sarcoma cell lines were treated with DDR and Roc, followed by cell proliferation assay, flow cytometry, and immunoblotting. Plasma concentrations of Roc or DDR in blood collected before and after dosing by intravenous or intraperitoneal injection or by oral gavage were analyzed using liquid chromatography coupled with tandem mass spectrometry. Orthotopic cell line-derived xenograft (CDX) and patient-derived xenograft (PDX) models for various pediatric and adult sarcomas were used to assess antitumor efficacy. The matrix high-throughput screening of the Mechanism Interrogation Plates (MIPE) oncology compound library, which contains ~3,000 compounds with diverse mechanisms of action, was used to identify agents that synergized with DDR in killing MPNST cells. Synergistic compound combinations were validated in multiple sarcoma cell lines, and their mechanisms of action were analyzed by Western blot and immunohistochemistry.

Results

We show that like Roc, DDR is also well-tolerated and exhibits oral bioavailability. Both Roc and DDR effectively inhibit tumor growth in multiple PDX models of MPNST, osteosarcoma, Ewing sarcoma, rhabdomyosarcoma, desmoplastic small round cell tumor, as well as the common adult sarcomas liposarcoma and leiomyosarcoma. In addition, these eIF4A inhibitors exhibit potent anti-tumor effects in an orthotopic intra-tibial osteosarcoma CDX model and a canine osteosarcoma PDX model by reducing multiple key growth signaling molecules, including IGF-1R, and inducing apoptosis. These results suggest that inhibition of eIF4A is a potential treatment strategy for multiple types of sarcoma. Based on these promising findings, the NCI Experimental Therapeutics (NExT) Program has approved and selected Roc and DDR for further development as sarcoma treatments. However, while these eIF4A inhibitors profoundly suppress tumor growth, they do not eliminate all sarcoma cells. By conducting a high-throughput screening of the MIPE oncology compound library for agents that synergized with DDR in killing MPNST cells, several targeted agents were identified, including several FDA-approved drugs. The synergistic growth-inhibitory activities of these agents were also found with Roc and were verified in multiple other types of sarcoma cells by enhancing apoptosis.

Conclusion

Collectively, these results suggest that a clinical trial for Roc and DDR to treat sarcomas is warranted. Further, our findings reinforce the notion that simultaneously blocking multiple aberrantly expressed oncogenic signaling molecules by eIF4A inhibitors and their combination with specific targeted drugs may be effective in completely eliminating pediatric and adult sarcomas. (We sincerely thank Larry W Anderson, Barry R O'Keefe, and Jerry M Collins of the NCI and the NExT program for pharmacokinetic and toxicity analysis and compound synthesis. This study is supported by CancerFree KIDS, Sunbeam Foundation, NF2 Biosolutions, and the US Department of Defense.)

Disclosure Information

FDA Disclosure
Not Applicable

Manufacturer's Name and Drugs or Devices

Financial Relationship
Yes

Abstract presented at the 2022 NF Conference (June 18-21, 2022)

Orthotopic Xenograft Models and Potential Treatments for *NF2*-Deficient Meningiomas

Long-Sheng Chang
Nationwide Children's Hospital & The Ohio State University

Neurofibromatosis 2 (NF2) is an extremely debilitating tumor predisposition syndrome in which afflicted patients frequently develop multiple nervous system tumors, including meningiomas. NF2 is caused by mutations that inactivate the *NF2*/merlin gene, which regulates multiple mitogenic signaling pathways including the receptor tyrosine kinase (RTK), PI3K/AKT/mTOR, and RAF/MEK/ERK pathways. As the most common intracranial tumors, meningiomas can also occur sporadically, and ~50% of sporadic meningiomas carry *NF2* mutations, suggesting an important role for merlin in meningioma tumorigenesis. Current treatment options for meningiomas are limited to surgery and radiation; however, these treatments can cause severe complications, such as seizure, intracranial bleeding, and stroke. Thus, identification of an effective medical therapy is urgently needed. To achieve this goal, we previously established a quantifiable orthotopic model for *NF2*-deficient meningiomas and used it to evaluate agents that target merlin-regulated pathways. We showed that telomerase-immortalized human meningioma Ben-Men-1 cells do not express merlin and that luciferase-expressing Ben-Men-1-LucB cells establish intracranial xenografts reminiscent of benign tumors. Interestingly, AR-42 (a.k.a. REC-2282), a histone deacetylase inhibitor with the ability to inhibit AKT, exerts differential effects on cell-cycle progression of normal meningeal and meningioma cells and causes regression of Ben-Men-1-LucB tumors in mice. AR-42-treated tumors also showed minimal regrowth following cessation of treatment. Based on these findings, Phase 1 and Phase 0 clinical trials were conducted and demonstrated that AR-42 is well-tolerated with some efficacy in NF2 patients, is concentrated in the tumors of treated patients, and decreases the levels p-AKT, p-ERK, and p-S6 in the majority of treated tumors. A Phase 2 study of REC-2282 is presently recruiting patients with progressive *NF2*-mutated meningiomas. Using the intracranial Ben-Men-1-LucB model, we also evaluated several potential drugs and drug combinations identified by the Synodos for NF2 team in collaboration with the NIH-National Center for Advancing Translational Sciences. We showed that the mTOR kinase inhibitor INK128 suppresses tumor growth and the multi-TK inhibitor brigatinib causes tumor shrinkage. These findings support the ongoing phase 2 trial of brigatinib in NF2 patients. Further, we found that combination of brigatinib and INK128 exhibited a trend toward enhanced tumor shrinkage compared to brigatinib alone but was not statistically significant. In addition, NF2-associated tumors express high levels of three components of the eukaryotic initiation factor 4F (eIF4F) translation initiation complex, including eIF4A. Genetic depletion of eIF4A using shRNA and pharmacological inhibition with eIF4A inhibitors strongly reduced meningioma cell proliferation, suggesting that blocking protein translation could be a potential treatment for meningiomas. Recently, we also generated an orthotopic xenograft model using meningioma cells derived from an NF2 patient's tumor. Additional drugs or drug combinations that block multiple signaling pathways are being sought. Our ultimate goal is to identify an effective drug to eradicate NF2-related tumors.

Full List Authors: Long-Sheng Chang[1], Sarah S. Burns[2], Janet L Oblinger[1], D. Bradley Welling[3]

[1]Center for Childhood Cancer & Blood Diseases, Nationwide Children's Hospital and Department of Pediatrics, The Ohio State University, [2]Indiana University School of Medicine, [3]Massachusetts Eyes and Ears, Massachusetts General Hospital and Harvard University

Funding: CancerFree KIDS, Department of Defense, NF2 Biosolutions, National Institute of Neurological Disorders and Stroke, and Children’s Tumor Foundation

Abstract presented at the 2022 NF Conference (June 18-21, 2022)

New patient-derived models of NF2-deficient vestibular schwannoma and meningioma to advance basic and preclinical investigations

Janet L Oblinger, PhD
Nationwide Children's Hospital

The authors have no relevant financial relationships to disclose.

Vestibular schwannoma (VS) and meningioma are two most commonly found tumors in patients with neurofibromatosis type 2 (NF2), which is caused by biallelic loss of the *NF2*/merlin gene. Although often benign, these nervous system tumors incur serious morbidities, such as deafness, facial paralysis, seizures, and potentially death. Also, they are unresponsive to traditional chemotherapy. One critical factor in identifying an effective therapy is the availability of disease-relevant models. Most of the existing VS and meningioma cell lines were immortalized by oncogenes, which confers aggressive growth, and some still express merlin. For these reasons, xenograft models using these cells do not recapitulate the benign characteristics of human tumors. Our objective is to establish new *NF2*-deficient cell lines derived from patients' VS and meningioma, characterize their growth behavior and molecular features, and develop them into quantifiable orthotopic xenograft models that can be used as platforms for drug testing. Lentiviral transduction of human telomerase was used to establish the immortalized cell lines AG-NF2-Men, derived from a grade-I meningioma of an NF2 patient, and hVS-16H, from a sporadic VS. The immortalized AG-NF2-Men and hVS-16H cells retain many characteristics of the original tumors. Western blot and immunostaining analysis confirmed that both cell lines did not express merlin protein but exhibited several cell type-specific markers and kinases commonly implicated in driving VS and meningioma growth, including EGFR, ErbB3, IGF-1R, and AKT. In addition, these cell lines are sensitive to growth inhibition by several targeted compounds, including the multi-kinase inhibitor brigatinib, mTOR kinase inhibitor INK128, HDAC inhibitor AR-42, proteasome inhibitors oprozomib and TAK-243, BRD4 inhibitor JQ1, XPO1 inhibitors selinexor and eltanexor, and eIF4A inhibitors rocaglamide and didesmethylrocaglamide, similar to primary VS and meningioma cell cultures. To generate a quantifiable NF2-associated meningioma model, luciferase-expressing AG-NF2-Men-Luc2 cells were isolated and implanted at the skull base or subcutaneous location in immunodeficient NSG mice and tumor growth monitored by bioluminescence imaging. Intriguingly, AG-NF2-Men-Luc2 established intracranial xenografts that grew steadily over time but grew poorly at the subcutaneous location. This orthotopic, NF2-associated meningioma model together with the sporadic meningioma Ben-Men-1-LucB model that we developed previously are being used to evaluate several drug candidates. Similarly, we also generated luciferase-expressing hVS-16H-Luc12 cells and will use them to establish a quantifiable xenograft model. The addition of these new models will allow us to further interrogate the biology of NF2-deficient tumors and help improve the predictiveness of existing preclinical drug testing protocols.

Full List Authors: Janet L Oblinger, PhD[1], Long-Sheng Chang, PhD[1,2]

[1]Center for Childhood Cancer & Blood Diseases, Abigail Wexner Research Institute at Nationwide Children's Hospital and [2]Department of Pediatrics, The Ohio State University College of Medicine

Funding: CancerFree KIDS, NF2 Biosolutions, Department of Defense, and NIH-NINDS